Sedimentological signatures of lacustrine tsunamis

Inauguraldissertation

der Philosophisch-naturwissenschaftlichen Fakultät

der Universität Bern

vorgelegt von

Valentin Nigg

von Gersau (SZ)

Leiter der Arbeit:

Prof. Dr. F. S. Anselmetti

PD Dr. H. Vogel

Institut für Geologie & Oeschger-Zentrum für Klimaforschung

Universität Bern

Sedimentological signatures of lacustrine tsunamis

Inauguraldissertation

der Philosophisch-naturwissenschaftlichen Fakultät

der Universität Bern

vorgelegt von

Valentin Nigg

von Gersau (SZ)

Leiter der Arbeit:

Prof. Dr. F. S. Anselmetti

PD Dr. H. Vogel

Institut für Geologie & Oeschger-Zentrum für Klimaforschung

Universität Bern

Von der Philosophisch-naturwissenschaftlichen Fakultät angenommen.

Bern, Montag, den 12. April 2021

Der Dekan:

Prof. Dr. Zoltan Balogh

This work is dedicated to my grandfather Werner Arnold.

*"*Besides chairs, tables, bookshelves, etc… there were several roofs of cottages, which had been transported almost whole… During my walk around the island, I observed that numerous fragments of rock, which, from the marine productions adhering to them, must recently have been lying in deep water, had been cast up high on the beach; one of these was six feet long, three broad, and two thick*."*

Charles Darwin, 1835
in *The Voyage of the Beagle*

Abstract

Lake tsunamis are considered to be natural hazards with high magnitudes and low recurrence rates. Because of their infrequent occurrence in space and time, little is known about the associated hazard and the risk to the vulnerable coastal areas that are now often heavily populated. However, historical reports and recent scientific achievements show that certain Swiss lakes may have been repeatedly affected by tsunamis during the last 15'000 years. This makes Switzerland an ideal case-study area to conduct fundamental research in the field of tsunamis and to gain new knowledge applicable to other lacustrine areas, as well as to the marine environment.

Lacustrine tsunamis can be generated by subaqueous and subaerial mass movements, volcanic eruptions, fault displacements within large lakes, and air-pressure disturbances. Mass movements, triggered by strong earthquakes, are considered one of the main causes. However, spontaneous delta collapses and subaerial impact, often related to artificial rock-mining activities, also have induced tsunami events on Swiss lake basins.

The geological record of mass-movement deposits in the seismically imaged stratigraphy of deep lake basins provides evidence for the occurrence of prehistoric lake tsunamis. However, because the dimensions (e.g., spatial distribution, volume, etc.) and dynamics (e.g., single-stage or multi-stage failures, initial acceleration, velocity, cohesion etc.) of mass movements strongly

influence tsunami generation, which is difficult to estimate, conclusive evidence for prehistoric lake tsunamis is lacking. Therefore, the geological record in the on- and offshore coastal environment may provide further evidence on past lacustrine tsunami events. These sedimentological signatures are examined in this thesis.

Recent marine (2018 Sulawesi earthquake and tsunami, Indonesia) and lacustrine (2007 landslide-generated tsunami in Chehalis Lake, Canada) tsunami events indicate that large amounts of sediment are mobilized during tsunami inundation and transported both landward and seaward with backwash currents. To date, a wide variety of sedimentological bed forms and characteristic depositional signatures have been described from various coastal environments. Nevertheless, hardly any tsunami deposits have been described from the on- and near-offshore of lakes, and none were investigated in and around Swiss lakes until today.

Yet, historical tsunami hazard descriptions from Swiss lakes provide documentation of inundation distances and run-up, and in specific cases, a limited description of the associated deposits left behind. These descriptions were used to characterize and locate tsunami deposits from lacustrine environments that were compared with descriptions of their marine counterparts.

In summary, a combination of geological field- and laboratory analysis, numerical tsunami propagation simulation, and historical documents is used to identify and characterize lacustrine tsunami deposits in several Swiss lakes. At field sites where positive evidence for tsunami deposits was observed, sedimentological characteristics are used to finally validate the robustness of numerical tsunami propagation simulations applied to mass movements observed from bathymetric and seismic reflection data in the lake.

Based on numerical tsunami simulation and a suite of sediment cores from the coastal on- and offshore environment of Lake Sils, we were able to reconstruct a prehistoric delta collapse-generated tsunami. An offshore tsunami deposit of the historic 1601 Lake Lucerne event was observed from sediment core transect in a coastal depression in the Lucerne Bay. Another sediment core recovered from the coastal offshore environment contains sedimentary signatures that are likely associated with bottom currents from prehistoric tsunami events at ~2200 and ~5400 Before Present at Lake Lucerne.

The observed sedimentological signatures of lake tsunamis were investigated using multi-proxy analysis including whole-core scans (density, magnetic susceptibility, and CT), as well as micro-CT scanning of sediment U-channels, radiocarbon dating, elemental analysis, and grain-size analysis. The identified sedimentological signatures consist of sharp lower and upper sedimentary contacts, successions of single and multiple normal graded sand, massive sand beds, and a characteristic fine-grained top. Based on radiocarbon dating, these signatures can be associated with large mass-movement deposits observed in sediment cores and seismic-reflection data of the deep lake basin.

Acknowledgements

First and foremost, I would like to express my gratitude for the invaluable support I received from my family and friends, as well as from the research associates and mentors who have guided me during the last four years of my doctoral studies. It has been an extraordinary journey of learning about new fields and places, making friends and, growing both scientifically and personally. Without your help, this work would not have been possible.

This acknowledgment goes to my supervisors Flavio Anselmetti and Hendrik Vogel, who closely guided this work. It has been a pleasure to work and learn with you, and I am grateful for your collective mentorship. As project leader, Flavio's openness to discussions allowed the project to evolve. I greatly appreciate the scientific exchanges we had during this period, as they took place at group retreats in remote cabins or at annual project meetings in various memorable locations. The last and probably most intense period of this project was strongly influenced by the Cov-19 global pandemic crisis. Nevertheless, we have continued close exchange despite the difficult circumstances. I thank you for your constructive and comprehensive as well as collegial support during this time.

My appreciation for the scientific and collegial support I received from Katrina Kremer, David Vetsch, Paola Bacigaluppi, Stefano Fabbri, Stephan Wohlwend, Michael Hilbe, Marina Morlock, Michael Strupler, Julijana Krbjanevic, Michael Strasser, Stéphanie Girardclos and the SNSF Sinergia research associates cannot be easily expressed in a few words. I have been very fortunate to spend my time with all of you. Without your support this project would have been considerably more difficult. I have been very lucky in having such committed collaborations and dynamic scientific environment.

I greatly appreciate the Swiss National Science Foundation for the financial support of this project. It was an honor to be involved in a national research project that conducts basic research in a socially relevant topic.

I would like to specifically thank Marc De Batist for examining and evaluating this thesis as an external expert. I thank Fritz Schlunegger for chairing the defense of my dissertation.

I would like to express my gratitude to the members of the SNSF Sinergia project: "Lake Tsunamis: Causes, Controls, and Hazard", the Quaternary Geology and Paleoclimatology working group and my office members for your company over the last four years. It has been a pleasure to discuss and study with you.

Words are not enough to thank my family, friends, and my beloved girlfriend. You have always sustained and motivated me. My gratitude is endless. I thank you for your support.

Contents

Lake Lucerne with Mount Pilatus in the distance.

1 Preface

The presented thesis deals with the rare natural phenomenon of lacustrine tsunamis, which have a destructive dimension and pose a potential threat to inhabited coastal areas and its infrastructure. The reader should be aware that natural hazards cannot be prevented. However, the vulnerability of a civilization depends on its risk assessment. Resilience is therefore necessary to cope with the local and global challenges of the 21st century. For resilient adaptation, however, natural hazards must be adequately studied to be better prepared for the future and mitigate possible consequences. This study is a contribution to this goal.

1.1 PhD project

This PhD project is embedded in the multidisciplinary Swiss National Science Foundation (SNSF) Sinergia Project: Lake Tsunamis: Causes, Controls, and Hazard (research grant no.: 171017). Within the holistic framework of the project, which consists of five synergetic work packages (WPs), the natural phenomenon of lacustrine tsunami is investigated in the field of fundamental research and in case studies at Swiss lakes. Within this PhD project the research questions of WP paleo were addressed.

The scientific studies of the different WP's were conducted at four different research institutes during 2017 to 2021:

- Institute of Geological Sciences (IfG), University of Bern, CH
- Swiss Seismological Service (SED), ETH Zurich, CH
- Institute of Hydraulics, Hydrology and Glaciology (VAW), ETH Zurich, CH
- Centre for Marine Environmental Sciences (MARUM), University of Bremen, DE

The work packages, their research institute affiliation, and their primary fields of research are:

- WP paleo (IfG): Geological record of lacustrine tsunami events
- WP response (SED, MARUM): Seismological geotechnical characterization of slope instabilities under seismic shaking
- WP wave (VAW): Sliding mechanisms and the associated tsunami generation and propagation based on numerical and hydrological models
- WP hazard (SED): Lake tsunami hazard assessment, which contributes to a sustainable and practice-oriented risk management in Switzerland
- WP delta (SED; IfG): Characterization of subaqueous slope failures in deltas

1.2 Organization of the thesis

This thesis is organized into an introduction, a series of four individual research papers, conclusions, and research paper appendices. The general introduction (Chapter 2), the four research papers (Chapters 3-6) and Chapter 7 (Conclusions and outlook) are briefly presented in the following. The research papers in Chapters 3, 4, and 5 were first-authored by myself, whereas I acted as co-author for the research paper in Chapter 6.

- Chapter 2 -

General introduction

The first chapter provides a broad background on the current understanding of the genesis of tsunami deposits and its implication for tsunami risk assessments. In addition, the objectives and research questions to be addressed are outlined. Finally, the applied methodological framework of this thesis is summarized.

- Chapter 3 -

Sedimentological signatures of historic tsunamis in Swiss lakes

This chapter defines the scientific basis for the research conducted as part of this dissertation. Emphasis is placed on the applied methodological workflow that was carried out for the study-site selection to locate and identify lacustrine tsunami deposits in the on- and offshore environment. Therefore, this chapter provides a guidance for future studies to investigate lake tsunami deposits in Switzerland and other countries.

- Chapter 4 -

A tsunamigenic delta collapse and its associated tsunami deposits in and around Lake Sils, Switzerland

The case study presented in this chapter was conducted at Lake Sils and combines a suite of geological field campaigns with numerical tsunami generation and propagation simulation. The observed sedimentological succession observed in the on- and offshore settings provide evidence for a basin-wide prehistoric tsunami that was generated by the partial collapse of the Isola Delta (Blass et al., 2005).

- Chapter 5 -

Tsunami offshore deposits: evidence from sediment cores and numerical wave propagation of the 1601 CE Lake Lucerne event

Deposits of the historically well-documented1601 CE Lake Lucerne tsunami were identified in the offshore setting of the Lucerne Bay. A strong regional earthquake caused multiple subaqueous slope failures, which are considered as the main cause of the lake tsunami (Hilbe & Anselmetti, 2015; Schnellmann et al., 2012; Siegenthaler et al., 1987). The second largest mass movement was simulated by an instantaneous collapse of 5 m of the sediment drape along the failed area, using the hydrodynamic modelling software BASEMENT (Vetsch et al., 2020). The simulated propagation of the tsunami waves and the dimensional bed shear-stress, used for a threshold criterion of incipient motion, were investigated in the Lucerne Bay area.

- Chapter 6 -

Freshwater (paleo)tsunamis – a review

This chapter is a review article on freshwater (paleo)tsunamis first-authored by Katrina Kremer and co-authored by the author of this thesis. The article summarizes the scientific progress that has been made since the 2011 Tohoku-oki tsunami in the field of freshwater tsunami research. It characterizes the generation mechanisms of freshwater tsunamis and reports on the characteristics of freshwater tsunami deposits by various authors.

- Chapter 7 -

Conclusions and outlook

The final chapter presents the main conclusions of this PhD thesis, the major achievements made within the SNSF Sinergia project: “Lake Tsunamis: Causes, Controls and Hazard” and recommendations for future work. In summary, this thesis uses historical reports on tsunami inundation and coastal damage combined with multiproxy sediment core analysis and numerical tsunami simulation to investigate and characterize the sedimentological signatures of lacustrine tsunami deposits in the on- and coastal offshore environment.

References

Blass A, Anselmetti FS, Grosjean M, Sturm M (2005) The last 1300 years of environmental history recorded in the sediments of Lake Sils (Engadine, Switzerland). Eclogae Geologicae Helvetiae 98:319-332.

Hilbe, M., and Anselmetti, F. S. (2015) Mass Movement-Induced Tsunami Hazard on Perialpine Lake Lucerne (Switzerland): Scenarios and Numerical Experiments. Pure Appl. Geophys. 172, 545–568.

Schnellmann, M., Anselmetti, F. S., Giardini, D., McKenzie, J. A., and Ward, S. N. (2002) Prehistoric earthquake history revealed by lacustrine slump deposits. Geology 30, 1131–1134.

Siegenthaler, C., Finger, W., Kelts, K., and Wang, S. (1987) Earthquake and seiche deposits in Lake Lucerne, Switzerland. Eclogae Geol. Helv. 80, 241–260.

Vetsch D., Siviglia A., Bacigaluppi P., Bürgler M., Caponi F., Conde D., Gerke E., Kammerer S., Koch A., Peter S., Vanzo D., Vonwiller L. & Weberndorfer M. (2020) System Manuals of BASEMENT, Version 3.1. Laboratory of Hydraulics, Glaciology and Hydrology (VAW). ETH Zurich. Available from https://www.basement.ethz.ch.

2 General introduction

This thesis focusses on tsunami deposits, which are the sedimentological traces of past tsunami events observed in different coastal environments (Fig. 2-1; Einsele et al., 1996). These signatures may be found in the on- and offshore setting in the marine and lacustrine environments. Because depositional signatures are strongly related to the coastal geomorphology (e.g., sediment availability, microtopography, flora), a variety of depositional signatures have been described, particularly in the marine (e.g., Dawson & Shi, 2000; Engel & Brückner, 2011), but also in the lacustrine environment (e.g., Kremer et al., 2020). These signatures include sharp to erosional bases as well as single and multiple graded fining and coarsening upward clastic sand-sized deposits with internal laminae of fine-grained sediment (silt and clay- sized). In addition to deposits of fines, homogenously distributed boulder deposits transported by tsunami inundation along the shallow coastal plains (e.g., Nandasena et al., 2013; Scheffers, 2008), as well as increased Cl, Ba, and Sr concentrations were found in coastal marine sediments where clastic traces were not present (e.g., Chagué-Goff, 2010).

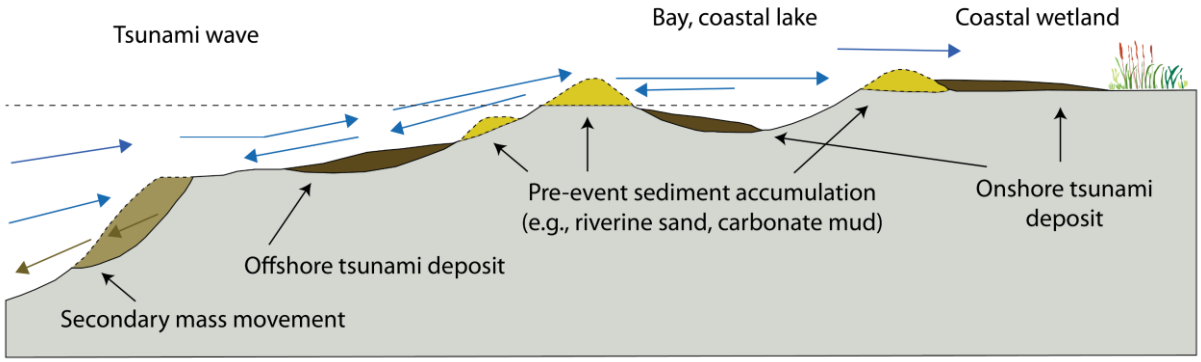

Fig. 2-1: Tsunami depositional model for different coastal settings (modified from Einsele et al., 1996).

The physical characteristics of tsunami waves differ from storm-induced waves by their long wavelengths, which are generated from water column displacement that occurs during tsunami initiation by megathrust earthquake ruptures along the seafloor (Bryant, 2014) and by

subaqueous mass movements (Tappin et al., 2001). Less commonly, tsunami waves can be generated by bolide impact (Papadopoulos & Kortekaas, 2003) or air-pressure disturbances that generate meteotsunamis (Monserrat et al., 2006). In addition, the propagation velocity of tsunamis differs from storm-induced wave currents. The phase velocity (c) of tsunami waves is determined by the depth of the water body (h) and the gravitational acceleration (g) according to $c = \sqrt{g\,h}$ (Röbke & Vögt, 2017; Synolakis & Bernard, 2006). In the open oceans, propagation velocity of tsunamis reaches speeds of up to 800 km h^{-1} and entire oceans can be traversed within hours.

As tsunami waves approach shallow waters of the continental shelf (water depths < 200 m), the water velocity decreases according to the rule abovementioned. However, due to the law of conservation of energy, the wave amplitude may increase from a few dm in the open ocean to several m on the coast. There, tsunami witnesses often report a drawback, the receding of the shoreline before the first pulse of tsunami inundation, but this does not necessarily always occur (Röbke & Vögt, 2017). Depending on the tsunami generation, a wave crest may also arrive at the coast first, which is followed by a wave trough. This is succeeded by several wave pulses that may inundate low-lying coastal areas several hundred to thousand meters. The maximum inland flooding is generally referred to the term inundation distance. Whereas the elevation above current water level (e.g., corrected for tides) at the location of the maximum inland flooding is usually referred to run-up or run-up height.

The high damage potential of tsunamis is attributed to the long wavelength of tsunami waves. Therefore, tsunami inundation may be illustrated by a wall of water that continuously floods the coastal environment. This is in contrast to storm-induced waves, which certainly also have high damage potential (e.g., Hurricane Katrina (Robertson et al., 2007); Typhoon Haiyan (Brill et al., 2016), but inundation of the coastal environment occurs in discrete surges with lower energies but often accompanied by strong wind gusts. Nonetheless, human population is heavily concentrated in low-lying coastal regions at a global scale (Nicholls & Small, 2002) and is therefore heavily affected during coastal floodings. For example, more than 200’000 people have lost their lives during the 2004 Indian Ocean tsunami event (Satake, 2014), around 20’000 people during the 2011 Tohoku-oki tsunami (Nakahara & Ichikawa, 2013). As a comparison, Hurricane Katrina caused more than 1’200 casualties in 2005 (Fritz et al., 2007).

A special case of tsunami waves are impulse waves generated by the impact of solid bodies (e.g., subaerial landslides and rockfalls, volcanic eruptions and meteoric bolides) on the water surfaces (Evers et al., 2019). These impulse waves have shorter wavelengths but higher wave amplitudes near the source, which generally decrease rapidly with propagation compared to subaqueous generated tsunamis. A well-known example for this type of tsunami is the earthquake-induced landslide impact generated mega-tsunami in Lituya Bay (Alaska, USA) on July 10, 1958, which caused total forest destruction up to 524 m above the current sea level (run-up) and erosion down to bedrock (Fritz et al., 2009). Another often referenced event is the K/T (Cretaceous/Tertiary boundary) impulse wave generated by a meteoric bolide impact that caused characteristic 1 to 3 m thick clastic tsunami event deposits in several coastal environments (Keller et al., 1997).

Waves that are generated by pressure perturbances in the atmosphere are referred to meteotsunamis (Nomitsu, 1935; Linares et al., 2016). Because these waves can travel far distances, they can hit coastal communities also with a calm sea and blue skies (e.g., Pattiaratchi and Wijeratne, 2015; Sallenger et al., 1995). Therefore, forewarning and effective mitigation is needed for both economic and social benefit (Thompson et al., 2020). Moreover, even seemingly modest meteotsunamis can produce strong currents with hazardous conditions at the coast (e.g., Monserrat et al., 2006; Shi et al., 2020). For example, on July 17, 2018 the Mediterranean coast of Spain was hit by a meteotsunami. In the Laurentian Great Lakes, Bechle et al. (2016) quantified meteotsunamis in terms of seasonality, causes, and recurrence rates and has found that they occur on average 106 times per year.

2.1 Current state of knowledge

Tsunami events occur not only in the marine setting, but also in the freshwater environment (Kremer et al., 2020). The main tsunami generation mechanisms are identical to the marine setting, whereas subaerial and subaqueous mass movements are the most common triggering mechanism. Tsunamis generated by fault displacements within a lake, however, are rare (Kremer et al., 2020). Impulse waves generated by the impact of meteoric bolides are not further considered in this work.

Historical accounts document several Swiss lakes that were affected once (Lake Lauerz 1806 (Bussmann & Anselmetti, 2010) or repeatedly (Lake Lucerne: 1601 & 1687 (Hilbe and

Anselmetti, 2015); Lake Geneva: 563 & 1584 (Kremer et al., 2015)) by lacustrine tsunamis during the historical period. Based on scientific advances in imaging the lake-floor morphology with multibeam swath bathymetry and its subsurface sediment architecture with high-resolution seismic reflection data, it has been shown that historically reported tsunami events were generated by large subaqueous and subaerial mass movements in the range of 10-100 10^6 m^3 and 0.005-10 10^6 m^3, respectively (Kremer et al., 2020, Nigg et al., in prep.). Simultaneously failed mass movements within a lake are likely triggered by peak ground acceleration during strong local to regional earthquakes (Schnellmann et al., 2006), while single mass movements and delta collapses may fail due to temporally confined high sedimentation rates or rapid pore pressure changes.

Although the mass-movement event stratigraphy of several Swiss lakes provides evidence for repeated tsunamis events during the prehistoric period, tsunami initiation by these mass movements is difficult to reconstruct from the geological record. While mass-movement morphology as well as failed volumes may be well reconstructed, mass movement behavior with respect to failure mechanism and kinematics (e.g., initial acceleration and velocity of slide, rheology, and timing of individual failures) are generally unknown but critical parameters for tsunami generation (Bornhold & Thomson, 2012). For example, it has been shown that some giant submarine landslides may generate tsunamis of only modest size due to their failure mechanisms (Løvholt et al., 2017). In particular, it is assumed that retrogressive subaqueous landslides are relative inefficient in generating tsunamis (Løvholt et al., 2017). However, when these voluminous landslides are rapidly converted into a fast-moving debris flow, they can generate large tsunamis (Løvholt et al., 2017).

The geological record from on- and offshore coastal environments may provide clues to past tsunami events in the lacustrine and marine realms. Examination of their signatures can help to reconstruct tsunami magnitude and recurrence rates at locations with limited historical records, but also extend the knowledge gap into the prehistoric period (e.g., Monecke et al., 2008; Kempf et al., 2017). However, the identification of lacustrine tsunami deposits is less well investigated compared to their marine counterparts. Nevertheless, tsunami deposits could provide the finale evidence for the concept of prehistoric tsunami events in Swiss lakes, which have been suspected from the mass-movement event stratigraphy (e.g., Schnellmann et al., 2006; Kremer et al., 2015; Reusch, 2016).

2.2 A brief history on the sedimentology of tsunami deposits

Tsunami is the Japanese term for harbor wave and describes the observation of fishermen returning from the open sea to a destroyed harbor without noting a wave at sea. This term was already established in the first publications on post-tsunami surveys (e.g., Shepard et al., 1950; Wright & Mella, 1963). These early studies indicated that tsunami inundation can erode and redistribute large amounts of coastal sediment and is capable of transporting coral debris, boulders, and sand for large distances inland (e.g., Shepard et al., 1950). However, the geological record of past tsunami events has only been recognized since the late 1980's (Bourgeois, 2009). For example, Atwater (1987) identified event deposits of anomalous sheets of sand and intertidal mud buried in well-vegetated lowlands in westernmost Washington State and associated the sand sheets to prehistoric tsunamigenic earthquakes from the Cascadia subduction zone, while the intertidal mud deposits were associated with rapid tectonic subsidence on the coast by earthquakes. At the same time, Dawson et al. (1988) identified and described a lateral continuous sandy event deposit with intraclasts of the embedding organic-rich peat-like coastal deposits in eastern Scotland. This deposit, together with a suite of later studies (e.g., coastal lake tsunami deposits in Norway (Bondevik et al., 1997; 2012, Bondevik, 2003), North Sea continental shelf "Doggerland" (Weninger et al., 2008)), related the event deposits to the prehistoric Storegga subaqueous mass movement-generated tsunami around 8150 years BP (Dawson et al., 2020).

The devastating 2004 Indian Ocean tsunami greatly amplified the study of event deposits from past tsunamis. Since then, a large number of publications have appeared examining the sedimentological signatures of tsunami deposits. This has led to a growing research field in sedimentology that uses both established and newly developed methods to shed light on the hidden history of past tsunami events worldwide. In summary, these multi-proxy approaches comprise sedimentological (particle-size distribution (e.g., Jaffe et al., 2003), textural analysis with X-ray tomography (e.g., Falvard and Paris, 2017; Kempf et al., 2017), geochemical elemental concentration (e.g., Judd et al., 2017), dating method (e.g., radiocarbon, U-Th, Cs activity profile, optically stimulated luminesce dating) (Ishizawa et al., 2020), biological species assemblages (e.g., diatoms (e.g., Dawson, 2007; Dura et al., 2016), foraminifera (e.g., Quintela et al., 2016; Uchida et al., 2010), and ancient sedimentary DNA (Szczuciński et al., 2016) analysis.

Due to the large number of case studies that investigated the sedimentary signatures of tsunami deposits, models for the texture of tsunami deposits have been proposed. The most commonly observed signatures are listed here:

- Sharp to erosive basal contact (e.g., Srinivasalu et al., 2009)
- Fining upward (e.g., Gelfenbaum & Jaffe, 2003)
- Landward fining and thinning (e.g., Srinivasalu et al., 2009)
- Intraclasts, also referred to rip-up clasts of reworked pre-tsunami deposits (e.g., Srisutam & Wagner, 2010)
- Distinc laminae of fines (e.g., Richmond et al. 2006)
- Geochemical signatures of seawater inundation: increased elemental concentrations of Na, S, Cl, Ca, Sr, Ba, and Mg (e.g., Szczuciński et al. 2006)

However, clear differentiation from storm-induced event deposits remains challenging (Engel and Brückner, 2011) as they have similar sedimentary characteristics.

Although a large number of publications have focused on the sedimentological signatures of tsunami deposits and post-tsunami surveys, primarily in marine settings, the processes involved in the lacustrine settings remain undeveloped. Few studies document the sedimentological signatures of past lacustrine tsunamis. For example, subaqueous boulder deposits and eroded shore terraces are attributed to a prehistoric lake tsunami by subaqueous landslides in Lake Tahoe (USA; Moore et al., 2014). Shore erosion and damage to trees were observed following the subaerial landslide-generated impulse wave at Lake Chehalis (Canada) in 2007 (Roberts et al., 2007). Nevertheless, the majority of tsunami deposits and post-tsunami surveys concern oceanic settings, and the associated processes are immaturely developed in the lacustrine setting. Therefore, documentation and investigation of lacustrine tsunami deposits is necessary.

2.3 Research motivation

Due to the immense growth of the tourism sector, coastal population and infrastructure, Swiss lakeshore communities must consider the lacustrine tsunami hazard from the adjacent lake. For example, Lake Lucerne and its shore areas are heavily used for recreational activities, especially during summer. Private motor- and sailboats gather on the lake and people sunbathe on the shores, play volleyball, or cool off with a swim in the lake. In addition, many people use

public transportation provided by shipping companies to experience the spectacular landscape on a trip on a historic steamboat, or they simple use it for their daily commute. In the case of a tsunami event, these people would be directly at risk and the warning time is particularly short. Moreover, coastal infrastructures may be severely damaged and the economic and reputational losses may be great, yet to be better estimated.

2.4 Objective of the thesis

This dissertation was carried out within the framework of the SNSF Sinergia project "Lake Tsunamis: Causes, Controls and Hazard". The driving research questions that accompanied the WP paleo that was carried out within this PhD studies can be formulated as follows:

- What are the sedimentological characteristics of lacustrine tsunami deposits?
- How do lake tsunami deposits differ from the better investigated ocean tsunami deposits?
- Are there geological records in the on– and offshore coastal environment of Swiss lakes that provide tsunami deposit-based event chronology over the past 15'000 years?
- How do reconstructed field-derived run-up and inundation models compare with numerical tsunami simulations?

2.5 Methodology

This work combines several different methodological approaches to address the research questions abovementioned. In particular, it uses historical documents, numerical tsunami simulations, and sediment core analysis. Historical documents (historical chronicles, artwork and photographs, and newspaper articles) were used to characterize described coastal damage from tsunami inundation to get an idea on potential sedimentological traces that may be preserved in the geological record. Numerical simulations were used to identify areas susceptible to tsunami inundation. High-resolution bathymetry and topography were used to identify the sedimentary archive of past tsunami events. In addition, the potential for erosion in the coastal offshore areas due to tsunami waves was investigated with numerical simulations of bed shear-stress. Various coring techniques (Gauge auger sediment corer, Geoprobe hydraulic coring, hammer bob-corer and piston coring) were used to recover sediment cores from the on- and offshore coastal environment. These sediment cores were analyzed with a

multitude of sediment core analyses using full core scanning techniques (multi-sensor core logger (MSCL), computed tomography (CT), and X-ray fluorescence (XRF) core scanner) and analysis on discrete samples (particle size, elemental composition, and smear slides). Dating of event deposits was performed on terrestrial organic macro-remains (e.g., leave fragments and conifer needles) with the radiocarbon dating method using accelerator mass spectrometry (AMS). The spatial extend of observed tsunami deposits was, where possible, reconstructed using seismic reflection data.

References

Atwater, B. F. (1987) Evidence for great Holocene earthquakes along the outer coast of Washington State. Science, 236(4804), 942-944.

Bechle, A. J., Wu, C. H., Kristovich, D. A., Anderson, E. J., Schwab, D. J., & Rabinovich, A. B. (2016). Meteotsunamis in the laurentian great lakes. Scientific reports, 6, 37832.

Bondevik, S. (2003) Storegga tsunami sand in peat below the Tapes beach ridge at Harøy, western Norway, and its possible relation to an early Stone Age settlement. Boreas, 32(3), 476-483.

Bondevik, S., Stormo, S. K., & Skjerdal, G. (2012) Green mosses date the Storegga tsunami to the chilliest decades of the 8.2 ka cold event. Quaternary Science Reviews, 45, 1-6.

Bondevik, S., Svendsen, J. I., Johnsen, G., Mangerud, J. A. N., & Kaland, P. E. (1997) The Storegga tsunami along the Norwegian coast, its age and run up. Boreas, 26(1), 29-53.

Bornhold, B. D., & Thomson, R. E. (2012) Tsunami hazard assessment related to slope failures in coastal waters. Landslides–Types, Mechanisms and Modeling, edited by: Clague, JJ and Stead, D., Cambridge University Press, 108-120.

Bourgeois, J. (2009) Geologic effects and records of tsunamis. The sea, 15, 53-91.

Brill, D., May, S. M., Engel, M., Reyes, M., Pint, A., Opitz, S., ... & Brückner, H. (2016) Typhoon Haiyan's sedimentary record in coastal environments of the Philippines and its palaeotempestological implications. Natural Hazards and Earth System Sciences, 16(12), 2799-2822.

Bryant, E. (2014) Tsunami: the underrated hazard. Springer.

Bussmann, F., & Anselmetti, F. S. (2010) Rossberg landslide history and flood chronology as recorded in Lake Lauerz sediments (Central Switzerland). Swiss Journal of geosciences, 103(1), 43-59.

Chagué-Goff, C. (2010) Chemical signatures of palaeotsunamis: a forgotten proxy?. Marine Geology, 271(1-2), 67-71.

Dawson, S. (2007) Diatom biostratigraphy of tsunami deposits: examples from the 1998 Papua New Guinea tsunami. Sedimentary Geology, 200(3-4), 328-335.

Dawson, A. G., and Shi, S. (2000) Tsunami Deposits. Pure Appl. Geophys. 157, 875–897.

Dawson, A. G., Dawson, S., Bondevik, S., Costa, P. J., Hill, J., & Stewart, I. (2020) Reconciling Storegga tsunami sedimentation patterns with modelled wave heights: A discussion from the Shetland Isles field laboratory. Sedimentology, 67(3), 1344-1353.

Dawson, A. G., Long, D., & Smith, D. E. (1988) The Storegga slides: evidence from eastern Scotland for a possible tsunami. Marine geology, 82(3-4), 271-276.

Dura, T., Hemphill-Haley, E., Sawai, Y., & Horton, B. P. (2016) The application of diatoms to reconstruct the history of subduction zone earthquakes and tsunamis. Earth-Science Reviews, 152, 181-197.

Engel, M., & Brückner, H. (2011) The identification of palaeo-tsunami deposits–a major challenge in coastal sedimentary research. Coastline Reports, 17, 65-80.

Einsele, G., Chough, S. K., & Shiki, T. (1996) Depositional events and their records—an introduction. Sedimentary Geology, 104(1-4), 1-9.

Evers, F. M., Heller, V., Fuchs, H., Hager, W. H., and Boes, R. M. (2019) Landslide-generated Impulse Waves in Reservoirs: Basics and Computation. VAW-Mitteilung. ed. R. M. Boes Zürich: Versuchsanstalt für Wasserbau, Hydrologie und Glaziologie (VAW), ETH Zürich.

Falvard, S., & Paris, R. (2017) X-ray tomography of tsunami deposits: Towards a new depositional model of tsunami deposits. Sedimentology, 64(2), 453-477.

Fritz, H. M., Blount, C., Sokoloski, R., Singleton, J., Fuggle, A., McAdoo, B. G., ... & Tate, B. (2007) Hurricane Katrina storm surge distribution and field observations on the Mississippi Barrier Islands. Estuarine, Coastal and Shelf Science, 74(1-2), 12-20.

Fritz, H. M., Mohammed, F., & Yoo, J. (2009) Lituya bay landslide impact generated mega-tsunami 50 th anniversary. In Tsunami Science Four Years after the 2004 Indian Ocean Tsunami (pp. 153-175). Birkhäuser Basel.

Gelfenbaum, G., & Jaffe, B. (2003) Erosion and sedimentation from the 17 July, 1998 Papua New Guinea tsunami. Pure and Applied Geophysics, 160(10-11), 1969-1999.

Hilbe, M., & Anselmetti, F. S. (2015) Mass movement-induced tsunami hazard on perialpine Lake Lucerne (Switzerland): scenarios and numerical experiments. Pure and Applied Geophysics, 172(2), 545-568.

Ishizawa, T., Goto, K., Yokoyama, Y., & Goff, J. (2020) Dating tsunami deposits: Present knowledge and challenges. Earth-Science Reviews, 200, 102971.

Jaffe, B., Gelfenbaum, G., Rubin, D., Peters, R., Anima, R., Swensson, M., ... & Riega, P. C. (2003) Identification and interpretation of tsunami deposits from the June 23, 2001 Peru tsunami. In Proceedings of the international conference on coastal sediments (p. 13).

Judd, K., Chagué-Goff, C., Goff, J., Gadd, P., Zawadzki, A., & Fierro, D. (2017) Multi-proxy evidence for small historical tsunamis leaving little or no sedimentary record. Marine Geology, 385, 204-215.

Keller, G., Lopez-Oliva, J. G., Stinnesbeck, W., & Adatte, T. (1997). Age, stratigraphy, and deposition of near-K/T siliciclastic deposits in Mexico: Relation to bolide impact? Geological Society of America Bulletin, 109(4), 410-428.

Kempf, P., Moernaut, J., Van Daele, M., Vandoorne, W., Pino, M., Urrutia, R., & De Batist, M. (2017) Coastal lake sediments reveal 5500 years of tsunami history in south central Chile. Quaternary Science Reviews, 161, 99-116.

Kremer, K., Anselmetti, F. S., Evers, F. M., Goff, J., & Nigg, V. (2020) Freshwater (paleo) tsunamis–a review. Earth-science reviews, 103447.

Kremer, K., Hilbe, M., Simpson, G., Decrouy, L., Wildi, W., & Girardclos, S. (2015) Reconstructing 4000 years of mass movement and tsunami history in a deep peri-Alpine lake (Lake Geneva, France-Switzerland). Sedimentology, 62(5), 1305-1327.

Linares, Á., Bechle, A. J., & Wu, C. H. (2016) Characterization and assessment of the meteotsunami hazard in northern Lake Michigan. Journal of Geophysical Research: Oceans, 121(9), 7141-7158.

Løvholt, F., Bondevik, S., Laberg, J. S., Kim, J., & Boylan, N. (2017) Some giant submarine landslides do not produce large tsunamis. Geophysical Research Letters, 44(16), 8463-8472.

Monecke, K., Finger, W., Klarer, D., Kongko, W., McAdoo, B. G., Moore, A. L., & Sudrajat, S. U. (2008) A 1,000-year sediment record of tsunami recurrence in northern Sumatra. Nature, 455(7217), 1232-1234.

Monserrat, S., Vilibić, I., & Rabinovich, A. B. (2006) Meteotsunamis: atmospherically induced destructive ocean waves in the tsunami frequency band. Natural hazards and earth system sciences, 6(6), 1035-1051.

Moore, J. G., Schweickert, R. A., & Kitts, C. A. (2014) Tsunami-generated sediment wave channels at Lake Tahoe, California-Nevada, USA. Geosphere, 10(4), 757-768.

Nakahara, S., & Ichikawa, M. (2013) Mortality in the 2011 tsunami in Japan. Journal of epidemiology, JE20120114.

Nandasena, N. A. K., Tanaka, N., Sasaki, Y., & Osada, M. (2013) Boulder transport by the 2011 Great East Japan tsunami: Comprehensive field observations and whither model predictions? Marine Geology, 346, 292-309.

Nicholls, R. J., & Small, C. (2002) Improved estimates of coastal population and exposure to hazards released. Eos, Transactions American Geophysical Union, 83(28), 301-305.

Nigg, V., Krermer, K., Girardclos, S., & Anselmetti, F. S. (in prep.) Sedimentological signatures of historic tsunamis in Swiss lakes.

Nomitsu, T. (1935) A Theory of Tunamis and Seiches produced by Wind and Barometric Gradient. Memoirs of the College of Science, Kyoto Imperial University. Series A, 18(4), 201-214.

Papadopoulos, G. A., & Kortekaas, S. (2003) Characteristics of landslide generated tsunamis from observational data. In Submarine mass movements and their consequences (pp. 367-374). Springer, Dordrecht.

Pattiaratchi, C. B., & Wijeratne, E. M. S. (2015) Are meteotsunamis an underrated hazard? Philosophical Transactions of the Royal Society A: Mathematical, Physical and Engineering Sciences, 373(2053), 20140377.

Quintela, M., Costa, P. J., Fatela, F., Drago, T., Hoska, N., Andrade, C., & Freitas, M. C. (2016) The AD 1755 tsunami deposits onshore and offshore of Algarve (south Portugal): sediment transport interpretations based on the study of Foraminifera assemblages. Quaternary international, 408, 123-138.

Reusch, A. M. (2016) Sublacustrine paleoseismology and fluid flow in the Western Swiss Molasse Basin: New constraints from the sedimentary archive of Lake Neuchâtel-Mass-transport deposits, subsurface sediment mobilization and geomorphology (Doctoral dissertation, ETH Zurich).

Richmond, B. M., Jaffe, B. E., Gelfenbaum, G., & Morton, R. A. (2006) Geologic impacts of the 2004 Indian Ocean tsunami on Indonesia, Sri Lanka, and the Maldives. Zeitschrift für Geomorphologie, 146, 235-251.

Roberts, N. J., McKillop, R. J., Lawrence, M. S., Psutka, J. F., Clague, J. J., Brideau, M. A., & Ward, B. C. (2013) Impacts of the 2007 landslide-generated tsunami in Chehalis Lake, Canada. In Landslide science and practice (pp. 133-140). Springer, Berlin, Heidelberg.

Robertson, I. N., Riggs, H. R., Yim, S. C., & Young, Y. L. (2007) Lessons from Hurricane Katrina storm surge on bridges and buildings. Journal of Waterway, Port, Coastal, and Ocean Engineering, 133(6), 463-483.

Röbke, B. R., & Vött, A. (2017). The tsunami phenomenon. Prog. Oceanogr. 159, 296–322.

Sallenger Jr, A. H., List, J. H., Gelfenbaum, G., Stumpf, R. P., & Hansen, M. (1995) Large wave at Daytona Beach, Florida, explained as a squall-line surge. Journal of Coastal Research, 1383-1388.

Satake, K. (2014) Advances in earthquake and tsunami sciences and disaster risk reduction since the 2004 Indian ocean tsunami. Geoscience Letters, 1(1), 15.

Scheffers, A. (2008) Tsunami boulder deposits. In Tsunamiites (pp. 299-317). Elsevier.

Schnellmann, M., Anselmetti, F. S., Giardini, D., & Mckenzie, J. A. (2006). 15,000 Years of mass-movement history in Lake Lucerne: Implications for seismic and tsunami hazards. Eclogae Geologicae Helvetiae, 99(3), 409-428.

Shepard, F. P., & Inman, D. L. (1950) Nearshore water circulation related to bottom topography and wave refraction. Eos, Transactions American Geophysical Union, 31(2), 196-212.

Shi, L., Olabarrieta, M., Nolan, D. S., & Warner, J. C. (2020) Tropical cyclone rainbands can trigger meteotsunamis. Nature communications, 11(1), 1-14.

Srinivasalu, S., Rao, N. R., Thangadurai, N., Jonathan, M. P., Roy, P. D., Mohan, V. R., & Saravanan, P. (2009) Characteristics of 2004 tsunami deposits of the northern Tamil Nadu coast, southeastern India. Boletín de la Sociedad Geológica Mexicana, 61(1), 111-118.

Srisutam, C., & Wagner, J. F. (2010) Tsunami sediment characteristics at the Thai Andaman coast. Pure and Applied Geophysics, 167(3), 215-232.

Synolakis, C. E., & Bernard, E. N. (2006) Tsunami science before and beyond Boxing Day 2004. Philos. Trans. R. Soc. A Math. Phys. Eng. Sci. 364, 2231–2265.

Szczuciński, W., Chaimanee, N., Niedzielski, P., Rachlewicz, G., Saisuttichai, D., Tepsuwan, T., ... & Siepak, J. (2006) Environmental and Geological Impacts of the 26 December 2004 Tsunami in Coastal Zone of Thailand--Overview of Short and Long-Term Effects. Polish Journal of Environmental Studies, 15(5).

Szczuciński, W., Pawłowska, J., Lejzerowicz, F., Nishimura, Y., Kokociński, M., Majewski, W., ... & Pawlowski, J. (2016). Ancient sedimentary DNA reveals past tsunami deposits. Marine Geology, 381, 29-33.

Tappin, D. R., Watts, P., McMurtry, G. M., Lafoy, Y., & Matsumoto, T. (2001) The Sissano, Papua New Guinea tsunami of July 1998—offshore evidence on the source mechanism. Marine Geology, 175(1-4), 1-23.

Thompson, J., Renzi, E., Sibley, A., & Tappin, D. R. (2020) UK meteotsunamis: a revision and update on events and their frequency. Weather.

Uchida, J. I., Fujiwara, O., Hasegawa, S., & Kamataki, T. (2010) Sources and depositional processes of tsunami deposits: Analysis using foraminiferal tests and hydrodynamic verification. Island Arc, 19(3), 427-442.

Weninger, B., Schulting, R., Bradtmöller, M., Clare, L., Collard, M., Edinborough, K., ... & Wagner, B. (2008) The catastrophic final flooding of Doggerland by the Storegga Slide tsunami. Documenta Praehistorica, 35, 1-24.

Wright, C., & Mella, A. (1963) Modifications to the soil pattern of South-Central Chile resulting from seismic and associated phenomenona during the period May to August 1960. Bulletin of the Seismological Society of America, 53(6), 1367-1402.

Historic painting by *Franz-Xaver Triner* shows the impact of the September 2, 1806 CE Rossberg landslide-generated impulse wave on Lake Lauerz, Switzerland with Mount Rigi (left) and Rossberg (right) in the distance (Swiss National Library).

3 Sedimentological signatures of historic tsunamis in Swiss lakes

Valentin Nigg [1 *], Katrina Kremer [1,2], Stéphanie Girardclos [3], Flavio S. Anselmetti [1]

[1] Institute of Geological Sciences & Oeschger Centre for Climate Change Research, University of Bern, Baltzerstrasse 1+3, 3012 Bern, Switzerland
[2] Swiss Seismological Service, ETH Zurich, Sonneggstrasse 5, 8092 Zürich, Switzerland
[3] Department of Earth Sciences and Institute of Environmental Science, University of Geneva, Rue des Maraîchers 13, 1205 Geneva, Switzerland

Abstract

Strong regional earthquakes can generate subaqueous mass movements in lakes. The displacement of the water column caused by the failure may be tsunamigenic, depending on mass-movement volumes and kinematics. Several lacustrine tsunami events have been historically reported in Switzerland. For example, the 1601 Lake Lucerne tsunami, which was caused by a magnitude Mw 5.9 earthquake. The historically documented tsunami wave height and run-up of the event have been well reconstructed in previous studies using numerical mass-movement and simulations of tsunami propagation. However, the geological record of past tsunami events in the onshore and coastal offshore environments have not been systematically investigated to date, even though these deposits could provide detailed insights into prehistoric mass movement-generated tsunami hazard and its recurrence rate. Here, we present a site-selection workflow based on historical documents and maps, geomorphological criteria, and numerical tsunami simulations to conduct site-specific field investigations to recover sediment cores from different coastal environments. Observed sedimentary signatures caused by past tsunamis in three Swiss lakes are discussed, together with observed negative evidence for tsunami deposits. The workflow presented can be applied to future studies of prehistoric and historic tsunami deposits in other lakes as well as in the marine environment.

3.1 Introduction

Lake tsunamis represent a low-recurrence rate hazard that can be generated by various triggering mechanisms, including plate displacements, subaerial and subaqueous landslides, rockfall impacts, volcanic eruptions, and air-pressure disturbances generating meteotsunamis (Kremer et al., 2020a and references therein). These events can have catastrophic effects on coastal communities and infrastructure due to shore erosion and high-energy flooding (e.g., Bryant, 2014). The characterization of lacustrine tsunami hazard, however, may be only sparsely accessible through historically reported (e.g., 1858 Common Era (CE) Lake Patzcuaro, Mexico (Garduno-Munroy et al., 2011); 1861/1862 CE Lake Baikal, Russia (Klyuchevskii et al., 2012); 1846 and 1910 CE Lake Taupo, New Zealand (Clark et al. 2015); 1905 and 1936 CE Lake Leon, Norway (Grimstad and Nesdal, 1991)) and a few recent, post-2000, lacustrine tsunami events (e.g., 2001 Lake Coatepeque, El Salvador (Gusiakov, 2009); 2007 CE Lake Chehalis, Canada (Roberts et al., 2013); 2014 Lake Askja, Alaska, USA (Gylfadóttir et al., 2017)). Because the historical record of lake tsunamis is too short to understand the full range of associated hazards, the geological record of tsunami deposits can provide useful information on the magnitude (e.g., tsunami run-up height, flow depth and inundation distance) and their recurrence rates for events that occurred also in the prehistorical period or in remote areas (e.g., Kempf et al. 2017; Monecke et al., 2008).

Tsunami deposits are the sedimentary traces of past tsunami events that are preserved in the geological record through time (e.g., Einsele et al., 1996; Dawson and Shi, 2000). They have been investigated at various coastal marine locations. As a result of the devastating 2004 Indian Ocean and 2011 Tohuku-Oki tsunami, numerous publications document the characteristics and spatial distribution of marine tsunamis deposits (e.g., Goto et al., 2011; Jaffe et al., 2012; Szczuciński et al., 2012) and their post-depositional alteration (e.g., Spiske et al., 2020). These signatures, studied from the sedimentary archive, may provide insights into inundation distance (e.g., Abe et al., 2012; Ishimura et al., 2019; Switzer et al., 2012), run-up height (e.g., Bondevik et al., 1997), number of inundation pulses (e.g., Richmond et al., 2006; Szczuciński et al. 2006), as well as the recurrence rate (e.g., Kempf et al. 2017; Monecke et al., 2008), all of which defining the magnitude of past tsunami events (e.g., Papadopoulos & Imamura, 2001). However, their lacustrine counterpart has not yet been adequately investigated (Kremer et al., 2020a).

Lacustrine tsunami events have been historically reported from several lakes in Switzerland. For example, in Lake Geneva (563 and 1584 CE: Kremer et al., 2012, 2015), Lake Lucerne (1601 and 1687 CE: Hilbe & Anselmetti, 2015), Lake Lauerz (1806 CE Goldau landslide: Bussmann & Anselmetti, 2010) and numerous locally confined impulse waves from subaerial mass-movement impacts (Huber, 1982). These tsunami events were caused by seismically triggered subaqueous mass movements (Hilbe & Anselmetti, 2015; Kremer et al., 2015;), delta failures (Girardclos et al., 2007; Hilbe & Anselmetti, 2015; Nigg et al., 2021) and subaerial mass-movements (Bussmann & Anselmetti, 2010), as well as rock mining at the lakeshores (Fuchs and Boes, 2010; Huber, 1982). Tsunami events that occurred in Swiss lakes prior to the historical record have been postulated from the mass-movement event stratigraphy observed in deep lake basins (e.g., Schnellmann et al. 2006; Kremer et al. 2015) as well as on- and offshore tsunami deposits (Nigg et al., 2021) However, subaqueous triggering mechanism of tsunamigenic mass movement is strongly controlled by mass-movement dynamics and kinematics (Løvholt et al., 2017). However, this information is difficult to access for prehistoric and events in remote areas where tsunami reports do not exist. Therefore, definitive evidence for these postulated prehistoric tsunami events is absent but may be achieved through the careful investigation of the on- and offshore sediment records that have preserved the sedimentological signatures of past tsunami inundation and backwash.

Careful site selection for geological investigations is fundamental to the scientific questions addressed in various research studies. However, there are no universally applicable criteria. Moreover, it is plausible that the criteria used depends on the scientific questions and the environment in which the study is conducted. Therefore, we developed a comprehensive site-selection workflow to obtain sedimentological signatures of past tsunami events preserved in the geological record. The workflow performed, and the criteria and data used are documented in this study. To achieve the goal of reconstruction of coastal impact and deposits from historic tsunamis, detailed analysis of historical documents of lake tsunamis in Switzerland are combined with sedimentary multiproxy analysis on recovered sediment cores from the coastal on- and offshore environment during several field campaigns. These results provide insights into the associated hazard of lake tsunamis generated by subaerial and subaqueous mass movements, but also highlight observed limitations and difficulties. Finally, we document the established workflow to provide guidelines for future investigations to localize promising sediment archives to study lacustrine tsunami deposits.

3.2 Study sites

Switzerland is characterized by moderate seismicity (e.g., Deichmann et al., 2000; Wiemer et al., 2009), with certain areas being more seismically active with more frequent strong earthquakes with moment magnitudes up to Mw 6 and larger in the historic period (e.g., Fäh et al., 2011; Gisler et al., 2004). From the historical record of earthquake damage, a total of 28 events with a magnitude Mw ≥ 5.5 are known over the last 800 years (Wiemer et al., 2009). The highest seismic activity is observed in the southwest and northwest of Switzerland in the region of Valais and Basel, respectively (Wiemer et al., 2009; Kremer et al., 2020b). In general, Mw 6 earthquakes are expected to occur in Switzerland every 50 to 150 years, while Mw 7 earthquakes occur approximately every 1000 years (Wiemer et al., 2016). Strong prehistoric earthquakes have been recorded in the sedimentary archive in the deep basin of large Swiss lakes from subaqueous mass-movement deposits (e.g., Kremer et al., 2015; Monecke et al., 2006; Schnellmann et al., 2006; Siegenthaler et al., 1987; Strasser et al., 2013) and earthquake-related deformation structures (Monecke et al., 2006). Kremer et al. (2017) found increased subaqueous mass-movement deposits at ~2200 Before Present (BP), ~3300 BP, ~6500 BP, and ~9700 BP in several Swiss lakes, providing evidence for repeated strong earthquakes (Mw ≥ 6) in Switzerland. These large prehistoric subaqueous mass-movement deposits with volumes in the range of 10^6 to 10^8 m^3 are likely tsunamigenic (Hilbe and Anselmetti, 2015; Kremer et al., 2014; Mountjoy et al., 2019; Nigg et al., 2021; Schnellmann et al., 2006; Strupler et al., 2018).

Lake tsunamis generated from subaqueous mass movements were reported from Swiss lakes in the historical period in Lake Lucerne (1601 and 1687 CE (Hilbe and Anselmetti, 2015)) and Lake Geneva (563 CE (Kremer et al., 2012) and 1584 CE (Fritsche et al., 2012; Kremer et al., 2015; Schwarz-Zanetti et al., 2018)). Additionally, subaerial mass movements have generated impulse waves with shore erosion at Lake Lucerne (e.g., 1963, 1964, and 2007 CE (Fuchs and Boes, 2010; Huber, 1982), Lake Walen (1924 and 1946 CE (Huber, 1982), and Lake Lauerz (1806 CE Rossberg landslide (Bussmann and Anselmetti, 2010)). For the localization and characterization of lake tsunami sedimentary signatures, Lake Lucerne, Lake Geneva, and Lake Sils were selected for further investigations among the several lakes with historical tsunami reports and extensive mass-movement deposits (Fig. 3-1 and Table 3-1).

Table 3-1: Historical reported tsunamis and large seismically imaged mass-movement deposits in Swiss lakes.

Index	Name	Mass-movement event stratigraphy	Numerical tsunami simulation	Largest historical reported tsunami (yr. CE)	Reported run-up (m)	Tsunami triggering mechanism
1	Lake Geneva	Kremer et al., 2015	Kremer et al., 2012	563	8–9	Subaqueous delta collapse
2	Lake Brienz	Girardclos et al. 2007; Haas et al., in prep.		1996	Greatly fluctuating lake level	Subaqueous delta collapse
3	Lake Lucerne	Schnellmann et al., 2006	Hilbe and Anselmetti, 2015	1601	3–4	Subaqueous mass movement
4	Lake Lauerz	Bussman and Anselmetti, 2010		1806	~15	Subaerial landslide shockwave
5	Lake Zug			1435	< 1	Shore collapse
6	Lake Walen	Zimmermann, 2008		1924	8–9	Rockslide impact
7	Lake Constance	Schwestermann, 2016		1720	Unusual wave action	
8	Lake Davos			1923	3	Subaqueous slope collapse
9	Lake Oeschinen	Knapp et al., 2018		1846	Lake outburst flood	Rockfall impact
10	Lake Thun	Wirth, 2008				
11	Lake Neuchatel	Reusch, 2016				
12	Lake Zurich	Strasser et al., 2013	Strupler et al., 2018			
13	Lake Sils	Blass et al., 2005	Nigg et al., 2021			
14	Lake Silvaplana	Bellwald, 2012				

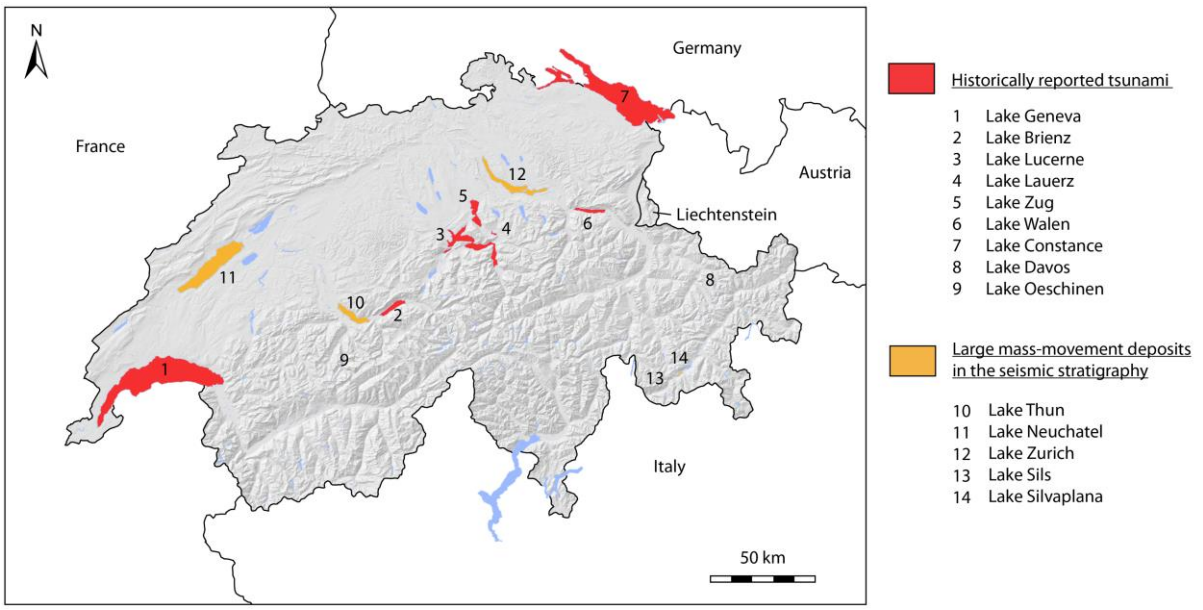

Fig. 3-1: Map of Switzerland (SwissAlti3D modified from swisstopo) shows Swiss lakes with historically reported tsunami events (red-colored lakes) and large, potentially tsunamigenic, mass-movement deposits in the deep basin (yellow-colored lakes). Note that Lake Geneva, Lake Lucerne, Lake Constance, and Lake Walen also have extended, potentially tsunamigenic mass-movement deposits within its seismic-stratigraphic event record (see Table 3-1 for further information).

3.3 Methods

For the localization of tsunami deposits in the coastal on- and offshore environment, a geomorphological database was compiled for selected lakes (Fig. 3-2). Based on the classification of the coastal areas, study sites were carefully chosen with a high potential for tsunami inundation, sediment deposition, and the preservation of its sedimentary signatures. Sediment cores were then recovered with different coring techniques and further sedimentologically investigated in the laboratory (Table 3-2).

3.3.1 Site-selection pathway

Site selection for the identification of lacustrine tsunami deposit in the geological record is crucial but complex. We use historical documents describing the coastal impact of lacustrine tsunami events in Swiss lakes, tsunami-inundation maps computed with numerical tsunami simulations from previous publications, and land-use classification applied on geomorphological maps (Fig. 3-2). Finally, a classification of the coastal areas was created to identify zones with high potential for deposition, preservation, and identification of tsunami-related sedimentary signatures.

Lake selection

Historical tsunami accounts, mass-movement event stratigraphy, and available numerical tsunami simulations are the main criteria applied for lake selection (Fig. 3-2): Historical documents (historical manuscripts, paintings, newspaper articles and photographs) analyzed in this study provide useful information on tsunami triggering mechanisms (seismic or aseismic subaerial and/or subaqueous mass movement(s)) and magnitude (flow depth, run-up, and inundation distance) of lacustrine tsunami events in Swiss lakes (Table 3-3). These documents provide a better understanding of the coastal impacts (e.g., shore erosion, tsunami related sediment deposition) from tsunami inundation and backwash. Special emphasis was put on historical documents describing tsunami deposits in various coastal domains. Prehistoric tsunami events were postulated from large mass-movement deposits previously imaged by reflection seismic data in deep lake basins. Mass-movement event chronologies based on radiocarbon dating were used for cross-correlation of prehistoric mass-movement deposits with the coastal event deposits (Table 3-1). Numerical tsunami simulations have been computed for several Swiss lakes in previous studies (e.g., Hilbe and Anselmetti, 2015, Kremer et al., 2012; Nigg et al., 2021; Strupler et al., 2018). These data provide information on tsunami inundation distance, flow depth, and run-up height and were used to identifying coastal areas prone to tsunami inundation.

Geomorphologic database

A geomorphological database was compiled for selected lakes using available data of topography, tsunami inundation, historical, and geological maps, as well as borehole logging data (Fig. 3-2). The individual datasets were compiled in the geographic information system software ArcMap (ESRI Inc., version 10.5). The public datasets SwissAlti3D hillshade map, SwissBathy3D bathymetric map, geological map GA25 and historical maps (Dufour, Siegfried and the national map of Switzerland) are provided by swisstopo. For areas on the French territory of Lake Geneva, freely available maps form the French geological survey (Bureau de Recherches Géologiques et Minières: BRGM) were used. Borehole logging data were requested from cantonal authorities and private geotechnical engineering companies. For most requests, these data could be used free of charge. Remote geomorphological characterization of the lakeshores was combined with field surveys and geomorphological mapping in the areas of interests. Based on these data, a land-use classification was created to provide a reasonable pathway for selecting coring sites. These levels include accessibility (e.g., natural protection

areas, ownership, and accessibility costs), land use (e.g., agricultural land, artificial landfill, and forest), and historical development (Fig. 3-2).

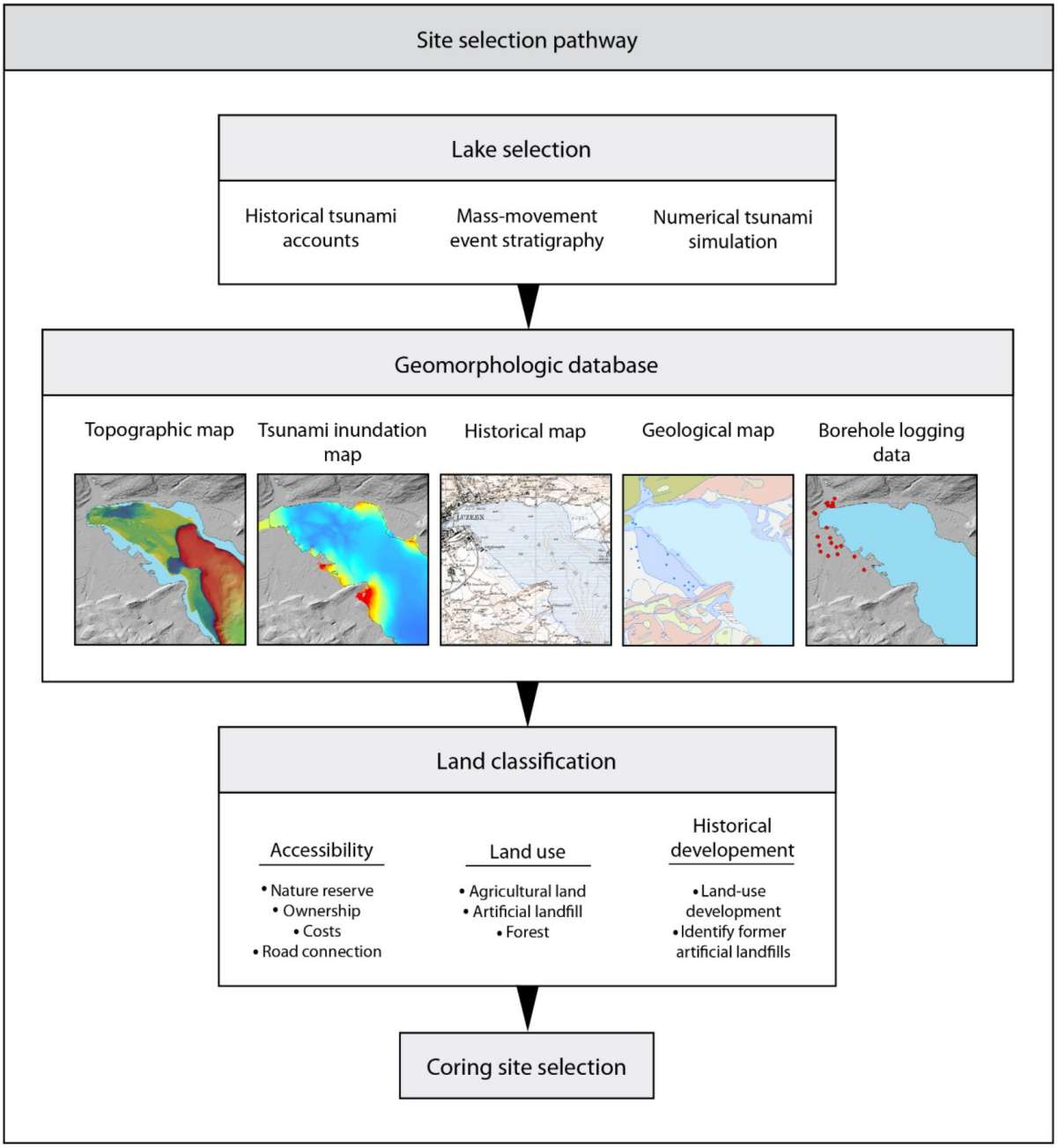

Fig. 3-2: Developed site selection workflow: lake selection criteria, compiled geomorphologic database, and land classification applied used for coring site selection. The data used consists of topographic map (hillshade map SwissAlti3D from swisstopo and Lake Lucerne bathymetric map from Hilbe et al. (2011)), tsunami inundation map of Lake Lucerne (Hilbe and Anselmetti, 2015), historical map (Dufour & Siegfried map from swisstopo), geological map (swisstopo GA25 map), and borehole logging data requested from cantonal authorities and private geotechnical engineering companies.

3.3.4 Sedimentological analysis

Terrestrial sediment cores were recovered up to a depth of 2 m using a Pürckhauer sediment corer. The recovered sediment sections were photographed and transferred to plastic tubes cut in half in the field for further analysis in the laboratory. At terrestrial sites with promising preliminary results, cores were recovered with a hydraulic-coring system (Geoprobe 6620DT; cored in collaboration with EAWAG, ETH Zurich). Short cores were recovered with a hammer-driven sediment corer, long cores (≥ 3 m) with an UWITEC piston-coring system from a floating platform, and a manual percussion-coring system from the frozen lake surface in coastal shallow-water environments. These sediment cores were scanned with a Geotek MSCL-S (Standard Multi Sensor Core Logger) at 5 mm for bulk density and magnetic susceptibility. Full-core computed tomography (CT) scans with a resolution of 100 µm per voxel size were performed with a Siemens Somatom Definition AS X-ray CT scanner at the Institute of Anatomy, University of Bern. CT scan data were analyzed using RadiAnt DICOM Viewer software (version 4.6.9.18463). Micro-CT scans with a resolution of 15 µm per voxel size were obtained from two sediment U-channels (take preferably plastic or carbon material, we used steel, which is problematic due to the low-density contrast to the sediment sample and the high absorption of X-rays) with a multi-scale X-ray nano-CT system (Bruker Skyscan 2211) at the Department of Geosciences University of Fribourg. Data visualization was performed after 3D reconstruction with NRecon software (version 1.6.10.5; Bruker Corporation) with Avizo software (version 9.4.0; Thermo Fisher Scientific). Sediment cores were split in two halves and line-scan images were acquired with the Geotek MSCL-S camera. Macroscopic sedimentological core analysis was performed, and sedimentological units were characterized by sediment color, grain size, diatom-species assemblages, and mineralogical composition. Radiocarbon dating was performed on terrestrial organic macro-remains with the Mini-RadioCarbon-dating System (MICADAS) at ETH Zurich and Department of Chemistry and Biochemistry, University of Bern.

Table 3-2: Investigation methods used to localize and identify the geologic archive for tsunami-related sedimentary signatures in the lacustrine on- and offshore environments.

Investigation method	Aim	Tools
Geomorphological mapping and reconnaissance	Identification of areas with sediment source and archive Investigate land-use change and development	Geographic information system ArcMap Geological maps Topography and bathymetry maps Aerial photographs Historical maps
Tsunami inundation maps	Identify areas with simulated tsunami inundation	Numerical tsunami propagation and inundation simulations
Historical document analysis	Characterization of lacustrine tsunami inundation, destruction, and deposition	Historical chronicles Historical newspaper articles Historical paintings Historical photographs
Sediment coring	Recover of sediment cores in the on- and offshore setting	Pürckhauer gouge auger Geoprobe Hammer-driven corer UWITEC piston corer
Sediment core analysis	Petrophysical core description Correlation of drill cores Sediment analysis Identification of tsunami deposits	MSCL core scanner X-ray tomography core scan X-ray fluorescence core scan Smear slides Particle size analysis
Dating method	Dating of tsunami event related sedimentary structures	Radiocarbon dating of terrestrial macro remains

Table 3-3: Compilation of historical documents consulted and investigated within this study.

Lake	Date (dd-mm-yyyy)	Event	Type of historical document	Reference
Lake Geneva	563 CE	Tauredunum rockfall and Lake Geneva tsunami	Chronicle	Montandon, 1925
			Chronicle	Favrod, 1991
			Chronicle	Schoeneich, 2015
Lake Geneva	11-03-1584	Aigle earthquake and small Lake Geneva tsunami	Collection of historical sources	Egli, 1901-1904
			Collection of historical sources	Reymond, 1917
			collection of historical sources	Schardt, 1892
			Chronicle	du Chesne, 1587
Lake Lucerne	18-09-1601	Unterwalden earthquake-generated subaqueous mass movements	Chronicle	Cysat, 1969
			Chronicle	Frank, 1950
Lake Lucerne	23-09-1687	Muota Delta collapse	Report	Bünti, 1973
			Chronicle	Billeter, 1923
			Chronicle	Dietrich, 1689
Lake Lucerne	27-02-1963	Obermatt quarry rockfall-generated impulse waves	Newspaper article	NZZ, 01-03-1963
	08-08-1964		Newspaper article	NZZ, 10-08-1964
			Newspaper article	NZZ, 13-08-1964
			Photographs	Historical archive Vitznau
Lake Lucerne	20-06-2007	Obermatt quarry rockfall-generated impulse wave	Newspaper article	NZZ, 13-12-2007

3.4 Results

Lake Lucerne, Lake Geneva, and Lake Sils were selected for this study based on historically reported tsunami events, large mass-movement deposits in the deep lake basins, and available numerical tsunami propagation and inundation simulations. The developed coring site selection workflow (Fig. 3-2) was applied to these three lakes with results presented in the following section.

3.4.1 Lake Lucerne

Lake Lucerne (113.6 km^2) is a perialpine fjord-type lake of glacial origin located in central Switzerland at an altitude of 434 m above sea level (a.s.l.; Fig. 3-3). The lake is characterized by seven steep-sided subbasins with flat basins plains that host multiple subaqueous mass-movement deposits. A total of six subaqueous mass-movement seismic horizons haven been attributed to strong regional earthquakes in 1601 CE, ~2200 BP, ~9870 BP, ~11'600 BP, ~13'770 BP, and ~14'590 BP (Schnellmann et al., 2006). But also, less extensive, smaller subaqueous and subaerial mass movements have been described from the seismic-reflection stratigraphy at ~3200 BP, ~3900 BP, ~5400 BP, ~6300 BP, ~8000 BP, and ~9310 BP (Schnellmann et al., 2006). Several historical chronicles report severe tsunami events on Lake Lucerne in 1601 and 1687, respectively (Hilbe and Anselmetti, 2015), as well as locally confined effects from subaerial mass movement-generated impulse waves (Fuchs and Boes, 2010; Huber, 1982). These historical documents were analyzed to characterize the tsunami-related coastal impact on Lake Lucerne. Additionally, numerical tsunami simulations of the historical events 1601 and 1687 CE by Hilbe and Anselmetti (2015) were used to identify areas prone to tsunami inundation.

Historically reported tsunami events on Lake Lucerne

i) 1601 CE Unterwalden earthquake and Lake Lucerne tsunami

The tsunami event of September 18, 1601 CE is documented in the chronicles of Renward Cysat, the Lucerne city clerk and the pastor Businger of Ennetbürgen. The chronicles describe a strong, regionally felt earthquake and a tsunami on Lake Lucerne. It is mentioned that shores have partially collapsed into the lake and coastal plains were inundated by several hundred meters (Cysat, 1969). Further it is documented that trees, boulders, boats, and fish were washed ashore (Cysat, 1969). The alluvial plain at Ennetbürgen was inundated by 800 m with a flow

depth of 2–4 m, so that fruit trees were washed away or partially covered (Businger in Frank, 1950). After the event, an oscillatory movement of the entire lake, a seiche, periodically drained the riverine outflow that continued for several days with decreasing seiche amplitude (Cysat, 1969). Two large (Weggis slide and Gersau basin slide) and several smaller subaqueous mass movements, as well as a rockfall impact, were recognized as the causes of the 1601 CE Lake Lucerne tsunami (Hilbe and Anselmetti, 2015; Schnellmann et al., 2002). Numerical tsunami simulation of the subaqueous Weggis slide (volume: ~11.4 x 10^6 m^3) and Gersau Basin slide (volume: ~20.8 x 10^6 m^3) by Hilbe and Anselmetti (2015) provide results (flow depth, inundation distance) that are in good agreement with the historically documented tsunami inundation distance and run-up height.

ii) 1687 CE Muota Delta collapse-generated Lake Lucerne tsunami

The tsunami event of September 23, 1687 CE was generated by an aseismic collapse of the Muota Delta (Hilbe and Anselmetti, 2015). The inundation and devastation in the village of Brunnen and the northern part of Uri Basin are reported in three independent contemporary chronicles by Bünti (1973), Billeter (1923) and Dietrich (1689). Ships were hurled on top of each other, pieces of wood and debris were washed far into the village of Brunnen, where flow depth (~4 m) reached up to the second floor of buildings near the shore (Bünti, 1973). On the opposite shore, at the guesthouse Treib, the wave knocked over the innkeeper at the entrance and tore away the windows shutters (Bünti, 1973). The jetty and the cheese in the cellar were washed away (Bünti, 1973). Hilbe and Anselmetti (2015) numerically simulated the delta collapse with a volume of 5.5 x 10^6 m^3 that generated a tsunami (flow depth, run-up, and inundation area) which is in good agreement with the historical documentation of the event.

iii) 1963, 1964, and 2007 CE Obermatt quarry rockfall-generated impulse waves

The northern flanks of Mount Bürgenstock is susceptible to generate rockfall-induced impulse waves. A large rockfall occurred during the 1601 CE Lake Lucerne tsunami event (Cysat, 1969). Three smaller, artificially induced rockfalls generated impulse waves in 1963, 1964 and 2007 CE from a nearby quarry ("Obermatt", Fig. 3-3: Fuchs and Boes 2010; Huber, 1982). On February 27, 1963 CE, a rockfall with a volume of ~20'000 m^3 caused 2 fatalities and considerable property damage (Huber, 1982). In addition, the rockfall impact on the lake surface generated an impulse wave with up to 4 m run-up, which locally caused shore erosion (NZZ from 01-03-1963). Another impulse wave was triggered by a rockfall (volume: ~70'000 m^3) on August 8, 1964 CE, probably related to improper blasting days before the event

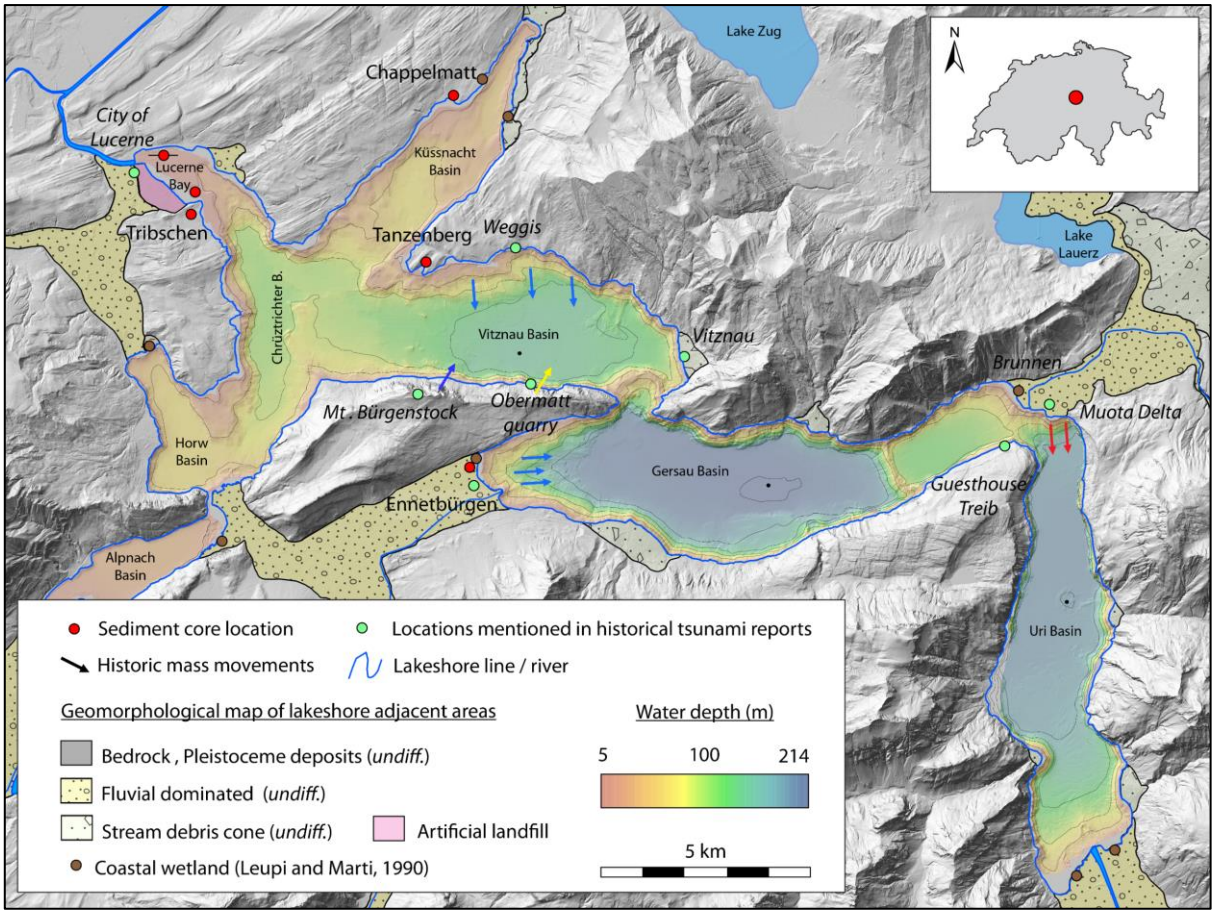

Fig. 3-3: Geomorphological map of Lake Lucerne and its adjacent areas shows locations of recovered sediment cores (red dots), historic mass movements (1601 CE (blue arrows), 1687 CE (red arrows), 1963, 1964, and 2007 CE subaerial rockfalls at the Obermatt quarry (yellow arrows)), mentioned in the historical tsunami reports (green dots), and coastal wetland (modified after Leupi and Marti, 1990; brown dots). Digital terrain model Swiss Alti3D (modified from swisstopo), and bathymetry of Lake Lucerne (modified from Hilbe et al., 2011).

(Huber, 1982). The impulse wave caused considerable damage at the quarry and along the shore at Vitznau and Weggis (ca. 3–4 km across the lake). Several newspaper articles document this event and provide good information on the run-up height and inundation distance of the wave (e.g., NZZ, 10-08-1964). In the quarry, the impulse wave had a run-up height of 20 m, destroyed a transport ship, and drowned several smaller boats. It is further reported that the harbor area in Weggis was first drained (ca. -1.5 m) and then inundated by a wave that approached the shore like a wall (NZZ from 10-08-1964). The few shallow coastal areas were flooded by several tens of meters, and coastal facilities, quay walls as well as about 100 boats were heavily damaged, and some were washed ashore (Fig. 3-4; NZZ from 13-08-1964). The most recent rockfall-generated impulse wave at the Obermatt quarry occurred on June 20, 2007 (Fuchs and Boes, 2010). Although the impulse wave was generated by substantial less rockfall volume (ca. 5'000–8'000 m^3) than in 1963/1964 CE, the wave caused considerable financial

losses and damage to properties, boats, and harbors at the opposite shore (Fuchs and Boes, 2010; NZZ from 13-12-2007).

Fig. 3-4: Photographs documenting the damage and shore erosion (lower left image) caused by a rockfall-generated impulse wave at Weggis in 2.5 km distance on August 8, 1964 CE (photographs: historical archive Vitznau).

Coring sites and its sedimentary records

At Lake Lucerne, sediment cores were recovered at six different locations within the coastal on- and offshore environment. At the four coastal localities Ennetbürgen, Chappelmatt, Tanzenberg, and Tribschen, Pürckhauer sediment cores were recovered (Fig. 3-3). Based on their results further sediment coring was conducted with a hydraulic Geoprobe coring system at Chappelmatt, Tanzenberg, and Tribschen, however, recovery rate was low at with ~40, ~35 and ~55% at Chappelmatt, Tanzenberg, and Tribschen, respectively (Fig. 3-5). In the offshore area of the Lucerne Bay, UWITEC piston cores were recovered along a transect from a coastal depression. Additionally, a solitary 7-m long core was recovered from an amphitheater-like setting in the southeast of the bay. In the following the investigations performed at Chappelmatt

and within the Lucerne Bay are presented below as examples for Lake Lucerne. All core coordinates can be found in the supplementary material (Appendix A).

i) Onshore localities

Ennetbürgen

Historical accounts (Businger in Frank, 1950; Cyat, 1969) and tsunami simulation (Hilbe and Anselmetti, 2015) document that the alluvial plain at Ennetbürgen (Fig. 3-3) was inundated by several hundred meters during the 1601 CE Lake Lucerne tsunami and was also affected by the tsunami generated by the collapse of the Muota Delta (Hilbe and Anselmetti, 2015). We identified a coring site at about 150 to 200 m distant from todays' lakeshore at a pastureland that had not been plowed recently, as reported by the local farmer reported. However, he was not aware of how the field had been farmed in the longer past. Additionally, based on geomorphological classification, the site was characterized as a fluvial floodplain that was repeatedly flooded by the Engelberger Aa (Fig. 3-3). Nevertheless, four Pürckhauer sediment cores were recovered at the site. The recovered sediment successions consist of a dark brown, organic-rich topsoil with poorly sorted gravelly sand in the upper 50 cm. Below this, the organic content gradually decreases and poorly sorted clastic components ranging from silt to medium gravel become more dominant between 50 to 100 cm depth. Color changes from dark brown to grayish brown and gray in the lowermost section. There, water-saturated clayey silt is dominant, and the fraction of gravel and sand is low. Due to this strongly clastic sediment succession observed along the fluvial floodplain at Ennetbürgen, no further cores were recovered with the hydraulic-coring system. Additionally, fluvial floodplains were further considered as poorly suited for the recognition of tsunami-derived clastic material in lacustrine environments.

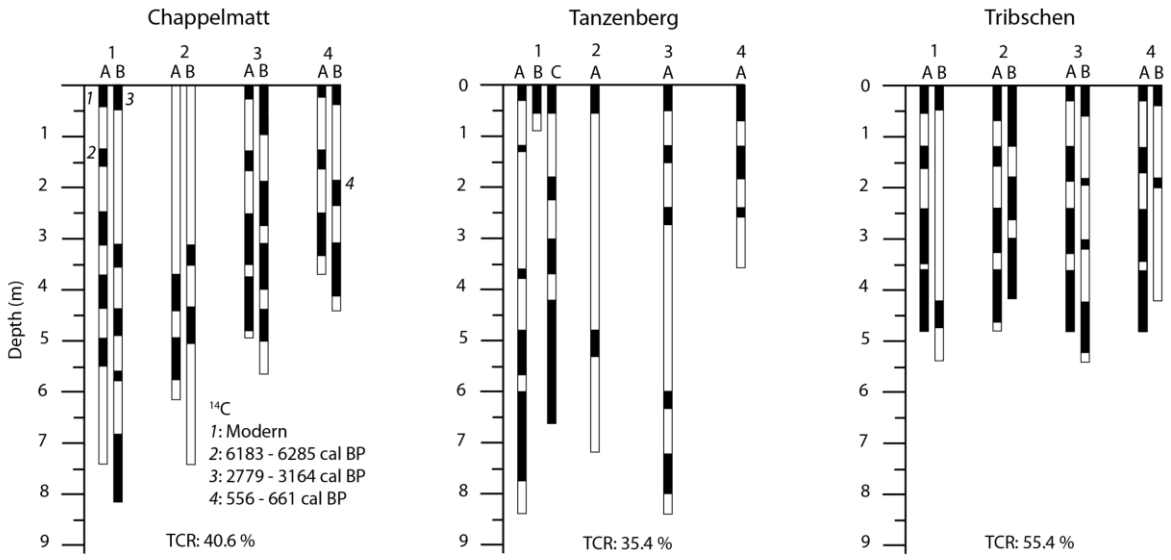

Fig. 3-5: Illustration of recovered sediment core (black) compared to run cored (black outlined rectangle) and total core recovery (TCR) obtained at Chappelmatt (40.6%), Tanzenberg (35.4%), and Tribschen 55.4%) with the hydraulic-coring system, indicates the difficulty of core-to-core correlation with the recovered sediment cores, even though duplicate cores (A and B) were generally taken. Location and calibration of radiocarbon ages performed from recovered sediment cores at Chappelmatt are indicated.

Chappelmatt

The pristine wetland at Chappelmatt (Fig. 3-6), located on the shore of the Küssnacht Basin (Fig. 3-3), was characterized as highly suitable for the recognition of tsunami-derived clastic material due to its organic-rich background sediment and low fluvial impact. Furthermore, since the area was likely inundated during the 1601 CE Lake Lucerne tsunami, as indicated from tsunami simulation (Hilbe and Anselmetti, 2015) and a historical account (Cysat, 1989), it was considered as one of the most promising onshore environments for our study. However, because of the pristine nature of the area and the rarity of these at Lake Lucerne, the area is a nature reserve. Nevertheless, permission for the investigation was granted by the cantonal authorities.

Sediment cores were recovered using a Pürckhauer sediment core and a hydraulic-coring system along a transect 10 to 200 m from the present shoreline (Fig. 3-6). The sedimentological succession consists of well to partly decomposed peat deposits that contains abundant fibrous peat fragments and occasionally detrital-rich sediment deposits the uppermost 1 to 2 m. Towards the lake, organic-rich clayey sediment was found in the lowermost part. In the area farther from the shore, the peat deposits overlies a dense, cohesive faintly laminated to massive

clay with angular gravel-sized clasts and layers of normally graded sand and gravel, which most likely representing Late Glacial (~15 kyr BP) deposits, sharp. Because total core recovery was low (~40.6%), probably due to high compaction of organic-rich units, meaningful core-to-core correlation of the clastic layers observed in the peat deposit was not possible. In addition, difficulties with proper radiocarbon dating of the units (Fig. 3-5; Table 3-4), have led us not to investigate the sedimentary succession further. However, prober coring with a monolith may provide better results in the future.

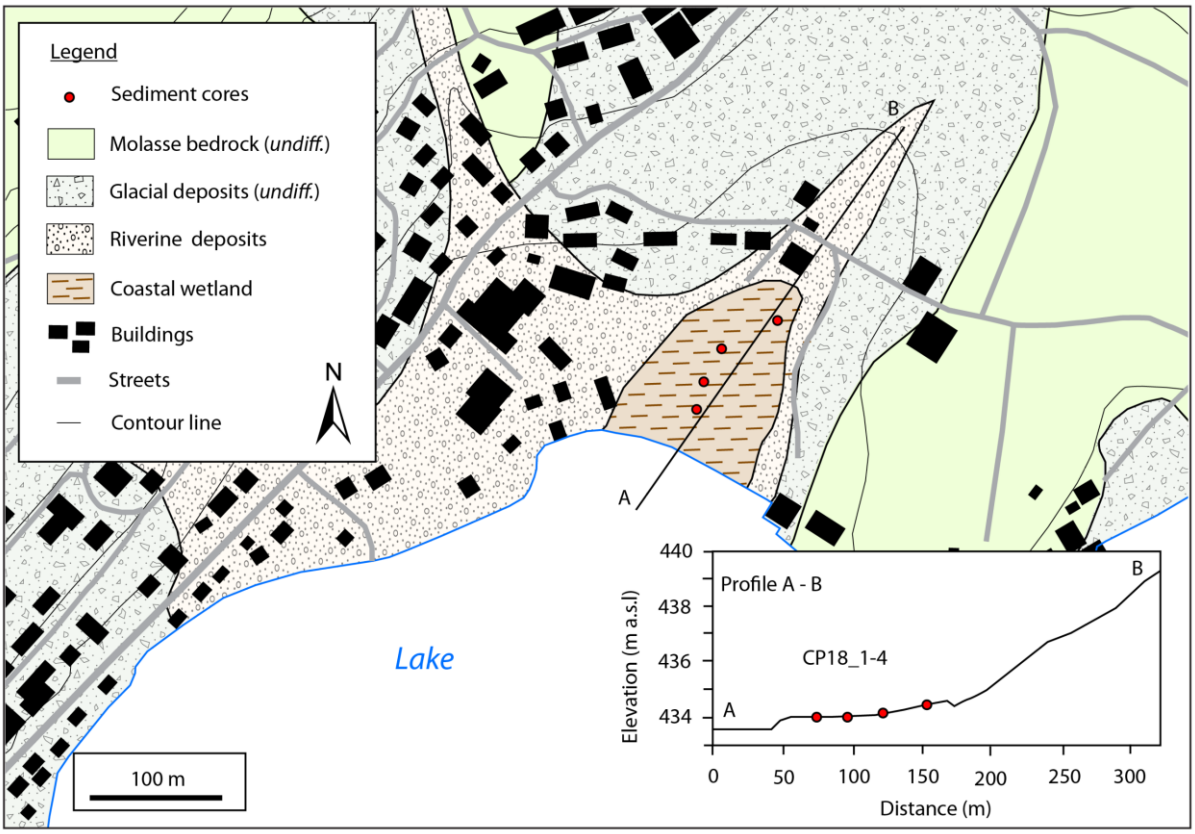

Fig. 3-6: Geomorphological map and Geoprobe sediment core location at the coastal wetland Chappelmatt, Lake Lucerne.

Tanzenberg

Tanzenberg is located at the northern shore of the Vitznau Basin and is characterized by an embayment protected from two 15 to 40 m high ridges of Molasse bedrock (Fig. 3-3). The landward area is characterized by an artificially created pond, which can be recognized on the historic Siegfried map (1889 CE), but not on the Dufour map (1861 CE). With the construction of a private residence of Ludwig II in the late 19th century, the pond was created by a lakeshore wall, which was built about 20 m into the lake and partly filled up behind. Over time, the pond

became silted by reed growth. Although the area was early anthropogenically influenced, it is supposed that the setting has not been excavated and "only" filled with debris. Underneath, however, the natural sedimentary archive has been preserved. Because of the well-suited geomorphological setting for the recognition of tsunami-derived sediment (not influenced by riverine discharge, small catchment area (10^5 m^2), organic-rich background deposits from reed vegetation), as well as considerable inundation simulated from the 1601 CE event (Hilbe and Anselmetti, 2015), we decided to recover sediment cores with the hydraulic-coring system along a transect at Tanzenberg.

Similar to the previous location, the total core recovery at Tanzenberg was low (35.4%; Fig. 3-5), therefore, meaningful core-to-core correlation was not possible. Nevertheless, the observed sedimentological succession can be reconstructed. From top to bottom, the succession consists of dark brown, very organic-rich deposits in the upper 30 cm, followed by artificially filled debris. The heterogeneous unit of landfill material has a variable thickness (10 to 40 cm) and is followed by another deposit of a very organic-rich lithology that is thickest proximal to the lake and thins landward. In one core, this is followed by a 10 cm thick yellowish lithology of silt with a density of 1.2 g cm^3, likely representing lacustrine deposits. In all cores, the lowermost section consists of dense, cohesive, faintly laminated clay deposits with angular gravel-sized intraclasts and section of gravel- and sand-dominated deposits, most likely representing Late Glacial (~15 kyr BP) deposits.

Tribschen

Tribschen is located on the southern shore of the Lucerne Bay in the eastern part of the City of Lucerne and place to a well-visited lido with outdoor sport facilities in the vicinity (Fig. 3-3). However, the area formerly hosted an extensive coastal wetland with reed vegetation that was drained and partially filled to level the surface in the early 20^{th} century. A 20 m high ridge of Molasse bedrock protects the area from the larger Chrienbach River drainage system, which build up a large fluviatile to deltaic system at Lucerne during the Holocene (Fig. 3-3). Additionally, the location has a small catchment area (7×10^5 m^2) and is not influenced by river runoff, however small streams do exist. The adjacent offshore bathymetry is relatively flat, thus tsunami-induced sediment remobilization and landward transport may be possible. Due to the geomorphological setting (coastal wetland, small catchment without riverine influences) and that the area was well-inundated in the numerical tsunami simulation (Hilbe and Anselmetti, 2015), the area was selected for sediment coring using the hydraulic-coring system. However,

the underground infrastructure of draining and electricity lines had a strong influence on the free choice of coring site.

Similar to the previous locations (Chappelmatt and Tanzenberg), the total core recovery at Tribschen was low (55.4%; Fig. 3-5), so that a meaningful core-to-core correlation was not possible. Nevertheless, the observed sedimentological succession can be reconstructed and is similar to the one observed at Tanzenberg. From top to bottom, the succession consists of dark brown, very organic-rich deposit in the upper 20 to 40 cm, followed by an artificially filled unit of debris. The heterogeneous fill material contains bricks, bituminous-smelling gravel-sized clasts, and a large proportion organic-rich, poorly sorted natural sand to gravel. This followed, in most of the cores by another well-decomposed, organic-rich unit of variable thickness (5 to 40 cm). This is followed proximal to the lake by a light grey homogeneous carbonate mud and dense, cohesive brownish yellow unit with angular intraclasts in a silty matrix with sections of faintly laminated with variable thickness landward, most likely representing Late Glacial (~15 kyr BP) deposits.

ii) Offshore setting

In the immediate vicinity of the City of Lucerne, three sediment cores were recovered with a piston-coring system from a floating platform from in an offshore depression at 200 m from the present shoreline along a 400-m transect (Figs. 3-3 and 3-7). The depression is characterized by a water depth of 8 m and is about 3 to 4 m deeper than the surrounding shallow water zone of the Lucerne Bay. From top to bottom, the sediment cores, up to 3 m long, consists of light gray carbonate mud in the uppermost 20 to 40 cm that is followed by a 60 to 70 cm thick, light brown, normal graded siliciclastic sand that overlies a brownish organic-rich Unit (2 to 10 cm thick) with beige laminae and carbonate shells with a sharp basal contact (Fig. 3-7). This is followed by a gradual transition towards the lowermost lithological Unit, which consists of faintly laminated, dense, cohesive silty clay with sandy lamina (Fig. 3-7). Because of the homogeneous density distribution observed from the MSCL scan and the presumably late-glacial character of the lowermost sedimentological Unit, not all sediment cores were opened for this study (Fig. 3-7).

The normal graded deposit was examined with laser-diffraction particle analysis of the siliciclastic sediment fraction, XRF scan, radiocarbon dated and associated with the 1601 CE Lake Lucerne tsunami by Nigg et al. (subm.). The observed offshore tsunami deposit is

characterized by a sharp lower contact with carbonate shell fragments and horizontally bedded wooden particles that become more abundant in the upper part. Mean grain-size of the siliciclastic sediment fraction varies from 200 μm at the base to 15 μm at the top, which is characterized by a sharp contact to the overlying carbonate mud. Si/Al ratio obtained from XRF can be well used as grain-size indicator and supports the normal graded grain-size distribution (Nigg et al., subm.). Radiocarbon dating of terrestrial derived organic macro remains (conifer needles and leave fragments), yield radiocarbon ages of 1306 to 1442 calibrated (cal) CE (Nigg et al., subm.). The radiocarbon ages obtained fit well with the proposed mechanism of tsunami-induced sediment remobilization from the Lucerne Bay and the adjacent onshore, which were then deposited from suspension in the offshore depression due to the decrease in tsunami flow speed at the location. Therefore, Nigg et al., (subm.) were able to link the offshore event deposit with the historically reported 1601 CE Lake Lucerne tsunami based on sediment core analysis (radiocarbon dating and grain size) and numerical bed shear stress simulation.

Another sediment core was recovered in an amphitheater-like setting in the southeastern part of the Lucerne Bay at 10 m water depth (Fig. 3-3). The 7 m long composite sediment core provides the longest record examined with a basal radiocarbon age of ~7000 years (Fig. 3-8). However, this core does not contain obvious sedimentary layers that correlate with the historical events described. Nevertheless, two clastic layers were radiocarbon dated with terrestrial organic macro remains (conifer needles, European beech seed and leave fragments; Table 3-4) in the lower part of the core that coincide with postulated prehistoric events at ~2200 BP and ~5400 BP (Schnellmann et al., 2006). The upper clastic layer, 5 cm thick, consists of a well-pronounced density peak and fragmented carbonate shells at 262 to 267 cm composite core depth and was radiocarbon dated to 2152-2339 cal. BP directly above the layer with a European beech seed (Fig. 3-8; Table 3-4). The CT-scan image shows well-pronounced laminated, high-density layers in the mm-scale with strong contrast and sharp contact with the overlying sediment (Fig. 3-8). However, the lower contact is not well visible from the line-scan image, CT-scan image also highlights a sharp lower contact here (Fig. 3-8). In the lower part, at 396 to 398 cm composite core depth, a very well-pronounced density peak can be recognized in the MSCL density data, which was radiocarbon dated to 5312-5571 cal. BP directly above with conifer needle fragments (Fig. 3-8; Table 3-4). There, the sediment is characterized by a 1 cm thick layer of well-pronounced mm-thick laminae of brownish gray and greenish gray color and a light gray top with a gradual transition to the overlying sediment (Fig. 3-8). Whole-core CT scan does not allow further textural descriptions here. Therefore, 3D micro-CT

analysis of a 2 x 1 x 1 cm thick U channel was made. The microtextural architecture of the layer that is characterized by strong density contrast to the background sediment, fold-thrust structures in the yz-orientation and cross-bedding in the xz-orientation. These sedimentary structures are probably related to strong bottom currents caused by prehistoric tsunamis triggered by subaqueous mass movements on Lake Lucerne at ~2200 and ~5400 BP.

3.4.2 Lake Geneva

Lake Geneva (580.03 km^2) is a perialpine lake of glacial origin situated at an altitude of 372 m a.s.l. in western Switzerland, that partly belongs to France. The lake is characterized by its curved morphology, which was carved into the bedrock by repeated advances of the Rhone Glacier during the Pleistocene (Fiore et al., 2011). The lake is divided into three subbasins: Haut Lac (Upper Lake) in the east, Grand Lac (Large Lake) in the central part, and Petit Lac (Small Lake) in the southwest. The max. lake depth of 310 m is reached in central part. Detailed investigation of Lake Geneva sedimentary infill was conducted with seismic reflection data and sediment cores in previous studies (Fiore et al., 2011). The sediment stratigraphy consists of a succession of basal lodgment till deposited on the bedrock, overlain by proglacial heterogeneous deposits and glacio-lacustrine fines, finally draped with Holocene lacustrine sediment (Fiore et al., 2011; Moscariello, 1997; Kremer et al., 2015). A total of six extensive subaqueous mass-movement deposits with volumes ranging from 22 to 250 x 10^6 m^3 have been deposited over the last 4000 years in Lake Geneva (Kremer et al., 2015). Accelerated ground motion during historic and prehistoric earthquakes likely caused mass-movements in 1584 CE, 1322 CE, ~2185 BP, and ~3683 BP (Kremer et al., 2015). However, the largest historically reported tsunami event on Lake Geneva was triggered by a large deltaic collapse of the Rhone Delta, most likely caused by the Tauredunum rockfall in 563 CE (Kremer et al., 2012).

The adjacent geomorphology of Lake Geneva can be roughly divided into an eastern and a western part. The eastern part is characterized by relatively steep shorelines dominated by exposed bedrock with a thin sedimentary cover of Holocene and Pleistocene deposits in some places, and by an extended fluvial environment between Bouveret and Villeneuve formed by the inflow of the Rhone River (Fig. 3-9). Several Gilbert-type deltas form cone-shaped sedimentary bodies that prograde into the lake (e.g., Montreux, Vevey). Locally, few early Holocene beach deposits of a 10 m high lacustrine terrasse are found. The western part of the

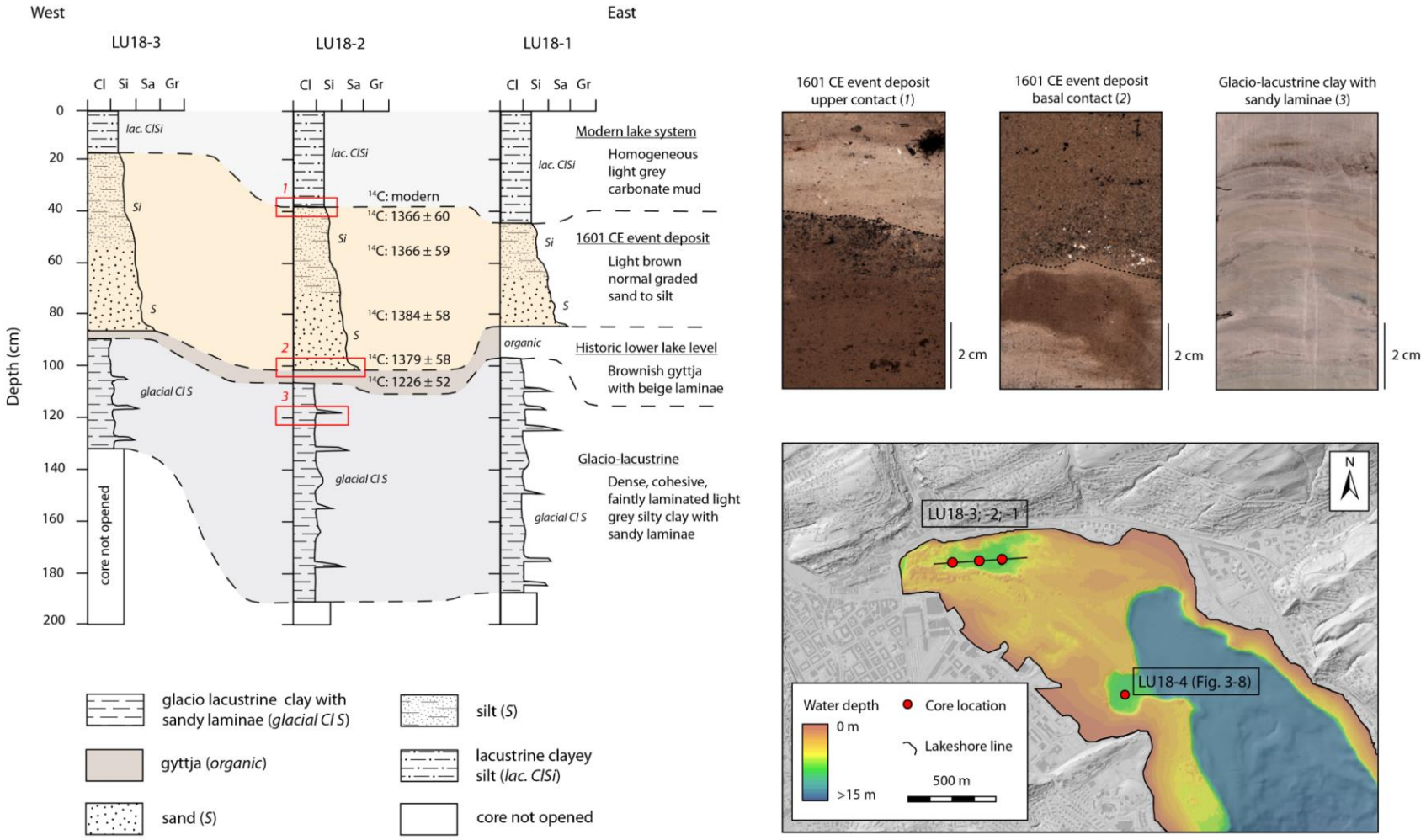

Fig. 3-7: Sediment core log and the 1601 CE offshore event deposit (left) recovered from a depression along a transect in the Lucerne Bay, Lake Lucerne (lower right). Line-scan images (upper right) show the sharp upper and lower contact of the light brown, normal graded sand to silt event deposits and the lowermost sedimentary lithology of dense, cohesive glacio-lacustrine clay with sandy laminae (modified from Nigg et al., subm.).

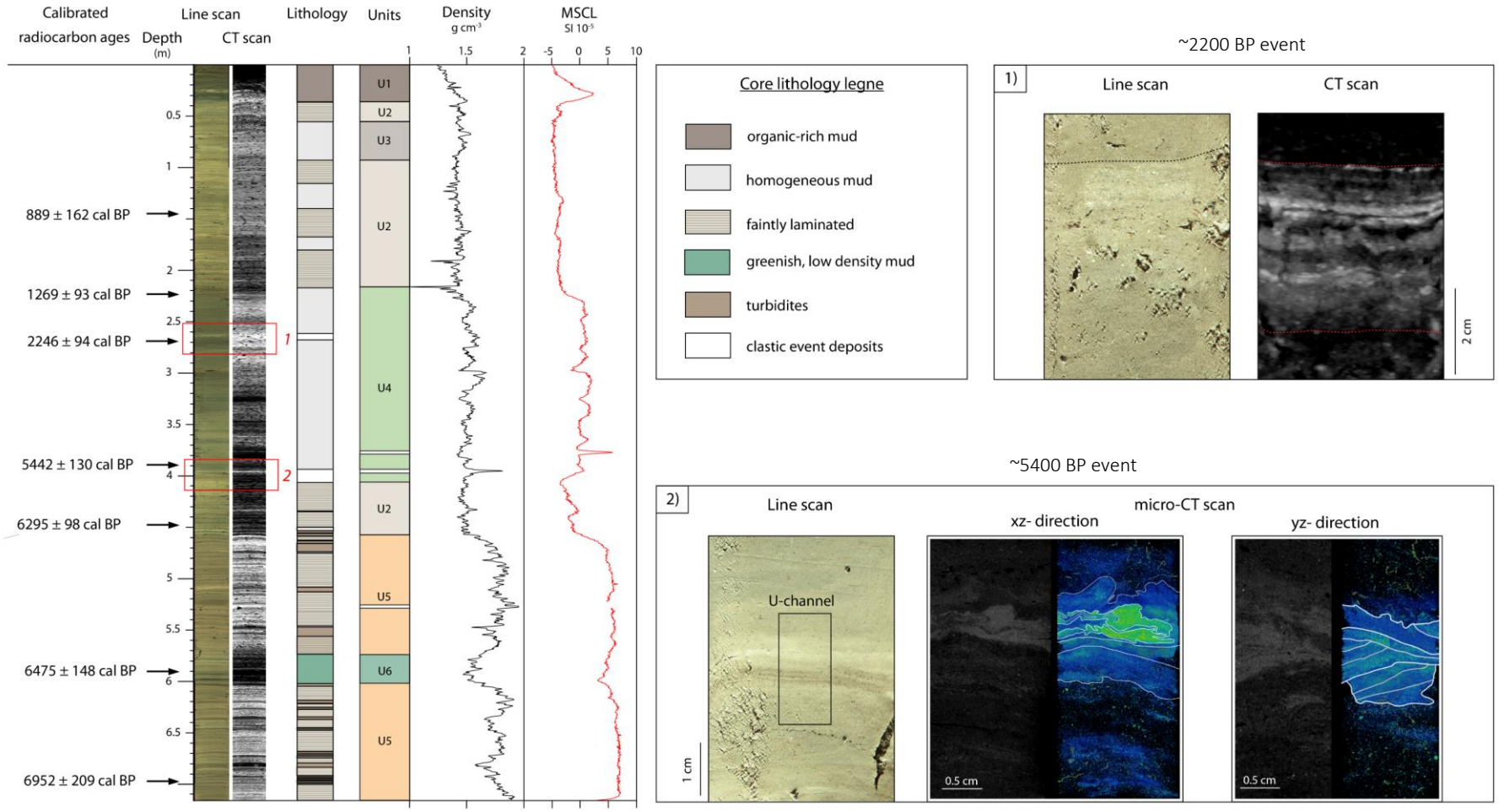

Fig. 3-8: Single sediment core recovered in an amphitheater-like setting in the southeastern part of the Lucerne Bay (see Fig. 3-7 for core location). Core log (lithology and units), line-scan image, CT-grayscale image, and MSCL data (density and magnetic susceptibility (Magn. susc.)). Radiocarbon ages obtained from terrestrial organic macro remains are shown on the left. Line-scan image, CT-scan images, and micro-CT scan of two clastic event deposits radiocarbon dated to previously postulated prehistoric mass movement generated tsunamis on Lake Lucerne at~2200 and ~5400 BP, and their textural interpretation (color scale adjusted for better visualization) are shown.

Table 3-4: AMS radiocarbon age, calibrated ages, and $\delta^{13}C$ results from terrestrial organic macro remains.

Location	Core ID	Sample	Core depth (cm)	Sample material	$\delta^{13}C$ (‰)	^{14}C age ± 1σ (^{14}C years BP)[a]	Calibrated 2σ range (cal CE)[b]	Calibrated 2σ range (cal BP)[b]
Chappelmatt	CP18-1A	BE-11499.1.1	13	Seeds	-30.9	-163 ± 65	Modern	–
Chappelmatt	CP18-1A	BE-12422.1.1	128	Nut shell	-28.8	5407 ± 26	–	6183–6285
Chappelmatt	CP18-1B	BE-12423.1.1	17	Leave fragments and seed	-32.6	2837 ± 78	–	2779–3146
Chappelmatt	CP18-4B	BE-12424.1.1	206	Seeds	-26.6	631 ± 21	1295–1396	556–661
Lucerne Bay	LU18-2	[c] BE-10751.1.1	35–36	Leave fragments	-28.7	-572 ± 31	Modern	–
Lucerne Bay	LU18-2	[c] BE-10752.1.1	41–42	Conifer needle	-28.7	570 ± 31	1306–1425	–
Lucerne Bay	LU18-2	[c] BE-10753.1.1	54–55	Conifer needle	-28.8	567 ± 30	1307–1425	–
Lucerne Bay	LU18-2	[c] BE-10754.1.1	79–80	Conifer needle	-27.4	527 ± 31	1326–1442	–
Lucerne Bay	LU18-2	[c] BE-10755.1.1	98–99	Leave fragments	-31.8	544 ± 30	1321–1437	–
Lucerne Bay	LU18-2	[c] BE-10756.1.1	102–103	Leave fragments	-29.7	812 ± 36	1174–1277	–
Lucerne Bay	LU18-4	BE-12170.1.1	145	Leave fragments	-30.0	965 ± 69	900-1224	–
Lucerne Bay	LU18-4	BE-12171.1.1	223	Conifer needle	-41.6	1373 ± 49	590-775	1176-1361
Lucerne Bay	LU18-4	BE-12172.1.1	269	European beech nut	-31.8	2243 ± 30	–	2152-2339
Lucerne Bay	LU18-4	BE-12770.1.1	389	Conifer needle fragments	-31.3	4674 ± 44	–	5312-5571
Lucerne Bay	LU18-4	BE-12173.1.1	447	Conifer needle fragment	-38.3	5481 ± 38	–	6197-6393
Lucerne Bay	LU18-4	BE-12771.1.1	590	Conifer needle	-36.6	5688 ± 59	–	6317-6633
Lucerne Bay	LU18-4	BE-12174.1.1	697	Seed	-27.4	6081 ± 81	–	6745-7163
Lake Sils	SIL10-1	[d] ETH-40776	50–51	Peat: plant remains	-30.5	1745 ± 35	241–403	–
Lake Sils	SIL06-8	[d] ETH-32595	79	Peat: 30 plant remains	-25.8	1735 ± 50	225–419	–
Lake Sils	Sis03-23	[e] Poz-5423	69-72	Three small twigs	NA	1300 ± 35	654–797	–
Lake Sils	Sis03-2	[e] Poz-5424	85	Leave fragments, small twig	NA	1465 ± 40	548–652	–

Uncertainties of ^{14}C ages refer to 1-sigma uncertainties. Ranges of calibrated ages represent 95.4% probabilities (2σ): [a] Stuiver and Polach, 1977; [b] Ramsey, 2009; Reimer et al., 2020; [c] Nigg et al., subm.; [d] Nigg et al., 2021; [e] Blass et al., 2005.

lake is characterized by more abundant shallow shorelines dominated by glacial deposits, fluvial environments with beaches, a few natural relicts of wetlands, and exposed bedrock that is partially covered with unconsolidated sediment. Shoreline infrastructures, sidewalks, and public gardens are abundant, especially in the urban areas around Lausanne and Geneva, but also elsewhere and strongly shaped both the eastern and western lakeshores.

Historically reported tsunami events on Lake Geneva

i) 563 CE Tauredunum rockfall and large Lake Geneva tsunami

The historical chronicles by Bishop Marius of Avenches and Grégoire of Tours report on the catastrophic Tauredunum rockfall and associated tsunami on Lake Geneva in 563 CE (Montandon, 1925; Schoeneich et al., 2015; Favrod, 1991) and were translated from Latin into French by Montandon (1925). Bishop Marius of Avenches accurately documents the disastrous Tauredunum rockfall at the Rhone river mouth: *"In that year the imposing mountain of Tauredunum in the territory of the Valais rushed so suddenly that it buried a nearby fortress with all their inhabitants"*. In the following lines Bishop Marius refers to the devastating tsunami that is directly related to the Tauredunum rockfall: *"... and so agitated the lake, sixty miles long and twenty miles wide, that, coming from both shores, it devastated ancient villages with people and herds; destroyed many of the holy gods with their servants, and destroyed the bridge of Geneva, mills, and men, and inundated the city of Geneva, causing many casualties there"*.

The chronicle by Bishop Grégoire of Tours describes a cascade of the event that differs from the chronicle by bishop Marius of Avenches: "*The damming of the Tauredunum rockfall cone created a lake upstream … Then a dam outburst flood caused the flooding of Lake Geneva shores. The flooding carried away everything and overtopped the Burgundian city walls at Geneva"*. However, this is not consistent with the observed mass-movement deposit with a volume of 250 x 10^6 m^3 observed in the Lake Geneva sediment record by Kremer et al. (2015). Thus, the Tauredunum rockfall impact destabilized the Rhone Delta and caused its collapse. The water displacement caused by the delta failure generated a basin-wide tsunami with severe inundation along the lakeshores and at the lake outlet (Kremer et al., 2012).

ii) 1584 CE Aigle earthquake and small Lake Geneva tsunami

The Aigle earthquake on March 11, 1584 CE, with a reconstructed epicentral moment magnitude (Mw) of 6.1 (Fäh et al., 2011), caused a tsunami and a seiche on Lake Geneva that

was historically reported (Fritsche al., 2012; Schwarz-Zanetti et al., 2018). The tsunami was likely caused by subaqueous mass movements that were triggered by the earthquake (Loizeau, 1991; Kremer et al., 2015). A mass-movement deposit with an estimated minimum volume of 1 x 10^6 m^3 was dated with the radiocarbon method to 1500 ± 100 cal CE (Kremer et al., 2015). Additional subaqueous mass movements may have originated in the area of the Rhone Delta. However, the associated failure scars were not identified in the multibeam bathymetry data, and the acquired seismic-reflection data by Kremer et al. (2015) did not include the delta area. Nevertheless, numerical tsunami simulations indicate that a minimum displaced sediment volume of 10^6 to 10^7 m^3 is required in the Rhone Delta area to generate a tsunami with 1 m run-up height at Montreux and Vevey, as reported in historical documents (Kremer et al., 2015).

Schwarz-Zanetti et al. (2018) compiled, analyzed, and verified the accuracy of various historical documents describing the secondary effects of the 1584 CE Aigle Earthquake. The effects of the tsunami and seiche on Lake Geneva were mentioned in several collections of historical sources (e.g., Egli, 1901-1904; Reymond, 1917; Schardt, 1892) and chronicles (e.g., du Chesne, 1587). For example, the tsunami was described by Jousua Wyttenbach: *"In the harbors of many places the lake was agitated and stormy, but a stone's throw away from the harbors the lake was calm. In some places the lake retreated, in others it expanded, at the end it rolled back in the old bed"* (Egli 1901–1904). Coastal erosion, inundation, and damage to vineyards near the shore were reported mainly from the northern shore of the lake near the Rhone Delta (Egli, 1901-1904). At Montreux, deep holes were created by the erosion of tsunami waves along the shore (Reymond, 1971). Several meters of run-up were reported at Grandvaux (Reymond, 1971). Additionally, entire shoreline sections have collapsed into the lake at Vevey, and a seiche with an amplitude of 1.5 m was observed at the lake outlet, exposing the Rhone riverbed three to four times at intervals of 15 min (Egli, 1901-1904).

Coring sites and its sedimentary records

Pürckhauer gauge auger sediment cores were recovered from 7 different onshore localities around Lake Geneva that exhibit geomorphological characteristics of beaches, coastal wetlands, and glacially dominated landscapes (Fig. 3-9; Table 3-5). Although these field surveys did not yield positive evidence of tsunami deposits and investigations were not intensified thereafter because the observed coastal sediments were considered poorly suited for tsunami deposit recognition, due to the predominantly clastic sedimentary environments even

in locations where organic-rich background sediments would have been expected. The results obtained at Collonge-Bellerive are presented below as an example for Lake Geneva.

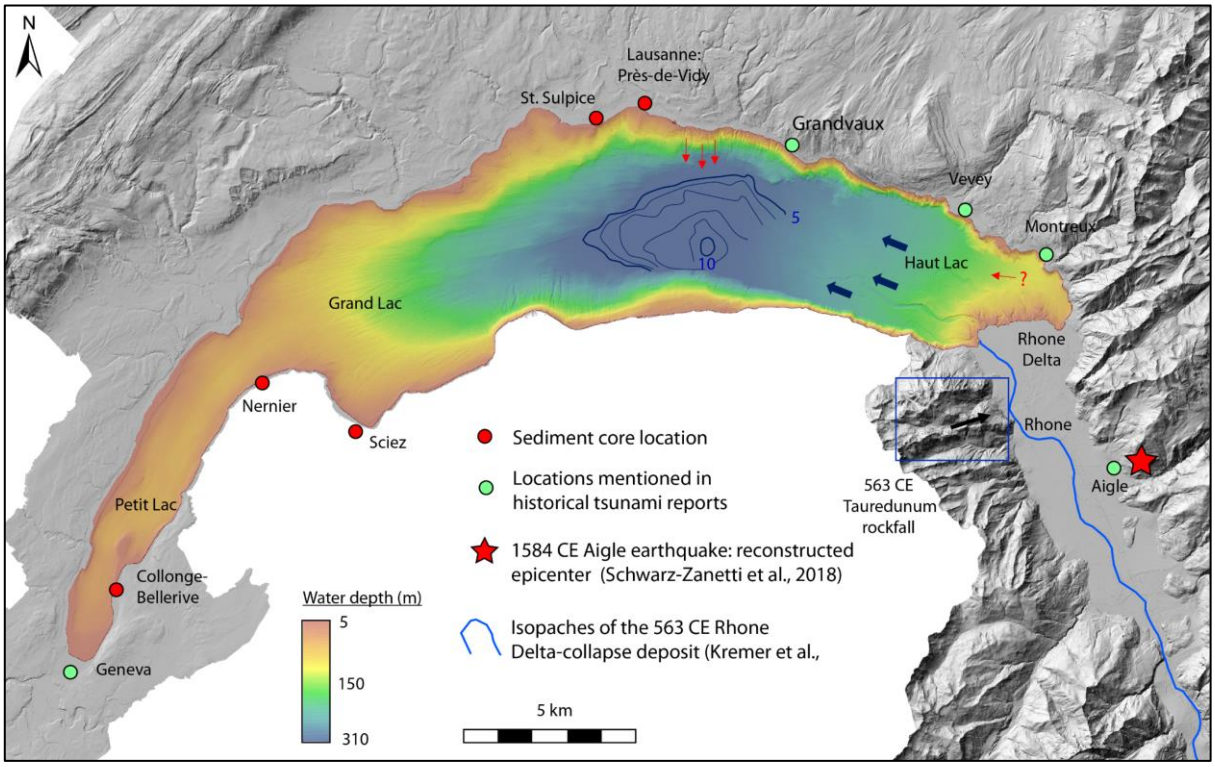

Fig. 3-9: Map of Lake Geneva shows the locations of recovered sediment cores (red dots) and historically reported tsunami waves (green dots). The reconstructed epicenter of the 1584 CE Aigle earthquake (red star) and the associated areas of triggered subaqueous mass movements are indicated (red arrows; modified from Kremer et al., 2015). The location of the 563 CE Tauredunum rockfall and the isopaches of the associated mass-movement deposit from the Rhone Delta collapse are shown in blue (modified from Kremer et al., 2015). High-resolution bathymetry is modified from Kremer et al. (2015), hillshade map is based on the SwissAlti3D from swisstopo.

Collonge-Bellerive: Point à la Bise

Point à la Bise hosts one of the few pristine wetlands on Lake Geneva (Fig. 3-10). It is located directly on the lakeshore and is adjacent to a campsite with artificially stabilized shoreline. The area is characterized by a wetland in the south, Holocene beach deposits to the north, and glacial deposits further inland. The wetland is a well-protected bird conservation area so that access for our geological surveys was denied. Nevertheless, 7 Pürckhauer cores were recovered at the campsite near the pristine wetland (Fig. 3-10). Because of several underground course of power lines, only a few cores could be recovered directly at the border of the nature reserve and at the northern end of the campground (Fig. 3-10).

The uppermost 2 m of the sediment stratigraphy at Collonge-Bellerive consists of poorly sorted gravel toward the lake (Fig. 3-11). There, however, core recovery was low, probably due to the very clastic, non-cohesive sediment properties. Landward, the succession from top to bottom consists of 20 to 40 cm thick unit of a brown, organic-rich soil with poorly sorted sand, and a few matrix-supported gravel clasts (Fig. 3-11). This is followed by a cohesive, light brown clayey soil with reddish oxidized horizons, and a variable thickness of 20 to 40 cm in Cores TCS-5, 6, and 7 (Fig. 3-11). In core TCS-4, however, the topsoil overlies the lakeward observed gravel with a sharp contact (Fig. 3-11). A well-sorted, dark grey sand is found below the light brown, clayey soil in Cores TCS-5, 6, and 7, and underlies the poorly sorted gravel in Cores TCS-3 and 4 (Fig. 3-11). The laterally continuous sand is massively bedded, varies in thickness from 20 to 60 cm, and is well sorted in parts, while larger proportions of silt occur in others (Fig. 3-11). In the lowermost section (100 to 200 cm), a massively bedded, light gray, homogeneous lacustrine carbonate mud with carbonate shells is observed based on the recovered Pürckhauer sediment cores (Fig. 3-11).

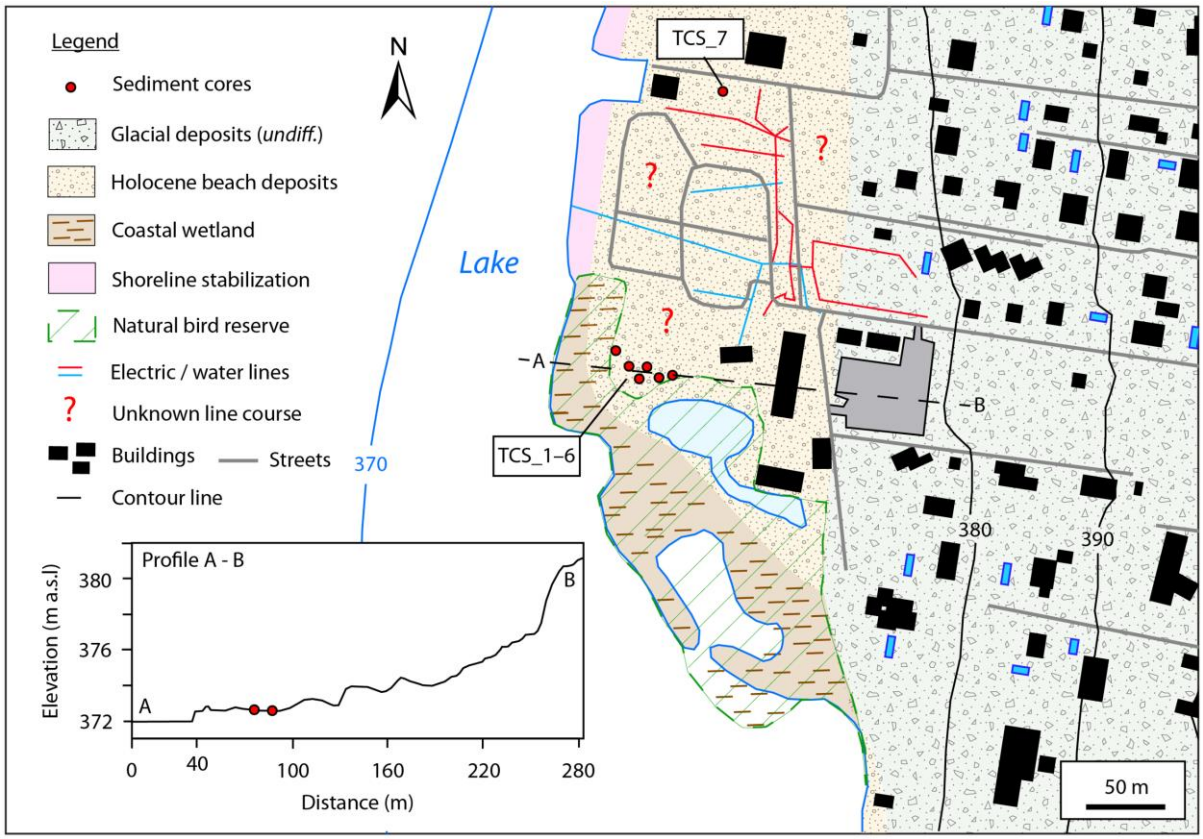

Fig. 3-10: Geomorphological map of Point à la Bise, Collonge-Bellerive show the location of recovered Pürckhauer sediment cores (red dots), elevation profile as well as mapped and unmapped electric lines and water pipes are indicated.

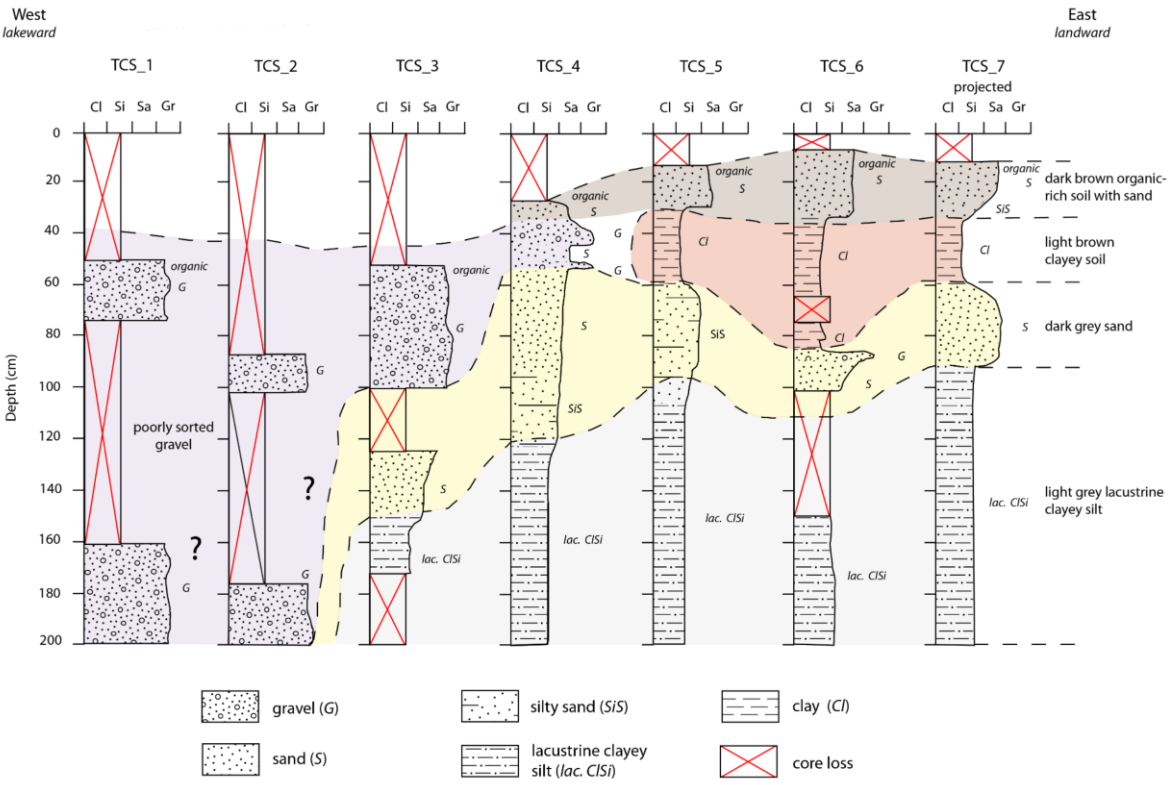

Fig. 3-11: Pürckhauer sediment core transect at Collonge-Bellerive. The sedimentological stratigraphy consists of poorly sorted gravel toward the lake and a succession of lacustrine mud, well sorted sand, clayey soil, and organic-rich soil further inland.

3.4.3 Lake Sils

Lake Sils (4.1 km^2) is the uppermost lake of a chain of four lakes (Lake Sils, Lake Silvaplana, Lake Champfèr, and Lake St. Moritz) in the Upper Engadine in southeastern Switzerland at an altitude of 1797 m a.s.l (Fig. 3-12). The longitudinally oriented alpine lake consists of four subbasins, Maloja, Lagrev, Silser, and Central Basin, with the Central Basin being the deepest, with a max. water depth of 72 m. The Central Basin hosts a large mass-movement deposit with an estimated minimum volume of 6.5°x 10^6 m^3 and a thickness of more than 6 m, which originates from a partial collapse of the Isola Delta around 700 CE (Fig. 3-12; Blass et al., 2005). Although no historical documents describe a tsunami on Lake Sils, this subaqueous mass movement was likely tsunamigenic and the area provides a unique opportunity to study coastal on- and offshore sediments in a pristine environment.

Based on numerical tsunami simulation the partial Isola Delta collapse likely generated a basin-wide tsunami, with an inundation distance of up to 250 m and a flow depth of up to 3 m at the coastal plains close to Sils Baselgia (Nigg et al., 2021). Although the area was an important

traffic axes during the Pax Romana (~1975–1750 BP) of the Roman period, there are no known historical accounts documenting the natural disaster. This is likely because with the collapse of the Roman Empire around 400 CE, the area became rural again (Ducrey, 2006).

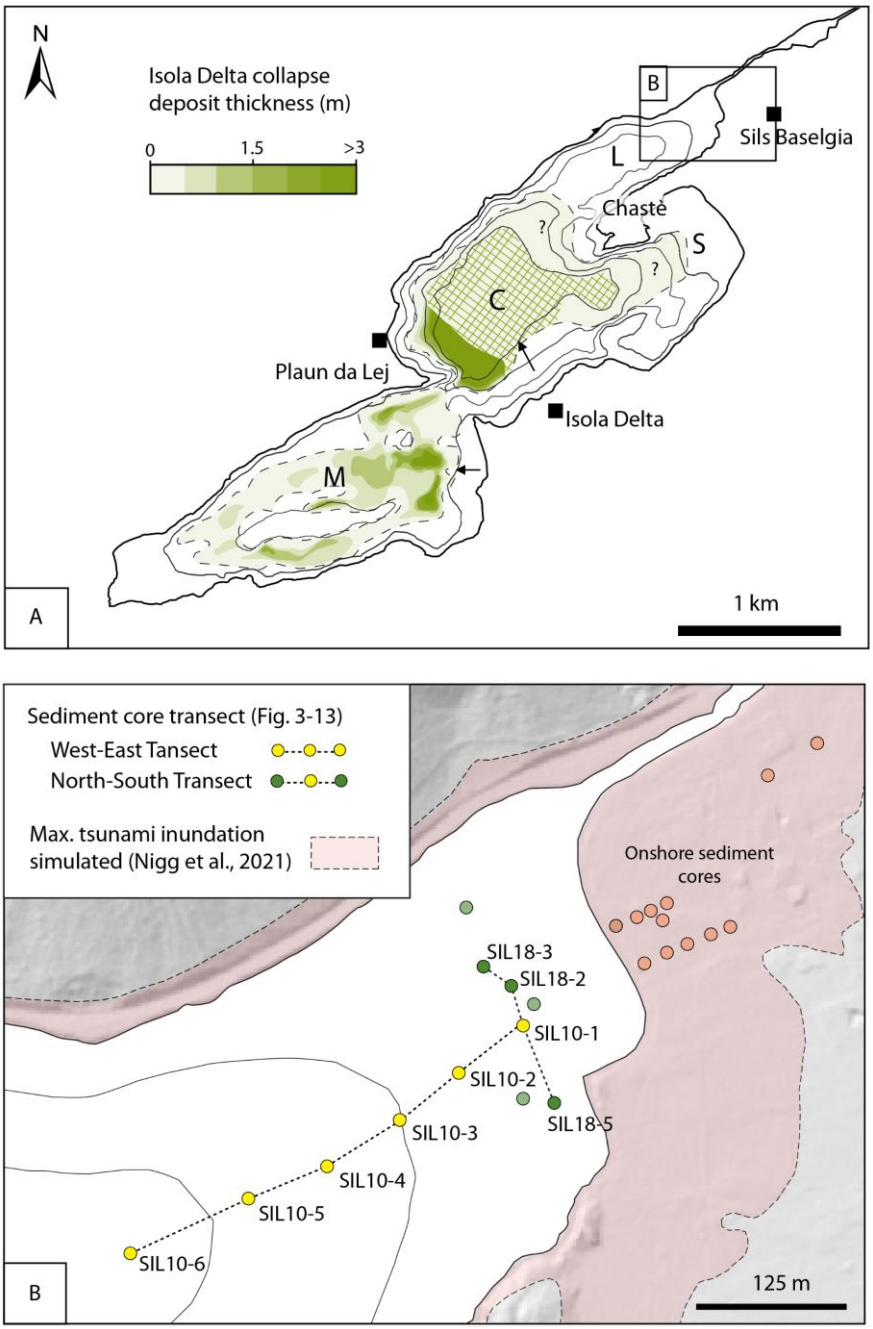

Fig. 3-12: A) Spatial extent of the Isola Delta collapse deposit in Lake Sils with its individual lake basins (M: Maloja Basin; C: Central Basin; L: Lagrev Basin, and S: Sils Basin (modified from Blass et al., 2005 and Nigg et al., 2021). B) Location of sediment core transects shown in Fig. 3-13 and area of tsunami inundation based on numerical simulations is shown in light red (modified from Nigg et al., 2021).

Coring sites and its sedimentary records

The lakeshore geomorphology of Lake Sils is characterized by the Gilbert-type Isola Delta in the southeast as well as steep shoreline with exposed bedrock and unconsolidated sediments on the south to southeast and north to northwest facing lakeshores. Along the main valley axes, coastal lowland plains with high alpine wetland, grass, and shrub vegetation are developed along the lakeshore. Based on the inundation map from the numerical tsunami simulation, Nigg et al. (2021) recovered 21 sediment cores along a transect encompassing the on- and offshore environment of Lake Sils (Fig. 3-12).

In the offshore, a coarse-grained, normal graded sand deposit with horizontally bedded gravel-sized clasts 10 to 20 cm thick with a clay cap a few cm thick on the top overlies a well-decomposed, organic-rich unit with a sharp lower contact (Fig. 3-13). This internally fining-upward sequence, the lower sharp contact, and horizontally bedded gravel-sized clasts are very well recognizable on whole-core CT-grayscale images (Fig. 3-13). Based on sediment cores recovered with a hydraulic-coring system on land, the lateral continuity of the deposit can be traced approximately 50 m inland until the deposit can no longer be distinguished from the overlying sediment, while the underlying organic-rich unit can be traced further inland. In the continuity of sediment cores recovered onshore, a landward thinning and fining (decrease in mean grain size) trend of the associated deposit is readily apparent (Fig. 3-13). In sediment cores recovered offshore in water depths of 4 to 40 m and at 150 to 500 m from the alluvial plain, the event deposit transitions to a more heterogeneous sediment package with variable thickness and composition (Fig. 3-13). The internal sediment architecture of the event deposit consists of poorly sorted gravel, single and multiple fining-upward sand sequences with lower sharp contacts, mud clasts of finely laminated pre-event lacustrine deposits, and a well-traceable clay cap at the top of the deposits. Sharp erosional contact to the underlying unit is observed in cores SIL10-2 and SIL10-1 (Fig. 3-13). Based on radiocarbon dating of the underlying unit of the event deposit to an age of 141-410 cal CE, the internal and spatial architecture of the observed sedimentary body as well as numerical tsunami simulation, Nigg et al. (2021) associated the event deposit with the Isola Delta collapse around 700 cal CE (Blass et al., 2005).

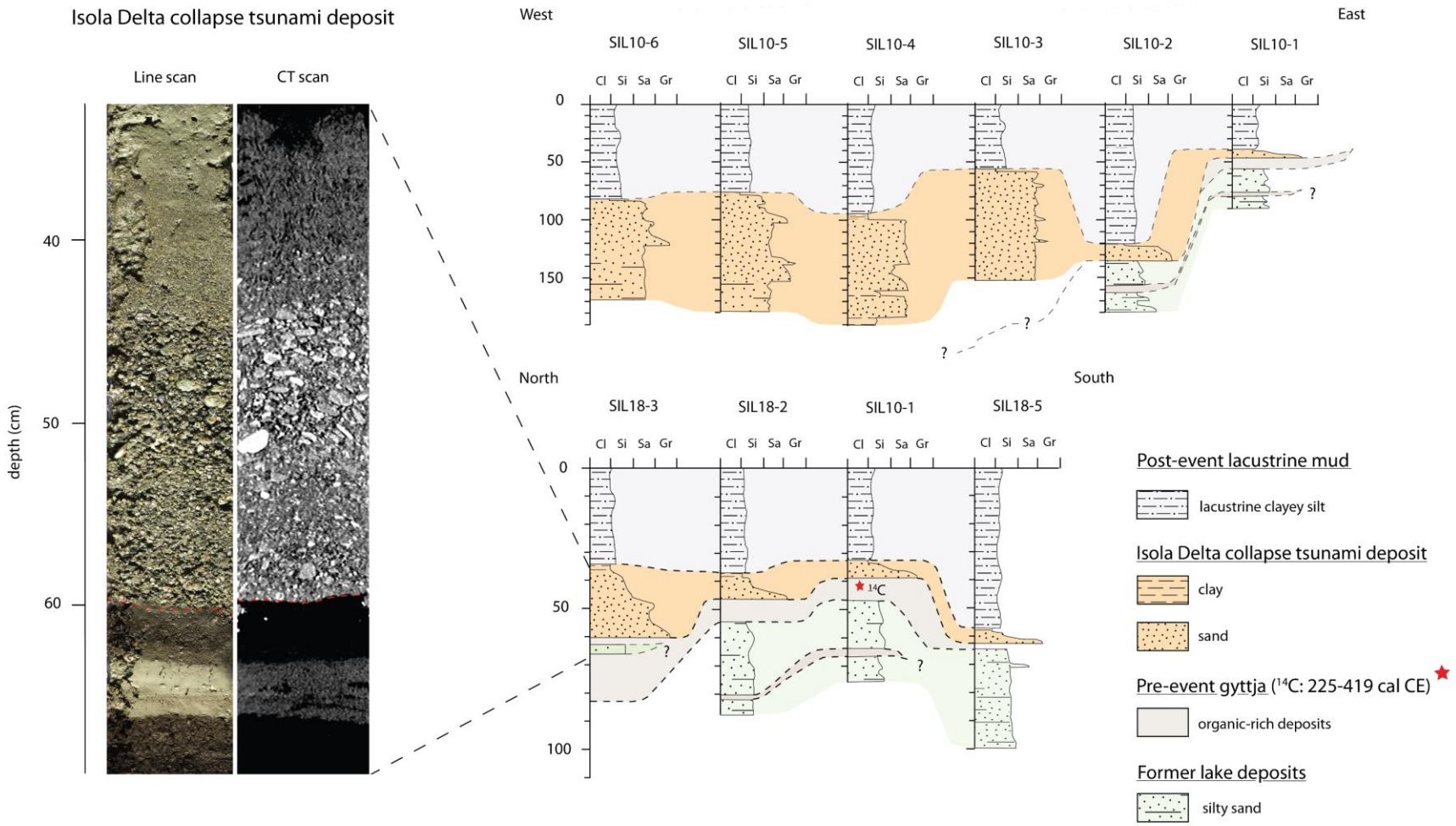

Fig. 3-13: Isola Delta collapse tsunami deposit and its lateral continuity observed in sediment cores from Lake Sils (see Fig. 3-12 for core location; modified from Nigg et al., 2021). CT-scan image shows sharp lower sedimentary contact on the underlying pre-event deposit radiocarbon dated to 225-419 cal CE, horizontally bedded gravel clast and the fining upward trend (modified from Nigg et al., 2021)

Table 3-5: Evidence for tsunami deposits observed in sediment cores recovered at various location in the on- and offshore environment of Lake Lucerne, Lake Geneva, and Lake Sils.

Lake	Location	Setting	Geomorphology	Core-type (number of recovered sediment cores)	Evidence for tsunami related sedimentary signatures
Lake Lucerne	Ennetbürgen	Onshore	Fluvial dominated alluvial plain	Pürckhauer (4)	Negative
	Weggis: Tanzenberg	Onshore	Coastal wetland	Pürckhauer (4); Geoprobe (4)	Negative
	Merlischachen: Chappelmatt	Onshore	Coastal wetland	Pürckhauer (4); Geoprobe (4)	Negative
	Lucerne: Tribschen	Onshore	Coastal wetland	Pürckhauer (4); Geoprobe (4)	Negative
	Lucerne Bay	Offshore	Depression	Piston-sediment cores (4)	Positive
Lake Geneva	Lausanne: Près-de-Vidy	Onshore	Beach	Pürckhauer (4)	Negative
	St. Sulpice	Onshore	Beach, basal lodgement till	Pürckhauer (4)	Negative
	Sciez (France)	Onshore	Coastal wetland	Pürckhauer (4)	Negative
	Nernier (France)	Onshore	Beach, basal lodgement till	Pürckhauer (4)	Negative
	Collonges-Bellerive: Point à la Bise	Onshore	Coastal wetland, beach	Pürckhauer (4)	Negative
Lake Sils	Sils Baselgia	Onshore	Alluvial plain	Pürckhauer (4); Geoprobe (12)	Positive
	Lagrev Basin	Offshore	Nearshore	Piston cores (6); Gravity cores (6)	Positive
	Sils Basin	Offshore	Nearshore	Gravity cores (4)	Positive

3.5 Discussion

3.5.1 Historical documents of past lake tsunamis

Because recent analogues of the sedimentary signature of lacustrine tsunamis are scarce, historical documents provide useful information about the characteristics of past tsunami events. However, intrinsic problems associated with this type of information need to be considered (Gusiakov, 2009). These problems may arise from the inaccuracy and fragmentary nature of available information on ancient or geographically remote events (Gusiakov, 2009). Therefore, the historical documents collected as part of this study, which consist of chronicles that include the authors' observations and compiled eyewitness accounts, as well as artwork, newspaper articles, and photographs, were subjected to a careful verification of authenticity. For the characterization of lake-tsunami hazard in Switzerland, in particular the historical chronicles from Cysat (1969), Bünti (1973), Billeter (1923), Dietrich (1689), Bishop Marius of Avenches (Montadon, 1925) and Bishop Gregoire de Tours (Montandon, 1925) provide detailed information on historical events at Lake Lucerne and Lake Geneva. Previous studies have generally focused on the physical wave parameters described in these documents for comparison with the numerical tsunami simulations performed (e.g., Hilbe and Anselmetti, 2015; Kremer et al. 2012) and on the secondary effects of strong historical earthquake (Schwarz-Zanetti et al., 2003, 2018). In this study, however, we put special emphasis on the historical documentation of tsunami-related coastal effects and, specifically, sediment remobilization and deposition. In the following, we elaborate (1) the nearshore effects of lacustrine tsunami waves and associated sedimentary signatures, and (2) triggering mechanisms of lake tsunamis based on the review of historical documents.

Sedimentary signatures reported in historical documents on lake tsunamis

Our study of historical documents highlights that lacustrine tsunamis have a very high erosion potential on lakeshores. For example, various chronicles mentioned entire shoreline sections that submerged. However, this could also be related to slopes that collapsed due to the earthquake itself. Therefore, it is not simple to disentangle this process and assign it to one cause or another. Nevertheless, historical documentation of aseismic subaqueous and subaerial mass movement-generated tsunami further supports these strong erosional signatures. Although, depositional signatures are poorly discernible from the historical descriptions analyzed, a few have been identified.

For example, the Lucerne city clerk Renward Cysat mentions boulders and debris as well as boats, fish, and fishing nets that were washed ashore by the 1601 CE Lake Lucerne tsunami (Cysat, 1969). For the same event, Pastor Businger reports destroyed and washed away houses and barns as well as fruit trees in Buochs. Bünti (1973) documents debris and large amounts of wood that were washed ashore and transported inland by the 1687 CE Muota Delta collapse-generated tsunami in Brunnen and Buochs. These documentations provide evidence that tsunami-related deposits likely exist in the onshore setting of lakes, but their sedimentary signatures may be more spatially heterogenous than extensive sand sheets as observed from some marine tsunami deposits (e.g., Dawson and Shi, 2000). Nonetheless, identification of the geomorphological conditions required to deposit these types of signatures likely leads to similar sedimentary signatures of past lake tsunamis. To fulfill these conditions, large amounts of unconsolidated sediment are needed to provide a sediment source that can be eroded, transported, and deposited along the tsunami inundation pathway. In addition, depositional environments are needed in which sedimentary signatures are preserved and distinct from background sediments. This is especially important because freshwater tsunami may have not chemical and biotic proxies that can be used for identification. Furthermore, it should be noted that the historically documented effects of tsunamis on coastal areas are highly erosive. Sediment may be transported into the lake with backwash currents because the coastal slopes in large areas of alpine lakes are too steep for effective sediment transport onshore.

3.5.2 Site selection pathway

A comprehensive site selection is required to choose ideal locations allowing identification of tsunami deposits from the geological record. In this study, a site selection workflow was developed to track the coring-site selection and to apply it to other lakes. First, lakes were selected based on available historical sources and numerical wave modelling of past tsunamis, as well as dated mass-movement event catalogues in the stratigraphic record of the lake (Fig. 3-2). Second, a geomorphological database was compiled that includes high-resolution topographic (swissAlti3D, swisstopo) and bathymetric models (SwissBathy3D, swisstopo), tsunami inundation maps, historical maps (Dufour and Siegfried map, swisstopo), geological maps (GA25, swisstopo), and borehole logging data. These information’s were used to apply a land-use classification scheme that finally led to the selection of specific locations for further investigations.

Lakeshore geomorphology and the potential for tsunami deposit recognition there

Of the three lakes (Lake Lucerne, Lake Geneva, and Lake Sils) considered in this study, we selected 15 location that appeared to be promising for the identification of tsunami depositional signatures according to our workflow. Various challenges in performing successful coring campaigns are discussed in the following sections:

i) General difficulties of logistics (private properties, nature reserves)

Several difficulties were observed during the planning of the fieldwork, especially in populated areas that are common on Swiss lake shores. First, property owner needed to be identified, contacted, and asked for permission to conduct the survey. Obviously, not everybody would agree to having their backyard altered by a sediment coring device, even if the disturbance would be temporary. In nature reserves, permits had to be requested from the cantonal authorities and in some cases were denied. At locations where we obtained permission for sediment coring, locations of numerous pipelines, such as telecommunications, water, electricity, had to be determined through non-centralized archives. As any potentially costly damage would still be in our responsibility, a careful and time-consuming planning was needed. Once Pürckhauer sediment cores were recovered, they required a careful sedimentological description before a decision could be made about the further investigation with a hydraulic Geoprobe coring device at the sites.

ii) Shoreline modifications

Swiss lakeshores have been heavily modified for coastal erosion protection, and coastal wetlands have been drained to gain areas for agricultural and infrastructure development, as well as for representative lakeside promenades and gardens. As a result, the former shoreline and shore morphology is difficult to reconstruct. However, the historical national maps by Dufour and Siegfried, published between 1845 and 1865 CE and 1870 and 1926 CE, respectively, provide useful information for the reconstruction the course and its vegetation type of the former shoreline. It should be noted here that historical maps are time windows into the period when they were mapped. But deltaic environments in particular are known to be dynamic and naturally rearrange the shoreline on short time scales (e.g., Woodroffe, 2000).

iii) Agricultural areas

In agricultural lands topsoil is regularly reworked the uppermost part of the soil. Due to increased runoff and erosion of these fields also deeper lying sediments become reworked

through time. Therefore, these areas are considered as being poorly suited for preserving tsunami signatures in the upper 50 cm. At greater depths, however, these localities may have preserved prehistoric events.

iv) Lakeshore geomorphology

The simplest classification of the lakeshore environment is probably the distinction between steep and shallow shores with the latter having a higher potential for the deposition and preservation of tsunami deposits. Steep shores may be characterized by vertical cliffs (e.g., Uri Basin of Lake Lucerne) and steep slopes dominated by gravitational process (e.g., northern shore of Lake Sils). Flat shores, on the other hand, consist of fluvially dominated environments with cone-shaped Gilbert-type deltas (e.g., the villages of Gersau and Sisikon at Lake Lucerne), extensive floodplains (e.g., Reuss River and Engelberger Aa at Lake Lucerne) and coastal wetland, which are usually rich in biodiversity and play a crucial role in lake ecology (e.g., Ostendorp, 1989).

3.5.3 Lake-level variations

Past lake-level fluctuations, similar to tidal correction in the marine environment for tsunami run-up and inundation distance estimations (e.g., Gelfenbaum et al., 2007; Hori et al., 2007), must be considered to identify potential tsunami depositional settings in the lacustrine environments. However, long-term (thousands of years) lake-level fluctuations are not well quantified for Swiss lakes. Nevertheless, a few studies indicate m-scale seasonal lake-level fluctuations as well as considerably lower and higher lake levels (e.g., Deàk et al., 2018: Keller et al., 2020; Wohlfarth & Schneider, 1991), before lake levels were stabilized at current levels through discharge controls at the lake outlet (e.g., Lake Lucerne (Keller et al., 2020); Lake Geneva (Girardclos et al., 2007; Moscariello 1997); Lake Sils (Grischott et al., 2017)). Therefore, information about former lake level needs to be considered for the site selection process, especially when establishing tsunami event chronology on millennial time scales.

3.5.4 The identification of lacustrine tsunami deposits

Marine fauna (e.g., brackish and/or saline diatom, calcareous shell producing mollusk, and planktonic foraminifera) has been used in numerous studies as one of several criteria for identification of marine tsunami deposits (e.g., Dawson et al., 1996; Hemphill-Haley, 1996;

Garrett et al., 2015; Minoura et al., 2000). However, this may have limited applicability to the case of lacustrine tsunamis, and further site-specific studies would be required to characterize the habitat of various potential biotic proxies first. Similarly, geochemical signatures of saline water flooding (e.g., elevated Na, Cl, and Ba concentration) in the terrestrial record of marine tsunami cannot be transferred directly to the lacustrine setting. Therefore, a high sedimentological contrast between background and tsunami-derived sediments is needed for the identification of lacustrine tsunami deposits. In clastic environments, fluvial or storm-induced reworking of sediments may produce sedimentological signatures similar to those expected from tsunami inundation. Therefore, also several marine examples (e.g., Dawson et al. (1988) on the Storegga landslide tsunami deposits) takes advantage of tsunami deposits being enveloped by organic-rich background sediments. This may also be applicable in lacustrine setting. Therefore, coastal wetlands are considered particularly promising for the identification of lacustrine tsunami deposits by sedimentological criteria when erodible sediment sources are available, and the area is significantly inundated.

Depositional environments

i) Fluvial environments

In fluvially dominated environments sediment is regularly reworked along the river channel (e.g., Delile et al., 2020) and the surrounding plains are frequently flooded (e.g., Woodroffe et al., 2000). Thus, the depositional signatures of these processes are considered to be similar to those expected from lake tsunamis. Additionally, tsunami-derived sediments may not be distinguishable from riverine sediment deposits based on biological criteria because sharp ecological boundaries do not exist in lacustrine environments. This is in contrast to marine environments where freshwater meets saline water at sharp ecological boundaries or in transition zones with brackish water, as observed in estuaries. Therefore, fluvially dominated environments were categorically excluded for further investigations, especially after several recovered Pürckhauer sediment cores in this environment were dominated by clastic deposits.

ii) Coastal wetlands

Low-lying coastal plains that are not influenced by fluvial processes delivering detrital components to the environment naturally consist predominantly of extensive wetlands with organic matter-rich deposits in temperate climate of Swiss lakes (Leupi & Marti, 1990). The historical Dufour and Siegfried maps indicate that these environments have been drastically reduced due to shoreline stabilization, agricultural land and infrastructure development.

Hürlimann (1951) reported a drastic retreat of reed belts around many Swiss lakes in the 1950s. Leupi and Marti (1990) quantified coastal peatland decrease at Lake Lucerne between 1900 to 1990 with ~75% from 470'000 to 120'000 m^2.

Because peatlands are considered a potential archive for past tsunami inundation, some limitations on the preservation of carbonate particles need to be considered. High concentrations of humic acids present in wetlands reduce the stability of carbonate and may dissolve the particles over time, but carbonate precipitation may also occur when the groundwater table is above a critical level (Almendigner & Leete, 1998). Consequently, only a small fraction of lake-derived clastic constituents, namely siliciclastic and oxide minerals, will be preserved in the long-term, because lacustrine sediments generally high in carbonate content.

Although, large amounts of reed belts have been destroyed due to coastal infrastructure and agriculture since the 1930s (e.g., Lucerne railway station area and adjacent area to the east). And although, few wetlands remain pristine but protected areas today. These environments are considered to have high potential for identifying sedimentary signatures of past lake tsunamis if the area was inundated and nearby sediment was available as stated earlier.

iii) Offshore environment

The offshore environment provides a relatively pristine lake environment. Although strong environmental pressures from public and private shipping are obvious. The effects on the uppermost sediment stratigraphy have not been systematically studied, but are considered as significant, especially in shallow waters. Additionally, sediment reworking above the wave-base need to be considered. Nevertheless, the offshore environment is regarded as a potential environment for identifying tsunami deposits in the marine setting as well, especially in areas where the terrestrial record is fragmentary for a variety reason (e.g., coastal infrastructures). An offshore depression at Lake Lucerne has been shown to be a suitable archive for the historical lacustrine tsunami event in 1601 CE (Nigg et al., subm.).

Multiproxy analysis

For the recognition of lake tsunami deposits, we used multiproxy analysis including core scanning (MSCL, CT, and XRF scanning), particle-size analysis, mineralogical composition, elemental concentration (C, N, and S), and radiocarbon dating. The full core scanning

techniques applied provide a rapid overview of the sedimentological properties of the recovered sediment cores. This can be helpful in the recognition of tsunami deposit candidates for more detailed investigation and is especially important when dealing with large numbers of sediment cores and study sites. Further, CT-scan data are very useful for characterizing three-dimensional sedimentary structures from the cm to the um-scale that are not obvious to the naked eye (Falvard & Paris, 2017) and elemental ratios obtained from XRF-scan data may further provide grain-size indicators (e.g., Wu et al., 2020). Particle-size distribution, mineralogical composition and elemental concentration may offer indications of sediment source. Adequate dating of the potential tsunami deposit using appropriate samples of short-lived (e.g., needles and seeds) terrestrial plant species, as well as correlatable well-dated and identified tsunami source is fundamental to their identification. The latter are provided from previous study of-lake bathymetry (Hilbe et al., 2011; Kremer et al., 2015), seismic-stratigraphic event catalogue (Kremer et al., 2015; Schnellmann et al., 2006), and historical sources (e.g., Cysat, 1969).

Sedimentary signatures

The sedimentary signatures of lacustrine tsunami events have been studied in only a few case studies (see review by Kremer et al., 2020a). The marine counterpart, however, is a growing field of research in sedimentology, greatly amplified by the devastating 2004 CE Indian Ocean tsunami and the 2011 CE Tohoku-oki tsunami. Hence, the criteria developed to identify tsunami deposits have been mainly established in the marine setting and are only partially applicable to lacustrine environments. Nevertheless, sedimentary textures of tsunami deposits in the marine and freshwater settings, are expected to be similar. But need to be better described, especially in the lacustrine environment, in order to make more robust statements.

Onshore tsunami deposits have been solely observed at Lake Sils and are characterized as clastic event deposits with internal fining-upward sequences and sharp lower contacts. In the offshore setting, the geological record of past lacustrine tsunami events may be divided into two types of sedimentary deposits. On the one hand, depositional signatures of voluminous subaerial and subaqueous mass movements that generated past tsunamis may be observable in the lake bathymetry, sediment cores, and seismic reflection data from the deep lake basins (e.g., Hilbe and Anselmetti, 2015; Kremer et al., 2015; Schnellmann et al., 2002). On the other hand, depositional signatures that recorded the effects of tsunami waves itself. This may be the deposition of finely laminated deposits on the top of mass-movement bodies in the deep lake

basin that were caused by bottom currents. However, it is likely that these signatures are related to the lake's response to the tsunami in the form of bottom currents of a seiche that causes oscillation of the entire lake and lasts for several days, as observed for the 1601 CE Lake Lucerne tsunami event. Therefore, this criterion could be used to demonstrate that also large prehistoric subaqueous mass movements-generated tsunami waves, especially for postulated events for which no other evidence has been found. However, this has not been investigated further.

The coastal offshore domain, however, has been found to provide a promising geological archive of past events. Large amounts of sediment is eroded, transported and remobilized from tsunami inundation and backwash currents and ultimately deposited in the geological archive. At Lake Lucerne and Lake Sils sedimentary signatures of past tsunamis have been identified in sediment cores and seismic reflection data of the shallow-water environment (Nigg et al., 2021, subm.). At Lake Lucerne a nearshore depression hosts an event deposit with an internal normal graded succession of siliciclastic medium sand to coarse silt (Nigg et al., subm.). Additionally, a single sediment core from an amphitheater-like setting in the southeastern area of the Lucerne Bay provides evidence for prehistoric tsunami-induced bottom currents and deposition of dense, clastic cm-thick layers with mm-scale lamina and cross-bedding structures that are associated with previously seismically mapped subaqueous mass movements around 2200 and 5400 BP (Schnellmann et al., 2006).

At Lake Sils Nigg et al. (2021) were able to reconstruct a prehistoric tsunami generated from a partial delta collapse on Lake Sils based on sediment cores recovered from the coastal on- and offshore environment combined with numerical mass-movement and tsunami propagation simulations. The described tsunami deposit consists of a heterogeneous sedimentary package with gravel, single and multiple normal graded sand sequences with a well-pronounced clay cap offshore and a landward continuous single-graded thinning and fining (Nigg et al., 2021).

3.5 Conclusions

Alpine lakes are susceptible to tsunami hazard from subaqueous and subaerial mass movements that can be triggered from strong regional earthquakes, lakeshore mining activities, and apparently spontaneous failures. The associated phenomena have been documented in contemporary chronicles, artwork, and newspaper articles. These documents provide a unique

opportunity to examine the effects of tsunami inundation in coastal areas of the lacustrine environment, as well as to localize their occurrence in space and time and characterize their ultimate triggering mechanisms.

To reconstruct the recurrence rate of lake tsunamis to the prehistoric period, lake bathymetry, and the mass-movement event stratigraphy previously used to study strong earthquakes may be useful. However, tsunami triggering by subaerial and subaqueous mass movements is strongly dependent on failure kinematics and slide mechanism. Therefore, tsunami deposits from the coastal on- and offshore areas need to be studied sedimentologically to ultimately reconstruct the chronology of lake tsunami events. Because, their sedimentological signatures have been sparsely investigated, we developed a sophisticated workflow for site selection based on geomorphological criteria. We then presented the evidence of tsunami-induced sediment remobilization and deposition from recovered sediment cores, but also discussed sediment cores where no traces could be associated with past events.

To identify lake tsunami deposits, we used sedimentological multi-proxy analysis, including whole-core scanning (density, magnetic susceptibility, CT, and XRF), as well as micro-CT scanning of sediment U-channels, radiocarbon dating, and grain-size analysis. Sedimentary signatures preserved from past events were observed predominantly in the coastal offshore area, whereas onshore deposits were only recognized at Lake Sils. This may be due to poor sediment preservation in the onshore, highly modified shoreline areas, but also to the difficulty of good core recovery within a heterogeneous sediment stratigraphy. However, the observed sedimentological signatures can be summarized as clastic event deposits in the cm- to dm range, with generally sharp lower and upper sedimentological contacts, single and multiple normal graded sand, massive sand, layering of fines and carbonate shell fragments, and fine-grained (clayey) deposits at the top from suspension settling at the terminal stage of a tsunami event when calm returned to the water body.

Acknowledgments

This work was funded by the Swiss National Science Foundation (research grant no.: 171017) and is embedded in the SNSF Sinergia Project “Lake tsunami: causes, controls and hazard”. Nicole Schwendener and the Institute of Anatomy, University of Bern are acknowledged for their support with the CT scanning. Daniela Fischer and the Institute of Geography, University

of Bern are thanked for their support with the grain-size determination. Sönke Szidat and the Department of Chemistry and Biochemistry, University of Bern are acknowledged for the radiocarbon dating. Julijana Krbanjevic is acknowledged for her help with the geochemical analysis. Firtz Schlunegger and Beat Keller are thanked for their useful comments on the manuscript. Franzyska Nyffenegger, Dominik Amschwand, Julijana Krbanjevic, Flavio Huber, Evelyne Margelisch, Anastasiia Shynkarenko, Patrick Schläfli, Katrina Kremer, Michael Strupler, Stefano Fabbri, Adrian Gilli and Marina Morlock are thanked very much for their support during the coring campaign. Anneleen Foubert, Christoph Neurur and Marina Morlock are acknowledged for the support with the micro-CT scanning analysis. We are very thankful to the following municipalities, institutions, and private person: Buchillon (VD), Collonge-Bellerive (GE), Weggis (LU), Küssnacht a.R. (SZ), Ennetbürgen (NW), Préverenges (VD), Sciex (France), Sils i.E. (GR), St. Sulpice (VD), City of Geneva (GE), Lausanne (VD), and Lucerne (LU) as well as the TCS camping Pointe à la Bise, Strandbad Tribschen in the City of Lucerne and Mr. Ital von Reding. Mathias Seifert and the Archeological Service of the Canton of Grisons are acknowledged for information about archeological findings in the Upper Engadine. We are very thankful to the municipality of Sils i.E. and Antonio Walther, who supported our study.

References

Abe, T., Goto, K., & Sugawara, D. (2012) Relationship between the maximum extent of tsunami sand and the inundation limit of the 2011 Tohoku-oki tsunami on the Sendai Plain, Japan. Sedimentary Geology, 282, 142-150.

Almendinger, J. E., & Leete, J. H. (1998) Peat characteristics and groundwater geochemistry of calcareous fens in the Minnesota River Basin, USA. Biogeochemistry, 43(1), 17-41.

Bellwald, B. (2012) Paleoseismologic Implications of the Sediment Stratigraphy in Lake Silvaplana (Engadine, Eastern Switzerland). MSc thesis. ETH Zürich.

Billeter, J. (1923) Pfarrer Jakob Billeter von Aegeri und seine Chronik. Heimat-Klänge, Sonntags-Beilage zu den «Zuger Nachrichten», 3. Jahrgang, Nr. 4, 28. January, 15–16.

Blass, A., Anselmetti, F. S., Grosjean, M., & Sturm, M. (2005) The last 1300 years of environmental history recorded in the sediments of Lake Sils (Engadine, Switzerland). Eclogae Geologicae Helvetiae, 98(3), 319-332.

Bondevik, S., Svendsen, J. I., Johnsen, G., Mangerud, J. A. N., & Kaland, P. E. (1997) The Storegga tsunami along the Norwegian coast, its age and run up. Boreas, 26(1), 29-53.

Bryant, E. (2014). Tsunami: the underrated hazard. Springer.

Bünti, J.L. (1973) Chronik des Johann Laurentz Bünti, Landammann, 1661–1736. Beiträge zur Geschichte Nidwaldens, 34,26–27.

Bussmann, F., & Anselmetti, F. S. (2010) Rossberg landslide history and flood chronology as recorded in Lake Lauerz sediments (Central Switzerland). Swiss Journal of geosciences, 103(1), 43-59.

Chesne, du, J. (1587) Le grand miroir du monde / par Joseph Du Chesne, sieur de La Violette, conseiller et médecin ordinaire du roy ; à la fin de chasque livre sont de nouveau adjoustées amples annotations et observations sur le texte, pour l'explication de plusieurs difficultez, et ce en faveur des personnes moins exercées ès diverses parties de la philosophie divine et humaine par S.G.S.

Clark, K., Upton, P., Carey, J. M., Rosser, B., & Strong, D. (2015) Tsunami and Seiche Hazard Scoping Study for Lakes Tekapo, Pukaki, Ohau, Alexandrina and Ruataniwha

Cysat, R. (1969) Collectanea Chronica und denkwürdige Sachen pro Chronica Lucernensi et Helvetiae. Erster Band, zweiter Teil (Eds J. Schmid and D. Schilling), pp. 879– 888. Diebold Schilling Verlag, Luzern.

Dawson, A. G., and Shi, S. (2000). Tsunami Deposits. Pure Appl. Geophys. 157, 875–897.

Dawson, A. G., Long, D., & Smith, D. E. (1988) The Storegga slides: evidence from eastern Scotland for a possible tsunami. Marine geology, 82(3-4), 271-276.

Dawson, S., Smith, D. E., Ruffman, A., & Shi, S. (1996) The diatom biostratigraphy of tsunami sediments: examples from recent and middle Holocene events. Physics and Chemistry of the Earth, 21(1-2), 87-92.

Deák, J., Magny, M., & Wüthrich, S. (2018) Late Neolithic to Middle Bronze Age (around 4900–3100 cal. BP) lake-level fluctuations at Lake Neuchâtel (Switzerland) as reflected by the sediment sequence of the site of Colombier/Les Plantées de Rive: Palaeoclimatic and archaeological implications. The Holocene, 28(1), 3-18.

Deichmann N, Baer M, Braunmiller J et al (2000) Earthquakes in Switzerland and surrounding regions during 1999. Grunthal 93:23–45.

Delile, H., & Salomon, F. (2020) Palaeotsunami deposits at the Tiber River mouth (Ostia Antica, Italy): Do they really exist?. Earth-Science Reviews, 103268.

Dietrich, J. (1689) Diarium von P. Josef Dietrich von Einsiedeln (1645–1704), Bd. 6. Klosterarchiv Einsiedeln, KAE A.HB.6, p. 202.

Ducrey P (2006) Die ersten Kulturen zwischen Alpen und Jura. In: Mesmer B (ed) Geschichte der Schweiz und der Schweizer, 4th edn. Schwabe, Basel, pp 27–5.

Egli, E. (1901-1904) Das Erdbeben im Waadtland 1584. Zwingliana. Mitteilungen zur Geschichte Zwinglis und der Reformation. Vol. 1, 1897–1904, 240–245.

Einsele, G., Chough, S. K., & Shiki, T. (1996) Depositional events and their records—an introduction. Sedimentary Geology, 104(1-4), 1-9.

Fäh, D., Giardini, D., Kästli, P., Deichmann, N., Gisler, M., Schwarz-Zanetti, G., Alvarez-Rubio, S., Sellami, S., Edwards, B., Allmann, B., Bethmann, F., Wössner, J., Gassner-Stamm, G., Fritsche, S. and Eberhard, D. (2011) ECOS-09 Earthquake Catalogue of Switzerland, Release 2011, Report SED/ECOS/R/001/20110417. Swiss Seismological Service, ETH Zürich, 42 pp.

Falvard, S., & Paris, R. (2017). X-ray tomography of tsunami deposits: Towards a new depositional model of tsunami deposits. Sedimentology, 64(2), 453-477.

Favrod, J. (1991) La Chronique de Marius d'Avenches (455-581): texte, traduction et commentaire (Vol. 4). Section d'histoire, Faculté des lettres, Université de Lausanne.

Fiore, J., Girardclos, S., Pugin, A., Gorin, G., & Wildi, W. (2011) Würmian deglaciation of western Lake Geneva (Switzerland) based on seismic stratigraphy. Quaternary Science Reviews, 30(3-4), 377-393.

Frank, J. (1950) 100 Jahre Bezirksgemeinde Ennetbürgen, 1850 – 1950, und ihre Vorgeschichte. Gemeinde Ennetbürgen, 128 pp.

Fritsche, S., Fäh, D., & Schwarz-Zanetti, G. (2012) Historical intensity VIII earthquakes along the Rhone valley (Valais, Switzerland): primary and secondary effects. Swiss Journal of Geosciences, 105(1), 1-18.

Fuchs, H., & Boes, R. M. (2010) Berechnung felsrutschinduzierter Impulswellen im Vierwaldstättersee. Wasser Energie Luft, 102(3), 215-221.

Garduño-Monroy, V. H., Soria-Caballero, D. C., Israde-Alcántara, I., Hernández Madrigal, V. M., Rodríguez-Ramírez, A., Ostroumov, M., ... & Mora-Chaparro, J. C. (2011) Evidence of tsunami events in the Paleolimnological record of Lake Pátzcuaro, Michoacán, Mexico. Geofísica internacional, 50(2), 147-161.

Garrett, E., Shennan, I., Woodroffe, S. A., Cisternas, M., Hocking, E. P., & Gulliver, P. (2015) Reconstructing paleoseismic deformation, 2: 1000 years of great earthquakes at Chucalén, south central Chile. Quaternary Science Reviews, 113, 112-122.

Gelfenbaum, G., Vatvani, D., Jaffe, B., & Dekker, F. (2007) Tsunami inundation and sediment transport in vicinity of coastal mangrove forest. In Coastal Sediments' 07 (pp. 1117-1128).

Girardclos, S., Schmidt, O. T., Sturm, M., Ariztegui, D., Pugin, A., & Anselmetti, F. S. (2007) The 1996 AD delta collapse and large turbidite in Lake Brienz. Marine Geology, 241(1-4), 137-154.

Gisler, M., Fäh, D., & Kästli, P. (2004) Historical seismicity in central Switzerland. Eclogae Geologicae Helvetiae, 97(2), 221-236.

Goto, K., Chagué-Goff, C., Fujino, S., Goff, J., Jaffe, B., Nishimura, Y., ... & Yulianto, E. (2011) New insights of tsunami hazard from the 2011 Tohoku-oki event. Marine Geology, 290(1-4), 46-50.

Grimstad, E., & Nesdal, S. (1991) The Loen rockslides—a historical review. Publikasjon-Norges Geotekniske Institutt, 182, 1-6.

Grischott, R., Kober, F., Lupker, M., Hippe, K., Ivy-Ochs, S., Hajdas, I., ... & Christl, M. (2017) Constant denudation rates in a high alpine catchment for the last 6 kyrs. Earth Surface Processes and Landforms, 42(7), 1065-1077.

Gusiakov, V. K. (2009) Tsunami history: recorded. The sea, 15, 23-53.

Gylfadóttir, S. S., Kim, J., Helgason, J. K., Brynjólfsson, S., Höskuldsson, Á., Jóhannesson, T., ... & Løvholt, F. (2017) The 2014 Lake Askja rockslide-induced tsunami: Optimization of numerical tsunami model using observed data. Journal of Geophysical Research: Oceans, 122(5), 4110-4122.

Haas, I., Fabbri, S. C., Kremer, K., Girardclos, S., & Anselmetti, F. S. (in prep.) Subaqueous geomorphology and delta-dynamics of Lake Brienz (Switzerland): implications for the sediment budget in the perialpine realm.

Hemphill-Haley, E. (1996) Diatoms as an aid in identifying late-Holocene tsunami deposits. The Holocene, 6(4), 439-448.

Hilbe, M., & Anselmetti, F. S. (2015) Mass movement-induced tsunami hazard on perialpine Lake Lucerne (Switzerland): scenarios and numerical experiments. Pure and Applied Geophysics, 172(2), 545-568.

Hilbe, M., Anselmetti, F.S., Eilertsen, R.S., Hansen, L. and Wildi, W. (2011) Subaqueous morphology of Lake Lucerne (Central Switzerland): implications for mass movements and glacial history. Swiss J. Geosci., 104, 425–433.

Hori, K., Kuzumoto, R., Hirouchi, D., Umitsu, M., Janjirawuttikul, N., & Patanakanog, B. (2007) Horizontal and vertical variation of 2004 Indian tsunami deposits: an example of two transects along the western coast of Thailand. Marine Geology, 239(3-4), 163-172.

Huber, A. (1982) Felsbewegungen und Uferabbrüche an Schweizer Seen, ihre Ursachen und Auswirkungen. Eclogae Geologicae Helvetiae, 75 (3): 563-578.

Hürlimann, H. (1951) Zur Lebensgeschichte des Schilfs an den Ufern der Schweizer Seen. Beiträge zur geobotanischen Landesaufnahme der Schweiz, 30:1-232.

Ishimura, D., & Yamada, K. (2019) Palaeo-tsunami inundation distances deduced from roundness of gravel particles in tsunami deposits. Scientific reports, 9(1), 1-8.

Jaffe, B. E., Goto, K., Sugawara, D., Richmond, B. M., Fujino, S., & Nishimura, Y. (2012) Flow speed estimated by inverse modeling of sandy tsunami deposits: results from the 11 March 2011 tsunami on the coastal plain near the Sendai Airport, Honshu, Japan. Sedimentary Geology, 282, 90-109.

Keller, B. (2020) Lake Lucerne and Its Spectacular Landscape. In Landscapes and Landforms of Switzerland (pp. 305-323). Springer, Cham.

Kempf, P., Moernaut, J., Van Daele, M., Vandoorne, W., Pino, M., Urrutia, R., & De Batist, M. (2017) Coastal lake sediments reveal 5500 years of tsunami history in south central Chile. Quaternary Science Reviews, 161, 99-116.

Klyuchevskii, A. V., Demyanovich, V. M., & Klyuchevskaya, A. A. (2012) The possibility of a tsunami on Lake Baikal. In Doklady Earth Sciences (Vol. 442, No. 1, pp. 130-134). SP MAIK Nauka/Interperiodica.

Knapp, S., Gilli, A., Anselmetti, F. S., Krautblatter, M., & Hajdas, I. (2018) Multistage rock-slope failures revealed in lake sediments in a seismically active Alpine region (Lake Oeschinen, Switzerland). Journal of Geophysical Research: Earth Surface, 123(4), 658-677.

Kremer, K., Anselmetti, F. S., Evers, F. M., Goff, J., & Nigg, V. (2020a) Freshwater (paleo) tsunamis–a review. Earth-Science Reviews, 103447.

Kremer, K., Gassner-Stamm, G., Grolimund, R., Wirth, S. B., Strasser, M., & Fäh, D. (2020b) A database of potential paleoseismic evidence in Switzerland. Journal of Seismology, 1-16.

Kremer, K., Hilbe, M., Simpson, G., Decrouy, L., Wildi, W., & Girardclos, S. (2015) Reconstructing 4000 years of mass movement and tsunami history in a deep peri-Alpine lake (Lake Geneva, France-Switzerland). Sedimentology, 62(5), 1305-1327.

Kremer, K., Simpson, G., & Girardclos, S. (2012) Giant Lake Geneva tsunami in ad 563. Nature Geoscience, 5(11), 756-757.

Kremer, K., Wirth, S. B., Reusch, A., Fäh, D., Bellwald, B., Anselmetti, F. S., ... & Strasser, M. (2017) Lake-sediment based paleoseismology: Limitations and perspectives from the Swiss Alps. Quaternary Science Reviews, 168, 1-18.

Leupi, E., & Marti, K. (1990) Die Riedgebiete am Vierwaldstättersee. Mitteilung der Naturforschenden Gesellscahft Luzern, 31, 135-149.

Loizeau, J.-L. (1991) La sédimentation récente dans le delta du Rhône, Léman: processus et évolution. Thèse No 2514, Université de Genève, 209.

Løvholt, F., Bondevik, S., Laberg, J. S., Kim, J., & Boylan, N. (2017) Some giant submarine landslides do not produce large tsunamis. Geophysical Research Letters, 44(16), 8463-8472.

Minoura, K., Imamura, F., Kuran, U., Nakamura, T., Papadopoulos, G. A., Takahashi, T., & Yalciner, A. C. (2000). Discovery of Minoan tsunami deposits. Geology, 28(1), 59-62.

Monecke, K., Anselmetti, F. S., Becker, A., Schnellmann, M., Sturm, M., & Giardini, D. (2006) Earthquake-induced deformation structures in lake deposits: A Late Pleistocene to Holocene paleoseismic record for Central Switzerland. Eclogae Geologicae Helvetiae, 99(3), 343-362.

Monecke, K., Finger, W., Klarer, D., Kongko, W., McAdoo, B. G., Moore, A. L., & Sudrajat, S. U. (2008) A 1,000-year sediment record of tsunami recurrence in northern Sumatra. Nature, 455(7217), 1232-1234.

Montandon, F. (1925) Les Eboulements de la Dent du Midi et du Grammont (Examen critique de la question de Tauredunum). Le Globe. Revue genevoise de géographie, 64(1), 35-91.

Mountjoy, J. J., Wang, X., Woelz, S., Fitzsimons, S., Howarth, J. D., Orpin, A. R., & Power, W. (2019) Tsunami hazard from lacustrine mass wasting in Lake Tekapo, New Zealand. Geological Society, London, Special Publications, 477(1), 413-426.

Moscariello, A. (1997) Lacustrine ooidal sands in Lake Geneva (Switzerland): Sedimentological evidence for high-energy conditions and lake-level rise in the Late Bronze Age. Climatic implications and constraints on the. Eclogae Geologicae Helvetiae, 90(1), 143-150.

Nigg, V., Wohlwend, S., Hilbe, M., Bellwald, B., Fabbri, S. C., de Souza, G. F., ... & Anselmetti, F. S. (2021) A tsunamigenic delta collapse and its associated tsunami deposits in and around Lake Sils, Switzerland. Natural Hazards, 1-35.

Nigg, V., Bacigaluppi, P., Vetsch, D. F., Vogel, H., Lremer K., & Anselmetti F. S. (subm.) Tsunami offshore deposits: evidence from sediment cores and numerical wave propagation of the 1601 CE Lake Lucerne event.

Ostendorp, W. (1989) 'Die-back'of reeds in Europe—a critical review of literature. Aquatic Botany, 35(1), 5-26.

Papadopoulos, G. A., & Imamura, F. (2001). A proposal for a new tsunami intensity scale. In ITS 2001 proceedings (Vol. 5, pp. 569-577).

Reusch, A. M. (2016) Sublacustrine paleoseismology and fluid flow in the Western Swiss Molasse Basin: New constraints from the sedimentary archive of Lake Neuchâtel-Mass-transport deposits, subsurface sediment mobilization and geomorphology (Doctoral dissertation, ETH Zurich).

Reymond, M. (1917) La chronique de Jehan Dumur (du Mur). Revue historique Vaudoise, 271–286.

Richmond, B. M., Jaffe, B. E., Gelfenbaum, G., & Morton, R. A. (2006) Geologic impacts of the 2004 Indian Ocean tsunami on Indonesia, Sri Lanka, and the Maldives. Zeitschrift für Geomorphologie, 146, 235-251.

Roberts, N. J., McKillop, R. J., Lawrence, M. S., Psutka, J. F., Clague, J. J., Brideau, M. A., & Ward, B. C. (2013) Impacts of the 2007 landslide-generated tsunami in Chehalis Lake, Canada. In Landslide science and practice (pp. 133-140). Springer, Berlin, Heidelberg.

Schardt H (1892) Notice sur l'effondrement du Quai du Trait de Baye à Montreux, précédée de quelques considérations générales sur la morphologie geophysique des rives lacustres, la formation des cones de déjection, etc. Bull. de la Soc. Vaudoise des Sciences Naturelles XXVIII(109):231–265.

Schnellmann, M., Anselmetti, F. S., Giardini, D., McKenzie, J. A., & Ward, S. N. (2002) Prehistoric earthquake history revealed by lacustrine slump deposits. Geology, 30(12), 1131-1134.

Schnellmann, M., Anselmetti, F. S., Giardini, D., & Mckenzie, J. A. (2006) 15,000 Years of mass-movement history in Lake Lucerne: Implications for seismic and tsunami hazards. Eclogae Geologicae Helvetiae, 99(3), 409-428.

Schoeneich, P., Weidmann, M. & Blomjous, C. (2015) L'énigme du Tauredunum enfin résolue? In: Le Rhône, entre nature et société. Emmanuel Reynard (Ed.). Sion, pp. 153-174.

Schwarz-Zanetti, G., Deichmann, N., Fäh, D., Giardini, D., Jimenez, M.-J., Masciadri, V., Schibler, R. and Schnellmann, M. (2003) The earthquake in Unterwalden on September 18, 1601: a historico-critical macroseismic evaluation. Eclogae Geol. Helv., 96, 441–450.

Schwarz-Zanetti, G., Fäh, D., Gache, S., Kästli, P., Loizeau, J., Masciadri, V., & Zenhäusern, G. (2018) Two large earthquakes in western Switzerland in the sixteenth century: 1524 in Ardon (VS) and 1584 in Aigle (VD). Journal of Seismology, 22(2), 439-454.

Schwestermann, T. (2016) Mass-movement Event Stratigraphy in Lake Constance. MSc Thesis, ETH Zürich.

Siegenthaler, C., Finger, W., Kelts, K. and Wang, S. (1987) Earthquake and seiche deposits in Lake Lucerne, Switzerland. Eclogae Geol. Helv., 80, 241–260.

Spiske, M., Tang, H., & Bahlburg, H. (2020) Post-depositional alteration of onshore tsunami deposits–Implications for the reconstruction of past events. Earth-Science Reviews, 202, 103068.

Strasser, M., Monecke, K., Schnellmann, M., & Anselmetti, F. S. (2013) Lake sediments as natural seismographs: A compiled record of Late Quaternary earthquakes in Central Switzerland and its implication for Alpine deformation. Sedimentology, 60(1), 319-341.

Strupler, M., Hilbe, M., Kremer, K., Danciu, L., Anselmetti, F. S., Strasser, M., & Wiemer, S. (2018) Subaqueous landslide-triggered tsunami hazard for Lake Zurich, Switzerland. Swiss journal of geosciences, 111(1-2), 353-371.

Switzer, A. D., Srinivasalu, S., Thangadurai, N., & Mohan, V. R. (2012) Bedding structures in Indian tsunami deposits that provide clues to the dynamics of tsunami inundation. Geological Society, London, Special Publications, 361(1), 61-77.

Szczuciński, W., Chaimanee, N., Niedzielski, P., Rachlewicz, G., Saisuttichai, D., Tepsuwan, T., ... & Siepak, J. (2006) Environmental and Geological Impacts of the 26 December 2004 Tsunami in Coastal Zone of Thailand--Overview of Short and Long-Term Effects. Polish Journal of Environmental Studies, 15(5).

Szczuciński, W., Kokociński, M., Rzeszewski, M., Chagué-Goff, C., Cachão, M., Goto, K., & Sugawara, D. (2012) Sediment sources and sedimentation processes of 2011 Tohoku-oki tsunami deposits on the Sendai

Plain, Japan—insights from diatoms, nannoliths and grain size distribution. Sedimentary Geology, 282, 40-56.

Wiemer S, Danciu L, Edwards B, Marti M, Fäh D, Hiemer S, Wössner J, Cauzzi C, Kästli P, Kremer K (2016) Seismic hazard model 2015 for Switzerland. Swiss Seismological Service (SED) at ETH Zurich, Zurich, pp 1–163.

Wiemer, S., Giardini, D., Fäh, D., Deichmann, N., & Sellami, S. (2009) Probabilistic seismic hazard assessment of Switzerland: best estimates and uncertainties. Journal of Seismology, 13(4), 449.

Wirth, S. (2008) Lake Thun sediment record: 300 years of human impact, flood events and subaquatic slides (Master's thesis, Federal Institute of Technology ETH, Department of Earth Sciences).

Wohlfarth, B., & Schneider, A. M. (1991) Late Glacial and Holocene lake level fluctuations in lake Biel, Western Switzerland. Journal of Quaternary Science, 6(4), 293-302.

Woodroffe, C. D. (2000) Deltaic and estuarine environments and their Late Quaternary dynamics on the Sunda and Sahul shelves. Journal of Asian Earth Sciences, 18(4), 393-413.

Wu, L., Wilson, D. J., Wang, R., Yin, X., Chen, Z., Xiao, W., & Huang, M. (2020) Evaluating Zr/Rb Ratio From XRF Scanning as an Indicator of Grain-Size Variations of Glaciomarine Sediments in the Southern Ocean. Geochemistry, Geophysics, Geosystems, 21(11), e2020GC009350.

Zimmermann, J. (2008) Der Walensee: eine sedimentologische Rekonstruktion seiner holozänen Ereignisgeschichte. PhD thesis, Geographisches Institut der Universität Zürich.

Historical map of the course of the Inn River and its tributaries in the Upper Engadine showing the chain of the four Engadine lakes Sils, Silvaplana, Champfèr and St. Moritz in 1707 (Scheuchzer, 1723).

4 A tsunamigenic delta collapse and its associated tsunami deposits in and around Lake Sils, Switzerland

Valentin Nigg [1], Stephan Wohlwend [2], Michael Hilbe [1], Benjamin Bellwald [3], Stefano C. Fabbri [1], Gregory F. de Souza [4], Florian Donau [2], Reto Grischott [2], Michael Strasser [5], Flavio S. Anselmetti [1]

[1] Institute of Geological Sciences & Oeschger Centre for Climate Change Research, University of Bern, Baltzerstrasse 1+3, 3012 Bern, Switzerland
[2] Geological Institute, ETH Zurich, Sonneggstrasse 5, 8092 Zürich, Switzerland
[3] Volcanic Basin Petroleum Research (VBPR), Høienhald, Blindernveien 5, 0361 Oslo, Norway
[4] Institute of Geochemistry and Petrology, ETH Zurich, Clausiusstrasse 25, 8092 Zürich, Switzerland
[5] Department of Geology, University of Innsbruck, Innrain 52, 6020 Innsbruck, Austria

Manuscript published in Natural Hazards (2021)
https://doi.org/10.1007/s11069-021-04533-y

Abstract

Large lacustrine mass movements and delta collapses are increasingly being considered as potential tsunamigenic sources and therefore hazardous for the population and infrastructure along lakeshores. Although historical reports document tsunami events in several lakes in Switzerland, and although the propagation of lake tsunamis has been studied by numerical wave modeling, only little is known about on- and offshore lacustrine tsunami deposits. In Lake Sils, Switzerland, a large prehistoric mass-movement deposit originating from the Isola Delta with a minimum estimated volume of 6.5 x 10^6 m^3 and a basinal thickness of > 6 m in the seismic record has been identified by previous studies and radiocarbon dated to around 700 Common Era. Here, we combine i) comprehensive sedimentological investigation of sediment cores recovered from the on- and offshore settings, ii) mineralogical fingerprinting of the

inflows from key catchments to characterize sediment provenance, and iii) numerical tsunami modeling, to test the hypothesis of a tsunamigenic delta collapse in Lake Sils. We observe a clastic event deposit consisting of coarse-grained, fining-upward sand overlying an organic-rich peat deposit in the shallow water. This layer thins and fines landward on the coastal plain. Toward the deeper water (20–40 m), the deposit transforms into a thicker and more heterogeneous sediment package with multiple sequences of fining-upward sand and a well-pronounced clay cap at the top. Radiocarbon dating of the peat underlying the event deposit yields a maximum age of 225–419 calibrated Common Era. The tsunami models, which indicate wave heights reaching up to 5 m, simulate areas of inundation that coincide with the location of event deposits. Based on our results, we propose that the historically undocumented Isola Delta collapse generated a basin-wide tsunami that inundated the lakeshore, transporting large amounts of unconsolidated sediment along the lakeshore toward the coastal plain and into the deeper lake basin.

4.1 Introduction

Historical documents and recent scientific investigations provide evidence that large subaqueous mass movements and delta collapses are capable of generating tsunamis in lakes (Hilbe and Anselmetti, 2015; Kremer et al., 2012). Besides impacts from rockfalls and subaerial landslides, subaqueous mass movements are considered as the most common triggering mechanism for lacustrine tsunami generation. Even though their wavelength is much shorter than that of their marine counterparts, lacustrine tsunamis have wavelengths of several hundred meters, which clearly distinguish them from wind-induced waves in these basins. At Lake Lucerne in central Switzerland, historical documents report anomalously large waves in 1601 and 1687 Common Era (CE) (Hilbe and Anselmetti, 2014). These effects were attributed to large subaqueous mass movements, which were adequately simulated with numerical tsunami generation and propagation models (Hilbe and Anselmetti, 2015). Other historical documents report a severe tsunami in Lake Geneva generated by the Rhone Delta collapse (Kremer et al., 2012). In Lake Brienz, a small-scale tsunami was observed following a partial collapse of the main delta in 1996 CE (Girardclos et al., 2007).

Although tsunamis are reported in lakes, the related on- and nearshore lacustrine tsunami deposits are rarely documented. For example, subaqueously generated boulder ridges, sediment-wave channels, and gently sloping tsunami erosion surfaces provide morphological

evidence for a prehistoric tsunami in Lake Tahoe (Nevada-California, USA; Moore et al. (2014)). In the shallow Lake Owens (California, USA), unusual poorly sorted and upward-graded pebbly sand with mud is likely related to the 1872 CE earthquake-induced seiche (wave height ~50 cm) that eroded much of the lakebed (Smoot et al., 2000). In Lake Patzcuaro (Mexico), heterogeneous sand and silt with angular lithoclasts, ceramic artifacts and abundant remains of fish bones, bivalves, gastropods and pelagic species are deposited above an erosional unconformity to the underlying unit (Garduño-Monroy et al., 2011). In Lake Chehalis (Canada), a subaerial landslide-generated tsunami caused severe shore destruction in 2007 CE (Roberts et al., 2013).

In marine settings, on the other hand, tsunami deposits are widely studied to infer past tsunami events in a broad range of coastal areas (e.g., Bourgeois et al., 2009; Costa and Andrade, 2020; Dawson and Stewart, 2007; Engel and Brückner, 2011). During tsunami inundation and backwash, a vast amount of shoreface and beach sediment is eroded, transported, and redeposited in the coastal environment, and subsequently moved offshore (e.g., Einsele et al., 1996; Fujiwara and Kamataki, 2007; Goto et al., 2011; Paris et al., 2010; Sakuna et al., 2012; Sugawara et al., 2008). The associated tsunami deposits are commonly site-specific and characterized by a wide range of sedimentological features depending on coastal geomorphology and microtopography (e.g., Hori et al., 2007; Matsumoto et al., 2016 Nishimura et al., 2015), sediment availability (e.g., Dawson and Shi, 2000; Goff et al., 2009; Meilianda et al., 2010), as well as tsunami magnitude (e.g., Yamaguchi and Sekiguchi, 2015; Ishimura and Yamada, 2019; Putra et al., 2019), and preservation potential (e.g., Brill et al., 2020; Goto et al., 2012; Spiske et al., 2020; Szczuciński, 2012). Hence, research on tsunami deposits requires multiproxy sedimentary analyses, including sedimentological, geochemical, and biological approaches (e.g., Goff et al., 2010; Judd et al., 2017; Ramirez-Herrera et al., 2012).

Sedimentary structures such as erosional basal contacts, fining-upward sequences and rip-up clasts are the most common physical textural characteristics found in onshore tsunami deposits in various coastal settings worldwide (e.g., Bondevik et al., 2005; Gelfenbaum and Jaffe, 2003; Srinivasalu et al., 2009). On the other hand, tsunami events may leave no traces in the geological record, especially along rocky coasts, where sediment supply is limited (e.g., Dawson and Shi, 2000), or tsunami inundation may be indicated through erosional unconformities in coastal sand barriers (e.g., Costa et al., 2016). Additionally, geochemical

proxies such as Na, S, and Cl concentrations (e.g., Goff et al., 2012; Szczuciński et al., 2006) and/or biogenic contents are used to identify marine tsunami deposits. For example pelagic and benthic fauna are used to infer tsunami deposits and their sediment source (e.g., Garrett et al., 2015; Kitamura et al., 2018; Smedile et al., 2020; Szczuciński et al., 2012; Tanigawa et al., 2018). Terrestrial sedimentary records are used to infer minimum tsunami inundation (e.g., Chagué-Goff et al., 2012; Moreira et al., 2017) and run-up height (e.g., Bondevik et al., 2005; Costa et al., 2016; La Selle et al., 2020; Paris et al., 2020). Based on the internal structure, composition, and spatial distribution of tsunami deposits, it may be possible to estimate magnitude and flow conditions by tsunami inverse modeling (e.g., Jaffe and Gelfenbaum, 2007; Jaffe et al., 2012; Spiske et al,. 2010; Woodruff et al., 2008). Such studies are directly applicable for coastal tsunami hazard assessments (e.g. Engel et al., 2016; Leonard et al., 2014 and references therein).

Compared to the onshore realm, the number of scientific publications describing offshore tsunami deposits is limited (e.g., Dawson and Stewart, 2008). Although the combined investigation of on- and offshore tsunami deposits may provide a more robust and accurate reconstruction of past events (Costa and Andrade, 2020), only few case studies describe offshore tsunami deposits (e.g., Goodman-Tchernov et al., 2009; Paris et al., 2010; Smedile et al., 2020; Tamura et al., 2015). For example, Sakuna et al. (2012) describe poorly-sorted mud including terrigenous and anthropogenic components, which were transported from backwash currents of the 2004 Indian Ocean tsunami into the shallow marine environment of the Andaman Sea off the coast of Thailand. Paris et al. (2010) characterize tsunami-derived boulder deposits from the 2004 CE Indian Ocean tsunami in the offshore setting Lhok Nga, Indonesia. Recently, tsunami backwash deposits from the 2009 CE South Pacific tsunami and 1960 CE Great Chilean earthquake tsunami were encountered in sediment cores from the sheltered Pago Pago Bay (USA) based on grain-size analysis, geochemical proxy analysis, sediment thin sections, and ^{137}Cs and ^{210}Pb dating (Riou et al., 2020). These deposits are characterized by terrigenous sediment transported as a dense and cohesive hyperpycnal flow that induced shearing of the underlying sediment (Riou et al., 2020).

Based on sediment cores collected on the coastal plain and in the shallow water, this study provides evidence for a lacustrine tsunami event in the proglacial Lake Sils, located in the Upper Engadine, Switzerland (Fig. 4-1). The proposed mechanism for the tsunami initiation is a large delta-slope collapse around 548–797 calibrated Common Era (cal CE) with an

estimated minimum volume of the mass-movement deposit in Lake Sils of 6.5 x 10^6 m^3 (Blass et al., 2005).

4.2 Study site

Lake Sils (surface area: 4.1 km^2) is located in the Upper Engadine in southeastern Switzerland at 1797 m above sea level (m a.s.l). The lake is connected downstream with Lake Silvaplana, Lake Champfèr, and Lake St. Moritz, draining the valley toward the northeast (Fig. 4-1). The Maloja Pass (1815 m a.s.l) in the southwest of Lake Sils separates the Engadine valley from the Val Bregaglia, which drains southward toward Chiavenna in northern Italy. The catchment of Lake Sils is situated in a complex geological area consisting of the Austroalpine and Penninic nappes (Fig. 4-1). The Austroalpine nappes consist of the Margna nappe to the south of the lake and the Err nappe north of the lake, respectively (Spillmann and Büchi, 1993). The Penninic Platta nappe in the northeast consists of an ophiolitic sequence originating from the South Penninic realm (Dietrich, 1970). A major regional tectonic element is the Engadine Line, an oblique sinistral strike-slip fault (Trümpy ,1977), which runs along the southeastern part of Lake Sils. This fault can be traced from Lake Sils 30 km toward the northeast and 25 km in southwest direction (Tibaldi and Pasquarè, 2008).

The major incoming tributary, the Aua da Fedoz, originates in the Val Fedoz and feeds the Isola Delta, the main delta of the lake (Fig. 4-1). The Ova dal Mulin, Ova de la Roda, Ova dal Crot, and Lavatera are minor tributaries draining from the northwest, and the Inn and the Valacia from the west and south, respectively. The Fedacla River currently feeds into Lake Silvaplana, but also fed into Lake Sils at least temporarily during high-discharge events (Ohlendorf, 1998). Lake Sils' four sub-basins form a longitudinal lake morphology along the main valley axis. The Central Basin is the deepest and reaches a depth of 72 m. The Lagrev Basin in the northeast is separated from the Sils Basin by the Chastè, a peninsula with outcropping bedrock composed of mylonitic granodiorites belonging to the Maloja Formation (Fig. 4-1). The Maloja Basin reaches a depth of 30 m and forms the southwestern part of the lake. Unlike delta areas, such as the Isola Delta on the southern shore, where sediments are dominated by coarse clastic sediments intercalated by few peaty horizons (Grischott et al., 2017), the coastal plain at Sils Baselgia is characterized by organic-rich swampy deposits onshore, fine clastic sediments, and lake-derived organics, which are occasionally interrupted by coarser clastic layers.

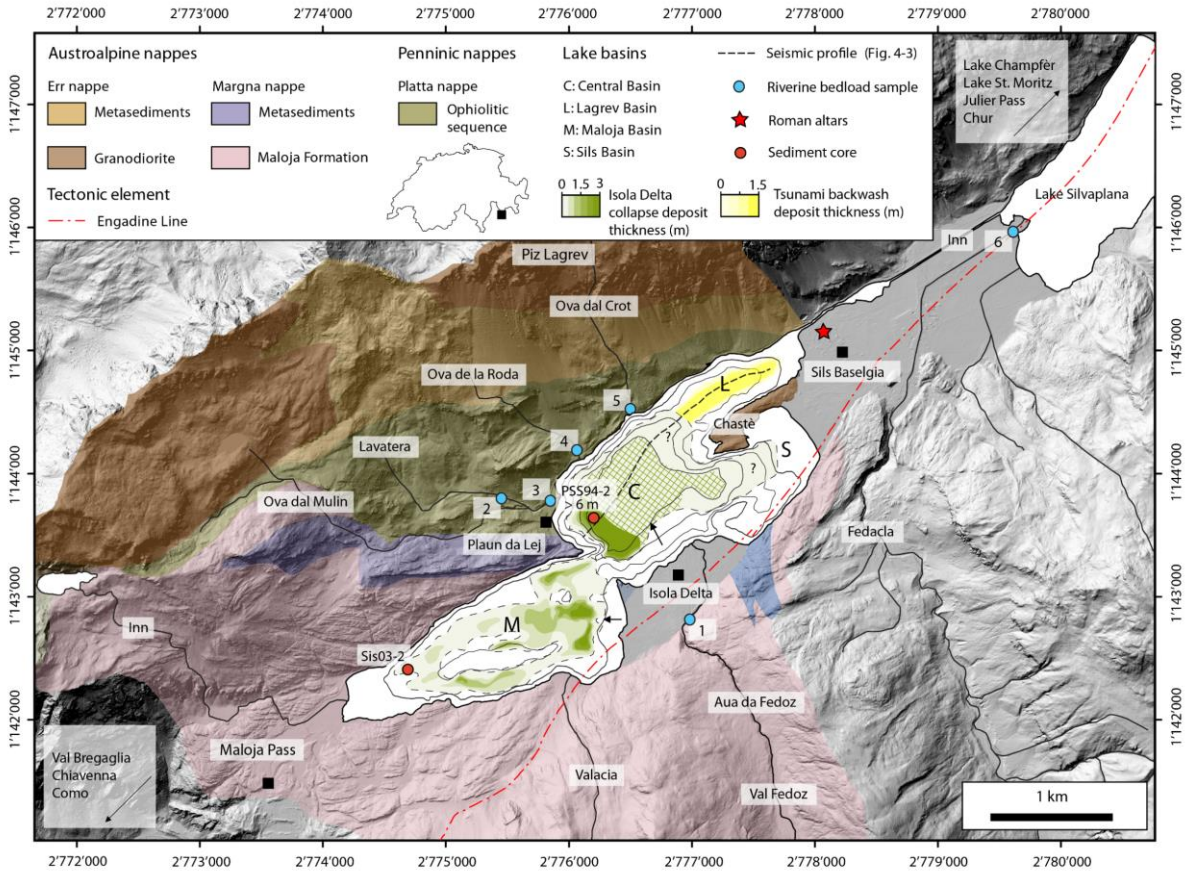

Fig. 4-1: Hillshade map showing Lake Sils and its catchment geology (swissALTI3D, swisstopo). The major tectonic and geological units are modified after Spillmann and Büchi (1993) and 1:25'000 Swiss geological map (GA24, swisstopo). Note the Engadine Line that runs along the southern shore of the lake. Lake Sils' four sub-basins are indicated (M: Maloja Basin, C: Central Basin; L: Lagrev Basin and S: Sils Basin). The Isola Delta collapse mass-movement deposit is highlighted in light green. Hashed green areas indicate area where thickness is not resolved by reflection seismic data due to limited penetration, but where the deposits is likely thicker than 2.5 m. Location of riverine bedload samples is indicated with numbered blue dots (1: Aua da Fedoz; 2: Lavatera 3: Lavatera + Ova dal Mulin; 4: Ova de la Roda; 5: Ova dal Crot; 6: Fedacla).

Pollen assemblages from sediment cores taken in Lake Champfèr and Lake St. Moritz provide evidence for first human impact in the Upper Engadine during the Neolithic Period around 5500 cal Before Present (BP) (Gobet et al., 2003). However, archeological findings are rather sparse for that time period in the area (Nauli, 1981; Rageth, 2000). Marked vegetation changes and regular cereal cultivation started around 3900 cal BP (Gobet et al., 2003). A late Bronze Age spring tapping, which is the only well-preserved wood building of the Swiss Alpine prehistory, was built at St. Moritz in 3361 cal BP (Oberhänsli et al., 2015). Although no permanent settlements are documented during that time, mule tracks were frequently used along the main passes in the Alpine environment as well as in the Upper Engadine (Roth-

Bianchi, 2007). During Roman times, the area of Lake Sils hosted an important traffic axis (Oberhänsli et al., 2015; Rageth, 2004). The directory of the most important Roman roads, the Itinerarium Antonini (230 CE), and the Tabula Peutingeriana (364 CE), an illustration of the Roman road network, report two main road connections in the area from Como in northern Italy to Chur in southeastern Switzerland. One of the two routes crossed the Upper Engadine from Chiavenna to Chur via the Maloja and Julier Passes, being the only route that was passable with two-wheeled carts in the province Raetia prima (Rageth, 2004; Roth-Bianchi, 2007). With the withdrawal of Roman troops from the province Raetia prima in 401 CE, the Roman presence in the area ended (Ducrey, 2006). Consequently, the use of the pass roads and mule tracks in the area decreased in the following centuries (Roth-Bianchi, 2007).

Initially, this study was stimulated by archeological findings in Sils Baselgia (Fig. 4-2), located at the northeastern shore of Lake Sils. During construction work in 1964 CE, four Roman votive altars were found (Erb et al., 1966). The excavated sacrificial altars are 40 to 47 cm high, made of serpentinite and dedicated to the Roman gods Silvanus, Diana, Pales and Mercury (Fig. 4-2B). These altars were found 2 m below today's surface, embedded in a clayey fine sandy silt with fine gravel (Erb et al., 1966). At the time of the discovery, the deposit was interpreted as a lacustrine deposit (Erb et al., 1966). Therefore, the archeologists proposed that the Roman altars fell from a ship during a phase of lake-level high stand connecting Lake Sils with Lake Silvaplana to the northeast (Erb et al., 1966). However, we are not aware of another study supporting the hypothesis of a significantly higher lake level during the Roman era. The fact would further imply massive hydrological changes along the Engadine valley. Based on our findings presented in this study, we propose an alternative hypothesis than regular lake sediments embedding the altars. We present evidence that the Isola Delta collapse generated a basin-wide tsunami that inundated the coastal plains around Lake Sils and partly buried the Roman altars with remobilized sediment around 548–797 cal CE.

4.2.1 The Isola Delta collapse in previous studies

High-resolution, single-channel seismic data from Lake Sils revealed two seismic units in the shallow subsurface that can be distinguished in the Maloja and Central Basins (Blass et al. 2005). The upper seismic unit is characterized by continuous high-amplitude reflections (Unit 1; Fig. 4-3), interpreted as representing distal deltaic and draping pelagic sediments. The

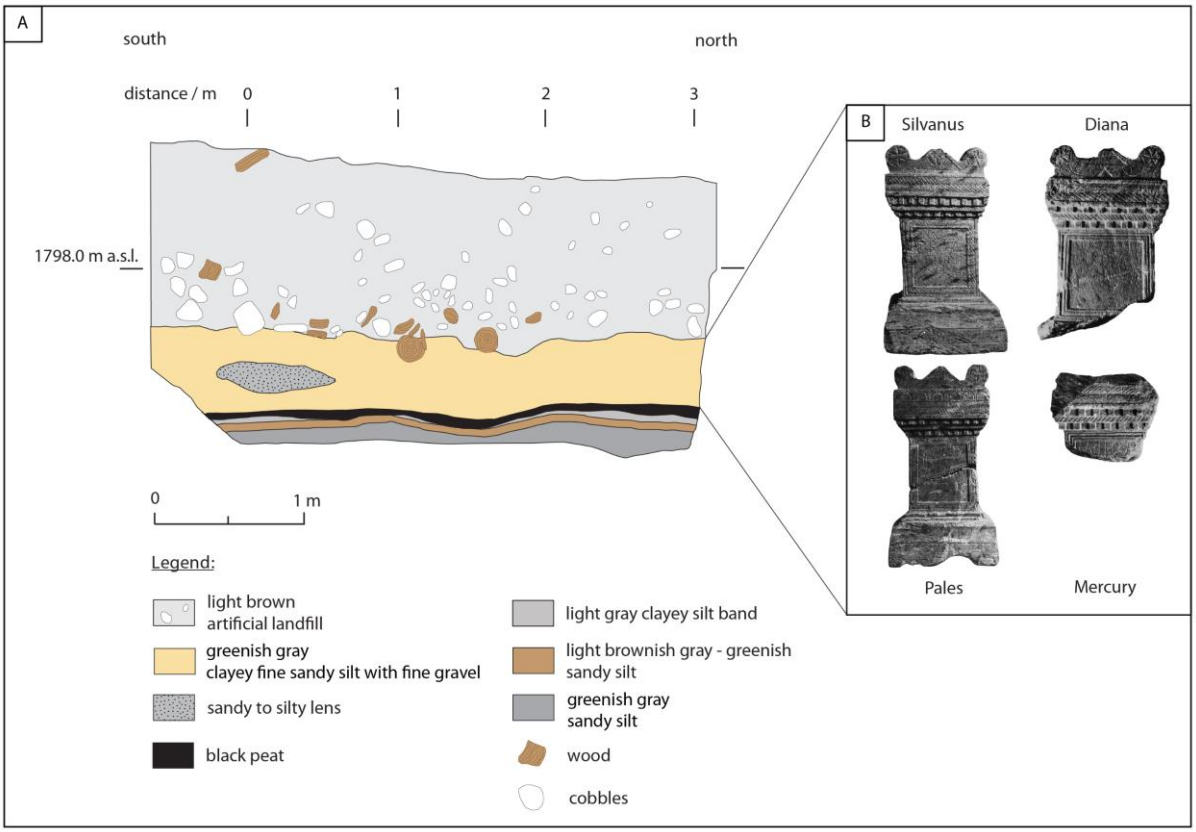

Fig. 4-2: A) Sketch of sedimentary section through an excavation site at Sils Baselgia (no vertical exaggeration; modified after Rageth (2002)). A peat horizon (black) with a fine band of clayey silt is overlain by a gray to greenish clayey fine sandy silt with fine gravel deposit (orange). It is supposed that the Roman altars (Fig. 4-2B) were buried in the equivalent unit 30 m away (Rageth, 2002). B) Photographs of the Roman altars that are dedicated to the Roman tutelary deity Silvanus, Diana, Pales and Mercury and excavated at Sils Baselgia in 1964 CE (Photographs: Archeological Service of Canton Grisons).

unit has a variable thickness distribution, being thickest at the base of the Isola Delta, and amounts up to 4 m in the Central Basin and 1–2 m in Maloja Basin, respectively (Fig. 4-1). Unit 1 encompasses smaller mass-movement deposits that are not individually mapped. The unit drapes a seismically transparent facies corresponding to the "homogenite" deposit (Subunit 2a; Fig. 4-3) of an extensive megaturbidite in the Central Basin (Blass et al., 2005). The homogeneous mud deposit represents the final phase of sedimentation of very fine particles from suspension in a calm water body (Kastens and Cita, 1981; Mulder et al., 2009; Schnellmann et al., 2006) after the Isola Delta collapse. Subunit 2c is characterized by a chaotic seismic facies with scattered diffraction hyperbolae that represents the large bedload transported mass-movement deposit of the Isola Delta collapse. The base of the mass movement is not imaged by the seismic data in the Central Basin. Subunit 2b and Unit 3 are

solely found along the seismic stratigraphy of the Lagrev Basin and will be discussed in Sections 3 and 4.

A sediment core recovered in the Central Basin by Ohlendorf et al. in 1994 CE (PSS94-2) was analyzed in detail by Blass et al. (2005). The lower part of the core contains an over 6 m thick mass-movement deposit with a base not reached by coring. Below a few cm thick clayey top, the deposit is characterized by a homogenous silty clay in the upper 3.5 m and a very heterogeneous, multiply graded sequence of coarse to very fine sand with varying organic content and increased variability of magnetic susceptibility (30–320 10^{-5} SI) in the lower 2.5 m (Blass et al., 2005). This large mass-movement deposit was radiocarbon dated to 548–797 cal CE, and interpreted as having originated from a partial collapse of the northern part of the Isola Delta (Blass et al., 2005). Based on high-resolution seismic data and recovered sediment cores, the minimum mass-movement volume was estimated to 6.5 x 10^6 m^3 in the Central Basin of Lake Sils (Blass et al., 2005).

4.3 Methods

4.3.1 Sediment coring

A total of 29 sediment cores (13 terrestrial and 16 lake cores) were recovered during multiple field campaigns between 2006 and 2018 (Fig. 4-4). In 2006 CE, a single, 85 cm long sediment core, SIL06-8 (Fig. 4.4B), was recovered using a gouge auger at the coastal plain in Sils Baselgia, 50 m from today's lakeshore. This core bore a 4 cm thick coarse silt deposit at 77 cm depth, overlying an organic-rich peat layer with a sharp basal contact. Radiocarbon dating of the peat layer revealed ages in the period of the delta collapse, motivating us to take 10 additional sediment cores, between 1.8 and 6 m length, which were recovered with a Geoprobe hydraulic-coring system along two onshore transects in 2009 CE. During the same campaign, two further sediment cores were recovered close to the site where the Roman altars were excavated in the year 1964 CE (Erb et al., 1966). One year later, in 2010 CE, lacustrine sediment cores were collected with a manual percussion-coring system from the frozen lake surface along an orthogonal transect (Transect T-I: Fig. 4-4B) with 100 to 500 m distance from the coastal plain at Sils Baselgia. These sediment cores reach core lengths between 0.8 and 2 m and were recovered in water depths from 1.7 to 40 m. Lastly, 10 short sediment cores (0.5–1 m long) were recovered in 2018 along a shoreline-parallel transect in the Lagrev (Transect T-II: 6 sediment cores) and Sils Basin (Transect T-III: 4 sediment cores), respectively. The sediment

cores were recovered in a water depth of ~2 m at 30 to 200 m distance from today's lakeshore with a manual percussion-coring system (Fig. 4-4). Core recovery of water-saturated sediments was high, and compaction is low when using a percussion-coring system. However, notable compaction was observed with the Geoprobe coring device in very organic-rich sediments that contains fibrous plant fragments. Moreover, low core recovery rates (60-70%) were observed in sandy lithologies with the same coring device.

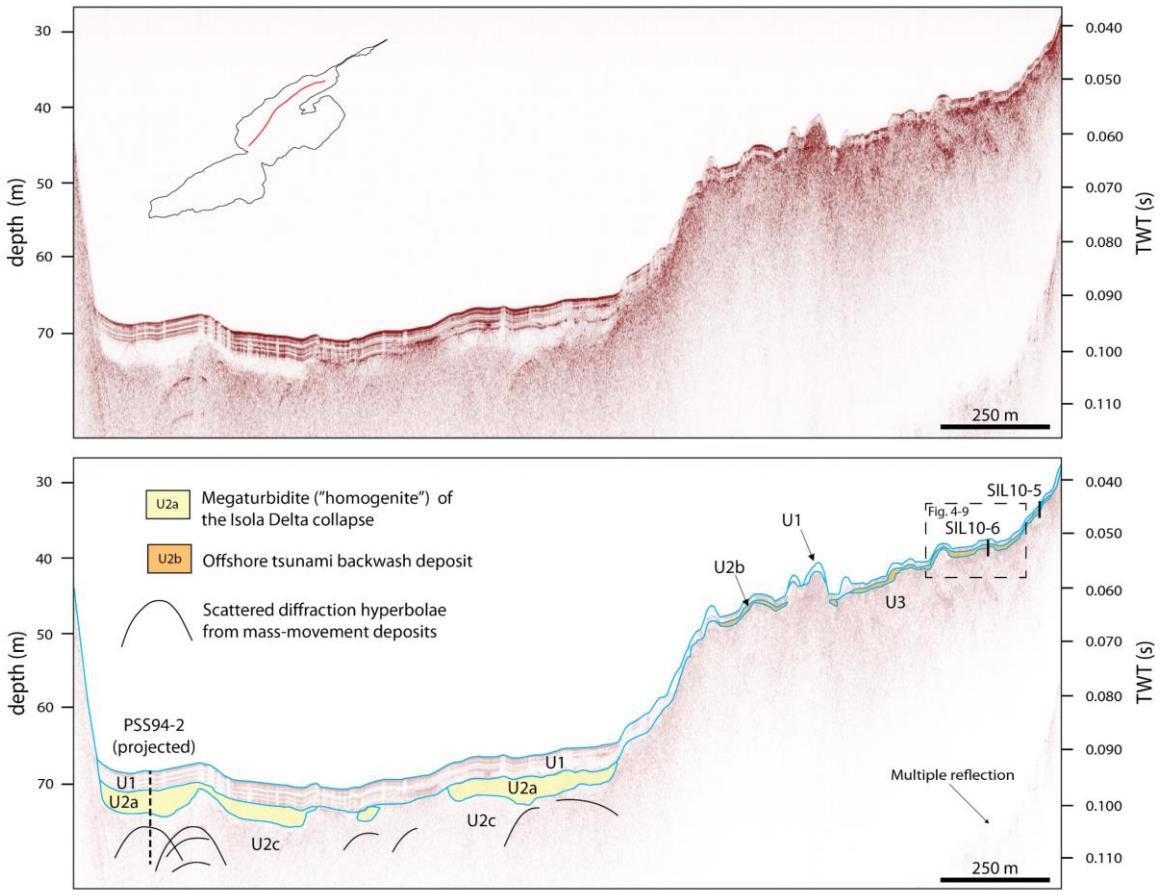

Fig. 4-3: Non-interpreted (top) and interpreted (bottom) seismic reflection profiles along the Central and Lagrev Basins, imaged by a 3.5 kHz single-channel pinger system (vertical scales: two-way travel time (TWT) in seconds (right) and depth in meters with a constant p-wave velocity of 1500 m s^{-1} applied for time-to-depth conversion (left)). Unit 1 (U1) is characterized by continuous high-amplitude reflections with draping character. The underlying Subunit 2a (U2a) represents a homogeneous mud of the Isola Delta collapse mass-movement deposit (Blass et al. 2015). The underlying chaotic Subunit 2c (U2c) represents the lower part of the Isola Delta collapse mass-movement deposit. Subunit 2b (U2b) and Unit 3 (U3) are solely found along the Lagrev Basin (see Fig. 4-9 for close-up view). Location of the recovered sediment Cores SIL10-5 and SIL10-6 are projected onto the seismic reflection profile (modified from Blass et al., 2005).

4.3.2 Core scanning

All cores were analyzed using a Geotek MSCL-S (Standard Multi Sensor Core Logger), except the gouge auger Core SIL06-8 and Core SIL18-2 which was opened prior to core scanning. Bulk density gamma-ray attenuation (using a 5 mm gamma beam) and magnetic susceptibility were measured with a resolution of 0.5 cm. Sediment cores recovered in 2018 were additionally scanned with a Siemens Somatom Definition AS X-ray computed tomography (CT) scanner at the Institute of Anatomy, University of Bern, prior to opening in order to obtain three-dimensional data of density variations at a voxel size of 100 µm. Computed tomography data were analyzed using the RadiAnt DICOM Viewer software (version 4.6.9.18463). Cores were subsequently split in two halves and line-scan images were captured with the Geotek MSCL-S camera.

4.3.3 Core analysis: sedimentology, mineralogy, and geochemistry

Macroscopic sediment description of lithologies including color, texture, grain-size distribution, and sediment composition were conducted on split sediment cores and in smear slides. Semiquantitative grain-size distribution was estimated visually on the sediment core for the coarse sediment fraction (sand and gravel) and with a microscope on smear slides for the fine sediment fraction (clay to silt). Further, semiquantitative descriptions of the diatom species assemblages, and mineralogical composition were estimated from smear-slide analysis. Discrete samples were collected from sediment cores to characterize the mineralogical composition by X-ray diffraction (XRD). For this purpose, subsampled sediment samples were dried with a freeze drier and milled. XRD measurements were performed with a powder X-ray Diffractometer (Bruker, AXS D8 Advance) at ETH Zurich. Elemental concentrations of total carbon (TC), total nitrogen (TN) and total sulfur (TS) were measured by gas chromatography (HEKAtech, Euro EA - CHNSO Elemental Analyzer) from discrete sediment subsamples at Eawag in Dübendorf. Total inorganic carbon (TIC) was measured on a coulometer (UIC, CM-5011 CO2 coulometer) at ETH Zurich. Total organic carbon (TOC) was calculated from the difference between measured TC and TIC. Sedimentary carbon-to-nitrogen (C/N) ratio was calculated from the ratio of molar TOC and TN concentrations.

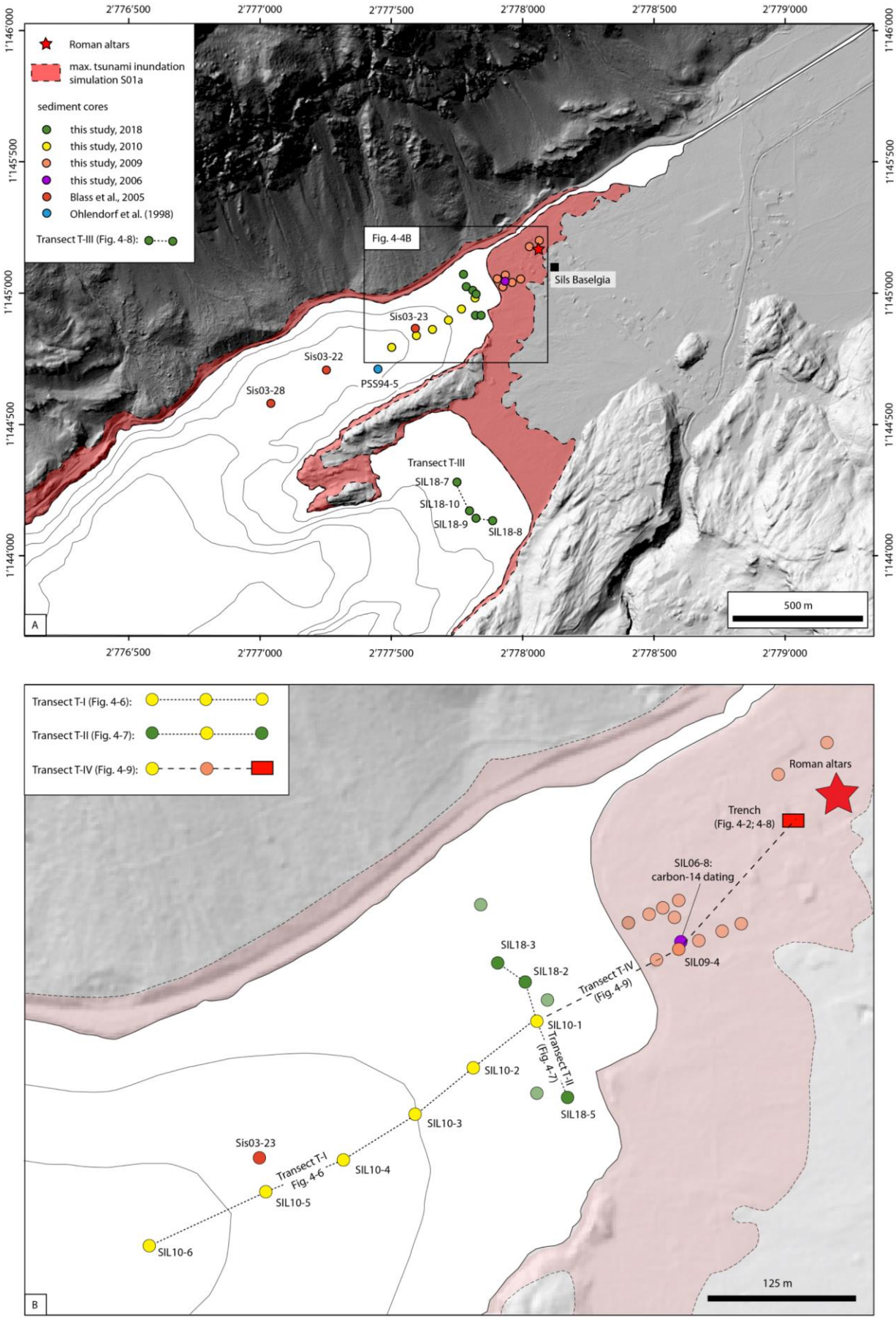
2'776'500
2'777'000
2'777'500
2'778'000
2'778'500
2'779'000
1'146'000
1'145'500
1'145'000
1'144'500
1'144'000
Roman altars
max. tsunami inundation simulation S01a
sediment cores
this study, 2018
this study, 2010
this study, 2009
this study, 2006
Blass et al., 2005
Ohlendorf et al. (1998)
Transect T-III (Fig. 4-8):
Fig. 4-4B
Sils Baselgia
Sis03-23
Sis03-22
PSS94-5
Sis03-28
Transect T-III
SIL18-7
SIL18-10
SIL18-9
SIL18-8
500 m
A
Transect T-I (Fig. 4-6):
Transect T-II (Fig. 4-7):
Transect T-IV (Fig. 4-9):
Roman altars
Trench
(Fig. 4-2; 4-8)
SIL06-8:
carbon-14 dating
SIL09-4
SIL18-3
SIL18-2
Transect T-IV
(Fig. 4-9)
SIL10-1
Transect T-II
(Fig. 4-7)
SIL18-5
SIL10-2
SIL10-3
Sis03-23
Transect T-I
Fig. 4-6
SIL10-4
SIL10-5
SIL10-6
125 m
B

◄ Fig. 4-4: A) Hillshade map of the northeastern area of Lake Sils (swissALTI3D; swisstopo) shows the excavation site of the four Roman altars in 1964 CE (red star), sediment core locations (blue: Core PSS94-5 (Ohlendorf, 1998); red: Cores Sis03-22; -23; -28 (Blass et al., 2005); orange: terrestrial cores recovered in 2009 CE with a Geoprobe; yellow: lacustrine sediment cores recovered in 2010; green: shallow-water cores recovered in 2018) and maximum tsunami inundation limit based on numerical tsunami modeling simulation S01a (red shaded area). Transect T-III is shown in Fig. 4-7. B) Close-up view of coring location along the Lagrev Basin and on the coastal plain at Lake Sils. Detail view of the different coring Transects T-I, T-II and T-IV (dashed lines) is illustrated in Figs. 4-5, 4-6, and 4-8. Terrestrial sediment cores were recovered along two transects oriented perpendicular to the lakeshore. Two sediment cores are located more distally close to the excavation site of the Roman altars and the archeological trench made in 2002 CE (red rectangle; Rageth, 2002). Single Core SIL06-8 (violet) was recovered in 2006 CE and used for radiocarbon dating.

4.3.4 Accelerator Mass Spectrometry (AMS) ^{14}C dating

Terrestrial organic macro-remains from a peat layer were used to date an organic-rich unit below the event deposit in Core SIL10-1 and SIL06-8 with the radiocarbon dating method. Another organic macro-remain was taken from siliciclastic lacustrine sediments above the event deposit in Core SIL10-1. For this purpose, sediment subsamples were wet sieved with deionized water prior to handpicking of terrestrial organic remnants under a binocular loupe. The samples were stored in the freezer until sample preparation for the AMS radiocarbon dating was done. Finally, prepared samples were measured with the Mini RadioCarbon Dating System (MICADAS) at ETH Zurich. Obtained results were calibrated using the OxCal software (version 4.4; Ramsey, 2009) and the IntCal20 Northern Hemisphere calibration curve (Reimer et al., 2020).

4.3.5 Provenance study: mineralogical signature of the major tributaries

Bedload samples were collected from Lake Sils' major incoming tributaries to characterize the mineralogical signature of the geologically highly complex catchment for provenance analysis of the detrital sediment components observed and analyzed in retrieved sediment cores (Fig. 4-1). Collected samples were sieved at 2 mm and 63 μm, respectively, to separate the sand-sized sediment fraction. Subsequently, sediment samples were freeze-dried, milled, and homogenized before analysis by powder XRD (X-ray Diffractometer Bruker, AXS D8 Advance) at ETH Zurich.

4.3.6 Numerical tsunami modeling

Numerical tsunami modeling was performed to assess the potential of the Isola Delta collapse to generate tsunami waves. The modeling approach, which is described in detail in Hilbe and Anselmetti (2015), uses the MassMov2D numerical model (version 0.91; Beguería et al., 2009) for subaquatic mass-movement simulation and the software package GeoClaw (version 4.6.3; Berger et al., 2011) for wave modeling. The input data include a comprehensive topography dataset that was created from the high-resolution swissALTI3D digital elevation model (swisstopo) and a raster dataset interpolated from the isobaths of the 1:25'000 national map (swisstopo). Both were resampled and combined into a single raster dataset with a grid cell size of 5 m. Two different subaqueous mass-movement scenarios with different failed volumes were simulated. The failed volumes, which were estimated from the mass-movement deposit in the lake basin and the present post-failure lake morphology, was added to the present-day Isola Delta. The subaqueous mass movement is simulated as a Bingham plastic in MassMov2D, with rheological parameters taken from Hilbe and Anselmetti (2015). The result of the landslide simulation is fed into GeoClaw as time-dependent changes of the lakebed topography. Tsunami generation, propagation and inundation are simulated in GeoClaw. Changes of the lakebed are directly transformed to the overlying water column and the water surface using a finite volume method to solve the nonlinear shallow-water equations (George and LeVeque, 2006).

4.3.7 Seismic reflection data

High-resolution, single-channel seismic reflection data were acquired using a 3.5 kHz pinger system with a vertical resolution of ~10 cm in the different sub-basins (Maloja Basin (this study); Central, Lagrev, and Sils Basin (Blass et al., 2005)). The acquired seismic reflection data were re-evaluated and interpreted using the seismic interpretation software SMT Kingdom suite 2015. A constant velocity of 1500 m s^{-1} was applied for time-to-depth conversion of both water column and sediment stratigraphy. A special focus was on the characterization of the seismic facies of the mass-movement deposit and its spatial extent in the individual lake basins, as well as on the seismic facies description along the Lagrev Basin.

4.4 Results

4.4.1 Sedimentology of sediment cores

The observed sedimentological composition along four different transects (T-I to T-IV) in the off- and onshore realms is presented in Figs. 4-5, 4-6, 4-7, and 4-8. The three Transects T-I, T-II, and T-IV contain Core SIL10-1 as the central "anchor" core, linking the different depositional environments of the three transects. Lithological units were correlated along the sediment cores where possible. Definition and numbering of lithological units in all transects follow the same scheme as defined in the Core SIL10-1. However, for terrestrial cores recovered along the low-lying plain at Sils Baselgia (part of Transect T-IV), newly introduced terrestrial-dominated lithological units are labeled with Roman Numerals. Sediment-core location (geographic coordinates) as well as results of the mineralogical and elemental analysis are reported in the Supplementary Material (Appendix B; Tables B1 to B6).

Transect T-I: Shore-perpendicular transect along the Lagrev Basin

Sediment cores of Transect T-I (Fig. 4-5) along the Lagrev Basin consist of six units in the shallow-water (1.7–4.3 m) and four units in water depths between 20.0 and 39.4 m. To enable comparison with the sedimentological description of Blass et al. (2005) the identical Units A to D were used. Sedimentologically, the uppermost lithological Units A to C are homogeneous and consist of light-gray siliciclastic massive to diffusely laminated silt to very fine sand with abundant diatoms.

The youngest unit is 2 to 10 cm thick, has the highest abundance of diatoms, smaller grain size, and the highest TOC content (2 to 3 wt%) compared to Units B and C (Blass et al., 2005). Unit B varies in thickness between 30 and 55 cm, is diffusely laminated and hosts two light-brownish graded detrital layers. Diatom abundance is lower than in Units A and C. Total organic carbon content is less than 1 wt% in Unit B and ~1 wt% in Unit C (Blass et al. 2005). The C/N ratio is around 7 to 8 mol mol^{-1} in Units A, B, and C (Blass et al., 2005). The silt-sized sediment consists mainly of siliciclastic minerals, carbonate minerals are accessory phases. The mineralogical composition in Unit C consists of chlorite (~34 vol%), white mica (~26 vol%), quartz (~11 vol%), amphibole (~9 vol%), K-feldspar (~6 vol%), plagioclase (~5 vol%), serpentine (~5 vol%), and minor amounts of clinopyroxene, calcite, and dolomite.

Unit D is a very heterogeneous and generally coarse-grained deposit that strongly varies in thickness and composition along the transect. The base of the unit is not reached in Cores SIL10-3 to SIL10-6, where it is up to 1 m thick. Toward the shoreline, Unit D thins to 10 to 15 cm in Cores SIL10-2 and SIL10-1. In Core SIL10-4, and SIL10-5, the unit is characterized by multiple fining-upward sequences composed of a coarse sandy matrix with gravels. A single fining-upward sequence overlies fine sandy silt in SIL10-6. These fining-upward sequences, observed in Cores SIL10-6, SIL10-5, and SIL10-4 consist of clast-supported, coarse sand with angular to sub-rounded gravel. In Core SIL10-4, Unit D hosts deformed and undeformed mud clasts of laminated silt. In Core SIL10-3, Unit D is composed of massive coarse sand with gravel clasts. The top of Unit D is marked, in all cores along the entire transect, by a pronounced and well-traceable light-gray clay cap, with an average thickness of 2 cm. Proximal to the shoreline, Unit D overlies the underlying Unit E with a sharp contact. The C/N ratio in Unit D varies between 10 and 40 mol mol^{-1} in Core SIL10-5. In Core SIL10-2, Unit D directly overlies Unit F with a sharp contact.

Along Transect T-I, Unit E is only present in Core SIL10-1. The unit consists of a 10 cm thick dark-colored organic-rich fibrous peat with finely dispersed white mica and is characterized by high TOC content (30–40 wt%), high TN concentration (2.2 wt%), and a C/N ratio of ~20 mol mol^{-1}.

Siliciclastic dominated Unit F is characterized by a C/N ratio between 10 and 15 mol mol^{-1}, low TOC content (~2 wt%), and an absence of diatoms. Grain size varies between coarse silt to medium sand. Units E and F will be discussed in more detail in the description of Transects T-II and T-III.

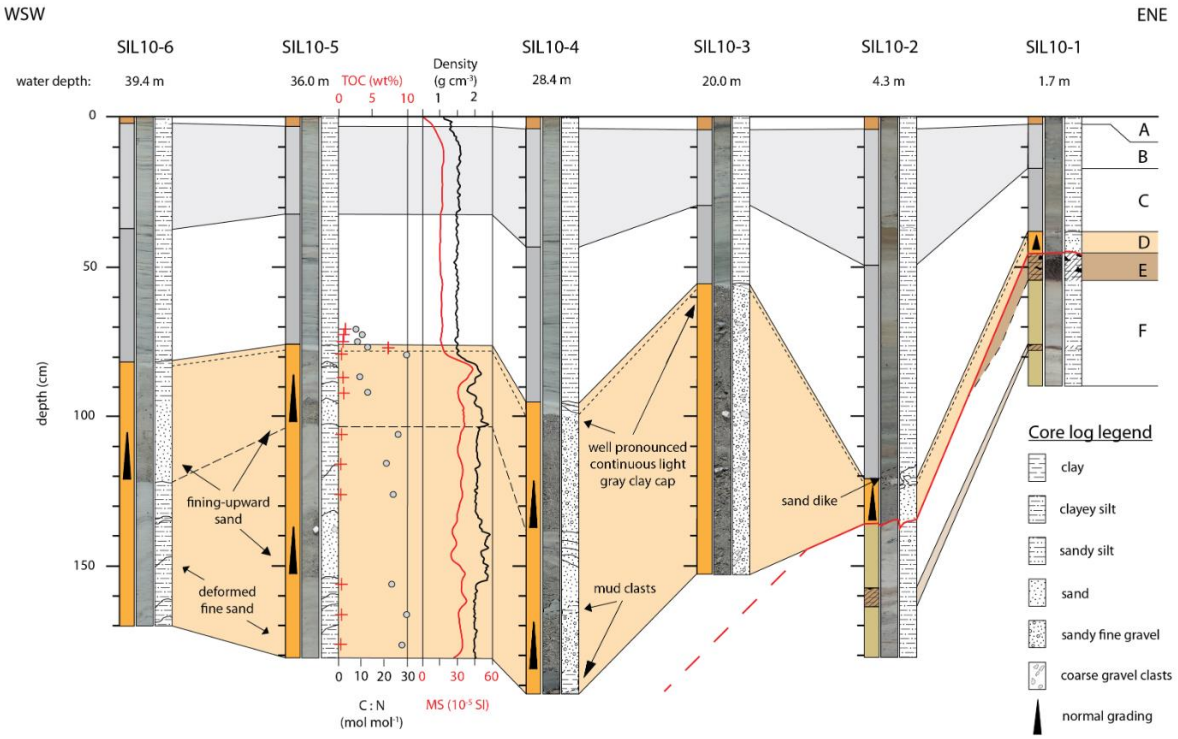

Fig. 4-5: Transect T-I located perpendicular to the shoreline at Sils Baselgia in the Lagrev Basin. Water depth and core ID are indicated above the corresponding sediment cores (see Fig. 4-4B for core location). The lithostratigraphic succession consists of six sedimentary units (A to F) with lateral thickness variations. Unit D (orange) can be traced along the transect and consists of a heterogeneous sandy deposit with gravels (SIL10-3), a single (SIL10-1 and -2) and multiple (SIL10-4, -5 and -6) fining-upward sequences, and a well-pronounced clay cap. Erosional contact to the underlying lithostratigraphic Units E and F is indicated in Cores SIL10-1 and SIL10-2 (red line). In Cores SIL10-3 to SIL10-6 the underlying sedimentary unit is not reached with coring.

Transect T-II: Shallow-water transect along the Lagrev Basin

Sediment cores of the shore-parallel Transect T-II (Fig. 4-6) were recovered from ~2 m water depth in 30 to 200 m distance from the shoreline along the Lagrev Basin (Fig. 4-4B). The lithostratigraphic succession consists of six different units, which can be correlated to the deeper-water Transect T-I (Fig. 4-5). The uppermost Unit A consists of silt-sized brownish-gray sediment with a high TOC content. Units B and C are light gray and consist of homogeneous silt to very fine sand. Units B and C have a lower TOC content compared to Unit A, with a TOC content of 3.3 to 4.5 wt% and a C/N ratio of 13 mol mol^{-1} in Unit C. The silt-sized sediment consists mainly of siliciclastic minerals with carbonate minerals only as accessories.

Unit D has an erosional contact to the underlying Unit E (red line in Fig. 4-6). The unit consists of a gravelly to sandy base that is overlain by a fining-upward sequence with a silty clay cap at the top. The sequence varies in thickness from 5 to 25 cm along the shore-parallel transect. In Core SIL18-3, the base of Unit D consists of fine gravelly sand, fining-upward to a medium-coarse sand (Fig. 4-6). Computed tomography scan images highlight horizontally bedded gravel clasts in a coarser section of the generally fining-upward sand at around 44 to 55 cm depth (Fig. 4-6). The uppermost part of Unit D is considerably finer and finishes with a pronounced light-gray clay cap. The most dominant mineral phases in Unit D are white mica (~30–40 vol%), chlorite (~18–36 vol%), quartz (~13–30 vol%), plagioclase (~6–17 vol%), and K-feldspar (<1–3 vol%).

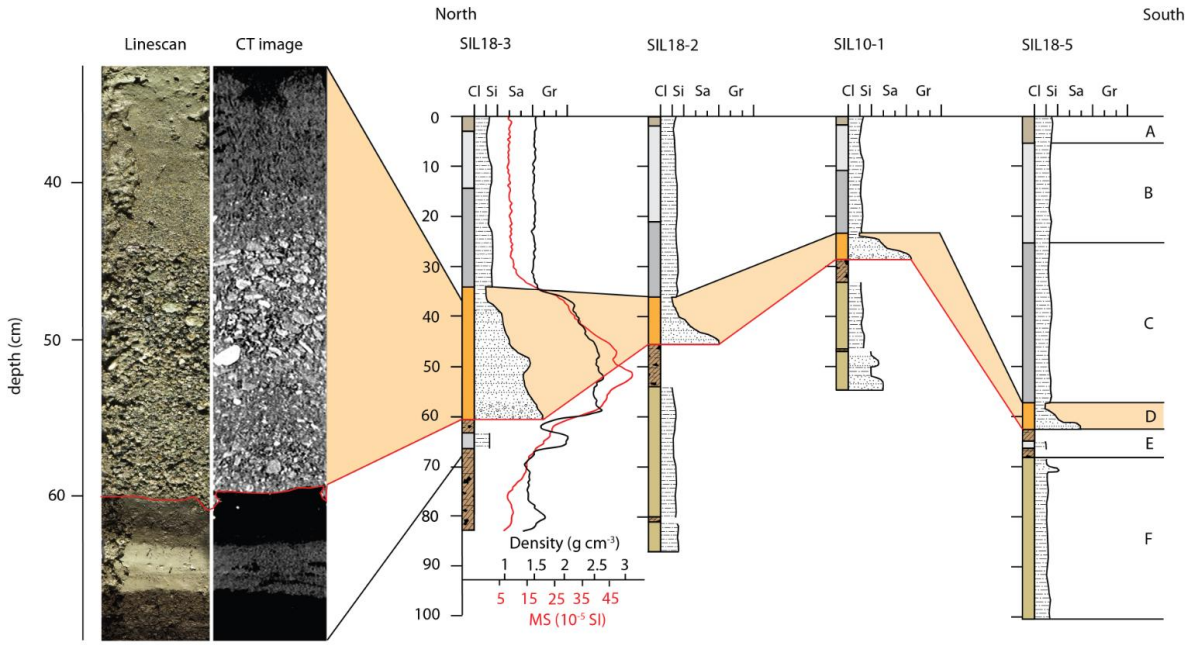

Fig. 4.6: Transect T-II located shore parallel in the Lagrev Basin (see Fig. 4B for core location). Left: Line scan image and CT-scan image of Core SIL18-3 with a gravelly fining-upward sand deposit (Unit D) overlying with an erosional contact (red line) Unit E. Computed tomography image of Core SIL18-3 shows horizontally bedded gravel clasts in a fining-upward sandy matrix in Unit D. Right: Lateral continuation of the event deposit along the shore of the Lagrev Basin. Bulk density and magnetic susceptibility are indicated for Core SIL18-3.

The underlying Unit E is a dark brown and very organic-rich (TOC content: ~30 wt%) peat deposit containing abundant organic fibrous fragments. The unit has a C/N ratio ranging from 15 to 20 mol mol^{-1}. Siliciclastic minerals, mostly white mica, are finely dispersed within the peat horizon. In Cores SIL18-3 and SIL18-5, a 2 to 4 cm thick, greenish-gray silty clay layer occurs within the organic-rich deposit.

Unit F, below the peat, consists of fine to medium siliciclastic sand with a C/N ratio that increases from 10 to 15 mol mol^{-1} upcore. Unlike Units A to C, diatoms are absent in Unit F. The sand-sized detrital components in Unit F consist of mica (~33 vol%), chlorite (~33 vol%), quartz (~17 vol%), and plagioclase (~5 vol%). Minor mineral phases comprise amphibole (~3 vol%), serpentine (~3 vol%), K-feldspar (~2 vol%), clinopyroxene (2 vol%), and dolomite (1 vol%).

Transect T-III: Shallow-water transect along the Sils Basin

A similar lithostratigraphic succession as discussed above occurs along a shore-parallel sediment core transect (Transect T-III: Fig. 4-7) in the Sils Basin (Fig. 4-4A). The uppermost strata in the cores are composed of fine-grained siliciclastic silt-sized deposits with abundant diatoms very similar to Units A to C in the Lagrev Basin (Transects T-I and T-II). The thickness of the uppermost Unit A varies between 3 and 8 cm along the transect. Unit A is dark brownish-gray, rich in diatoms, and consists of finer sediment particles compared to Units B and C below, apart from a few distinct coarse high-density laminae. Unit A is characterized by a higher TOC content compared to Units B and C. Units B and C vary markedly in thickness between 10 and 40 cm, are greenish-gray and massive to very diffusely laminated.

A sharp density contrast is observable at the contact to Unit D (Fig. 4-7). Units A to C have a density of 1.3–1.4 g cm^{-3}. In Unit D a very uniform density distribution occurs in Core SIL18-9 (~2 g cm^{-3}), whereas a more variable density distribution is observed in Cores SIL18-7, -10, and -8 (1.5–2.5 g cm^{-3}). The coarse-grained detrital and fining-upward high-density deposit of Unit D occurs along the entire Transect T-III and seems to correspond to Unit D of Transect T-II in the Lagrev Basin (Fig. 4-7). Accordingly, density generally decreases upcore in Cores SIL18-7, -10, and -8. In contrast to Transect T-II, in Transect T-III Unit D is characterized by discrete layers with increased density, darker colors and coarse sand. The internal multiple stacked fining-upward sequence varies laterally in thickness and has a light-gray clay cap in Cores SIL18-8 and SIL18-10. Vertically oriented, sand-sized, wavy laminae are observable in Unit D in Core SIL18-9. The base of Unit D is only recovered in SIL18-7, where a tree trunk, which was partly recovered in the sediment core, likely represents the equivalent to Unit E in the Lagrev Basin, marked as Unit “E” (Fig. 4-7).

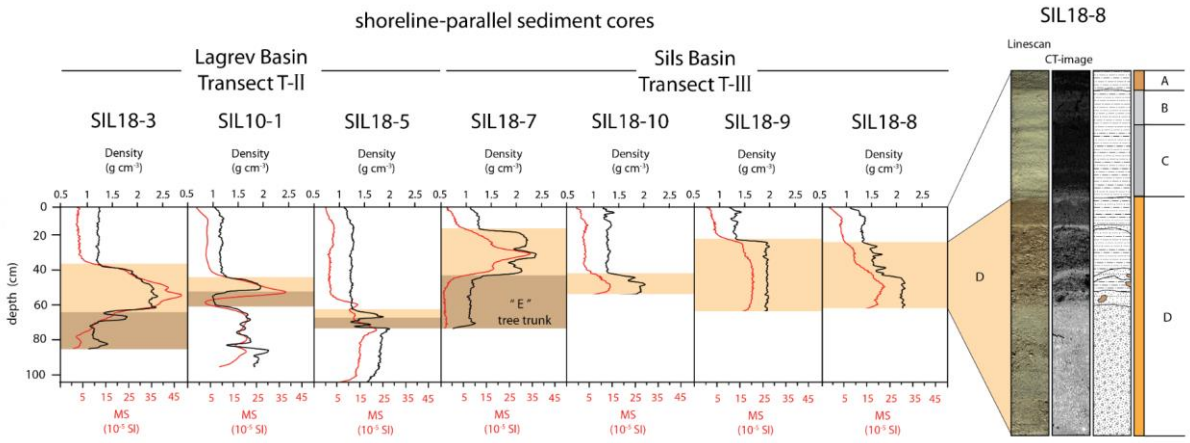

Fig. 4-7: Variation of bulk density and magnetic susceptibility in sediment cores of Transects T-II and T-III. Sediment cores recovered in the Sils Basin (Transect T-III) do not penetrate Unit E except Core SIL18-7 where a tree trunk was partially cored below (Unit "E"). Core photograph and CT-scan image of Core SIL18-8 show a high-density massive sand in the lower part of Unit D. In the upper part, Unit D is brownish gray with higher concentrations of terrestrial and aquatic macro-remains and two laminae of detrital fine sand and rip-up clasts (brown) are observable.

Transect T-IV: Cores across the shoreline at Sils Baselgia

Terrestrial sediment cores recovered in the low-lying plain at Sils Baselgia and an archeological trench close to the excavation site of the Roman altars (Fig. 4-2) show a similar lithological succession. Core SIL09-4 provides one of the best-preserved and longest records. Therefore, Core SIL09-4 is chosen as terrestrial core reference (Fig. 4-8). Six main lithological units (I–VI) can be distinguished in the terrestrial cores.

The uppermost Unit I varies between 20 and 40 cm in thickness, is yellowish to reddish oxidized, and characterized by heterogeneous organic-rich soil to more clastic-dominated, poorly sorted gravel and sand. At the top, Unit I consists of 10 to 20 cm organic-rich soil, which is underlain by a 5 cm thick gravelly layer and another organic-rich soil with a thickness of 10 to 15 cm. At the base, Unit I is characterized by a fine to coarse sandy gravel with very low TOC content (~0.5 wt%) and a C/N ratio of ~10 mol mol^{-1}. The sand fraction consists of white mica (~25–30 vol%), K-feldspar (~25–30 vol%), plagioclase (~10–20 vol%), chlorite (~10–15 vol%), and quartz (~10 vol%). Minor abundances are measured for amphibole (~3–4 vol%) and serpentine (>1 vol%). Talc and clinopyroxene are absent or occur only in minor amounts.

Unit II varies in thickness along the transect with largest values (~22 cm) at the most proximal location and thinning landward (1–2 cm). Unit II is light gray, diffusely laminated and consists

of silt to fine sand with some diatoms. Unit II has a low TOC content (0.4–0.6 wt%), and a variable C/N ratio between 5 and 17 mol mol^{-1}. The mineralogical composition consists of abundant K-feldspar (30–45 vol%), white mica (20–28 vol%), quartz (12–15 vol%), plagioclase (10–13 vol%), and chlorite (~8 vol%), and minor abundances of amphibole (~2 vol%), clinopyroxene (~1.5 vol%), and serpentine (<1 vol%). The boundary to Unit I above is gradual with a reddish to orange oxidized appearance.

Units III and IV can be correlated to Units D and E in Transects T-I and T-II, respectively, and are therefore called D(III) and E(IV) hereafter. However, the thickness of Unit D(III) is variable along the onshore sediment cores. It is generally up to 4 cm thick at a distance of ~40 m from today's shoreline and thins to 1 cm further away from the shore (~80-90 m), until it disappears or is not distinguishable from overlying Unit II (see Supplementary Material for core photos: Appendix B; Fig. B1 & B2). The unit is characterized by poorly sorted siliciclastic silt to fine sand with fragmented diatoms. The diffusely laminated and fining-upward deposit has a high concentration of TOC (~1.2 wt%), low TN concentration (~0.1 wt%), and a C/N ratio of ~13. The deposit shows a sharp to erosional contact to the underlying organic-rich Unit E(IV) (Fig. 4-8). The distinct clay cap observed in the offshore sediment cores is absent or only very slightly expressed in the onshore setting. Additionally, the upper boundary is gradual and difficult to trace when no clay cap is present. The internal structure of Unit D(III) is variable showing layering at the mm-scale, and normal grading. At the base flame structures are visible. However, such structures might also be artifacts related to the coring process.

Unit E(IV) is a dark brown to black porous 10 cm thick peat deposit with fragmented to well-decomposed organic macro-remains. The peat deposit can be correlated along the transect with substantial thickness variations. Total organic carbon content amounts up to 40 wt% with a C/N ratio of 15 to 25 mol mol^{-1}. The transitional contact to the underlying Unit V is characterized by a sharp color change from brownish black to brownish gray, a strong decrease of TOC content, and a C/N ratio with a minimum ratio of 10 mol mol^{-1} at 82 cm depth. The fine- to medium-sand siliciclastic fraction becomes more dominant in Unit V. The mineralogical composition of Unit V is characterized by white mica (~23 vol%), K-feldspar (~20 vol%), quartz (~19 vol%), chlorite (~18 vol%), and plagioclase (~15 vol%) with minor abundances of amphibole (~2.5 vol%), serpentine (~1 vol%), and clinopyroxene (<1 vol%). The lowermost Unit VI is composed of a light-gray, massive to faintly laminated silt with low TOC content (<1 wt%), and a C/N ratio of ~15 mol mol^{-1}.

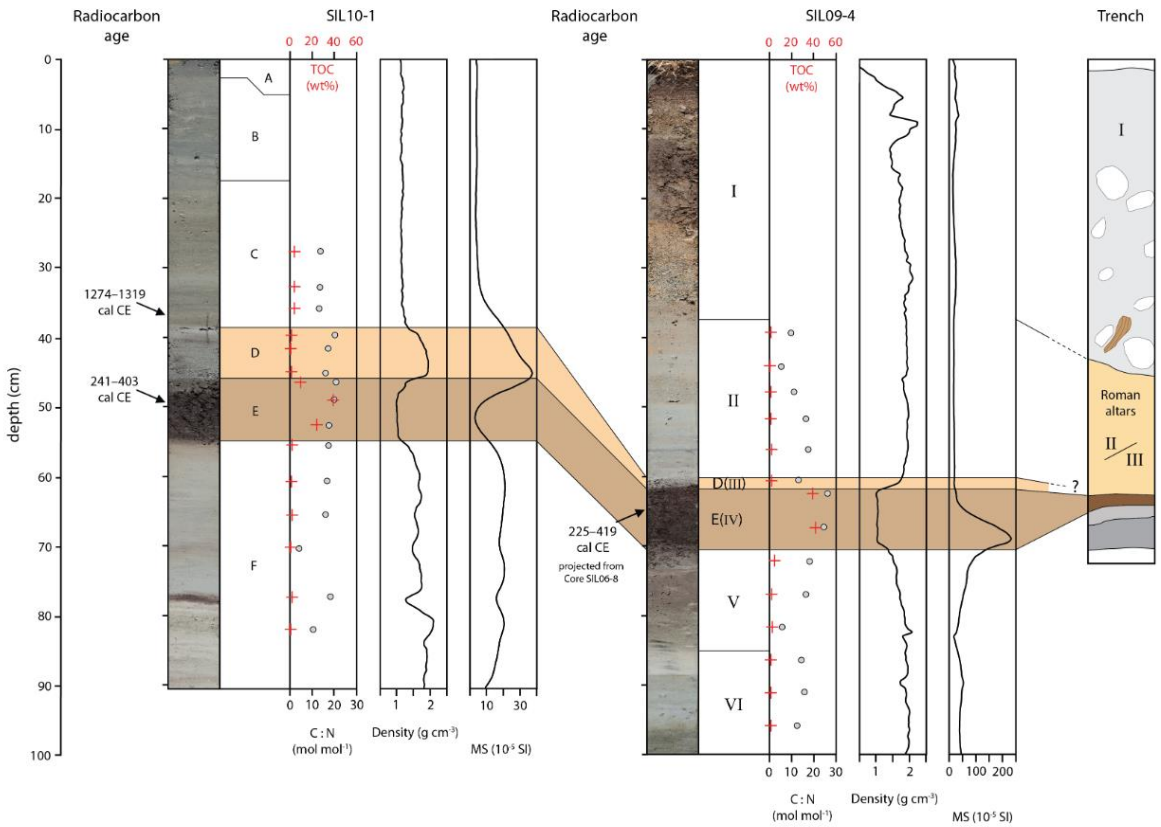

Fig. 4.8: Transect T-IV shows the two Cores SIL10-1 (shallow-water), SIL09-4 (terrestrial) and the archeological trench described in Rageth (2002) (see Fig. 4-2 for details). The organic-rich Units V and D(V) are radiocarbon dated to 241–401 cal CE and 225–419 cal CE, respectively. The base of Unit C was dated to 1274–1319 cal CE. Note that the age from the terrestrial record in Core SIL09-4 is projected from Core SIL06-8 (see Fig. 4.4B for core locations).

Rageth (2002) documents a similar lithostratigraphic succession as described above in an archaeological trench at Sils Baselgia at ~125 m distance from Core SIL09-4, close to the excavation site of the Roman altars found in 1964 (Figs. 4-2, 4-4B, and 4-9. The upper 40 to 50 cm of the trench a consists of an artificial fill containing wood fragments and variable-sized debris with discrete organic-rich horizons, representing recent and medieval cultural horizons and fills (Rageth, 2002), and is equivalent to Unit I in Transect T-IV. Below, Rageth (2002) describes a 50 to 60 cm thick greenish-gray silt-sized sediment package with sandy to gravelly lenses, in which the Roman altars most likely were found. This deposit is probably the equivalent of Unit II in Transect T-IV. Below this, Rageth (2002) describes at 60 cm depth a 5 to 15 cm thick organic-rich deposit with finely dispersed white mica that contains charcoal, bone fragments, processed serpentinite fragments and Roman brick fragments. This organic-rich unit is very likely the equivalent of Unit E(IV) in Core SIL09-4. The lowermost sediment

unit is described as brownish-gray to greenish sandy silt with minor gravel (Rageth, 2002). This unit is most likely the equivalent to the lithological Units V and VI (Fig. 4-8).

4.4.2 Seismic reflection data and seismic-to-core correlation

The seismic reflection data of the Central Basin (Fig. 4-3) shows a 3 to 4 m thick seismic Unit 1, characterized by continuous high-amplitude parallel reflections representing undisturbed background deposits (Blass et al. 2005). Below seismic Unit 1, an acoustically transparent facies (Subunit 2a, Fig. 4-3) correlates to the uppermost part of the 548–797 cal CE mass-movement deposit (Blass et al., 2005). No energy is absorbed in the acoustically transparent facies Subunit 2a, most likely indicating fine-grained deposits. Typically, the finest particles of a megaturbidite settle during the final phase of an event, causing a homogenous deposit and a transparent seismic facies (Schnellmann et al., 2002). Below the acoustically transparent seismic facies, a chaotic to patchy facies with some scattered diffraction hyperbolae can be recognized (Subunit 2c, Fig. 4-3), representing a partly blocky mass-movement unit (e.g., Sammartini et al., 2020). The base of the more than 6 m thick mass-movement deposit is not imaged, probably due to high sand and gas content in the Central Basin. For seismic-to-core correlation, sediment core PSS94-2, recovered in the Central Basin (Fig. 4.1) by Ohlendorf et al., in 1998, was used. The upper 3.5 m consists of hemipelagic silty clay with intercalations of distal turbidite deposits. The uppermost part of the mass-movement deposit consists of a 4 cm thick light-gray clay cap at the top and a homogeneous silty clay with low variations in density and magnetic susceptibility in the lower 3.5 m that corresponds to the seismic Subunit 2a. The lower seismic Subunit 2c corresponds to a heterogeneous sediment deposit with deformed silty clay sediment packages and several graded sequences with coarse sand to silt (Blass et al., 2005). The base of Unit 2 is not imaged by the seismic data, nor was the base of the mass-movement deposit reached with coring.

Along the Lagrev Basin, a sedimentary body consisting of chaotic to internally stratified low-amplitude seismic reflections (Subunit 2b) is observed above an undulating topography (Unit 3; Fig. 4-9). The limited continuity reflections of seismic Subunit 2b are parallel to subparallel oriented and show onlapping reflections onto the underlying highs of Unit 3. The sedimentary body can be traced along the entire Lagrev Basin and is characterized by a smooth surface and ponding geometry. Subunit 2b fills geomorphological depressions and reaches thicknesses of 0.5 to 1 m. The lowermost seismic facies (Unit 3) is characterized by chaotic,

low-amplitude seismic reflections with many scattered diffraction hyperbolae and an undulating topography. The base of Unit 3 is not imaged by the seismic data (Fig. 4-3). Seismic-to-core correlation is based on Core SIL10-6 along the Lagrev Basin (Fig. 4-9). Seismic Unit 1 corresponds to faintly laminated hemipelagic silt-sized sediment in the upper 80 cm (Units A to C). Below seismic Unit 2b correlates with a sediment package of deformed clayey silt and a fining-upward coarse sand with a light-gray clay cap at the top of the lithological Unit D.

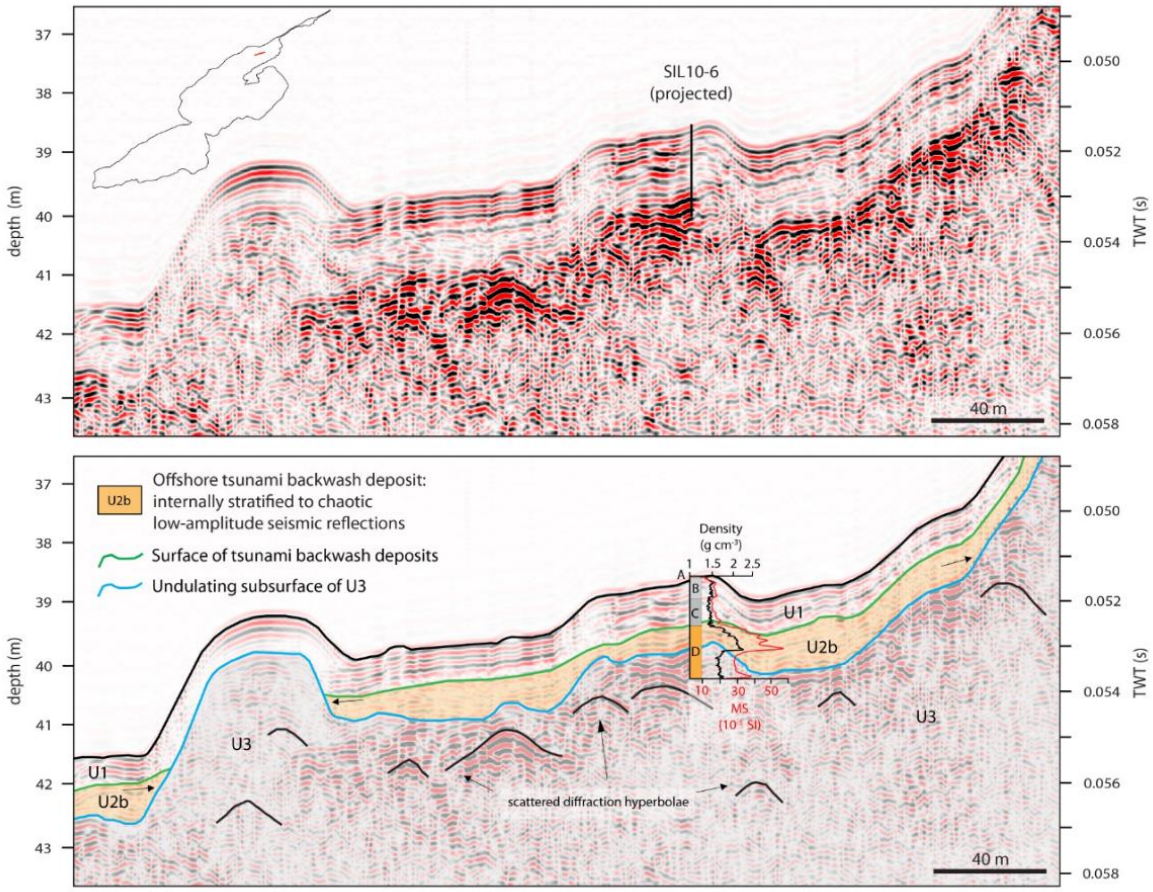

Fig. 4-9: Close-up view of the seismic reflection profile along the Lagrev Basin shown in Fig. 4-3. Non-interpreted (top) and interpreted (bottom) seismic reflection data and seismic-to-core correlation of Core SIL10-6. The profile location is shown in the inset (top). Overview of the seismic stratigraphy shows continuous high-amplitude reflections of Unit 1 (U1) and chaotic to internally stratified low-amplitude reflections in Unit 2b (U2b). Black arrows mark onlapping of U2b onto surface highs of Unit 3 (U3).

4.4.3 Age of the event deposit

Radiocarbon dating of terrestrial macr-organic remains from the organic-rich peat layer (Unit E) reveals a calibrated radiocarbon age range of 241–403 cal CE in Core SIL10-1 and 225–419 cal CE in Core SIL06-8. The radiocarbon age range is given within a 2σ confidence level, representing a probability of 95.4% (Table 4-1; Fig. 4-8). A sample collected in the lowermost part of Unit C is dated to 1274–1319 cal CE. However, due to high $\delta^{13}C$ (-11.7 ± 1.1 ‰) and very young ^{14}C age the sample is rejected. Blass et al. (2005) dated two samples from the uppermost part of the mass-movement deposit in the Central Basin (Core Sis03-23; Poz-5423) and the Maloja Basin (Core Sis03-2; Poz-5424) using the radiocarbon dating method. Calibration of the two ^{14}C ages yield a minimum age for the Isola Delta collapse of 548–797 cal CE (Table 4-1).

Table 4-1: Radiocarbon data and calibrated ages of terrestrial organic macro-remains from Cores SIL10-1 and SIL06-8.

Sample code	Core ID	Depth (cm)	Unit	^{14}C age ± 1σ (^{14}C years BP) [a]	Calibrated 2σ ranges (cal CE) [b]	Relative probability (%)	$\delta^{13}C$ (‰)	sample material
ETH-40236	SIL10-1	37–38	C	685 ± 30	1274–1319	62.1	-11.7 ± 1.1	Organic plant remains
					1359–1389	33.4		
ETH-40776	SIL10-1	50–51	E	1745 ± 35	241–403	95.4	-30.5 ± 1.1	Peat: plant remains
ETH-32595	SIL06-8	79	E(IV)	1735 ± 50	225–419	95.4	-25.8 ± 1.2	Peat: 30 plant remains
[c] Poz-5423	Sis03-23	69-72	D (top)	1300 ± 35	654–797	95.4	-	Three small twigs
[c] Poz-5424	Sis03-2	85	D (top)	1465 ± 40	548–652	95.4	-	Leave fragments, small twig

Uncertainties of ^{14}C ages refer to 1-sigma uncertainties. Ranges of calibrated ages represent 95.4% probabilities (2σ): [a] Stuiver and Polach, 1977; [b] Ramsey, 2009; Reimer et al. 2020; [c] Blass et al., 2005.

4.4.4 Mineralogical composition of the riverine bedload

Mineralogical composition of the sand-sized sediment fraction of Lake Sils tributaries was quantified by X-ray diffraction from the bulk sediment samples taken from the riverbeds of Aua da Fedoz, Lavatera, Ova dal Mulin, Ova de la Roda, Ova dal Crot, and Fedacla (Fig. 1). In general, the mineralogical composition is characterized by a high quartz concentration (60–88 vol%) and minor percentages of plagioclase (5–20 vol%), K-feldspar (<1–8 vol%), clinopyroxene (1–3 vol%), and mica (<1–5 vol%). Accessory minerals are chlorite, dolomite, serpentine, and amphibole (Appendix B; Table B3). The Aua de Fedoz, feeding the Isola Delta, is characterized by the lowest concentration of quartz (61 vol%) and highest concentration of mica (5 vol%) and amphibole (3.5 vol%) compared to the northern tributaries and the Fedacla, draining into Lake Silvaplana (Fig. 4-10). Dolomite is delivered by the southern tributaries Aua de Fedoz (3 vol%) and Fedacla (4.5 vol%), whilst of the northern tributaries it is solely delivered by the Lavatera (<1 vol%). Serpentine is only delivered by the northern tributaries. Considerable amounts of K-feldspar are delivered by the Ova dal Crot (8 vol%) and Ova de la Roda (7 vol%), draining from the northern slopes.

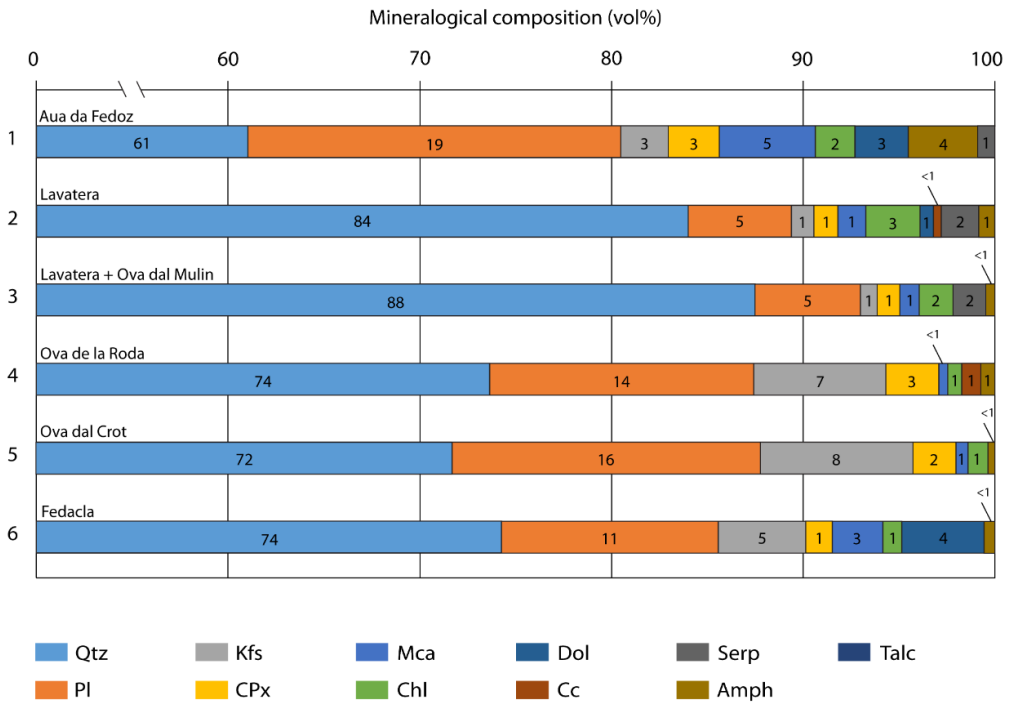

Fig. 4-10: Mineralogical composition of the sand-sized riverbed samples collected at Lake Sils major tributaries given in volume percentage (see Fig. 1 for sample locations). Used mineral abbreviations are Qtz: quartz; Pl: plagioclase; Kfs: K-feldspar; CPx: clinopyroxene; Mca: white mica; Chl: chlorite; Srp: serpentine; Am: amphibole; Tlc: talc; Dol: dolomite and Cc: calcite.

4.4.5 Tsunami generation and propagation model

The failed volume of the Isola Delta collapse was estimated on the basis of the deposit volume given by Blass et al. (2005), using geometrical information from bathymetric data, and a tentative reconstruction of the Isola Delta prior to its collapse (see Supplementary Material: Appendix B, Fig. B3). The mass-movement volumes of the two scenarios are considerably smaller than the volume estimated by Blass et al. (2005). This conservative estimate accounts for the fact that volumes estimated based on mapped chaotic seismic facies may be greater than actual failed volumes, because the former may include considerable amounts of deformed pre-existing basin sediments (Hilbe and Anselmetti, 2014). Therefore, we modelled the delta failure applying two different mass-movement volumes (Table 4-2). Due to the lack of detailed information on the pre-failure topography, the estimated volumes were simply added to the present topography, bearing in mind the considerable uncertainties that exist regarding the volume and geometry of the failed mass. Additionally, and for simplicity, only the mass movement toward the Central Basin was simulated, whilst the much smaller mass movement toward the Maloja Basin is neglected. A Bingham plastic rheology was used for the landslide simulation with initial bulk density, yield strength, dynamic viscosity, and constant Manning's roughness coefficient as given in Table 4-2.

Table 4-2: Model parameters of the mass-movement, tsunami generation, and propagation simulations.

Scenario	Volume (10^6 m^3)	Rheology (constitutive model)	Bulk density (kg m^{-3})	Yield strength (Pa)	Dynamic viscosity (Pa s)	Manning's roughness coefficient (s m$^{-1/3}$)
S01a	1.71	Bingham plastic	750	5	50	0.03
S01r	1.33	Bingham plastic	750	5	50	0.03

The numerical tsunami model provides an estimation for the order of magnitude of the lacustrine tsunami that might have been generated by the Isola Delta collapse (e.g., inundation, run-up height, depth-averaged velocity, and flow depth). Two different scenarios, S01a and S01r (Table 4-2), with different initial landslide volumes were run and show comparable results (see Appendix B for simulated mass-movement deposit thickness and mass-movement velocity: Figs. B4 & B5). Final mass-movement deposit thickness locally reaches up to 6 m for the two scenarios. Maximum mass-movement thickness locally reaches up to 8.5 m in scenario S01a and 6.5 m in scenario S01r (see Appendix B: Fig. B4). Maximum mass-movement

velocity of 23 m s^{-1} and 18 m s^{-1} is reached after 14 s in simulation scenario S01a and after 12 s in S01r, respectively, at the Isola Delta slope (see Appendix B: Fig. B5).

Tsunami initiation occurs within seconds after the Isola Delta collapse begins (Fig. 4-11a). A complex interference pattern of waves develops within less than two minutes after slide initiation, spreading along the different sub-basins (Fig. 4-11b). The wave train reaches the coastal plain at Sils Baselgia after 1 minute, and inundation reaches up to 200 m from today's shoreline, with run-up heights of 2 to 3 m (Fig. 4-11c).

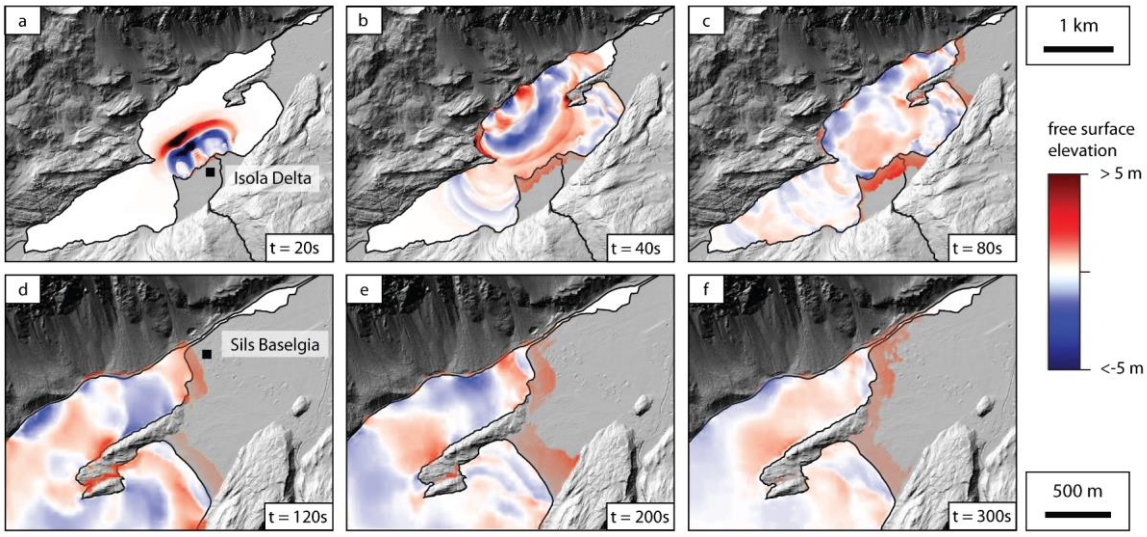

Fig. 4-11: Time steps of the wave amplitude (free surface elevation) of the numerical tsunami propagation model scenario S01a.

Maximum depth-averaged flow velocity and flow depth reached onshore are shown for scenario S01a in Fig. 4-12. Highest values are observed on the steep opposite slope at Plaun da Lej along the northwestern shore. Maximum inundation distance (280–300 m) is highest proximal to the tsunami source on the Isola Delta. Here, maximum depth-averaged flow velocity is ~5 m s^{-1} and flow depth is ~2.5 m. Flow velocity is very high within the first 150 m and drops quickly to near zero at 200 m. Highest maximum flow depths (5 m) are directly observed at the shore, drop quickly to ~2.5 m within the first 50 m, and become lower 150 m inland (0–1 m). On the low-lying plain at Sils Baselgia maximum depth-averaged flow velocity drops within the first 100 m from 5 m s^{-1} to 2.5 m s^{-1} (120–170 m) and to near zero in 250 m distance from today's shoreline. Maximum flow depth is 2.5 m within the first 80 m of inundation and drops continuously to 0 m at the maximum inundation distance at 250 to 280 m. Maximum depth-averaged velocity (2.5 m s^{-1}) and maximum flow depth (<2.5 m) is generally

lower at the low-lying plain adjacent to the Sils Basin. Maximum inundation distance remains around 220 m.

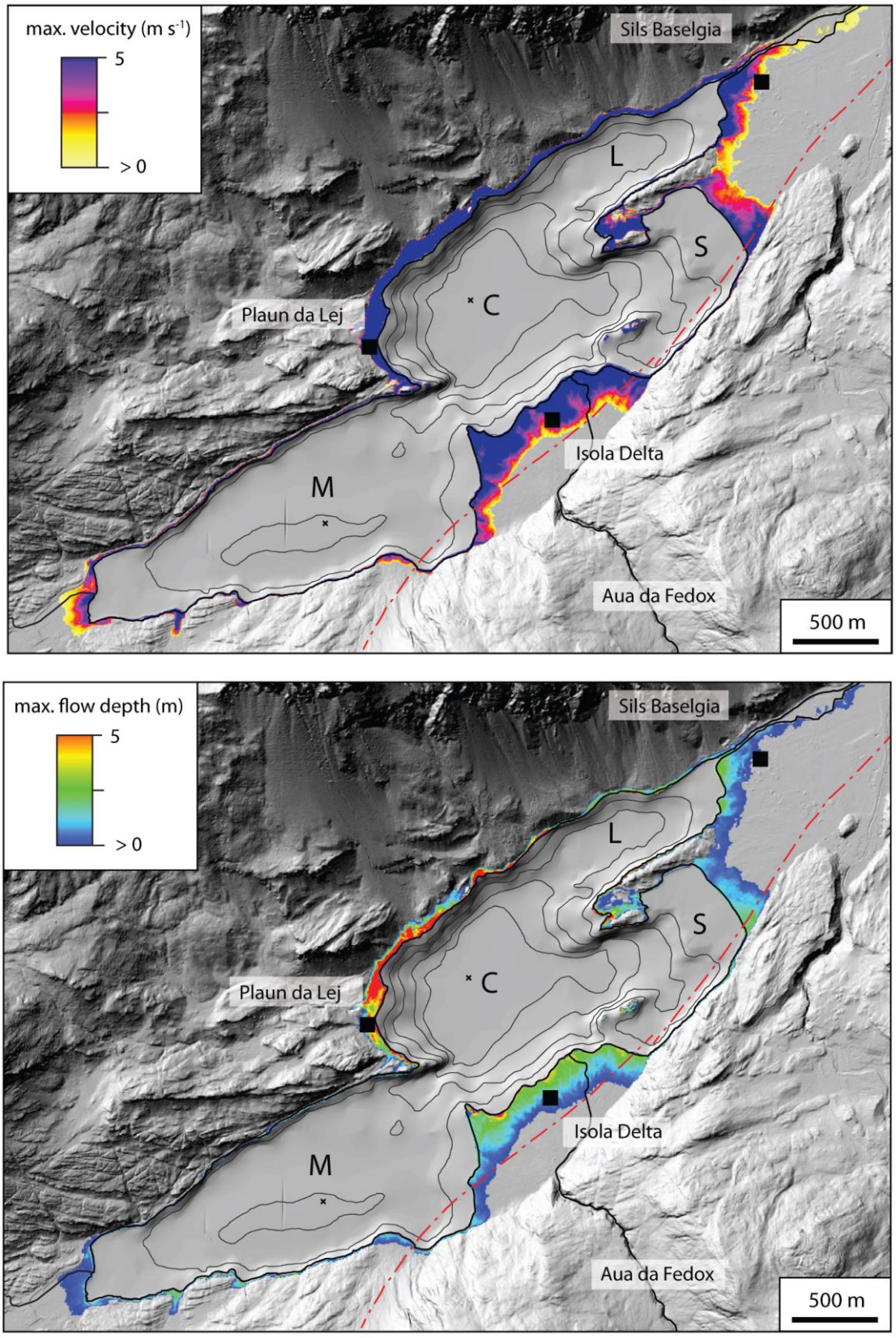

◄ Fig. 4-12: Maximum depth-averaged velocity (left) and maximum flow depth (right) of the numerical tsunami propagation model scenario S01a. Lake Sils' four sub-basins are indicated with capital letters (M: Maloja Basin, C: Central Basin; L: Lagrev Basin and S: Sils Basin).

4.5 Discussion

4.5.1 Sedimentology

A complex, and apparently laterally continuous, event deposit (Units D and D(III)) was identified across different depositional environments within an amphibious transect from onshore areas to the deeper water of Lake Sils. This event layer consists of massive sand and fining-upward gravelly sand sequences with a pronounced clay cap in the shallow-water areas of the Lagrev and Sils Basins. The event deposit transforms into a thicker unit with multiple packages of fining-upward sand to silt and a thicker clay cap toward the deeper water. Large amounts of unconsolidated sediment likely were transported from the northern shore towards the offshore area of the Lagrev Basin by a complex interference of opposing tsunami waves and backwash currents on the shore-based Transect T-IV, the contact to the underlying peat horizon is marked by an unconformity with a sharp erosional contact (Fig. 4-8). Horizontally bedded gravel clasts that are embedded in an overall fining-upward sequence indicate high bed shear-stress. Therefore, we assume that vast amounts of unconsolidated sediment were transported as bedload and in suspension from the lake landward. Along the coastal plain, the event layer generally thins and fines landward, with varying thicknesses from several cm in the proximal shore area to 1 cm in the more distal part. Although the coastal plain is relatively flat, with ~1 m elevation change along the 100 m long sediment core transect, paleo-microtopography have an important effect on deposit thickness and sedimentary structures of tsunami deposits (Nishimura et al., 2015). Therefore, the variable observed thickness and sedimentological structures likely are a direct consequence of the paleo-microtopography. A pronounced clay cap can only be deposited from standing water over some hours, and therefore, its partial absence can be explained by variations of the paleo-microtopography. The gradual transition toward the upper unit reflects erosion and bioturbation, mechanisms that usually alter tsunami deposits directly after sedimentation (e.g., Goto et al., 2012; Szczuciński, 2012; Spiske et al., 2020). The observed trend of decreasing mean grain size landward is consistent with decreasing tsunami velocity with increasing inundation distance, as confirmed by the numerical wave models and was described in various marine tsunami deposits (e.g., Bondevik et al., 2005; Dawson, 1995; Gelfenbaum and Jaffe, 2003). The landward thinning of the event deposit is

explained by the decreasing transport capacity of the flow, entraining less sediment the further it travels inland. Moreover, the erosional contacts, the massive and fining-upward sand layers, and horizontally bedded coarse components (Fig. 4-6) are typical sedimentological signatures found in past and recent coastal plain tsunami deposits. Similar structures have been described for tsunami deposits by Szczuciński et al. (2006), who observed landward thinning of normally graded coarse silt to medium sand along the Andaman Sea coast of Thailand after the 2004 Indian Ocean tsunami. Furthermore, tsunami deposits from the Storegga Slide tsunami are characterized by a remarkably continuous sand layer with evidence of erosion of underlying sediments in Montrose, eastern Scotland (Dawson et al., 1988). For the same event, Bondevik et al. (2003) investigated a generally continuous and normally graded sand layer that thins and fines landward and contains pebbles and organic-rich rip-up clasts. The 1755 CE Lisbon tsunami deposit at Boca do Rio is characterized as a continuous fining-upward sequence that ranges from coarse sand to clayey sandy silt (Dawson et al., 1995). Although the abovementioned similarities are convincing, tsunami deposits are characterized by a wide range of sedimentological characteristics depending on sediment availability and microtopography (Nishimura et al., 2015). For example, discontinuous sheets of sands are described at Koh Phra Thong, in southern Thailand (Engel and Brückner, 2011). Other examples of complex sediment architecture are often caused by shore erosion attributed to tsunami inundation and backwash, as described at many different locations including the Sendai coastal plain after the 2011 CE Tohoku-oki tsunami (Richmond et al., 2012), at Kalpakkam, India, due to the 2004 CE Indian Ocean tsunami (Srinivasalu et al., 2007) and at the north coast of Papua New Guinea caused by the 1998 CE Papua New Guinea Tsunami (Gelfenbaum and Jaffe, 2003).

Offshore tsunami deposits in the Sendai Bay following the devastating 2011 CE Tohoku-Oki tsunami were characterized by distinct layer of beach-derived coarse sand, transported by backwash currents into water depths between 14 and 30 m (e.g., Tamura et al., 2015, Yoshikawa et al., 2015). Channel-like erosion surfaces were identified in offshore seismic profiles in the same area (Yoshikawa et al., 2015) and large subaqueous dunes and bathymetric changes were observed in the Kesennuma Bay, Japan (Haraguchi et al., 2013). Following the 2004 CE Indian Ocean tsunami multiple studies were conducted on sedimentary deposits on the inner shelf offshore of Khao Lak in the Andaman Sea off the coast of Thailand (e.g., Paris et al., 2010, Sakuna et al., 2012). Sakuna et al., 2012 compared the offshore sedimentary signatures with offshore tsunami deposits in the Portuguese shelf offshore Lisbon (Van den

Bergh et al., 2003) and in the Mediterranean (coastal zone of Israel; Goodman-Tchernov et al., 2009 and Augusta Bay, Italy; Smedile et al., 2011). The described sedimentary signatures include a sharp erosional basal contact, thickness between a few cm and m, and grain size in the range of mud to gravel (Sakuna et al., 2012 and references therein). These signatures are well comparable with the offshore deposits in Lake Sils, which are characterized by erosional lower contact, multiple stacks of normal graded coarse sand and massive gravel.

Based on our sedimentological observations and numerical wave modeling, we hypothesize that the Isola Delta collapse generated a tsunami that impacted the northern lakeshore strongly and transported large amounts of unconsolidated sediment along the lakeshore and toward the deeper basin. The complex interference pattern of waves led to several inundation pulses, so that the back-flowing waters eventually caused downslope currents into the Lagrev Basin. The multiple-pulse flow transported terrestrial sediments into the lake, which were deposited as backwash deposits along the Lagrev Basin. After flow velocities decreased, a distinct clay cap overlying the coarse layer, identified along Transect T-I (Fig. 4-5), was deposited out of suspension.

Geochemical and mineralogical analysis were conducted to fingerprint the detrital source of the event deposit. Because the geological catchment of Lake Sils is composed of a complex tectonic architecture with many different units, it may be possible to characterize and differentiate detrital components originating from the Aua da Fedoz, the Fedacla, and the northern lakeshore (Fig. 4-1). The Lavatera and the Ova dal Mulin, draining from the north, are the only riverine bedload samples containing serpentine (1.8–2.0 vol%). The Aua da Fedoz and the Fedacla, draining from the south, deliver dolomite (2.9–4.6 vol%). Comparison between the mineralogical composition of the riverine bedload samples and discrete sediment-core samples indicate that quartz is strongly depleted in the sediment cores (15–30 vol%) relative to the riverine bedload (>60%). In contrast, mica (20–40 vol%) and chlorite (13–35 vol%) are enriched in the sediment cores, although measured mineral concentrations are very variable compared to the sand-sized riverine bedload sediment fraction. The characterization of the mineralogical composition of the event layer thus supports a local sediment source from the northern slopes. Serpentine is a minor constituent of the detrital event deposit and solely delivered from the northern tributaries of Lake Sils (Fig. 4-10). Based on the mineralogical composition, we assume that during tsunami propagation, large amounts of sediment were remobilized along the northern slopes between Plaun da Lej and Sils Baselgia.

4.5.2 Age estimation of the deposit

A good age estimation of the depositional timing of the laterally continuous fining-upward and landward-thinning sand event layer is provided by radiocarbon dating on terrestrial organic macro-remains from the peat layer underlying the event deposit. Two radiocarbon samples were retrieved from the organic-rich Unit E in sediment Cores SIL10-1 and SIL09-4 (Fig. 8). Calibration of radiocarbon dating yields ages of 241–403 cal CE and 225–419 cal CE for these core samples, respectively. Assuming that tsunami inundation could substantially erode the alluvial plain close to the shore at Sils Baselgia, and knowing that peat accumulation is a slow process and that the large Isola Delta collapse occurred around 548–797 cal CE (Blass et al., 2005), the obtained radiocarbon ages for the peat layer underlying the event deposit fit well to the proposed mechanism of a tsunamigenic delta collapse, with resulting sediment deposition along the alluvial plain at Sils Baselgia eroding and burying pre-existing soils.

4.5.3 Tsunami generation and propagation model

Numerical modeling of the delta-slope collapse and associated tsunami waves indicates that a partial Isola Delta collapse would be able to generate a basin-wide tsunami inundating the surrounding nearshore and coastal plain environment. Large amounts of unconsolidated sediment likely were transported from the northern shore towards the offshore area of the Lagrev Basin by a complex interference of opposing tsunami waves and backwash currents. However, model limitations and uncertainties regarding the simulation of tsunami-wave height, run-up and inundation distance need to be considered. For instance, initial delta geometry and landslide volume are not well constrained and were simply added to today's delta geomorphology in our models. It should also be considered that seismic reflection data and recovered sediment cores in the deep basin do not reach the base of the mass-movement deposit. Therefore, total volume estimation by Blass et al. (2005) is a rough estimate and represents rather a lower bound.

We simulated two conservative delta-collapse scenarios with slightly different initial volumes. Scenarios S01r (1.33×10^6 m^3) and S01a (1.71×10^6 m^3) have much lower volumes than the estimated Isola Delta collapse mass-movement deposit in the Central Basin (6.5×10^6 m^3; Blass et al., 2005). Hilbe and Anselmetti (2015) use failed volumes calculated from the scar height and area for modeling the subaqueous mass movement-generated tsunami in Lake Lucerne. These volumes typically amount to half of the volumes observed in the mass-

movement deposits. The observed difference is attributed to a suspected incorporation of basin sediments into the mass-movement deposits (Hilbe and Anselmetti, 2014). The obtained results, especially in the far field, are satisfactory and comparable with well-documented historical tsunami inundation and run-up (Hilbe and Anselmetti, 2015), although the nonlinear shallow-water equations used for the modeling tend to overestimate the height of mass movement-generated tsunamis with shorter wavelengths compared to earthquake-generated tsunamis in the ocean (Lynett, 2010). At Lake Sils, neither the total mass-movement deposit in the Central Basin nor the failure scar along the Isola Delta is traceable due to highly dynamic sedimentation mechanism in the deltaic environment.

Subaqueous mass-movement rheology may be another important source of uncertainty. Although the rheological parameters used are equivalent to the parameters used by Hilbe and Anselmetti (2015) for the Muota Delta collapse, which is thought to be comparable to the Isola Delta collapse, evidence revealing the kinematics of submarine landslides remain scarce (Løvholt et al., 2015). Yet, tsunami generation, amplitude, and wavelength are influenced by mass-movement kinematics (Løvholt et al., 2015) and mainly determined by the volume, the initial acceleration, and the maximum velocity (Harbitz et al., 2006). Maximum mass-movement velocities simulated (16 to 24 m s^{-1}) are comparable to other simulated subaqueous mass movement-generated tsunamis in the same order of volume (e.g., 2014 CE Statland Tsunami, Norway; Glimsdal et al., 2016). Sensitivity analysis of the mass-movement rheology parameters for the Muota Delta collapse-generated tsunami at Lake Lucerne indicates that the initial volume and mass-movement geometry as well as the dynamic viscosity are the most important parameters controlling tsunami run-up and wave height (Hilbe and Anselmetti, 2015). Although shore texture and land cover, expressed as bottom roughness, can significantly affect tsunami inundation and velocity (Kaiser et al., 2011), and we do not know the land cover at the time of the collapse, a constant Manning's value was used for bottom roughness of 0.03 s $m^{-1/3}$ on the alluvial plain.

Tsunami sediment erosion and transport capacity depend mainly on bed shear-stress and shear velocity (e.g., Ontowirjo et al., 2013; Paris et al., 2010). Simulated tsunami flow velocity ranges from 0 to 5 m s^{-1} along the alluvial plain at Sils Baselgia. Such flow velocities exceed critical threshold conditions for incipient motion of silt-, sand- and fine gravel-sized siliciclastic particles. Therefore, erosion of sediment particles along the slope and in the foreshore area, as well as erosion of the paleosol along the alluvial plain may be caused due to tsunami

inundation. Silt- and sand-sized particles are transported in suspension, larger blocks, and gravel as bedload fraction. With decreasing velocity, a normally graded layer (Units D and D(III)) is deposited from sediment falling out of suspension in the onshore and in the shallow-water setting, respectively, whereas multiple deposits of fining-upward sequences along Transect T-I probably were deposited during pulse-like localized backwash currents.

4.5.4 Other potential event deposit mechanisms

Besides the tsunamigenic Isola Delta collapse, some other sedimentary processes could potentially have caused the investigated event deposit. In the following, we discuss why we consider these mechanisms less plausible:

Debris flows

Although debris flows show a wide range of characteristics, they are commonly characterized by the sediment transport of particles ranging from clay to large boulders in a dense viscous flow. Water velocities range between 0.5 and 20 m s^{-1} (Takahashi, 1981) on alluvial or debris cones with a slope usually between 4 and 8° containing channels with well-developed boulder-rich lateral levees (Takahashi, 1981). The sedimentary deposits consist of poorly sorted mixture of particles and are generally fine distal from the source. In the lowermost areas off-fan deposition of winnowed fines may be observable (Blair and McPherson, 1998).

Rockslides

Rockslides are characterized by transport of debris from disaggregated bedrock with a relatively shallow-seated glide plane (Voight et al., 1981). The rate of movement can be very slow to extremely rapid, with an abrupt disintegration of the slope (Allen, 2009). The associated sedimentary deposits are usually very poorly sorted and often contain wooden debris and tree trunks. However, sorting is more effective when large amounts of water is involved, and the rockslide gradually transforms into a debris flow.

Lake-level changes

Submerged paleo-shorelines are formed by gradual water-level rise in a transgressive phase and may leave site-specific depositional signatures in the geological record. Often these deposits consist of a fining-upward sequence above an unconformity with an erosional to sharp contact due to a relatively abrupt water-level rise (e.g., Merzeraud et al., 2019). Such a

transgressional facies pattern is characterized by a change from coastal sediments to coarse clastic nearshore deposits, which are overlain by fine-grained deposits.

These geological processes may generate similar depositional signatures as the observed fining-upward and landward thinning and fining Unit D at the coast of Lake Sils. But certain aspects clearly speak against their genesis. (*i*) A debris-flow cone is characterized by a decreasing particle size distal to its origin. At Lake Sils the Fedacla river, draining the Val Fex, certainly flooded the alluvial cone at Sils repeatedly. Associated flood layers were described by Blass et al. (2005) in recovered sediment cores from Lake Sils. But the investigated Unit D is thinning and fining landward, therefore a deposition from a debris flow can be excluded. Additionally, the southern tributaries have different sediment provenance than the mineralogical composition observed in the event deposit. (*ii*) Rockslides originate from the northern shore at Lake Sils, as indicated by several talus and block deposits on the slopes of Piz Lagrev. Associated sedimentary deposits are expected to be less sorted due to the proximity of the steep slope. Moreover, these deposits would only occur in the proximal Lagrev Basin as they would not reach the distant Sils Basin (Fig. 4-1). (*iii*) A lake-level rise is indicated by the buried peat layer (Unit E), but an abrupt rise is considered not to be able to transport the amount of sediment needed to deposit Unit D in the lacustrine setting. Moreover, none of these alternate processes would generate the observed clay cap at the top of Unit D in Transects T-I, T-II, and T-III, which clearly indicates an event deposition with very large suspension involved, favoring a large delta collapse.

4.5.5 Unifying hypothesis: delta collapse-generated tsunami

Tsunamigenic delta collapses are historically reported in Lake Geneva (563 CE Rhone Delta collapse (Kremer et al., 2012), Lake Lucerne (1687 CE Muota Delta collapse (Hilbe and Anselmetti, 2014)), and Lake Brienz (1996 CE Aare Delta collapse (Girardclos et al., 2007). Compared to these tsunamigenic delta collapses, the observed depositional volume of the Isola Delta mass movement is best comparable with the 1687 CE Muota Delta collapse (14×10^6 m^3) in Lake Lucerne (Hilbe and Anselmetti, 2015). Historical documents of this event report a tsunami run-up of 5 m at the opposing lakeshore, about 1.2 km distant, and severe demolition of coastal infrastructures (Dietrich, 1689). The shore behind the delta was considerable damaged in the proximal area of the village Brunnen by two main pulses of inundation and subsequent backwash currents (Dietrich, 1689).

Although the (conservatively calculated) mass-movement volume involved in the Isola Delta collapse is almost half of the volume of the Muota Delta collapse at Lake Lucerne, delta morphology and major constituents are thought to be very similar. This is especially important with respect to mass-movement rheology and tsunami generation mechanism. Because tsunami modeling results obtained for the Muota Delta collapse correlate well with historical documented wave parameters (Hilbe and Anselmetti, 2015), the simulated Isola Delta collapse-generated tsunami, calculated using the same numerical codes, is thought to provide a realistic frame. Further, previous studies have shown that tsunamis generated by submarine landslides often have very large run-up heights close to the source area and are most dangerous when generated in shallow waters (Harbitz et al., 2006).

Despite the lack of direct historical reports documenting a tsunami event in Lake Sils, the observed sedimentological succession in sediment cores from the onshore and shallow-water setting provides insights into a severe depositional event. Radiocarbon dating of the event underlying peat layer indicates that the event occurred after 225–419 cal CE. The large Isola Delta collapse with a depositional volume of at least 6.5 x 10^6 m^3 and dated to 548–797 cal CE (Blass et al., 2005) is the best and obvious candidate to cause the event deposits. Firstly, it postdates the organic-rich sediment underlying the event layer by a short period. Secondly, the observed sedimentological characteristics points toward tsunami sediment transport and deposition. Thirdly, sediment provenance indicates that a local sediment source from the northern shore is very likely the major sediment contributor for the observed event deposit along the Lagrev Basin and the coastal plain. Fourthly, our numerical tsunami simulations indicate that the mass-movement volume of the Isola Delta collapse is sufficiently large to displace large amounts of water so that the required inundation and run-up can be reached.

4.5.6 Triggering mechanism of the Isola Delta collapse

Subaquatic mass movements may have variable trigger mechanisms, ranging from seismic to climatic causes (Kremer et al., 2017). Multiple synchronous mass movements on statically stable lateral lake slopes are usually triggered by seismic shaking (Kremer et al., 2017), while potentially unstable delta slopes may also collapse spontaneously (Girardclos et al., 2007; Hilbe and Anselmetti, 2014). The timing of the Isola Delta collapse (548–797 cal CE) coincides, within the resolution of the radiocarbon dating method, with multiple subaquatic mass movements identified on reflection seismic data and sediment cores in nearby Lake

Silvaplana at 571–650 cal CE (Bellwald, 2012 in Kremer et al., 2017). Moreover, a large mass-movement deposit was identified in Lake Como 60 km to the south and dated to ~530 CE (Fanetti et al., 2008). Such multiple coevally triggered mass movements deposited along the same horizon within a restricted basin and in different lakes are strong evidence for an earthquake-triggered collapse (Kremer et al., 2017; Schnellmann et al., 2002), so that the Lake Sils event may have been also triggered by a strong regional seismic event.

4.6 Conclusions

A large subaqueous delta collapse emplaced a mass-movement deposit with a maximum thickness of more than 6 m and a total estimated minimum volume of 6.5×10^6 m^3 in the Central Basin of Lake Sils around 548–797 cal CE (Blass et al., 2005). Our sedimentological analysis of sediment cores retrieved on the coastal plain and in the shallow water of Lake Sils supports the hypothesis that this mass movement generated a basin-wide tsunami that was able to substantially erode unconsolidated sediment along the lakeshores, especially along the northern shore. Recovered sediment cores show a prominent fining-upward sequence above an erosional sharp contact to the underlying paleosol that can be correlated across all sediment core transects. Based on radiocarbon dating, this paleosol was formed 225–419 cal CE, indicating a 2–3 m lower lake level at the time. The overlying coarse-grained event deposit consists of horizontally bedded gravel in a fining-upward sandy matrix thinning and fining landward. Cores recovered in the deeper part of the Lagrev Basin host a tsunami backwash deposit that contains multiple successions of fining-upward sequences with underlying erosional contacts. A clay cap marks the top of the event deposit, indicating sedimentation of the finest particles from suspension in the latest phase of the event.

Based on numerical tsunami-wave modeling, the Isola Delta collapse could have mobilized enough sediment to generate a basin-wide tsunami. Our simulations indicate that the delta collapse generated an initial wave with a free surface elevation exceeding 3 m in the direction of the emerging delta-slope failure. The wave train traveled along the main direction in which the slope failed and inundated the opposite shore. Due to restricted basin morphology, complex interference of waves caused them to spread along the different basins, resulting in a main wave direction traveling into the Lagrev and Sils Basins. These waves inundated the alluvial plain at Sils Baselgia with a maximum run-up of 2–3 m up to 200 m inland with initial flow velocities of up to ~5 m s^{-1}. Although the performed numerical tsunami simulations suggest that the area

where the Roman altars have been excavated was flooded, it remains questionable whether the entire fine-grained deposits embedding the altars represent tsunami deposits. Yet, it is likely that the Roman altars were tilted and displaced by the tsunami. They eventually became buried by deposits from the inundation as well as by overlying lake sediments, indicating also a post-event lake-level rise of over 2 m.

Because the described megaturbidite and its associated shallow-water and coastal deposits are the only identified major mass-movement deposit in the Central Basin and around Lake Sils (reflection seismic data and sediment cores do not penetrate further into the postglacial fill of the deep basin), recurrence rates of similar delta failures cannot be constrained. Nevertheless, high sedimentation rates and oversteepening in delta areas such as the Isola Delta are the ideal preconditioning factors for causing multiple failures in relatively short time, as was observed in other lacustrine case studies (e.g., Girardclos et al., 2007). These processes and phenomena need to be taken into consideration when evaluating the hazard potential of future subaqueous delta collapse-generated tsunamis in inhabited areas.

Acknowledgments

This work was funded by the Swiss National Science Foundation (Research Grant No.: 171017) and is part of the SNSF Sinergia Project “Lake tsunami: causes, controls and hazard”. We are very thankful for the constructive reviews by Pedro J.M. Costa and an anonymous reviewer, which improved the quality and clarity of the manuscript. Nicole Schwendener and the Institute of Anatomy are acknowledged for their support during the CT scanning. We thank Mathias Seifert and the Archeological Service of the Canton of Grisons to provide information about archeological findings in the Upper Engadine. The municipality of Sils i.E. and Antonio Walther are very sincerely thanked for their support during fieldwork.

References

Allen, P. A. (2009). Hyperconcentrated and Mass Flows. In: Earth surface processes. John Wiley & Sons. ISBN 978-0-632-03507-6.

Beguería, S., Van Asch, T. W., Malet, J. & Gröndahl, S. (2009) A GIS-based numerical model for simulating the kinematics of mud and debris flows over complex terrain. Natural Hazards and Earth System Sciences 9:1897-1909.

Berger, M. J., George, D. L., LeVeque, R. J. & Mandli, K. T. (2011) The GeoClaw software for depth-averaged flows with adaptive refinement. Advances in Water Resources 34:1195-1206.

Blair, T. C. & McPherson, J. G. (1998). Recent debris-flow processes and resultant form and facies of the Dolomite alluvial fan, Owens Valley, California. Journal of Sedimentary Research 68(5):800-818.

Blass, A., Anselmetti, F. S., Grosjean, M. & Sturm, M. (2005) The last 1300 years of environmental history recorded in the sediments of Lake Sils (Engadine, Switzerland). Eclogae Geologicae Helvetiae 98:319-332.

Bondevik, S., Løvholt, F., Harbitz, C., Mangerud, J., Dawson, A. & Svendsen, J. I. (2005) The Storegga Slide tsunami—comparing field observations with numerical simulations. In: Solheim, Berg & Mienert (eds) Ormen Lange–an Integrated Study for Safe Field Development in the Storegga Submarine Area. Elsevier, pp 195-208, ISBN 978-0-08-044694-3.

Bondevik, S., Mangerud, J., Dawson, S., Dawson, A. & Lohne, Ø. (2003) Record-breaking height for 8000-year-old tsunami in the North Atlantic. Eos, Transactions American Geophysical Union 84:289-293.

Bourgeois, J., Bernard, E. & Robinson, A. (2009) Geologic effects and records of tsunamis. In: Robinsin & Bernard (eds) The Sea: Ideas and Observations on Progress in the study of the Seas, Volume 15: Tsunamis. Harvard University Press, World, pp 53-91, ISBN 9780674031739

Brill, D., Seeger, K., Pint, A., Reize, F., Hlaing, K. T., Seeliger, M., Opitz, S., Win, K. M. .M., Nyunt, W. T., Aye, N. & Aung, A. (2020) Modern and historical tropical cyclone and tsunami deposits at the coast of Myanmar: Implications for their identification and preservation in the geological record. Sedimentology 67(3):1431-1459.

Costa, P. J. & Andrade, C. (2020) Tsunami deposits: Present knowledge and future challenges. Sedimentology 67:1189-1206.

Costa, P. J., Costas, S., González-Villanueva, R., Oliveira, M. A., Roelvink, D., Andrade, C., Freitas, M. C., Cunha, P. P., Martins, A., Buylaers, J.-P. & Murray, A. (2016). How did the AD 1755 tsunami impact on sand barriers across the southern coast of Portugal? Geomorphology 268:296-311.

Chagué-Goff, C., Andrew, A., Szczuciński, W., Goff, J. & Nishimura, Y. (2012) Geochemical signatures up to the maximum inundation of the 2011 Tohoku-oki tsunami—implications for the 869 AD Jogan and other palaeotsunamis. Sedimentary Geology 282:65-77.

Dawson, A. G., Hindson, R., Andrade, C., Freitas, C., Parish, R. & Bateman, M. (1995) Tsunami sedimentation associated with the Lisbon earthquake of 1 November AD 1755: Boca do Rio, Algarve, Portugal. The Holocene 5:209-215.

Dawson, A. G., Long, D. & Smith, D. (1988) The Storegga slides: evidence from eastern Scotland for a possible tsunami. Marine Geology 82:271-276.

Dawson, A. G. & Shi, S. (2000) Tsunami deposits. Pure and Applied Geophysics 157:875-897.

Dawson, A. G. & Stewart, I. (2007) Tsunami deposits in the geological record. Sedimentary Geology 200:166-183.

Dawson, A. G. & Stewart, I. (2008) Offshore tractive current deposition: the forgotten tsunami sedimentation process. In: Shiki, Yamazaki, Tsuji & Minoura (eds) Tsunamiites. Elsevier, pp 153-161, ISBN 978-0-444-51552-0.

Dietrich, J. (1689) Diarium von P. Josef Dietrich von Einsiedeln, Bd. 6 (1687-1688). Klosterarchiv Einsiedeln KAE, A.HB.6:202

Dietrich, V. (1970) Die Stratigraphie der Platta-Decke: facielle Zusammenhänge zwischen Oberpenninikum und Unterostalpin. Eclogae Geologicae Helvetiae 63:631-671

Ducrey, P.. (2006) Die ersten Kulturen zwischen Alpen und Jura. In: Mesmer B (ed), Geschichte der Schweiz und der Schweizer, 4rd edn. Schwabe, Basel, pp 27-57, ISBN 978-3-7965-2067-9

Einsele, G., Chough, S. & Shiki, T. (1996) Depositional events and their records—an introduction. Sedimentary Geology 104:1-9.

Engel, M. & Brückner, H. (2011) The identification of palaeo-tsunami deposits – a major challenge in coastal sedimentary research. In: Karius, Hadler, Deicke, Eynatten, Brückner & Vött (eds) Dynamische Küsten - Grundlagen, Zusammenhänge und Auswirkungen im Spiegel angewandter Küstenforschung. Coastline Reports (17), Rostock, pp 65-80, ISBN 978-3-939206-00-2

Engel, M., Oetjen, J., May, S. M. & Brückner, H. (2016) Tsunami deposits of the Caribbean–Towards an improved coastal hazard assessment. Earth-Science Reviews 163:260-296.

Erb, H., Meyer, E. & Bruckner, A. (1966) Römische Votivaltäre aus dem Engadin und neue Inschriften aus Chur. In Helvetia Antiqua, Festschrift Emil Vogt 9:223-232

Fanetti, D., Anselmetti, F. S., Chapron, E., Sturm, M., & Vezzoli, L. (2008) Megaturbidite deposits in the Holocene basin fill of Lake Como (southern Alps, Italy). Palaeogeography, Palaeoclimatology, Palaeoecology, 259(2-3), 323-340.

Fujiwara, O. & Kamataki, T. (2007) Identification of tsunami deposits considering the tsunami waveform: an example of subaqueous tsunami deposits in Holocene shallow bay on southern Boso Peninsula, Central Japan. Sedimentary Geology 200(3-4):295-313.

Garduño-Monroy, V. H., Soria-Caballero, D. C., Israde-Alcántara, I., Hernández Madrigal, V. M., Rodríguez-Ramírez, A., Ostroumov, M., ... & Mora-Chaparro, J. C. (2011) Evidence of tsunami events in the Paleolimnological record of Lake Pátzcuaro, Michoacán, Mexico. Geofísica internacional, 50(2), 147-161.

Garrett, E., Shennan, I., Woodroffe, S. A., Cisternas, M., Hocking, E. P., & Gulliver, P. (2015). Reconstructing paleoseismic deformation, 2: 1000 years of great earthquakes at Chucalén, south central Chile. Quaternary Science Reviews, 113, 112-122.

Gelfenbaum, G. & Jaffe, B. (2003) Erosion and sedimentation from the 17 July, 1998 Papua New Guinea tsunami. Pure and Applied Geophysics 160:1969-1999.

George, D. L. & LeVeque, R. J. (2006) Finite volume methods and adaptive refinement for global tsunami propagation and local inundation. Science of Tsunami Hazards 24(5):319-328.

Girardclos, S., Schmidt, O. T., Sturm, M., Ariztegui, D., Pugin, A., & Anselmetti, F. S. (2007) The 1996 AD delta collapse and large turbidite in Lake Brienz. Marine Geology, 241(1-4), 137-154.

Glimsdal, S., L'Heureux, J. S., Harbitz, C. B. & Løvholt, F. (2016) The 29th January 2014 submarine landslide at Statland, Norway—landslide dynamics, tsunami generation, and run-up. Landslides 13(6):1435-1444.

Gobet, E., Tinner, W., Hochuli, P., Van Leeuwen, J. & Ammann, B. (2003) Middle to Late Holocene vegetation history of the Upper Engadine (Swiss Alps): the role of man and fire. Vegetation History and Archaeobotany 12:143-163.

Goff, J., Chagué-Goff, C., Nichol, S., Jaffe, B. & Dominey-Howes, D. (2012) Progress in palaeotsunami research. Sedimentary Geology 243:70-88.

Goff, J., Lane, E. & Arnold, J. (2009) The tsunami geomorphology of coastal dunes. Natural Hazards and Earth System Sciences 9:847-854.

Goff, J., Pearce, S., Nichol, S. L., Chagué-Goff, C., Horrocks, M. & Strotz, L. (2010) Multi-proxy records of regionally-sourced tsunamis, New Zealand. Geomorphology 118(3-4):369-382.

Goodman-Tchernov, B. N., Dey, H. W., Reinhardt, E. G., McCoy, F. & Mart, Y. (2009) Tsunami waves generated by the Santorini eruption reached Eastern Mediterranean shores. Geology 37(10):943-946.

Goto, K., Chagué-Goff, C., Fujino, S., Goff, J., Jaffe, B., Nishimura, Y., ... & Yulianto, E. (2011) New insights of tsunami hazard from the 2011 Tohoku-oki event. Marine Geology, 290(1-4), 46-50.

Goto, K., Takahashi, J. & Fujino, S. (2012) Variations in the 2004 Indian Ocean tsunami deposits thickness and their preservation potential, southwestern Thailand. Earth, planets and space 64(10):923-930.

Grischott, R., Kober, F., Lupker, M., Hippe, K., Ivy-Ochs, S., Hajdas, I., ... & Christl, M. (2017) Constant denudation rates in a high alpine catchment for the last 6 kyrs. Earth Surface Processes and Landforms, 42(7), 1065-1077.

Haraguchi, T., Goto, K., Sato, M., Yoshinaga, Y., Yamaguchi, N., & Takahashi, T. (2013) Large bedform generated by the 2011 Tohoku-oki tsunami at Kesennuma Bay, Japan. Marine Geology, 335, 200-205.

Harbitz, C. B., Løvholt, F., Pedersen, G. & Masson, D. G. (2006) Mechanisms of tsunami generation by submarine landslides: a short review. Norwegian Journal of Geology/Norsk Geologisk Forening 86(3).

Hilbe, M. & Anselmetti, F. S. (2014) Signatures of slope failures and river-delta collapses in a perialpine lake (Lake Lucerne, Switzerland). Sedimentology 61:1883-1907.

Hilbe, M. & Anselmetti, F. S. (2015) Mass movement-induced tsunami hazard on perialpine Lake Lucerne (Switzerland): scenarios and numerical experiments. Pure and Applied Geophysics 172:545-568.

Hori, K., Kuzumoto, R., Hirouchi, D., Umitsu, M., Janjirawuttikul, N., & Patanakanog, B. (2007) Horizontal and vertical variation of 2004 Indian tsunami deposits: an example of two transects along the western coast of Thailand. Marine Geology, 239(3-4), 163-172.

Ishimura, D. & Yamada, K. (2019) Palaeo-tsunami inundation distances deduced from roundness of gravel particles in tsunami deposits. Scientific reports 9(1):1-8.

Jaffe, B. E. & Gelfenbuam, G. (2007) A simple model for calculating tsunami flow speed from tsunami deposits. Sedimentary Geology 200(3-4):347-361.

Jaffe, B. E., Goto, K., Sugawara, D., Richmond, B. M., Fujino, S., & Nishimura, Y. (2012) Flow speed estimated by inverse modeling of sandy tsunami deposits: results from the 11 March 2011 tsunami on the coastal plain near the Sendai Airport, Honshu, Japan. Sedimentary Geology, 282, 90-109.

Judd, K., Chagué-Goff, C., Goff, J., Gadd, P., Zawadzki, A., & Fierro, D. (2017) Multi-proxy evidence for small historical tsunamis leaving little or no sedimentary record. Marine Geology, 385, 204-215.

Kaiser, G., Scheele, L., Kortenhaus, A., Løvholt, F., Römer, H., & Leschka, S. (2011) The influence of land cover roughness on the results of high resolution tsunami inundation modeling. Natural Hazards and Earth System Sciences, 11(9), 2521-2540.

Kastens, K.A. & Cita, M. B. (1981) Tsunami-induced sediment transport in the abyssal Mediterranean Sea. Geological Society of America Bulletin 92:845-857.

Kitamura, A., Ito, M., Ikuta, R. & Ikeda, M. (2018) Using molluscan assemblages from paleotsunami deposits to evaluate the influence of topography on the magnitude of late Holocene mega-tsunamis on Ishigaki Island, Japan. Progress in Earth and Planetary Science 5(1):41.

Kremer, K., Simpson, G. & Girardclos, S. (2012) Giant Lake Geneva tsunami in AD 563. Nature Geoscience 5:756-757.

Kremer, K., Wirth, S. B., Reusch, A., Fäh, D., Bellwald, B., Anselmetti, F. S., ... & Strasser, M. (2017) Lake-sediment based paleoseismology: Limitations and perspectives from the Swiss Alps. Quaternary Science Reviews, 168, 1-18.

La Selle, S., Richmond, B. M., Jaffe, B. E., Nelson, A. R., Griswold, F. R., Arcos, M. E., ... & Gelfenbaum, G. (2020) Sedimentary evidence of prehistoric distant-source tsunamis in the Hawaiian Islands. Sedimentology, 67(3), 1249-1273.

Leonard, L. J., Rogers, G.C. & Mazzotti, S. (2014) Tsunami hazard assessment of Canada. Natural Hazards 70:237-274.

Løvholt, F., Pedersen, G., Harbitz, C. B., Glimsdal, S. & Kim, J. (2015) On the characteristics of landslide tsunamis. Philosophical Transactions of the Royal Society A: Mathematical, Physical and Engineering Sciences 373:20140376.

Lynett, P. (2010) Hydrodynamic modeling of tsunamis generated by submarine landslides: generation, propagation, and shoreline impact. In: Mosher, Shipp, Moscardekk, Chaytor, Baxter, Kee & Urgeles (eds) Submarine Mass Movements and Their Consequences. Springer, pp 685-694.

Matsumoto, D., Sawai, Y., Tanigawa, K., Fujiwara, O., Namegaya, Y., Shishikura, M., ... & Kimura, H. (2016) Tsunami deposit associated with the 2011 Tohoku-oki tsunami in the Hasunuma site of the Kujukuri coastal plain, Japan. Island Arc, 25(5), 369-385.

Merzeraud, G., Achalhi, M., Cornée, J. J., Münch, P., Azdimousa, A., & Moussa, A. B. (2019) Sedimentology and sequence stratigraphy of the late-Messinian-Early pliocene continental to marine deposits of the Boudinar basin (North Morocco). Journal of African Earth Sciences, 150, 205-223.

Meilianda, E., Dohmen-Janssen, C. M., Maathuis, B. H. P., Hulscher, S. J., & Mulder, J. P. M. (2010) Short-term morphological responses and developments of Banda Aceh coast, Sumatra Island, Indonesia after the tsunami on 26 December 2004. Marine geology, 275(1-4), 96-109.

Moore, J. G., Schweickert, R. A., Kitts & C. A. (2014) Tsunami-generated sediment wave channels at Lake Tahoe. California-Nevada, USA, Geosphere 10:757-768.

Moreira, S., Costa, P. J., Andrade, C., Lira, C. P., Freitas, M. C., Oliveira, M. A., & Reichart, G. J. (2017) High resolution geochemical and grain-size analysis of the AD 1755 tsunami deposit: Insights into the inland extent and inundation phases. Marine Geology, 390, 94-105.

Mulder, T., Zaragosi, S., Razin, P., Grelaud, C., Lanfumey, V., & Bavoil, F. (2009) A new conceptual model for the deposition process of homogenite: Application to a cretaceous megaturbidite of the western Pyrenees (Basque region, SW France). Sedimentary Geology, 222(3-4), 263-273.

Nauli, S. (1981) Zur Urgeschichte und römischen Epoche im Engadin Schriften zur urgeschichtlichen und römischen Besiedlung des Engadins. In: Conrad (ed) Schriften zur urgeschichtlichen und römischen Besiedlung des Engadins. Engadin Press AG, Samedan, pp 57-61.

Nishimura, Y., Nakamura, Y. & Putra, P. S. (2015) The influence of sediment source vegetation and microtopography on tsunami deposit characteristics. In: Wang, Rosati & Cheng (eds) The Proceedings of the Coastal Sediments 2015. World Scientific, ISBN 978-981-4689-98-4.

Oberhänsli, M., Seifert, M. & Sormaz, T. (2015) Zurück zur Quelle. Archäologie Schweiz 38(4):16-23.

Ohlendorf, C. (1998) High Alpine lake sediments as chronicles for regional glacier and climate history in the Upper Engadine, southeastern Switzerland. Dissertation, ETH Zurich.

Ontowirjo, B., Paris, R. & Mano, A. (2013) Modeling of coastal erosion and sediment deposition during the 2004 Indian Ocean tsunami in Lhok Nga, Sumatra, Indonesia. Natural hazards 65(3), 1967-1979.

Paris, R., Falvard, S., Chagué, C., Goff, J., Etienne, S., & Doumalin, P. (2020) Sedimentary fabric characterized by X-ray tomography: A case-study from tsunami deposits on the Marquesas Islands, French Polynesia. Sedimentology, 67(3), 1207-1229.

Paris, R., Fournier, J., Poizot, E., Etienne, S., Morin, J., Lavigne, F., & Wassmer, P. (2010) Boulder and fine sediment transport and deposition by the 2004 tsunami in Lhok Nga (western Banda Aceh, Sumatra, Indonesia): a coupled offshore–onshore model. Marine Geology, 268(1-4), 43-54.

Putra, P. S., Aswan, A., Maryunani, K. A., Yulianto, E., & Kongko, W. (2019) Field survey of the 2018 Sulawesi tsunami deposits. Pure and Applied Geophysics, 176(6), 2203-2213.

Rageth, J. (2000) Kleine Urgeschichte Graubündens. Archäologie der Schweiz 23(2):32-46.

Rageth, J. (2002) Sils i. E./Segl, Baselgia/nördlich Haus Suosta Veglia. Jahresberichte des Archäologischen Dienstes Graubünden und der Denkmalpflege Graubünden 141-146.

Rageth, J. (2004) Römische Fundstellen Graubündens: Schriftenreihe des Rätischen Museums Chur.

Ramírez-Herrera, M. T., Lagos, M., Hutchinson, I., Kostoglodov, V., Machain, M. L., Caballero, M., ... & Quintana, P. (2012) Extreme wave deposits on the Pacific coast of Mexico: Tsunamis or storms?—A multi-proxy approach. Geomorphology, 139, 360-371.

Ramsey, C. B. (2009) Bayesian analysis of radiocarbon dates. Radiocarbon 51:337-360.

Reimer, P. J., Austin, W. E., Bard, E., Bayliss, A., Blackwell, P. G., Ramsey, C. B., ... & Talamo, S. (2020) The IntCal20 Northern Hemisphere radiocarbon age calibration curve (0–55 cal kBP). Radiocarbon, 62(4), 725-757.

Richmond, B., Szczuciński, W., Chagué-Goff, C., Goto, K., Sugawara, D., Witter, R., ... & Goff, J. (2012) Erosion, deposition and landscape change on the Sendai coastal plain, Japan, resulting from the March 11, 2011 Tohoku-oki tsunami. Sedimentary Geology, 282, 27-39.

Riou, B., Chaumillon, E., Schneider, J. L., Corrège, T., & Chagué, C. (2020) The sediment-fill of Pago Pago Bay (Tutuila Island, American Samoa): New insights on the sediment record of past tsunamis. Sedimentology, 67(3), 1577-1600.

Roberts, N. J., McKillop, R. J., Lawrence, M. S., Psutka, J. F., Clague, J. J., Brideau, M. A., & Ward, B. C. (2013) Impacts of the 2007 landslide-generated tsunami in Chehalis Lake, Canada. In Margottini, Canuti & Sassa (eds) Landslide science and practice. Springer, Berlin, pp 133-140, ISBN 978-3-642-31319-6.

Roth-Bianchi, W. (2007) Die Geschichte des Kanton Graubünden ist die Geschichte seiner Alpenpässe und Verkehrswege. In: Historische Verkehrswege im Kanton Graubünden, Eine Publikation zum Inventar historischer Verkehrswege der Schweiz IVS. Bundesamt für Strassen (ASTRA), Bern, pp 8-21.

Sakuna, D., Szczuciński, W., Feldens, P., Schwarzer, K. & Khokiattiwong, S. (2012) Sedimentary deposits left by the 2004 Indian Ocean tsunami on the inner continental shelf offshore of Khao Lak, Andaman Sea (Thailand). Earth, planets and space 64(10):11.

Sammartini, M., Moernaut, J., Anselmetti, F. S., Hilbe, M., Lindhorst, K., Praet, N. & Strasser, M. (2020) An Atlas of Mass-Transport Deposits in Lakes. In: Ogata, Festa & Pini (eds) Submarine Landslides: Subaqueous Mass Transport Deposits from Outcrops to Seismic Profiles. Geophysical Monograph 246, American Geophysical Union – John Wiley & Sons, pp 201-226, ISBN 978-1-119-50058-2.

Schnellmann, M., Anselmetti, F. S., Giardini, D. & Mckenzie, J. A. (2006) 15,000 Years of mass-movement history in Lake Lucerne: Implications for seismic and tsunami hazards. Eclogae Geologicae Helvetiae 99:409-428.

Schnellmann, M., Anselmetti, F. S., Giardini, D., McKenzie, J. A. & Ward, S. N. (2002) Prehistoric earthquake history revealed by lacustrine slump deposits. Geology 30:1131-1134.

Smedile, A., De Martini, P. M., Pantosti, D., Bellucci, L., Del Carlo, P., Gasperini, L., ... & Boschi, E. (2011) Possible tsunami signatures from an integrated study in the Augusta Bay offshore (Eastern Sicily—Italy). Marine Geology, 281(1-4):1-13

Smedile, A., Molisso, F., Chagué, C., Iorio, M., De Martini, P. M., Pinzi, S., ... & Pantosti, D. (2020) New coring study in Augusta Bay expands understanding of offshore tsunami deposits (Eastern Sicily, Italy). Sedimentology, 67(3), 1553-1576.

Smoot, J., Litwin, R., Bischoff, J. & Lund, S. (2000) Sedimentary record of the 1872 earthquake and "Tsunami" at Owens Lake, southeast California. Sedimentary Geology 135:241-254.

Spillmann, P. & Büchi, H. (1993) The Pre-Alpine Basement of the Lower Austro-Alpine Nappes in the Bernina Massif (Grisons, Switzerland; Valtellina, Italy). In: Raumer & Neubauer (eds) Pre-Mesozoic geology in the Alps. Springer, pp 457-467, ISBN 978-3-642-84640-3.

Spiske, M., Tang, H. & Bahlburg, H. (2020) Post-depositional alteration of onshore tsunami deposits–Implications for the reconstruction of past events. Earth-Science Reviews 202:103068.

Spiske, M., Weiss, R., Bahlburg, H., Roskosch, J. & Amijaya, H. (2010) The TsuSedMod inversion model applied to the deposits of the 2004 Sumatra and 2006 Java tsunami and implications for estimating flow parameters of paleo-tsunami. Sedimentary Geology 224:29–37.

Srinivasalu, S., Rao, N. R., Thangadurai, N., Jonathan, M., Roy, P., Mohan, V. R. & Saravanan, P. (2009) Characteristics of 2004 tsunami deposits of the northern Tamil Nadu coast, southeastern India Boletín de la Sociedad. Geológica Mexicana 61:111-118.

Srinivasalu, S., Thangadurai, N., Switzer, A. D., Mohan, V.R. & Ayyamperumal, T. (2007) Erosion and sedimentation in Kalpakkam (N Tamil Nadu, India) from the 26th December 2004 tsunami. Marine Geology 240:65-75.

Stuiver, M. & Polach, H. (1977) Discussion Reporting of 14C Data. Radiocarbon 19:255-363.

Sugawara, D., Minour, K. & Imamura, F. (2008) Tsunamis and tsunami sedimentology. In: Shiki, Yamazaki, Tsuji & Minoura (eds) Tsunamiites. Elsevier, pp 9-49, ISBN 978-0-444-51552-0.

Szczuciński, W. (2012) The post-depositional changes of the onshore 2004 tsunami deposits on the Andaman Sea coast of Thailand. Natural Hazards 60:115–133.

Szczuciński, W., Chaimanee, N., Niedzielski, P., Rachlewicz, G., Saisuttichai, D., Tepsuwans, T., Lorenc, S. & Siepak, J. (2006) Environmental and Geological Impacts of the 26 December 2004 Tsunami in Coastal Zone of Thailand-Overview of Short and Long-Term Effects. Polish Journal of Environmental Studies 15:793-810.

Szczuciński, W., Kokociński, M., Rzeszewski, M., Chagué-Gof,f C., Cachão, M., Goto, K. & Sugawara, D. (2012) Sediment sources and sedimentation processes of 2011 Tohoku-oki tsunami deposits on the Sendai Plain, Japan — insights from diatoms, nannoliths and grain size distribution. Sedimentary Geology 282:40-56.

Takahashi, T. (1981). Debris flow. Annual review of fluid mechanics 13(1):57-77.

Takagi, H., Pratama, M. B., Kurobe, S., Esteban, M., Aránguiz, R. & Ke, B. (2019) Analysis of generation and arrival time of landslide tsunami to Palu City due to the 2018 Sulawesi Earthquake. Landslides 16:983-991.

Tamura, T., Sawai, Y., Ikehara, K., Nakashima, R., Hara, J.& Kanai, Y. (2015) Shallow-marine deposits associated with the 2011 Tohoku-oki tsunami in Sendai Bay, Japan. Journal of Quaternary Scienc 30(4):293-297.

Tanigawa, K., Sawai, Y.. & Namegaya, Y (2018) Diatom assemblages within tsunami deposit from the 2011 Tohoku-oki earthquake along the Misawa coast, Aomori Prefecture, northern Japan. Marine Geology 396:6-15.

Tibaldi, A. & Pasquarè, F. A. (2008) Quaternary deformations along the 'Engadine–Gruf tectonic system', Swiss–Italian Alps. Journal of Quaternary Science: Published for the Quaternary Research Association 23:475-487.

Trümpy, R. (1977) The Engadine Line: A sinistral wrench fault in the central alps. Memoir of the Geological Society of China 2:1-12.

Van den Bergh, G. D., Boer, W., De Haas, H., Van Weering, T. C., & Van Wijhe, R. (2003) Shallow marine tsunami deposits in Teluk Banten (NW Java, Indonesia), generated by the 1883 Krakatau eruption. Marine Geology, 197(1-4), 13-34.

Voight, B., Glicken, H., Janda, R. J., Douglass, P. M., & Lipman, P. W. (1981) Catastrophic rockslide avalanche of May 18. In The 1980 Eruptions of Mount St. Helens, Washington (Vol. 1250, pp. 347-377). US Geological Survey Professional Paper 1250:347-377.

Woodruff, J. D., Donnelly, J. P., Mohrig, D., & Geyer, W. R. (2008) Reconstructing relative flooding intensities responsible for hurricane-induced deposits from Laguna Playa Grande, Vieques, Puerto Rico. Geology, 36(5), 391-394.

Yamaguchi, N., & Sekiguchi, T. (2015) Effects of tsunami magnitude and terrestrial topography on sedimentary processes and distribution of tsunami deposits in flume experiments. Sedimentary Geology, 328, 115-121.

Yoshikawa, S., Kanamatsu, T., Goto, K., Sakamoto, I., Yagi, M., Fujimaki, M., ... & Sakaguchi, H. (2015) Evidence for erosion and deposition by the 2011 Tohoku-oki tsunami on the nearshore shelf of Sendai Bay, Japan. Geo-Marine Letters, 35(4), 315-328.

The City of Lucerne, Switzerland in 1597 by *Martinus Martini*, copperplate engraving (Staatsarchiv Luzern, StALU PL 5255)

5 Offshore tsunami deposits: evidence from sediment cores and numerical wave propagation of the 1601 CE Lake Lucerne event

Valentin Nigg [1 *], Paola Bacigaluppi [2], David F. Vetsch [2], Hendrik Vogel [1], Katrina Kremer [1, 3], Flavio S. Anselmetti [1]

[1] Institute of Geological Sciences & Oeschger Centre for Climate Change Research, University of Bern, Baltzerstrasse 1+3, 3012 Bern, Switzerland
[2] Laboratory of Hydraulics, Hydrology and Glaciology, ETH Zurich, Hönggerbergring 26, 8093 Zürich
[3] Swiss Seismological Service, ETH Zurich, Sonneggstrasse 5, 8092 Zürich, Switzerland

Abstract

The 1601 Common Era earthquake (M_w ca. 5.9) in "Unterwalden", Central Switzerland triggered multiple subaqueous mass movements and a subaerial rockfall that generated tsunami waves with devastating run-up heights of up to 4 m and several hundred meters of inundation along the coastal lowland plain of Lake Lucerne. In the shallow Lucerne Bay at the outlet of the perialpine lake, historical chronicles reported a seiche with an initial amplitude of ~1–2 m and a period of 10 min that decreased with time but persisted for several days after the event. The impact and erosion potential of the tsunami wave on the Lucerne Bay is assessed with sediment core analysis and numerical simulation of wave propagation. A 60 cm thick offshore event deposit was recovered and radiocarbon dated along a sediment-core transect. The event deposit has a sharp basal contact with carbonate shell fragments and a normal graded succession of siliciclastic sand to silt with high amount of terrestrial-derived horizontally bedded wooden particles. The simulated tsunami waves have a water-surface displacement of up to 1.5 m and bed shear-stresses that are likely capable of remobilizing large amounts of sediment in the Lucerne Bay area. Our study thus successfully links the sedimentology of event deposits with physical principles of sediment mobilization derived from numerical wave

modeling, providing a tool to improve the identification and interpretation of potential tsunami deposits.

5.1 Introduction

Tsunami hazard is frequently associated with megathrust earthquakes at convergent plate boundaries in the marine environment (e.g., 2011 Common Era (CE) Tohoku-Oki tsunami (e.g., Goto et al., 2011a; Suzuki et al., 2011)). But also, earthquake-triggered subaqueous mass movements have generated devastating tsunami inundation in the recent past (e.g., 2018 CE Sulawesi earthquake (e.g., Heiderzadeh et al., 2019)). Moreover, tsunamis in lakes have been recognized as a considerable natural hazard with high magnitudes and low recurrence rates (e.g., Hilbe and Anselmetti, 2015; Kremer et al., 2015; Kremer et al., 2020; Nigg et al., 2021; Strupler et al., 2018a, 2018b). Large subaqueous and subaerial mass movements are considered to be the most common triggering mechanism for the tsunami generation in lakes (e.g., Hilbe and Anselmetti, 2015; Kremer et al., 2020; Mountjoy et al., 2019; Nigg et al., 2021; Roberts et al., 2013; Strupler et al., 2020). Historic chronicles document that lacustrine tsunamis have caused severe shore erosion, inundation, and fatalities (e.g., Cysat, 1969; Hilbe and Anselmetti, 2015; Kremer et al., 2014; Nigg et al., in prep.). For example, lacustrine tsunamis have been reported in historical chronicles at Lake Geneva (564 CE Tauredunum rockfall (Montandon, 1925; Favrod, 1991)), Lake Baikal (1861 CE Tsagan earthquake (Klyuchevskii et al., 2011)), Lake Lucerne (1601 CE Unterwalden earthquake (Cysat, 1969) and 1687 CE Muota Delta collapse (Bünti, 1973; Billeter, 1923; Dietrich, 1689)). Additionally, they have been proposed to occur in the prehistoric period as a consequence of large subaqueous and subaerial mass movements (e.g., Hilbe and Anselmetti, 2014; Kremer et al., 2015; Nigg et al., 2021; Schnellmann et al., 2006; Siegenthaler et al., 1987). And have also been suggested from numerical tsunami simulations (e.g., Hilbe and Anselmetti, 2015; Kremer et al., 2012; Mountjoy et al., 2019) and subaqueous lake morphology (e.g., Gardner et al., 2000; Moore et al., 2006). However, depositional signatures of tsunami impact in the on- and offshore have received little attention in the lacustrine environment. Nevertheless, Roberts et al. (2013) document onshore sedimentary signatures of the 2007 CE subaerial landslide-generated tsunami in Lake Chehalis and Nigg et al. (2021) found sedimentary evidence of a prehistoric tsunami generated by a delta collapse in the shallow water and coastal area of Lake Sils, Switzerland, that are comparable to marine tsunami deposits.

Tsunami deposits are the accumulation of remobilized sediment from tsunami inundation and backwash in the on- and offshore setting (e.g., Einsele et al., 1996), which have been predominantly investigated in marine environments. These deposits have been increasingly studied following the devastating 2004 CE Indian Ocean tsunami (e.g., Feldens et al., 2009; Paris et al., 2010; Sakuna et al., 2012; Sugawara et al., 2009) and 2011 CE Tohoku-Oki tsunami (e.g., Goto et al., 2014; Haraguchi et al., 2013; Ikehara et al., 2014; Yoshikawa et al., 2015; Tamura et al., 2015). Although offshore deposits may contribute to improved tsunami-hazard assessment in the future (Costa et al., 2020), especially in areas with fragmented terrestrial records (Goodman-Tchernov and Austin, 2015), anthropogenically influenced coastal areas (e.g., Fritz et al., 2008; Spiske et al., 2013), limited tsunami preservation (Spiske et al., 2013), and sediment-limited coastal settings (Apotsos et al., 2011), the number of publications examining their signatures is rather small compared to their onshore counterparts (e.g., Dawson and Stewart, 2008; Costa et al., 2020). This may be related to poor preservation of the primary deposits, especially due to reworking by wind-induced bottom currents above the storm-wave base within months (Weiss and Bahlburg, 2006) and by bioturbation from aquatic organisms (van den Bergh et al., 2003). Nevertheless, previous studies have successfully identified historic and prehistoric offshore tsunami deposits in the shallow marine setting (e.g., Abrantes et al., 2008; Goodman-Tchernov et al., 2009; Riou et al., 2020; Smedile et al., 2011; van den Bergh et al., 2003). Their depositional signatures are characterized by a wide range of sedimentological characteristics (e.g., Fujiwara, 2008) including lower erosional surfaces (e.g., Ikehara et al., 2014; Riou et al., 2020; Smedile et al., 2020; Yoshikawa et al., 2015), coarse-grained clastic materials (Abrantes et al., 2008; Goodman-Tchernov et al., 2009; Paris et al., 2010; Sakuna et al., 2012; van den Bergh et al., 2003), terrestrial-derived organics (Goodman-Tchernov et al., 2009; Paris et al., 2010; Sakuna et al., 2012), as well as single- and multiple-graded sandy deposits (e.g., Tamura et al., 2015). Yet, no universal criteria for the recognition offshore tsunami deposits are defined. Nevertheless, multiproxy-based sedimentological and geophysical methods combined with numerical simulation of sediment transport will help to improve the understanding of tsunami-induced sediment remobilization and deposition (e.g., Goto et al., 2011b; Noda et al., 2007).

Tsunami sediment-transport and deposition have increasingly been studied using inverse (e.g., Huntington et al. 2007; Jaffe and Gelfenbaum, 2007; Jaffe et al., 2011; Jaffe et al., 2012; Johnson et al., 2017; Spiske et al., 2010; Tang and Weiss, 2015; Woodruff et al., 2008) and forward modelling (e.g., Apotsos et al., 2011; Apotsos et al., 2012; Ontowirjo et al., 2013;

Pritchard and Dickinson, 2008) in the onshore setting to reconstruct tsunami flow speed based on the grain-size distribution of tsunami deposits (Jaffe and Gelfenbaum, 2007). Moreover, forward models combine hydrodynamics and sediment transport models (including erosion and deposition) to simulate observed sedimentary deposits (e.g., grain-size distribution and spatial thickness distribution) (Apotsos et al., 2011). Although, little attention has been drawn to the quantification of tsunami erosion in the nearshore area to date (Yoshikawa et al., 2015), Goto et al. (2011b) determined severely impaired stability of coastal infrastructures due to strong localized scouring and sediment rearrangement. Additionally, remarkable bathymetric changes caused by tsunamis have been numerically simulated (e.g., Orai Port, Japan (Kuriyama et al., 2020)) and observed in several nearshore areas (e.g., Kirinda Harbor, Sri Lanka (Goto et al., 2011b)), suggesting substantial sediment remobilization by tsunami waves in the shallow offshore area.

The particle entrainment by flows has been quantified from flume experiments (e.g., MAntz, 1977; Shields, 1936) and identified as being strongly dependent on the bed shear-stress, flow regime, as well as grain-size distribution, grain shape, grain packing, and density of the bed surface sediment (e.g., Boggs, 2014; Buffington and Montgomery, 1977). The resulting hydrodynamic description may be partially transferable to tsunami-induced sediment transport in shallow water (Kihara et al., 2012). Therefore, for the incipient motion of sediment particles by tsunami propagation, the fluid force, which consists of the bed-parallel drag force and the horizontal lift force, need to be larger than the resistance force of the particles to be moved (e.g., Lee and Balachandar, 2012; Van Rijn, 2007). Here, the Shields diagram that relates the dimensionless bed shear-stress and the grain Reynolds number, can be used for determining the threshold of sediment motion in uniform and non-uniform flows (Shields, 1936).

The main objective of this study is to find evidence for sediment remobilization in the Lucerne Bay caused by the 1601 CE tsunami in Lake Lucerne (Hilbe and Anselmetti, 2015; Schwarz-Zanetti et al., 2003) using sediment cores, lake-surface samples, and numerical simulations of tsunami wave propagation. First, we investigate the sedimentary properties in the Lucerne Bay through a series of collected sediment cores and modern lake-surface samples. Then we simulate tsunami generation by one of the largest subaqueous mass movements triggered by the 1601 CE earthquake and examine the simulated wave characteristics (water-surface displacement, and flow-velocity magnitude) and spatial extend of threshold conditions for

incipient motion using the dimensionless bed shear-stress (Shields parameter) in the Lucerne Bay of Lake Lucerne.

5.2 Study site

Lake Lucerne is a perialpine lake located in Central Switzerland at an altitude of 433.6 m above sea-level (m a.s.l). It geologically lies between the Helvetic nappes, the Subalpine Molasse, and the Swiss Molasse basin (Fig. 5-1; Funk et al., 2013; Hantke et al., 2005; Kopp et al., 1955). The fjord-like lake consists of several sub-basins with a maximum (max.) water depth of 214 m and predominantly steep-sided lakeshores.

Lucerne Bay is a relatively shallow sub-basin in the western part of the lake with a water depth between 2.5 to 5 m (max. water depth 8 m) and a sharp transition leading to deeper parts of the lake in the east (Fig. 5-2A). The basin is glacially eroded into Burdigalian sandstones of the Upper Marine Molasse (UMM) and Aquitanian sandstones and conglomerates of the Lower Freshwater Molasse (USM; Kopp et al., 1955; Schlunegger et al., 1997). The top of the bedrock occurs at a lowermost elevation of 408.8 m a.s.l at the lake outlet (Keller, 2020) and at ~335 m a.s.l at the Lucerne railway station in the southwest of the Lucerne Bay (Keller, 2013). The up to 100-m-thick overlying Quaternary deposits consist of a sedimentary succession formed by a thick package of Late Pleistocene sediments characterized by glacially overconsolidated basal lodgment diamicts, and local esker gravels above the bedrock surface, which are overlain by heterolithic glaciolacustrine silts with sand lenses (Keller, 2020). Around 14’700 years Before Present (yr. BP), the area of the Lucerne Bay was filled with Late Pleistocene sediments up to 422 m a.s.l at the Lucerne railway station and up to 426 m a.s.l at the northern lakeshore (Keller, 2020). These sediments are overlain by a relatively thin (1–4 m) sequence of transgressive-regressive Holocene deposits that comprise shallow lake to alluvial plain deposits, peat-rich swamp deposits, carbonate mud, as well as deltaic deposits and gravelly lobes at the toe of incoming rivers (Keller, 2020). Major inflowing tributaries of the Lucerne Bay are the Würzenbach River in the northeast and the Krienbach River in the west, delivering dominantly siliciclastic material (Fig. 5-2A). The Würzenbach, entering the lake at the northern shore, is today artificially canalized, but formed a large delta over time. In the southwestern area of the City of Lucerne, the Krienbach formed an extensive Holocene flood plain with gravelly alluvial fan deposits and overbank sands that repeatedly clogged temporarily the lake outlet caused high lake levels (Keller, 2013; Keller, 2020). Nowadays, the

river is artificially diverted underground with tunnels feeding into the River Reuss, the main outflow of Lake Lucerne (Fig. 5-1).

Lake level is relatively stable at 433.6 m a.s.l., with high lake levels in spring and late summer and low lake levels in winter and peak summer (BAFU, 2009). At the time of the city foundation (~1200 CE) lake level was around 432.2 to 433.2 m a.s.l. (Keller, 2013). Through the construction of mills and a weir at the lake outlet in the 13th to 14th century, lake level was stabilized at 433.0 m a.s.l. (Keller, 2013). Prior to the historical record, lake level was presumably lower, with greater seasonal fluctuations (±1.5 m; Keller, 2020). In the Late Glacial Interstadial (~15'000–13'000 yr. BP), lake level was at ~432 m a.s.l (Keller, 2020) and during the Neolithic Period (5000–6000 yr. BP) lake was presumably lowest at around 428.6–429.5 m a.s.l. (Keller, 2013; Michel et al., 2012). After 1800 CE until today, strong artificial shoreline changes were carried out, especially around the City of Lucerne, but also around the lake in smaller villages.

5.2.1 The 1601 CE earthquake and Lake Lucerne tsunami

The 1601 CE earthquake with an epicenter in "Unterwalden", Central Switzerland (Mw ca. 5.9; Fäh et al., 2011; Schwarz -Zanetti et al., 2003) triggered multiple subaqueous mass movements (e.g., Hilbe et al., 2011; Siegenthaler et al., 1987; Schnellmann et al., 2002, 2006) and a subaerial rockfall (e.g., Keller, 2017; Schnellmann et al., 2006; Schwarz-Zanetti et al., 2003). All of these mass movements generated a basin-wide tsunami with wave heights exceeding 4 m and devastating inundation and run-up along the lakeshore (e.g., Cysat, 1969; Hilbe and Anselmetti, 2015). Several casualties caused by the tsunami waves were reported (Cysat, 1969). In the shallow Lucerne Bay, at the outflow of the lake, historical chronicles report a seiche with an amplitude of about 1 to 2 m and an initial period of 10 min. Its amplitude decreased with time but the seiche persisted for several days after the event (Cysat, 1969).

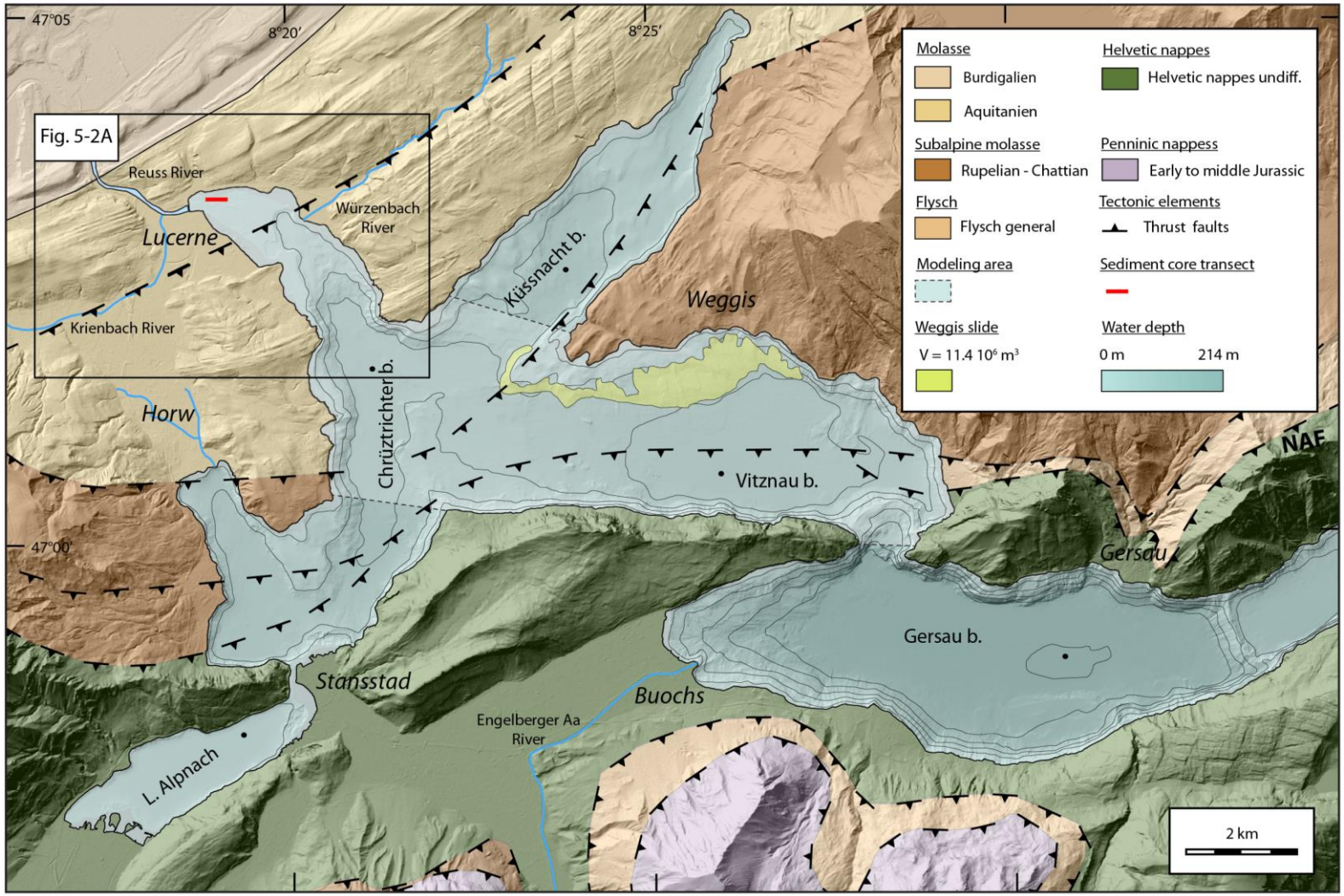

Fig. 5-1: Western part of Lake Lucerne with individual lake basins (note that the Uri Basin in the east is not shown), extent of numerical simulation (light-blue area), dashed line indicating open weir boundary condition towards adjacent lake basins), and areal extent of the simulated Weggis-slide mass movement (yellow). The map is based on the swisstopo swissALTI3D digital terrain model, geological map of swisstopo (GK500-Geol) and the bathymetry map of Hilbe et al. (2011).

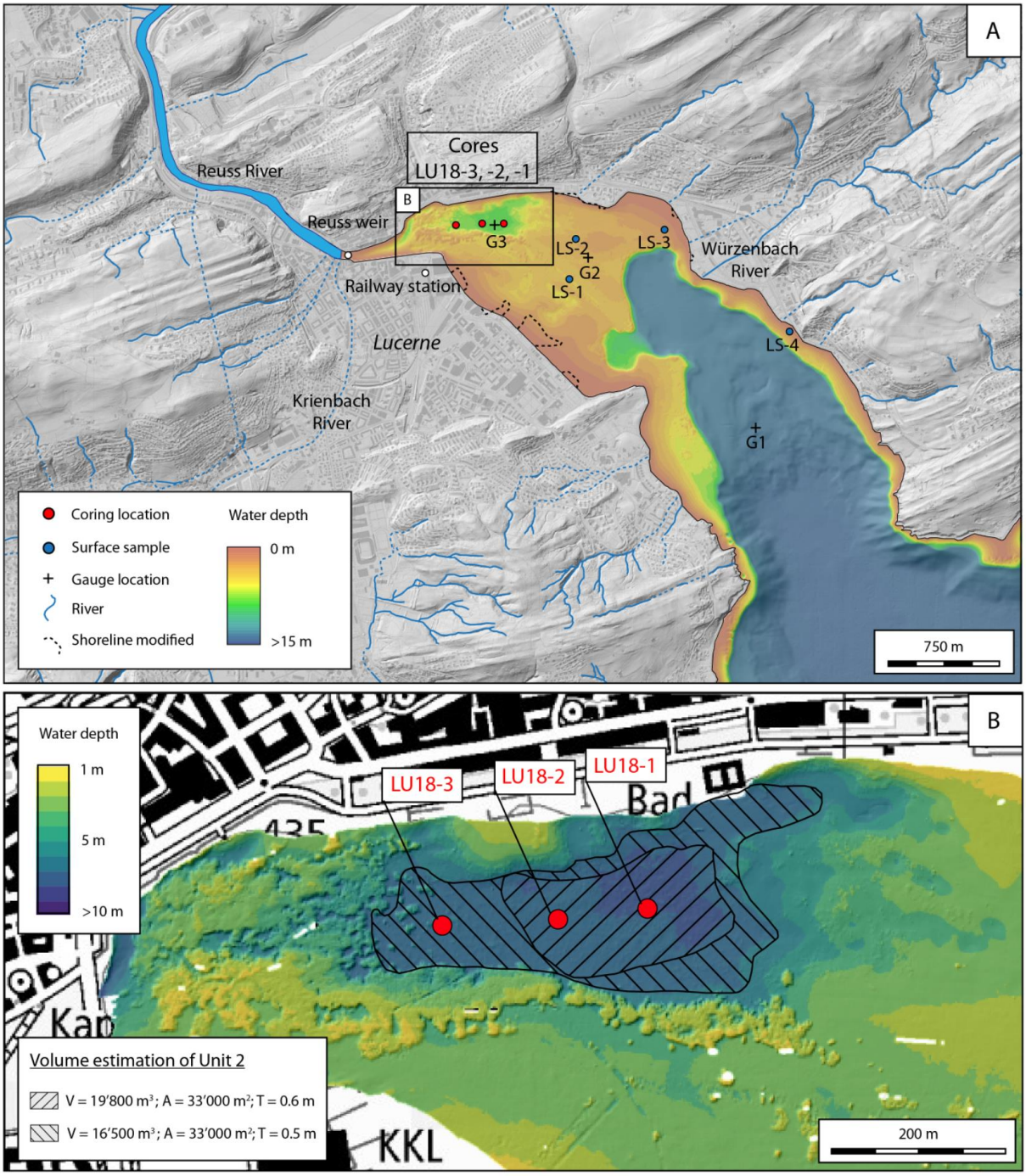

Fig. 5-2: A) Detailed map of the Lucerne Bay with the interpolated bathymetry (modified from Hilbe et al., 2011) used for the numerical simulation with its outline (solid black line) and artificial obstacles such as landfills and coastal infrastructure that were cut off (exact shoreline course: dashed line). The map is based on the swisstopo digital terrain model swissALTI3D and the national map LK50 from swisstopo. The sediment core location (red dots), sediment core ID (red), surface sediment samples (blue dots) and virtual gauges (black crosses) plotted in Fig. 5-9 are shown. B) Detailed high-resolution bathymetric map (Hilbe et al., 2011) of the east-west oriented depression shows the location of the sediment cores (red dots) and the area (black shaded) used for the volume estimation of the siliciclastic-rich normally graded Unit 2. The shallowest and rugged topography represents artifacts caused by aquatic plants.

5.3 Methods

5.3.1 Sedimentological investigations

High-resolution (1 m grid cell) bathymetrical data of Lake Lucerne (Hilbe et al., 2011) were used for the coring-site selection (Fig. 5-2B). Three sediment cores (Core LU18-1, -2, and -3) were recovered from a floating platform in water depth between 7 to 8 m (Fig. 5-2B) with a 3-m-long percussion piston-coring system (UWITEC Co. Austria) up to a subsurface depth of 3.5 m. A gravity corer was used to recover the undisturbed water-sediment interface. The observed lithological units are visually correlated. Lake-surface samples were collected at four locations along the Lucerne Bay.

Sediment cores

Petrophysical properties (bulk density gamma-ray attenuation, magnetic susceptibility, and p-wave velocity) were measured on all recovered whole round cores with a Geotek multi-sensor core logger (MSCL-S). Whole round cores also underwent X-ray computed tomography (CT) imaging using a medical Siemens Somatom Definition AS scanner. Full core CT-scan data were obtained at a voxel size of 100 μm and visualized with the RadiAnt DICOM Viewer software (version 4.6.9.18463). Sediment cores were split longitudinally, imaged with the MSCL-S core logger line-scan camera, and sedimentologically described. A complete composite sediment record was obtained by visual correlation of overlapping piston and gravity cores. High-resolution assessment of sediment geochemistry by means of X-ray fluorescence (XRF) scanning was performed on split core surfaces of Core LU18-2 with an ITRAX-XRF core scanner (Cox Ltd., Sweden). Measurements were performed with a Cr-tube set to 30 kV and 50 mA using longitudinal 2 mm integrals and 20 s integration times. Here we report relative intensities of calcium (Ca) and silicon (Si) to aluminum (Al) and titanium (Ti), respectively.

Sediment samples were continuously taken at 10 cm intervals in Unit 1 and 2 (Core LU18-2) and at 1 cm intervals in Unit 3 (Core LU18-1). Only two subsamples were taken from the top of Unit 4 (Core LU18-1) due to its presumably glacio-lacustrine sediment appearance. All sediment sub-samples were freeze-dried and homogenized using mortar and pestle. Total carbon (TC), total nitrogen (TN) and total sulfur (TS) concentrations were measured on these samples with a Flash 2000 NCS (Thermo Fisher Scientific Co.) flash combustion elemental analyzer configured with a MAS plus autosampler (Thermo Fisher Scientific Co.) and thermal

conductivity detector. For analysis samples were weighed into tin (5–8 mg) capsules for TC, TN, and TS measurements and silver (4–5 mg) capsules for total organic carbon (TOC) measurements. For TOC concentration measurements samples were treated with 1M HCl until no visual reaction occurred. The remaining HCl was evaporated prior to flash combustion analysis. Total inorganic carbon (TIC) was calculated from the differences between TC and TOC. The molar carbon-to-nitrogen (C/N) ratio was determined from TOC and TN concentrations. $CaCO_3$ was calculated from TIC using the stoichiometric conversion factor of 8.33.

A sandy deposit (Unit 2) was continuously subsampled at 1 cm intervals between 37 and 120 cm depth in Core LU18-2 for grain-size analysis. Subsamples with a wet weight of 1 g were treated with 10%vol HCl and 10%vol H_2O_2 to remove solid carbonate species and organic matter. A dispersion solution containing $Na_6P_6O_{18}$ and Na_2CO_3 was added to the remaining clastic fraction and shaken in aqueous suspension for an 1 h prior to analysis. Laser diffraction analysis (LDA) was then carried out with a Malvern Mastersizer 3000 particle size analyzer. Volume percentages (%vol) was calculated for each sample from the average of 3 aliquot measurements. Grain-size classes are presented after the classification proposed by Wentworth (1922).

Radiocarbon dating of terrestrial plant macro-remains from Core LU18-2 was used to date a sandy deposit (Unit 2). In total 6 samples were measured by accelerator mass spectrometry (AMS) with the Mini RadioCarbon Dating System (MICADAS) at the Department of Chemistry and Biochemistry, University of Bern. Radiocarbon ages were calibrated into calendar years Common Era (cal CE) using the OxCal software (version 4.3; Ramsey 2009) and the IntCal20 Northern Hemisphere calibration curve (Reimer et al. 2020).

Lake-surface sediment

Lake surface samples (uppermost ~10 cm) were collected by diving with a shovel and a bucket during summer from a sailboat. The collected lake-surface sediment samples (Fig. 5-2A) were described macroscopically using a binocular. Total carbon, TN, TS, and TOC concentrations were measured, and TIC and $CaCO_3$ concentrations as well as the molar C/N ratio was calculated according to the procedure described above. For the grain-size analysis the same procedure as described in the previous section was performed.

Estimation of sediment volume for Unit 2

The depositional volume of Unit 2 was estimated based on the high-resolution bathymetric data from Hilbe et al. (2011) and the thickness of Unit 2 observed in sediment cores. Polygons of the estimated areal extent of the sediment packages were drawn, and the area was calculated using ArcMap (version 10.8.1). Due to high gas content of sediment in the Lucerne Bay area, previously acquired seismic reflection data could not be used to characterize the spatial distribution of sedimentary units.

5.3.2 Numerical simulation, visualization, and sensitivity analysis of the bed shear-stress

The wave generation, propagation, and inundation were numerically simulated with the software BASEMENT (BAsic-Simulation-EnvironMENT). The software, originally designed for quasi-1D and 2D simulations of river hydro- and morphodynamics in alpine and subalpine regions (Vanzo et al., subm.), has been recently validated for the hydrodynamic modelling of tsunami waves on lakes (Bacigaluppi et al., in prep.).

BASEMENT is a freeware (www.basement.ethz.ch). The numerical modelling tool is used in academic research as well as engineering practice and provides a user-friendly environment for study of manifold problems. It enables the simulation of steady and unsteady hydraulic flow conditions with complex geometries as well as sediment transport. The underlying mathematical description is based on a decoupled system of equations given by the 2D-depth averaged non-linear shallow-water model for the hydrodynamics and the Exner equation for morphodynamical modelling. Finite volume spatial discretization in combination with Riemann solver guarantees the stability and robustness of the numerical solution (Vetsch et al., 2020). Due to its highly optimized design, the software allows for accelerated simulations using multi-core CPUs, GPUs (graphic processing unit), and hybrid CPU-GPU. For hydrodynamic simulations, BASEMENT computes water-surface elevation h and specific discharges q_x and q_y in a selected computational domain. From these quantities, the water-surface displacement

$$A = h - h_{ref},$$

with h_{ref} initial still water reference-level and the flow-velocity magnitude

$$u = \frac{\sqrt{q_x^2 + q_y^2}}{h}$$

can be derived (Fig. 5-3).

The bed shear-stress is defined as

$$\tau = \frac{u^2 \rho_f}{c_f^2},$$

with ρ_f fluid density, c_f friction coefficient for fully turbulent flow computed according to Chézy as

$$c_f = 5.75 \log(12 \frac{h}{k_b})$$

(e.g., Bobrowsky and Marker, 2018) and bed roughness (k_b), which may range from grain roughness to total physical bed-roughness as mentioned in Houwman and van Rijn (1999). The dimensionless form of the bed shear-stress derived by Shields (1936) based on dimensional analysis (also known as the Shields parameter) is defined as

$$\theta = \frac{\tau}{(\rho_s - \rho_f) g d_s},$$

where ρ_s represents the sediment density, g the gravitational acceleration and d_s the grain diameter of bed surface sediment.

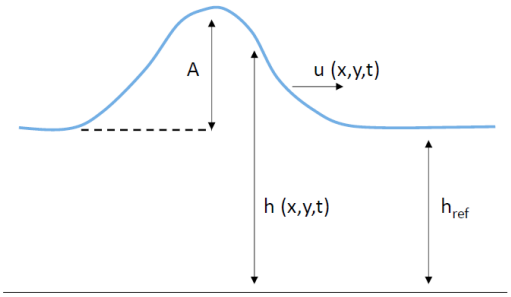

Fig. 5-3: Sketch of computed numerical quantities: initial still-water reference-level (h_{ref}), water-surface elevation (h), water-surface displacement (A) and flow-velocity magnitude (u).

The considered computational domain is limited to the Vitznau Basin and the Lucerne Bay with open boundaries (non-reflective boundary condition) to allow a natural outflow towards the Gersau, Küssnacht, and Horw Basins and at the lake outlet in the Lucerne Bay (Fig. 5-1). The digital elevation model is based on the high-resolution bathymetric data obtained by Hilbe et al. (2011), which was resampled to a cell size of 25 m^2. Shallow-water areas (water depth 0–4 m), which are not entirely covered by the bathymetrical data were linearly interpolated to the current shoreline, whereas large artificial obstacles (islands and port facilities) were cut out (Fig. 5-2). From the resampled bathymetry, the computational grid with 787.4k triangular elements with an average cell size of 115 m^2 in the central Vitznau Basin and 25 m^2 in the Lucerne Bay area was created. Details on the computational performance are summarized in Table 5-1 to allow an estimation on the computing time requirements for the numerical simulation performed.

The initial volume of the mass movement was taken from the bathymetric reconstruction prior to the 1601 CE earthquake (Hilbe and Anselmetti, 2015). The initial displacement of the water column caused by the "Weggis-slide", was modelled with an instantaneous downward vertical displacement of the identified area by 5 m (2.3 km^2 area with a total failed volume of 11.4 x 10^6 m^3; Fig. 5-1).

Table 5-1: Details of the numerical set-up and performance of the simulation via BASEMENT.

number of mesh elements	element area range [m^2]	simulation time [s]	computing time [s]	GPU card
787.4k	25-115	1800	312	TeslaP100-PCIE-12GB

Data visualization was performed with the numerical data visualization software Paraview (V5.8.1, www.paraview.org). Three virtual gauges were placed in the Lucerne Bay: gauge 1 is located at the entrance of the Lucerne Bay, gauge 2 in the shallow-water area and gauge 3 in the east-west oriented depression (Fig. 5-2A). Time series of water-surface displacement, flow-velocity magnitude, specific discharge, bed shear-stress and dimensionless bed shear-stress (Shields parameter) were investigated using gauge data (see Appendix C: Figs. C1, C2, and C3). In addition, the spatial variability of the variables at different time steps was analyzed on map scale. Flow-field vectors were used to reconstruct the flow path and direction of potential sediment transport.

5.4 Results

5.4.1 Lake-surface sediments

The lake-surface sediment samples (Table 5-2) are characterized as carbonate mud with coarse organic remains (Sample LS-1 and LS-2), poorly sorted siliciclastic sand with fine gravel and carbonate shells (Sample LS-3), and a mixture of siliciclastic fines and carbonate mud with coarse organic remains (Sample LS-4). Sample LS-1 and LS-2 are collected in the central part of the Lucerne Bay (Fig. 5-2A). Sample S-3 is taken in the western part of the Würzenbach river delta, and Sample LS-4 on the northeastern lakeshore of the Lucerne Bay (Fig. 5-2A).

Table 5-2: Lake-surface sediment samples collected in the shallow area of the Lucerne Bay: sample ID, macroscopic description, TOC and $CaCO_3$ concentrations, molar C/N ratio, D_{50} of the grain-size distribution as well as the volume percentage of the clay-, silt- and sand fraction.

Sample ID	Macroscopic description	TOC (wt.%)	$CaCO_3$ (wt.%)	C/N ratio (mol mol^{-1})	D_{50} (µm)	Clay (vol.%)	Silt (vol.%)	Sand (vol.%)
LS-1	Carbonate mud with coarse organic	2.208	80.8	6.7	45	3	60	37
LS-2	Carbonate mud with coarse organic	2.424	78.4	6.8	58	3	50	47
LS-3	Poorly sorted siliciclastic sand with fine gravel	0.427	5.1	7.5	340	0	3	97
LS-4	Carbonate mud with coarse organic	2.481	26.9	9	45	3	62	35

5.4.2 Sediment-core data

Based on high-resolution bathymetric data (Hilbe et al., 2011) a topographic depression was identified in the Lucerne Bay near the lake outlet (Fig. 5-2B). The depressional feature is characterized by an east-west oriented longitudinal shape with a length of ~400 m and width of ~200 m, and an average water depth of 7.5 m, while the surrounding plateau of the Lucerne Bay has a water depth of ~3.5 m. This depression surrounded by shallow water provide an ideal depositional environment suitable for trapping remobilized sediment from tsunami inundation and backwash. Three sediment cores (LU18-1, LU18-2, and LU18-3) were retrieved along an east-west oriented transect within the depression to study sedimentary composition and structures.

Recovered sediment cores have a complete composite sediment record of 284 cm (Core LU18-1); 288 cm (Core LU18-2) and 218 cm (Core LU18-3). The lithostratigraphy consist of four well-traceable sedimentary units (Fig. 5-4) observed along the offshore sediment core transect (Fig. 5-5), which were identified by visual appearance and core-log data.

Sedimentary unit description

i) Unit 1: carbonate mud

Unit 1 is light gray in color, varies in thickness between 17 and 43 cm, consists of shell fragments embedded in an endogenous carbonate mud matrix, with siliciclastic minerals only as accessories. It has a $CaCO_3$ concentration of 70–80 wt.%, a gradual downcore decrease in TOC (3.3–1.5 wt.%), and an increase in the C/N ratio (7–13 mol mol^{-1}) and density (1.2–1.5 g cm^{-3}, Fig. 5-5). Magnetic susceptibility is slightly negative in the upper 20 cm (-4 SI 10^{-5}) and has a peak at 27.5 cm depth (197.5 SI 10^{-5}), which is due to metallically shiny, black, gravel-sized coal particles.

ii) Unit 2: normal graded sand to silt

Unit 2 is dark brown in color and consists of a thick (40 - 67 cm), dense, siliciclastic normal graded fine to medium sand with sharp lower and upper contacts and four internal subunits (Subunit 2_A to 2_D, Fig. 6). Coarse sand-sized shell fragments are finely dispersed in a fine siliciclastic sand at the bottom of the 40 to 67 cm thick normal graded sand to silt deposit with sharp lower and upper sedimentary contacts observed by sediment core line scan and CT grayscale images (Fig. 5-5). The enrichment of macroscopically observed carbonate shell fragments at the bottom is also expressed in the distinct XRF Ca/Ti ratio peak at the base (Fig. 5-5). In the upper part, carbonate is homogeneously present (13.5–16.5 wt.%) and is occasionally found as fine sand-sized shell fragments. The C/N ratio (14 to 20 mol mol^{-1}) could only be calculated in the top three sub-samples at 40, 50, and 60 cm core depth, but not in the lower sub-samples due to nitrogen concentrations below detection limit (Fig. 5-5). The high C/N ratio fits well to the large amount of macroscopic, horizontally embedded wood fragments, whose abundance decreases toward the base. Magnetic susceptibility ranges from 3 to 18 SI 10^{-5}, and density increases downcore from 1.5 to 2.1 g cm^{-3}. Similarly, the mean grain size (D_{50}) and sorting increases downcore from poorly to moderately sorted silt to well sorted fine sand (Fig. 5-6). Four subunits were identified from the LDA grain-size data, (2_A (37-55 cm), 2_B (55-60 cm), 2_C (60-95 cm) and 2_D (37-55 cm)), which are grouped based on their mean grain size

(D_{50}) and grain-size distribution. The XRF Si/Al ratio correlates well with the LDA grain-size data and can be used as grain-size indicator (Fig. 5-5).

iii) Unit 3: light brown gyttja

Unit 3 is a light brown gyttja with occasional beige laminae, variable thickness between 2 to 10 cm with coarse sand and carbonate shell fragments embedded in an organic-rich matrix with low density (1.7 g cm^{-3}), and a gradual transition over > 2 cm at the base (Subunit 3_T). The low density of the unit is well pronounced in the CT grayscale image, which has sand-sized particles (siliciclastic grains as well as complete and fragmented carbonate shells) embedded in an organic matter-rich matrix (Fig. 5-7). Total organic carbon is high (1.5–2 wt.%) in the upper part (83–91 cm) and decreases to ~0.2 wt.% at the base of the unit. The C/N ratio varies between 9.5 to 13 mol mol^{-1} and sulfur is present (0–0.2 wt.%). $CaCO_3$ varies between 13–54 wt.% and is highest within the beige laminae. Magnetic susceptibility is ~3 SI 10^{-5}. A gradual transition with variable thickness along the sediment-core transect is evident at the base of the unit on the CT grayscale image (Fig. 5-7). The transitional base of Unit 3 is brownish gray in color and consists of fine to medium sand with carbonate shell fragments (Fig. 5-5) and a distinct peak in the XRF Ca/Ti ratio (Fig. 5-5).

iv) Unit 4: dense – cohesive silty clay

Unit 4 is light gray in color and consists of a cohesive, very dense (~2.1 g cm^{-3}) silty, clay-rich sedimentary deposit. Magnetic susceptibility varies only slightly within the unit (7–12 SI 10^{-5}). Fine laminae of variable thickness and graded fine sand to silt are well recognizable on CT grayscale images (Fig. 5-5). These graded intervals are also well expressed in the XRF Si/Al ratio that may be used as grain-size indicator (Fig. 5-5).

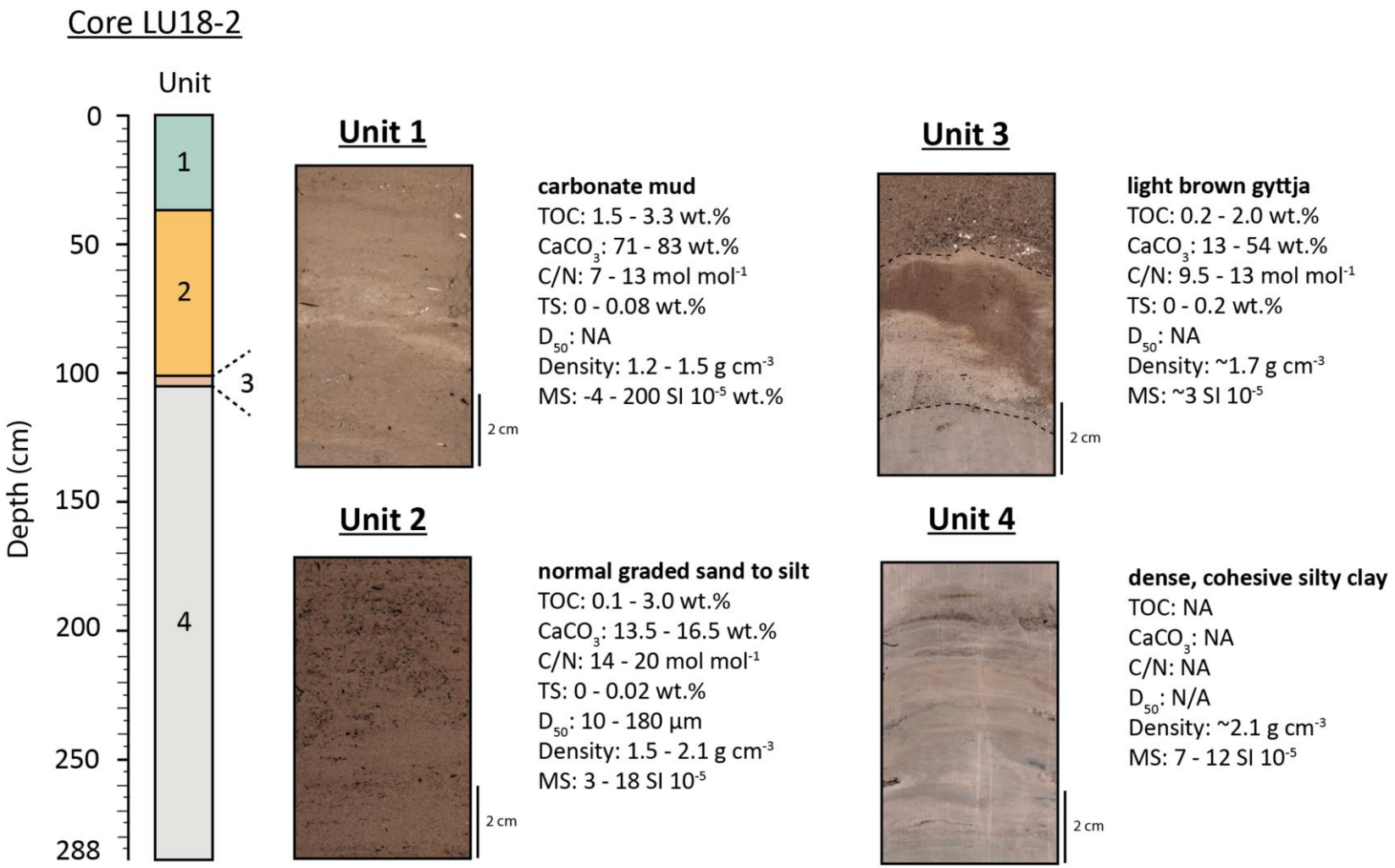

Fig. 5-4: Complete composite sediment Core LU18-2, selected line-scan images of the four lithologic units, and its sedimentologic properties (TOC, $CaCO_3$, and TS concentrations, and molar C/N ratio, D_{50} of the LDA grain-size distribution, density, and magnetic susceptibility (MS)) of the four sedimentary units. Note that in the line-scan image of Unit 3, the lower gradual contact and upper sharp contact are indicated with a dashed black line.

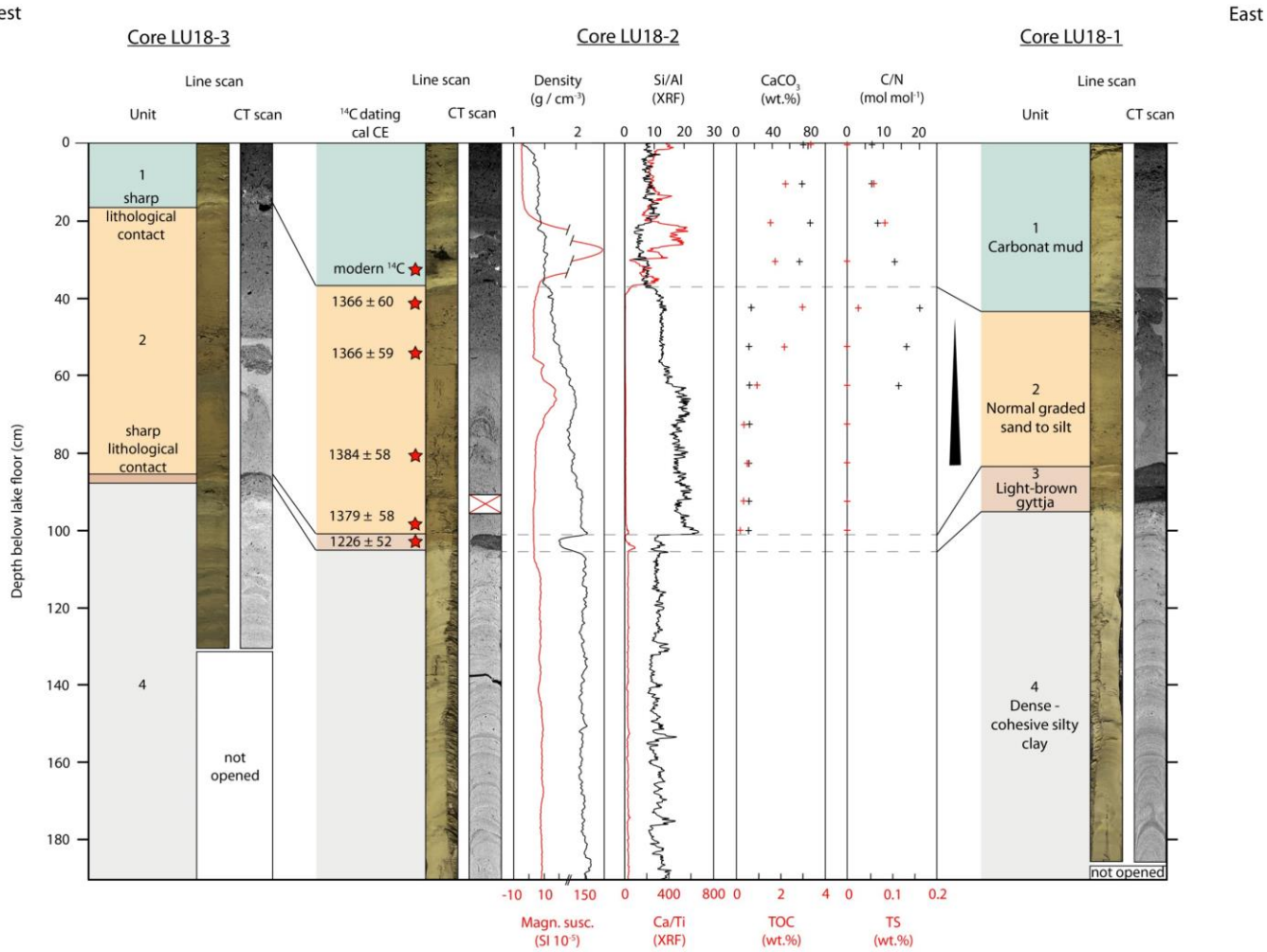

Fig. 5-5: Sediment core transect of core LU18-1, -2 and -3 recovered along the east-west oriented depression in the Lucerne Bay (Fig. 5-2B). The sedimentological transect overview shows calibrated radiocarbon ages, sedimentary units, line-scan images, CT-grayscale images, density, magnetic susceptibility (Magn. susc.), Si/Al- and Ca/Ti ratio from the XRF scans, $CaCO_3$, TOC and TS concentrations, and molar C/N ratio (see Fig. 5-7 for results of Unit 3).

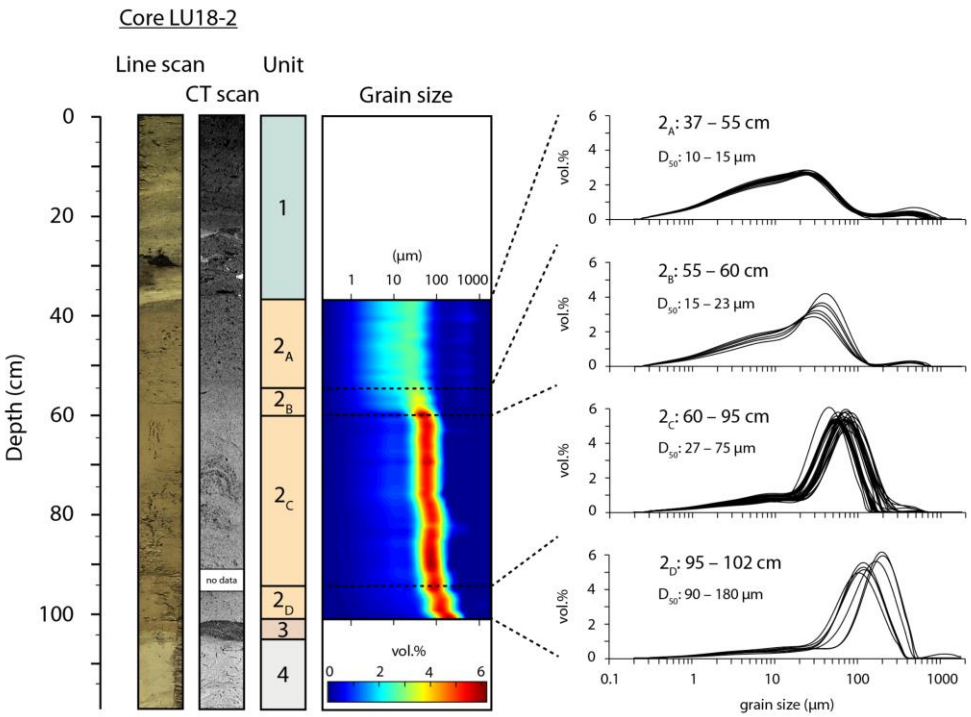

Fig. 5-6: Line-scan image, CT-grayscale image, and particle-size distribution from the LDA of Unit 2 in Core LU18-2. The grain-size distribution of the siliciclastic fraction shows a pronounced fining upward trend in Unit 2, which is divided into 4 subunits (2_A to 2_D).

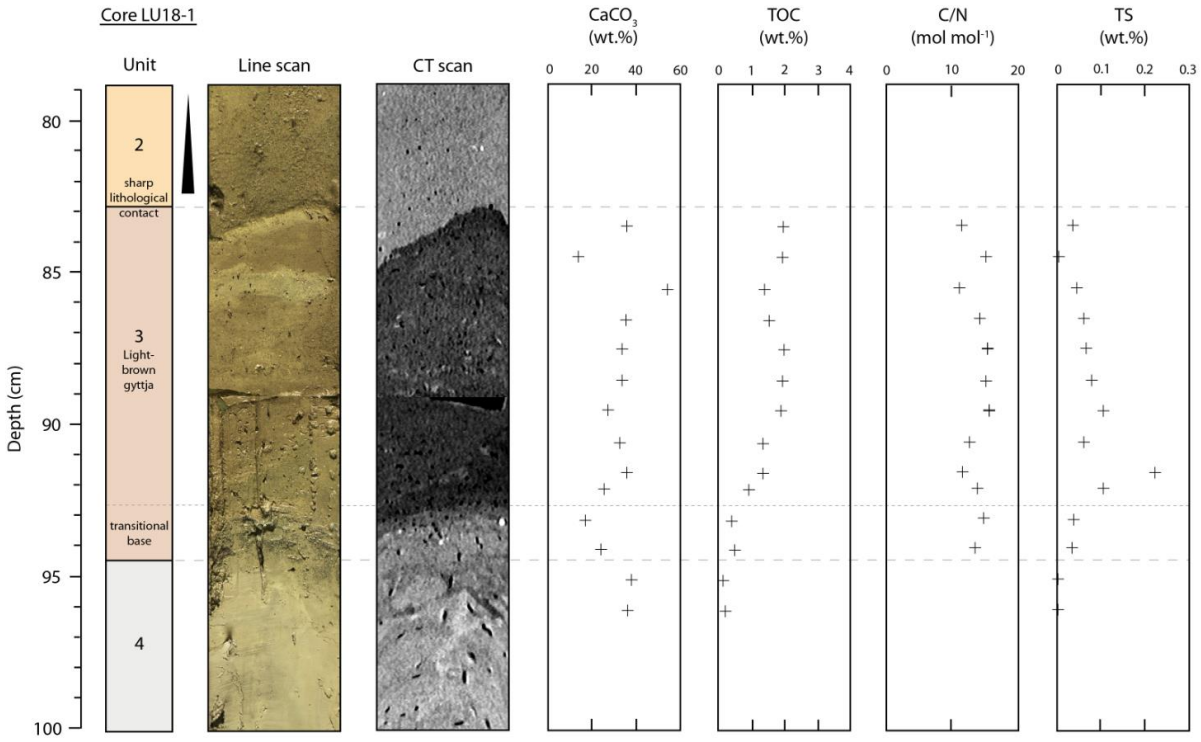

Fig. 5-7: Line-scan image, CT-grayscale image, $CaCO_3$, TOC and TS concentrations, and the molar C/N ratio of sub-samples from Unit 3, its lower transitional base and the uppermost of Unit 4 in Core LU18-1. The sharp basal contact of Unit 2 is well recognizable in the CT-grayscale image.

5.4.3 Radiocarbon dating

Four radiocarbon dates obtained from terrestrial organic macro remains found in Unit 2 have calibrated radiocarbon ages in the range of 1306–1442 cal CE (Table 5-3 & Fig. 5-5). The four samples were collected at regular intervals throughout the unit. One sample of fragmented leaves from Unit 3 yields a radiocarbon age of 1174–1277 cal CE. Another sample of leaf fragments in Unit 1 has a modern radiocarbon age (Table 5-3). The calibrated radiocarbon age ranges presented are given within a 2σ confidence level, which corresponds to a 95.4% probability.

Table 5-3: AMS radiocarbon age and $\delta^{13}C$ results from terrestrial organic macro remains from Core LU18-2. Radiocarbon age uncertainties refer to 1-sigma uncertainties. Range of calibrated represent 95.4% probability (2σ).

Sample	Core depth (cm)	Sample material	$\delta^{13}C$ (‰)	14C age ± 1σ (14C years BP)[a]	Calibrated 2σ range (cal CE)[b]
BE-10751.1.1	35–36	Leave fragments	-28.7	-572 ± 31	Modern
BE-10752.1.1	41–42	Conifer needle	-28.7	570 ± 31	1306–1425
BE-10753.1.1	54–55	Conifer needle	-28.8	567 ± 30	1307–1425
BE-10754.1.1	79–80	Conifer needle	-27.4	527 ± 31	1326–1442
BE-10755.1.1	98–99	Leave fragments	-31.8	544 ± 30	1321–1437
BE-10756.1.1	102–103	Leave fragments	-29.7	812 ± 36	1174–1277

[a] Stuiver and Polach (1977); [b] Ramsey (2009); [b] Reimer et al. (2020).

5.4.4 Volume estimation of Unit 2

The estimation of the total volume of Unit 2 along the east-west oriented depression is based on high-resolution bathymetrical data and retrieved sediment cores. Three polygons with areas of 10’395 m^2, 14’507 m^2 and 8’148 m^2, with a corresponding thickness of 0.4 m, 0.64 m, and 0.67 m, respectively, yield an estimated total depositional volume of 18’902 m^3 (Fig. 5-2B).

5.4.5 Numerical tsunami model

Tsunami generation and propagation

The 1601 CE Weggis-slide collapse with a volume of 11.4 x 10^6 m^3 (Hilbe and Anselmetti, 2015) was simulated by an instantaneous collapse of a 5 m thick sediment drape located on the northern lateral slope of the Vitznau Basin (Fig. 5-1). This moving slab and the affected area

(> 2 km^2) correspond to the well-defined 1601 CE Weggis-slide described by Schnellmann et al. (2005) and Hilbe et al. (2011). The numerically simulated wave generation and propagation can be divided in three phases: wave generation (phase 1), wave propagation in the Vitznau Basin (phase 2), and arrival of a first wave trough in the Lucerne Bay that is followed by 3 main wave pulses (phase 3).

A wave trough with a water-surface displacement with respect to the lake at rest of more than -3 m forms immediately after the instantaneous collapse along the failed area (Fig. 5-8). After 20 s the first waves reach the nearest shore with wave crests of 2 m forming after 40 s. The tsunami wave reaches the steep southern shore within 60 s and is reflected into the Vitznau Basin. A complex wave pattern is formed along the northern shoreline. In the initial phase, a wave trough approaches the shore (after 10 s), which is followed by a long lasting spatially heterogeneous wave crest with water-surface displacements up to 2 m (from 40 to 100 s), until the reflected wave trough from the southern shore superposes the established wave crest (after 80 s).

Figure 5-9 shows four time-snapshots of the computed tsunami propagation and water-surface displacement in the Lucerne Bay. A train of waves arrives in the narrow and shallow Lucerne Bay with an initial wave trough and a water-surface displacement of up to -1 m after 410 s. At the transition from the deeper to the more shallow-water area of the Lucerne Bay, a strong surge occurs in the direction of the wave trough with a flow-velocity magnitude greater than 2 m s^{-1}. At ~550 s the first wave crest with a water-surface displacement between +0.2 and +0.5 m inundates the bay with a bore-like appearance and max. flow-velocity magnitudes of 2.2 m s^{-1} at the wave front. The second wave trough is characterized by a complex and heterogeneous flow field, which inundates the bay at ~755 s. The second wave crest has an impressive bore-like wave with a max. flow-velocity magnitude of ~2.4 m s^{-1} at gauge 1 and ~0.9 m s^{-1} at gauge 3 (Fig. 5-10). The third wave has a smaller water-surface displacement than the first two, but flow-velocity magnitudes reached at gauges 2 and 3 are similar (Fig. 5-10). The third wave is followed by waves with smaller water-surface displacements and flow-velocity magnitudes (Fig 5-10).

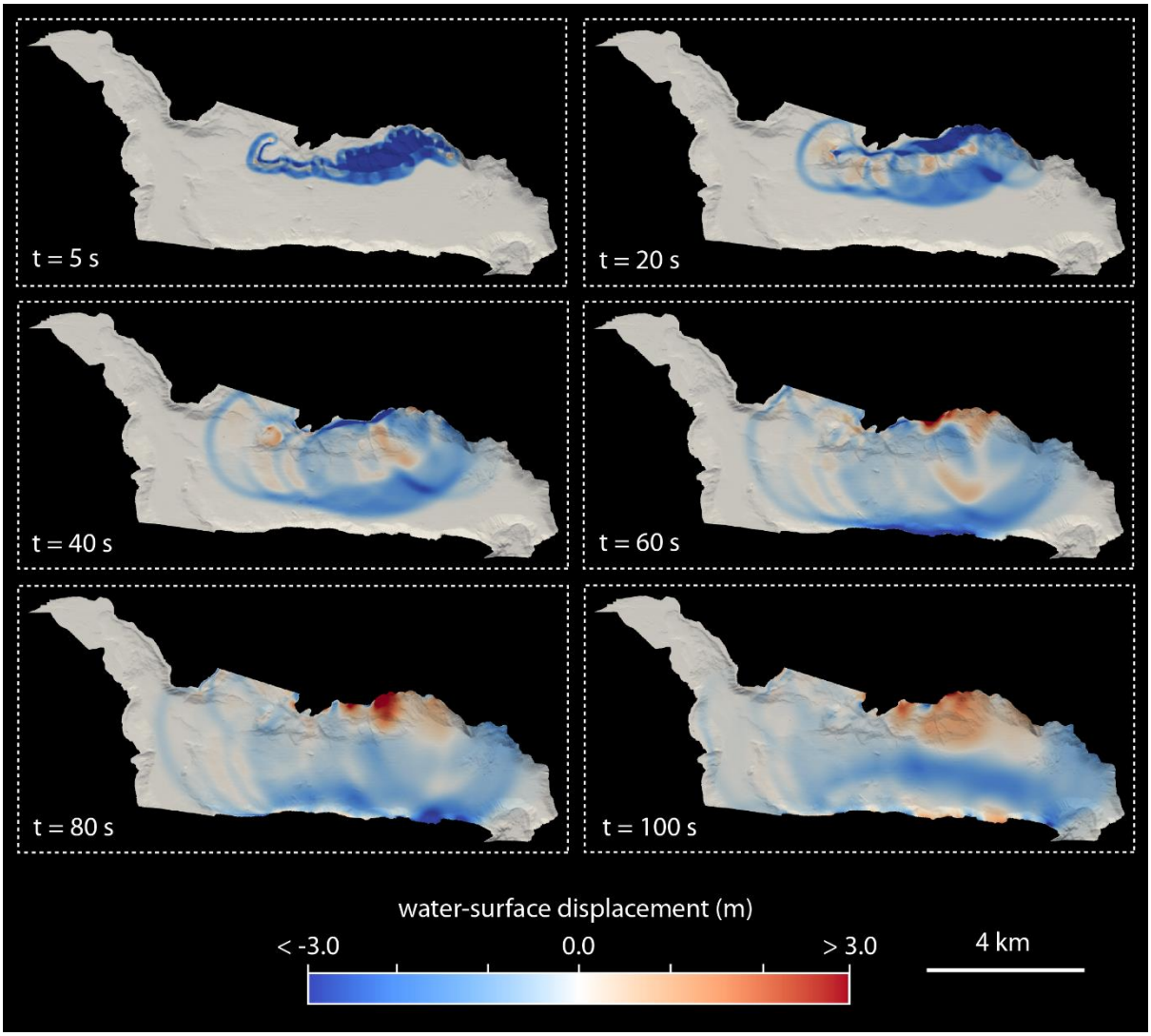

Fig. 5-8: Time snapshots of the computed tsunami propagation and water-surface displacement (-3 to +3 m with respect to the lake at rest) of the 1601 CE Weggis-slide (simulation LU18-S4) within the first 100 s after the simulated slope collapse.

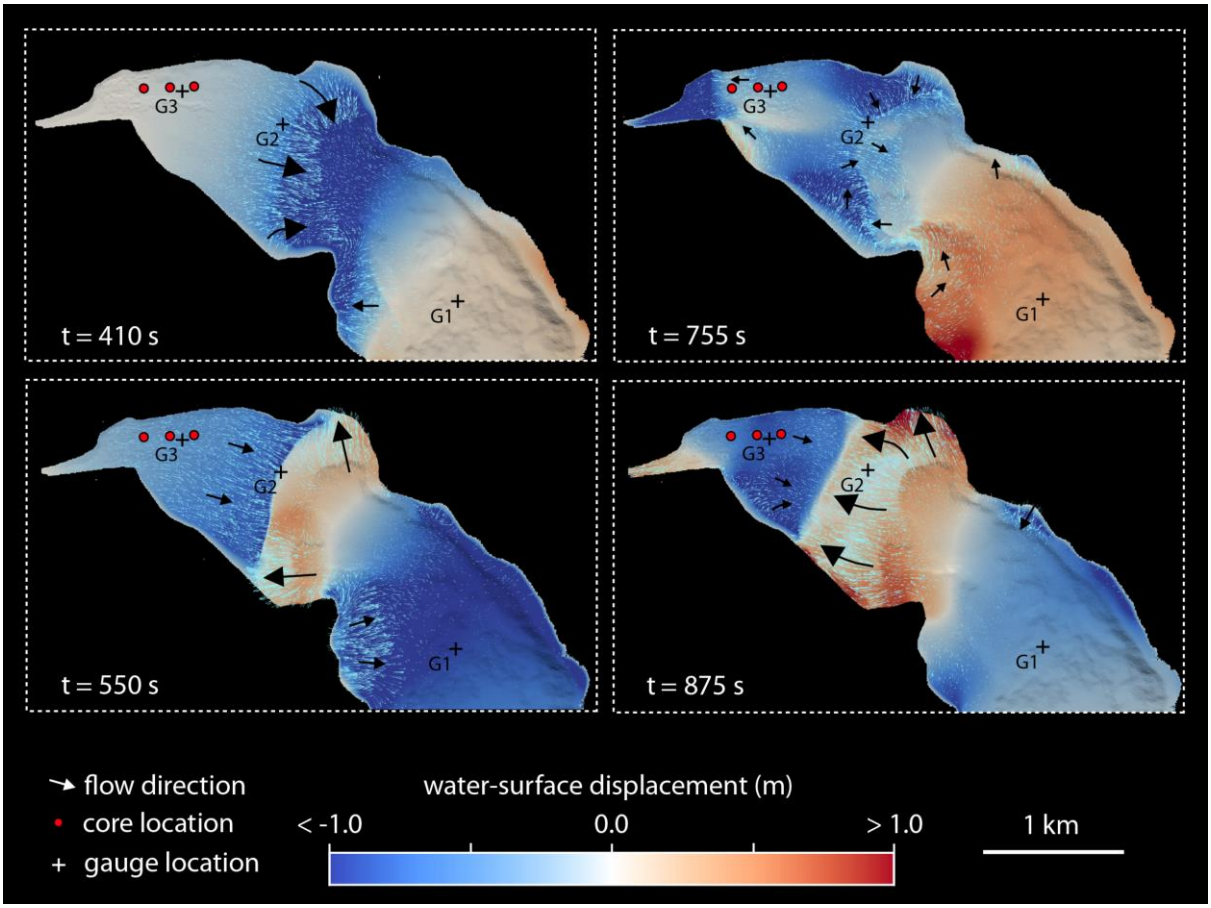

Fig. 5-9: Time snapshots of the computed tsunami propagation and water-surface displacement of the 1601 CE Weggis slide (simulation LU18-S4) in the Lucerne Bay. The water-surface displacement (-1 to +1 m) and flow-velocity direction (black arrows redrawn for better visualization of actual model data indicated with fine, light-blue arrows) are shown at four distinct time steps (410, 550, 755, and 875 s). Time series of water-surface displacement and flow-velocity magnitude at the virtual gauges 1, 2, and 3 (black crosses) are plotted in Figure 5-10. Core locations (red dots) are shown in the map.

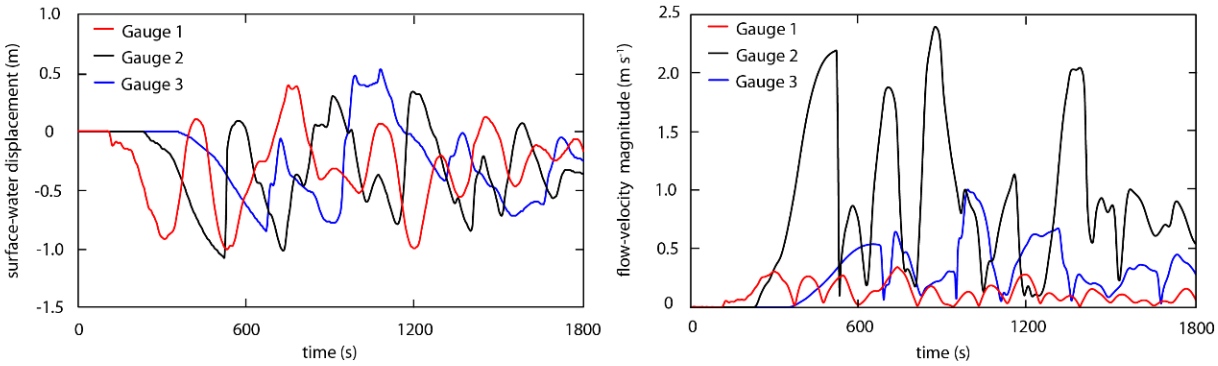

Fig. 5-10: Timeseries of water-surface displacement (left) and flow-velocity magnitude (right) at gauges 1–3 (see Fig. 5-9 for location) of the simulation LU18-S4.

Sensitivity analysis of bed shear-stress

To determine the dependency and robustness of the computed flow parameters, a sensitivity analysis of the bed roughness k_b was performed. Six scenarios were simulated with different bed roughness values (k_b) ranging from 0.0002 to 0.1 m (Table 5-4). The sensitivity of the bed roughness (k_b) on the dimensionless bed shear-stress (θ) was evaluated by simulations computed with different bed roughness values (k_b) between 0.0002 and 0.1 m, keeping fluid density (1 g cm^{-3}), sediment density (2.65 g cm^{-3}), and sediment porosity (0.4 vol%) constant (Table 5-4). The area with a dimensionless bed shear-stress $\theta \geq 0.03$ (Table 5-4) was calculated with ArcMap (version 10.8.1).

Table 5-4: Sensitivity analysis of the dimensionless bed shear-stress to the bed roughness (k_b): applied bed roughness in the different scenarios computed with BASEMENT and the calculated area with a dimensionless bed shear-stress $\theta \geq 0.03$.

	LU-S1	LU-S2	LU-S3	LU-S4	LU-S5	LU-S6
Bed roughness k_b (m)	0.0002	0.001	0.01	0.02	0.06	0.1
Area with $\theta \geq 0.03$ (10^6 m^2)	0.20	0.28	0.38	0.43	0.52	0.57

The analysis of the computed data on map-scale and gauge data indicates that the applied bed roughness k_b has a strong effect on the dimensionless bed shear-stress. However, water-surface displacement, flow-velocity magnitude, and specific discharge are hardly affected. For example, flow-velocity magnitude has a variance of less than 10% within the range of the different simulations at gauge locations. Whereas the computed dimensionless bed shear-stress is strongly influenced by the applied bed-roughness coefficient as shown in Figure 5-11.

The max. dimensionless bed shear-stress (θ) computed at gauge locations range from 0.0001 to 0.0003 at gauge 1, 0.01 to 0.03 at gauge 2, and 0.001 to 0.003 at gauge 3 (see Appendix C: Figs. C1, C2, and C3). From the map-based analysis, it is evident that the highest observed max. dimensionless bed shear-stresses in the Lucerne Bay are most pronounced along the shoreline and in the shallow water area at the sharp transition from the deep to shallow water (Fig. 5-11). The area with a max. dimensionless bed shear-stress $\theta \geq 0.3$ ranges from 0.2 to 0.6 x 10^6 m^2 for the various simulated bed-roughness coefficients (Table 5-4).

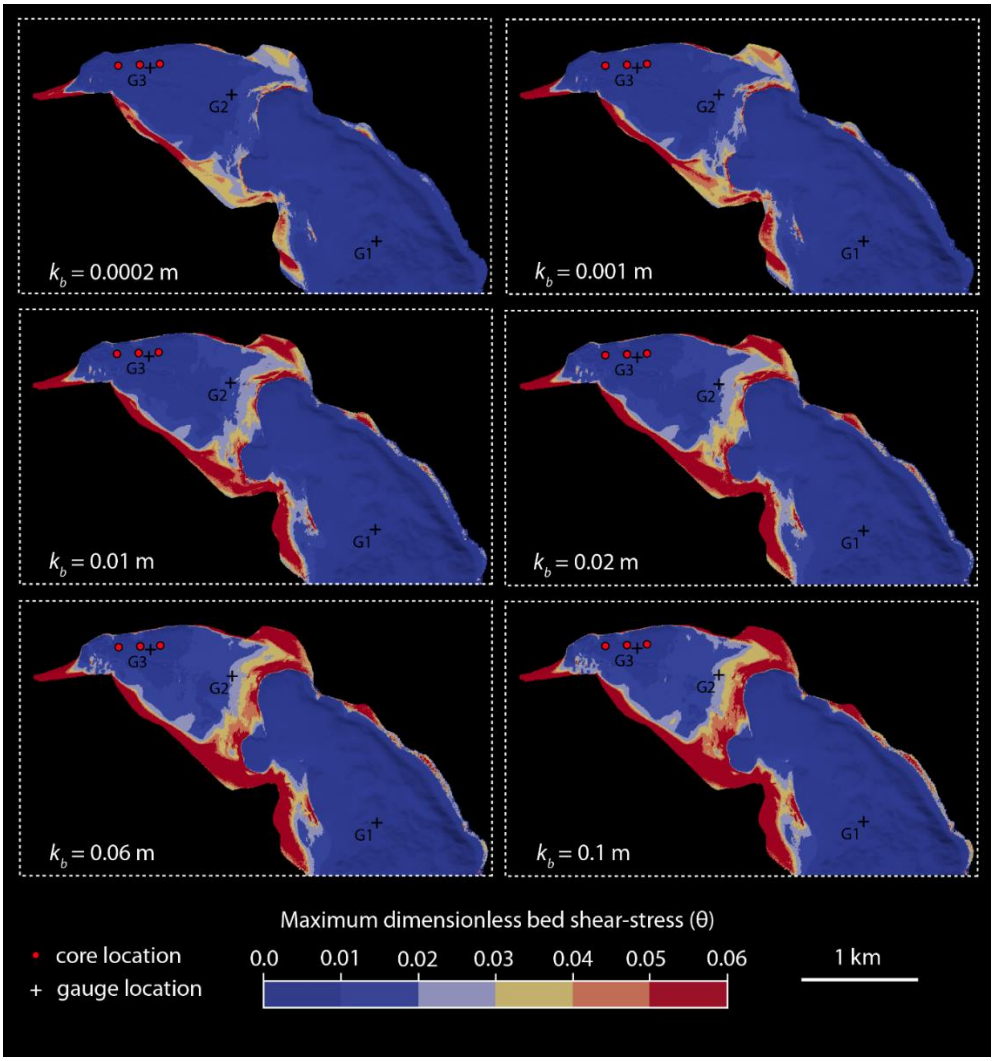

Fig. 5-11: Results of the sensitivity analysis of bed roughness to the dimensionless bed shear-stress. The max. dimensionless bed shear-stress reached in each computational cell throughout the simulated time is shown for the simulation with different bed roughness (k_b: 0.0002–0.1 m). Sediment core (red dots) and gauge (black crosses) locations are shown on the map.

5.5 Discussion

5.5.1 Depositional history

Unit 4: The lowermost Unit 4, characterized as a dense, cohesive, light-gray clay to silt deposit has been previously described in other sediment cores in the area (Keller et al., 2020). These deposits are interpreted as glacio-lacustrine sediments deposited during an early lake phase around 15’000 yr. BP (Keller et al., 2020). The fine-grained cohesive sediment originates from the retreating Reuss Glacier and probably corresponds to rock flour delivered by glacial runoff. A gradual transition overlies Unit 4 discordant with a hiatus of several 1000 years. This hiatus

is probably caused by the incision of the eroding outflowing Reuss River during lake-level low stands.

Unit 3: With the construction of mills in the 13th century at the outflow of the lake, lake level was stabilized at today's level (Keller et al., 2020 and references therein). This early stabilized lake-level phase corresponds to the Unit 3, dated to 1174–1411 cal CE, which is characterized by organic-rich deposits with limited carbonate production and variable thickness along the coring transect (Fig. 5-7).

Unit 2: The normally graded Unit 2 overlies Unit 3 with a sharp basal contact, indicating an abrupt deposition reflecting a severe event on Lake Lucerne. The narrow radiocarbon age range (1306–1437 cal CE) with minor age reversals as well as the normally graded sedimentary sequence of Unit 2 (Fig. 5-5) indicate event deposition. Unit 2 is characterized by a fine sandy base and fines gradually upwards to a poorly sorted fine silt (Figs. 5-5 and 5-6). A clear shift in the grain-size distribution is observable in Core LU18-2 at a depth of 95 and 60 cm (Fig. 5-6). The two lowermost subunits have a well sorted grain-size distribution whereas the two uppermost subunits are moderately to poorly sorted. Such types of normal grading haven been described for high-energy flows such as tsunamis and turbidity currents (Kuene and Menard, 1952; Middleton, 1967; Jaffe et al., 2011). The gradual upwards decrease in grain size is a signature of deposition from suspension (Jaffe et al., 2012). This specific type of normal grading is termed suspension grading (Jaffe et al., 2012) and is primary caused by the settling velocity of the particles, but also by the flow velocity (Woodruff et al., 2008; Johnson et al., 2017). Thick normal graded deposits have been reported from the off- (e.g., Sakuna et al., 2012; Tamura et al., 2015) and onshore (e.g., Jaffe et al., 2012 and references therein) environment deposited by the inundation and backwash of marine tsunamis. For example, Kempf et al. (2015) have observed normal and multiple graded sand deposits with mud caps and variable thicknesses (5–60 cm) in two Chilean coastal lakes, that record the local inundation of the 1960 Great Chilean Earthquake tsunami. Of the few offshore tsunami deposits studied worldwide, several authors describe sharp lower and/or upper sedimentary contacts (e.g., van den Bergh et al., 2003; Sakuna et al., 2012; Abrantes et al., 2008; Goodman-Tchernov et al., 2009; Smedile et al., 2020) as observed at the basal contact of Unit 2. In Lake Sils, Nigg et al. (2021) observed thick normal graded sand deposits that were formed by the backwash currents of a prehistoric lake tsunami. Although the radiocarbon ages in Unit 2 are ~200 years younger than the historically described 1601 CE Lake Lucerne tsunami, the observed siliciclastic-rich, normally

graded deposit (Unit 2) is interpreted to have been formed by this event. The single normally graded siliciclastic sand succession was deposited during a unique event. The sediment originates from the uppermost part of the lakebed in the Lucerne Bay, which was reworked by the erosive power of the wave, as is simulated in the numeric model and discussed in detail in Section 5.5.3 below. The event deposit was then formed at the depression by sediment deposition from suspension as the flow-velocity decreased. However, another historically reported tsunami event on Lake Lucerne in 1687 CE is unlikely to have the same order of magnitude in the Lucerne Bay because the tsunami was generated by a single subaqueous mass movement in a more distant basin and therefore no preserved sedimentary structures were observed in the sediment cores associated with this later event.

Unit 1: Uppermost Unit 1 represents a modern lake system with high endogenous carbonate production in an oligotrophic lake (Bossard et al., 2001) that became more nutrient-rich during a period of eutrophication in the 1970s to 1980s (Theveneon et al., 2012). The high magnetic susceptibility is attributed to combustion particles associated with the development of steam navigation on Lake Lucerne from the beginning of the late 1830s.

5.5.2 Numerical simulation

The selected tsunami generation mechanism, relying on the collapse of a selected area of the bathymetry is, despite its strongly simplified dynamics, in good agreement with similar, relying on more complex, approaches (Hilbe et al., 2015), reflecting a reasonable generated wave pattern. From both historical reports (e.g., the tsunami occurred in 1998 along the shores of the Sissano Lagoon in Papua New Guinea (Davies et al., 2003), it is well known that usually shorelines are hit by a wave train, with the first incoming wave characterized by a smaller amplitude with respect to the succeeding ones. Nevertheless, as also well described in (Lampela, 2019), near the shore the water most often undergoes a first drawback, forming a bore in a shallow area near the coast. This behavior is well reproduced by the numerical simulation obtained via BASEMENT. Indeed, considering for instance Figure 5-9, at 410 s, the water flows towards the center of the lake, i.e., creating a drawback, while at 550 s one observes the formation of a bore in the shallow area, represented by the two distinct flow directions which meet to form a steep wave front, i.e., the bore. Further, confirming the overall observations of tsunami behavior (e.g., Davies et al., 2003), the first simulated wave in the considered 1601 CE event results to be lower in height with respect to the subsequent ones, as

can be seen for instance for the water-surface displacement over time in Figures C1, C2, and C3 (see Appendix C). The reported hydrodynamic quantities for the sensitivity analysis of the bed roughness height in the selected area of interest appear to not undergo significant changes where the water column is large (gauge 1). Indeed, as one may observe from Figures C1, C2, and C3 (see Appendix C), the wave amplitude and flow velocities appear less deformed in gauge 1, whereas in gauges 2 and 3 which are in shallow water, the wave amplitude displays several minor displacements when considering different k_b, as expected.

5.5.3 Sediment erosion, transport, and deposition

Erosion, maximum dimensionless bed shear-stress, and bed roughness

The max. dimensionless bed shear-stress is the key value that defines whether sediment is eroded by flow events (Van Rijn, 2007). The bed shear-stress reached during the propagation of the tsunami generated by the 1601 CE Weggis-slide (Fig. 5-1) in the Lucerne Bay was numerically simulated with BASEMENT to better understand the erosion and mobilization potential of the tsunami waves. For this purpose, the influence of bed roughness on the incipient motion of particles was considered. Sediment may be eroded when the effective dimensionless bed shear-stress is larger than the dimensionless critical bed shear-stress, i.e., $\theta > \theta_{cr}$ (Choi and Kwak, 2001). However, critical dimensionless bed shear-stress depends on the grain-size distribution and cohesion of the sediment bed (Houwing and Van Rijn, 1998). For the given situation, the threshold for incipient motion was chosen at $\theta = 0.03$, which has been previously suggested to be a reasonable number based on flume experiments (e.g., Shields, 1936; Houwing and Van Rijn, 1998). As soon as the threshold for incipient motion is reached, sediment particles may be entrained by the flow (van Rijn, 2007). Once sediment particles are set in motion, less energy is generally required to keep particles in motion after entrainment (Boggs, 2014).

The applied physical bed roughness (k_b) varies from 0.0002 to 0.1 m (Fig. 5-11), which is a reasonable range from grain roughness to total physical bed roughness (Houwman and van Rijn, 1999). Total physical bed-roughness may be influenced by sedimentary bed forms (e.g., ripples and dunes), superimposed bed forms (e.g., megaripples), grain-size distribution and packing, mineralogical sediment composition, and the presence of an organic biofilm on the lakebed (van Rijn, 2007). Therefore, accurate estimates of total physical bed roughness are difficult to obtain. Houwman and van Rijn (1999), for example, have found that physical bed

roughness of 0.1 m gives best agreement between measured and predicted current velocities in the North Sea at water depths of 5–10 m and a d_{50} of 200 µm. Thus, considering the above-mentioned factors and that surf beats are less expressed in the Lucerne Bay than at the North Sea coast, physical bed roughness of 0.02 to 0.06 m is a reasonable and realistic value for the given situation.

Considering the above limitations in the estimation of incipient motion, our simulation shows large areas with a dimensionless bed shear-stress $\theta \geq 0.03$ (Fig. 5-11), indicating large amounts of sediment may have been eroded, transported, and resuspended by the main wave pulses of the 1601 CE tsunami in the Lucerne Bay. The areal extent of max. dimensionless bed shear-stress $\theta \geq 0.03$ computed for different physical bed-roughness is in the order of 0.2–0.6 x 10^6 m^2 and follows the regression curve $y = 0.8225\ k_b^{0.163}$ (Fig. 5-12A). A simple estimate of the erosion volume (4 to 11.5 x 10^4 m^3; Fig. 5-12B) can be calculated based on a homogeneous thickness of erosion (0.02–0.2 m) on the area with $\theta \geq 0.03$. Thus, our simulations show clearly that substantial amount of sediment gets eroded and mobilized by the wave. The erosion mostly affects the uppermost water-rich layer near the lakebed. The age data of Unit 2 (1306 to 1442 cal CE; Table 5-3) with radiocarbon ages of up to 200 years older than the tsunami event confirms that sediment may get mobilized to a chronostratigraphic depth of 200 years, corresponding to a thickness of up to 20 cm at a sedimentation rate of 0.1 cm yr^{-1}. Therefore, eroded volume in the Lucerne Bay is likely in the order of 10^4 to 10^5 m^3 (Fig. 5-12B; k_b: 0.02–0.06 m) with an erosional thickness of 0.2 m.

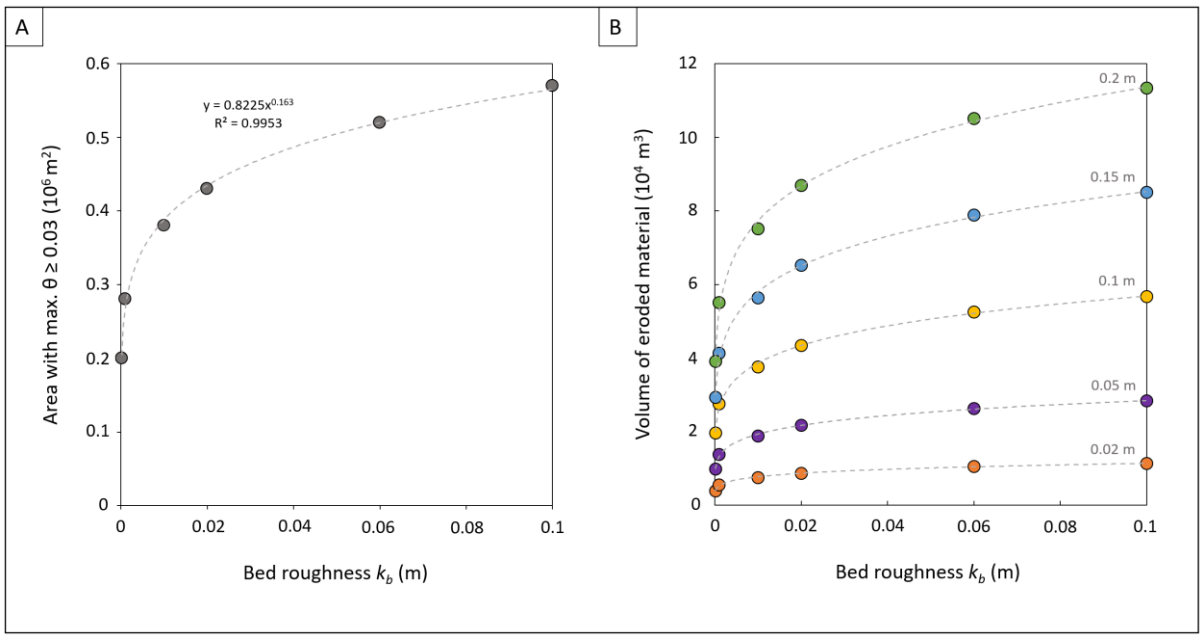

◄ Fig. 5-12: A) Mapped area with a max. dimensionless bed shear-stress $\theta \geq 0.03$ reached computed with different bed roughness k_b. B) Estimation of remobilized sediment volumes with different homogeneous erosional thicknesses and bed roughness k_b.

Sediment source

The numerical simulations clearly show where and when the tsunami wave causes bed shear-stress in the Lucerne Bay capable of substantial sediment erosion and mobilization (Fig. 5-12). Erosional forces are pronounced in the shallow-water area of geomorphological obstacles marking the transition from the deeper to the shallower area of the Lucerne Bay and along the lakeshore, as indicated by the computed max. dimensionless bed shear-stress (Fig. 5-11). These areas are likely the sediment source of remobilized sediment particles during the 1601 CE tsunami inundation of the Lucerne Bay. Another important sediment source is the lakeshore, where predominantly siliciclastic sand is found (e.g., lake-surface sediment Sample LS-3). At these locations, constant wave motion leads to sandy-dominated surface sediments from winnowing of fines.

Sediment transport and deposition

The sediment transport towards the coring site can be observed by visualizing vectors of flow-velocity magnitude indicating the sediment transport direction (Fig. 5-9). Three main wave pulses propagate in the Lucerne Bay in the first 1800 s after the instantaneous simulated Weggis-slide collapse (Fig. 5-10). During the first wave, a strong surge towards the wave trough is observable (Fig. 5-9). At this stage, sediment particles may be mobilized and brought into suspension. With the arrival of the 2nd wave expressed as an impressive bore-like wave, particles are then transported westwards towards the coring location. These main wave pulses have high flow velocities (> 2 m s^{-1}; Fig. 5-10) and specific discharges (> 4 m^3 s^{-1}; see Appendix C: Figs. C1, C2, and S3) that are capable to transport large amounts of sediment from the areas with high bed shear-stress towards the coring location. At the coring location, due to the geomorphological depression, flow velocity drops instantaneously, and sediments are deposited from suspension forming the graded event deposit.

A depositional volume of 2 x 10^4 m^3 is estimated from the thickness of Unit 2 in recovered sediment cores and multibeam bathymetry map (Fig. 5-2B). This estimate fits well with the proposed eroded sediment volume in the order of 10^4 to10^5 m^3, that is estimated with the numerical model more accurate estimation of eroded volume would be possible by using a fully

featured model for suspended-sediment transport, which is currently still under development. Such a model would allow for simulation of variable erosion related to the dimensionless bed shear-stress and provide more realistic transport of the sediment with the flow. However, many uncertainties may persist, e.g., sediment-erosion thickness is likely not homogenous over the area and sediment erosion may be strongly influenced by local variations of sediment composition (e.g., mineralogy, grain-size distribution, and bed roughness). However, the presented methodology proves to be a reasonable simplification of the complex mechanism of erosion by tsunami waves and allows for basic reconstruction of related events and processes involved.

5.6 Conclusions

An offshore event deposit was observed in sediment cores recovered along a transect across a depression in the shallow-subaqueous environment of Lucerne Bay. The normally graded deposit with a thickness of up to 60 cm consists predominantly of siliciclastic sand- to silt-sized particles with increased amounts of coarse sand-sized carbonate shell fragments at the base. The deposit has a sharp basal contact with horizontally bedded organic, mostly woody particles that become more abundant in the upper part of the deposit. Radiocarbon dates of terrestrial plant macro remains isolated from the clastic deposit yield ages in the range of 1306-1442 cal CE.

The sedimentary features clearly reflect deposition from a high-flow event, which we interpret to be the historically reported 1601 CE Lake Lucerne tsunami. This interpretation is supported by i) the grain-size pattern of Unit 2 indicating suspension settling, ii) the narrow 200 years age offset of the event deposit indicating erosion, mobilization of the uppermost sediment column, as well as iii) the performed numerical tsunami-wave propagation and bed shear-stress simulation in the Lucerne Bay, providing a criterion for incipient motion of sediment by the incoming waves.

The numerical simulation of the 1601 CE Lake Lucerne tsunami was simulated using the software BASEMENT by an instantaneous collapse of the second largest subaqueous mass movement failed during the 1601 CE earthquake. In addition to simulating the wave propagation, water surface-displacement and flow-velocity magnitude, the dimensionless bed shear-stress was used to characterize and locate areas of tsunami-induced sediment erosion in

the shallow-subaqueous environment of Lucerne Bay. The simulated results clearly show that the critical dimensionless bed shear-stress is exceeded in large areas where significant erosion must have occurred. Flow direction pointing from the erosional areas toward the sediment sink in the depression indicate sediment transport towards the coring locations.

Our study thus documents the high potential of combining sedimentological observations of event deposits with numerical simulations of water motion. This approach is not restricted to lacustrine systems and mass movement-induced tsunami waves but can be applied to any basin where high-flow events occur.

Acknowledgments

This work was funded by the Swiss National Science Foundation (research grant no.: 171017) and is embedded in the SNSF Sinergia Project "Lake tsunami: causes, controls and hazard". We acknowledge Nicole Schwendener and the Institute of Anatomy, University of Bern for their support with CT scanning, Daniela Fischer and the Institute of Geography, University of Bern for their support with the grain-size determination. Sönke Szidat and the Department of Chemistry and Biochemistry, University of Bern are acknowledged for the radiocarbon dating. Julijana Krbanjevic is acknowledged for her help with the geochemical analysis. Firtz Schlunegger and Beat Keller are thanked for their useful comments on the manuscript. Franzyska Nyffenegger, Dominik Amschwand, Julijana Krbanjevic, Flavio Huber, Evelyne Margelisch, Michael Strupler, Stefano Fabbri, Adrian Gilli and Marina Morlock are acknowledged for their support during the coring campaign. Nikola Janevski is acknowledged for his help in collecting lake-surface samples from a sailboat.

References

Abrantes, F., Alt-Epping, U., Lebreiro, S., Voelker, A., & Schneider, R. (2008) Sedimentological record of tsunamis on shallow-shelf areas: The case of the 1969 AD and 1755 AD tsunamis on the Portuguese Shelf off Lisbon. Marine Geology, 249(3-4), 283-293.

Apotsos, A., Gelfenbaum, G., Jaffe, B., Watt, S., Peck, B., Buckley, M., & Stevens, A. (2011) Tsunami inundation and sediment transport in a sediment-limited embayment on American Samoa. Earth-Science Reviews, 107(1-2), 1-1.

Apotsos, A., Gelfenbaum, G., & Jaffe, B. (2012) Time-dependent onshore tsunami response. Coastal Engineering, 64, 73-86.

Bacigaluppi, P.- Boes, R., & Vetsch, D.F (in prep) On an accurate, robust and efficient simulation tool for lake-scale tsunamis.

BAFU (Ed.) (2009) Hydrologisches Jahrbuch der Schweiz 2008, Umwelt-Wissen Nr. 0921, Swiss Federal Office for the Environment, Bern, 578 pp.

Billeter, J. (1923) Pfarrer Jakob Billeter von Aegeri und seine Chronik. Heimat-Klänge, Sonntags-Beilage zu den «Zuger Nachrichten», 3. Jahrgang, Nr. 4, 28. January, 15-16.

Bobrowsky, P. T., & Marker, B. (Eds.) (2018) Encyclopedia of Engineering Geology. Cham: Springer.

Boggs Jr, S. (2014) Principles of Sedimentology and Stratigraphy, Fifth Edition. Pearson, Harlow, pp. 564.

Bossard, P., Gammeter, S., Lehmann, C., Schanz, F., Bachofen, R., Bürgi, H. R., ... & Zimmermann, U. (2001) Limnological description of the lakes Zürich, Lucerne, and Cadagno. Aquatic Sciences, 63(3), 225-249.

Buffington, J. M., & Montgomery, D. R. (1997) A systematic analysis of eight decades of incipient motion studies, with special reference to gravel-bedded rivers. Water Resources Research, 33(8), 1993-2029.

Bünti, J.L. (1973) Chronik des Johann Laurentz Bünti, Landammann, 1661–1736. Beiträge zur Geschichte Nidwaldens, 34,26–27.

Choi, S. U., & Kwak, S. (2001) Theoretical and probabilistic analyses of incipient motion of sediment particles. KSCE Journal of Civil Engineering, 5(1), 59-65.

Costa, P. J., & Andrade, C. (2020) Tsunami deposits: Present knowledge and future challenges. Sedimentology, 67(3), 1189-1206.

Cysat, R. (1969) Collectanea Chronica und denkwürdige Sachen pro Chronica Lucernensi et Helvetiae. Erster Band, zweiter Teil (Eds J. Schmid and D. Schilling), pp. 879-888. Diebold Schilling Verlag, Luzern.

Davies, H. L., Davies, J. M., Perembo, R. C. B., and Lus, W. Y. (2003). The Aitape 1998 tsunami: Reconstructing the event from interviews and field mapping. Pure and Applied Geophysics, 160(10-11), 1895-1922.

Dawson, A. G., & Stewart, I. (2008) Offshore tractive current deposition: the forgotten tsunami sedimentation process. In Tsunamiites (pp. 153-161). Elsevier.

Dietrich, J. (1689) Diarium von P. Josef Dietrich von Einsiedeln (1645–1704), Bd. 6. Klosterarchiv Einsiedeln, KAE A.HB.6, pp. 202.

Einsele, G., Chough, S. K., & Shiki, T. (1996) Depositional events and their records—an introduction. Sedimentary Geology, 104(1-4), 1-9.

Fäh, D., Giardini, D., Kästli, P., Deichmann, N., Gisler, M., Schwarz-Zanetti, G., Alvarez-Rubio, S., Sellami, S., Edwards, B., Allmann, B., Bethmann, F., Wössner, J., Gassner-Stamm, G., Fritsche, S. & Eberhard, D. (2011) ECOS-09 Earthquake Catalogue of Switzerland, Release 2011, Report SED/ECOS/R/001/20110417. Swiss Seismological Service, ETH Zürich, 42 pp.

Favrod, J (1991) La Chronique de Marius d'Avenches (455-581): Texte, Traduction et Commentaire (Vol. 4). Section d'histoire, Faculté des lettres, Université de Lausanne.

Feldens, P., Schwarzer, K., Szczucinski, W., Stattegger, K., Sakuna, D., & Somgpongchaiykul, P. (2009) Impact of 2004 Tsunami on Seafloor Morphology and Offshore Sediments, Pakarang Cape, Thailand. Polish Journal of Environmental Studies, 18(1).

Fujiwara, O. (2008) Bedforms and sedimentary structures characterizing tsunami deposits. In Tsunamiites (pp. 51-62). Elsevier.

Funk, H., Buxtorf, A., Christ, P., Egli, D., Estoppey, D., Gebel, Ch., Geiger, M. E., Graf, A., Gübeli, A., Klemenz, W., Ramseyer, K., Roesli, F., Schaub, H., Schindler, C., Steinhauser, V. & Wanner, M. (2013) Geologischer Atlas der Schweiz, Blatt 1170, Alpnach (Nr. 137): Schweizerische Geologische Kommission, scale 1:25 000, 1 sheet.

Fritz, H. M., Kalligeris, N., Borrero, J. C., Broncano, P., & Ortega, E. (2008) The 15 August 2007 Peru tsunami runup observations and modeling. Geophysical Research Letters, 35(10).

Gardner, J. V., Mayer, L. A., & Hughs Clarke, J. E. (2000) Morphology and processes in lake Tahoe (California-Nevada). Geological Society of America Bulletin, 112(5), 736-746.

Goodman-Tchernov, B. N., & Austin Jr, J. A. (2015) Deterioration of Israel's Caesarea Maritima's ancient harbor linked to repeated tsunami events identified in geophysical mapping of offshore stratigraphy. Journal of Archaeological Science: Reports, 3, 444-454.

Goodman-Tchernov, B. N., Dey, H. W., Reinhardt, E. G., McCoy, F., & Mart, Y. (2009) Tsunami waves generated by the Santorini eruption reached Eastern Mediterranean shores. Geology, 37(10), 943-946.

Goto, K., Chagué-Goff, C., Fujino, S., Goff, J., Jaffe, B., Nishimura, Y., ... & Witter, R. C. (2011a) New insights of tsunami hazard from the 2011 Tohoku-oki event. Marine Geology, 290(1-4), 46-50.

Goto, K., Ikehara, K., Goff, J., Chagué-Goff, C., & Jaffe, B. (2014) The 2011 Tohoku-oki tsunami—Three years on. Marine Geology, 358, 2-11.

Goto, K., Takahashi, J., Oie, T., & Imamura, F. (2011b) Remarkable bathymetric change in the nearshore zone by the 2004 Indian Ocean tsunami: Kirinda Harbor, Sri Lanka. Geomorphology, 127(1-2), 107-116.

Hantke, R., Bollinger, D., & Kopp, J. (2005) Geologischer Atlas der Schweiz, Blatt 1151, Rigi (Nr. 116). Schweizerische Geologische Kommission, scale 1:25 000, 1 sheet.

Haraguchi, T., Goto, K., Sato, M., Yoshinaga, Y., Yamaguchi, N., & Takahashi, T. (2013) Large bedform generated by the 2011 Tohoku-oki tsunami at Kesennuma Bay, Japan. Marine Geology, 335, 200-205.

Heidarzadeh, M., Muhari, A., & Wijanarto, A. B. (2019). Insights on the source of the 28 September 2018 Sulawesi tsunami, Indonesia based on spectral analyses and numerical simulations. Pure and Applied Geophysics, 176(1), 25-43.

Hilbe, M., & Anselmetti, F. S. (2014) Signatures of slope failures and river-delta collapses in a perialpine lake (Lake Lucerne, Switzerland). Sedimentology, 61(7), 1883-1907.

Hilbe, M., & Anselmetti, F. S. (2015) Mass movement-induced tsunami hazard on perialpine Lake Lucerne (Switzerland): scenarios and numerical experiments. Pure and Applied Geophysics, 172(2), 545-568.

Hilbe, M., Anselmetti, F.S., Eilertsen, R.S., Hansen, L. & Wildi, W. (2011) Subaqueous morphology of Lake Lucerne (Central Switzerland): implications for mass movements and glacial history. Swiss Journal of Geosciences, 104, 425–433.

Houwman, K. T., & Van Rijn, L. C. (1999) Flow resistance in the coastal zone. Coastal Engineering, 38(4), 261-273.

Huntington, K., Bourgeois, J., Gelfenbaum, G., Lynett, P., Jaffe, B., Yeh, H., & Weiss, R. (2007) Sandy signs of a tsunami's onshore depth and speed. Eos, Transactions American Geophysical Union, 88(52), 577-578.

Ikehara, K., Irino, T., Usami, K., Jenkins, R., Omura, A., & Ashi, J. (2014) Possible submarine tsunami deposits on the outer shelf of Sendai Bay, Japan resulting from the 2011 earthquake and tsunami off the Pacific coast of Tohoku. Marine Geology, 358, 120-127.

Jaffe, B. E., & Gelfenbuam, G. (2007) A simple model for calculating tsunami flow speed from tsunami deposits. Sedimentary Geology, 200(3-4), 347-361.

Jaffe, B.E., Buckley, M., Richmond, B., Strotz, L., Etienne, S., Clark, K., ... & Goff, J. (2011) Flow speed estimated by inverse modeling of sandy sediment deposited by the 29 September 2009 tsunami near Satitoa, east Upolu, Samoa. Earth-Science Reviews, 107(1-2), 23-37.

Jaffe, B. E., Goto, K., Sugawara, D., Richmond, B. M., Fujino, S., & Nishimura, Y. (2012) Flow speed estimated by inverse modeling of sandy tsunami deposits: results from the 11 March 2011 tsunami on the coastal plain near the Sendai Airport, Honshu, Japan. Sedimentary Geology, 282, 90-109.

Johnson, J. P., Delbecq, K., & Kim, W. (2017) Predicting paleohydraulics from storm surge and tsunami deposits: Using experiments to improve inverse model accuracy. Journal of Geophysical Research: Earth Surface, 122(4), 760-781.

Keller, B. (2013) Geologische Geschichte der Luzerner Reuss. In Gestautes Wasser – Regulierter See: Geschichte, Bau und Betrieb der Reusswehranlage in Luzern (pp. 105-123). Lehrmittelverlag Kanton Luzern.

Keller, B. (2017) Massive rock slope failure in Central Switzerland: history, geologic–geomorphological predisposition, types and triggers, and resulting risks. Landslides, 14(5), 1633-1653.

Keller, B. (2020) Lake Lucerne and Its Spectacular Landscape. In Landscapes and Landforms of Switzerland (pp. 305-323). Springer, Cham.

Kopp, J., Bendel, L., & Buxtorf, A., (1955) Geologischer Atlas der Schweiz, Blatt 1150, Luzern (Nr. 28): Schweizerische Geologische Kommission, scale 1:25 000, 1 sheet.

Kempf, P., Moernaut, J., Van Daele, M., Vermassen, F., Vandoorne, W., Pino, M., ... & De Batist, M. (2015) The sedimentary record of the 1960 tsunami in two coastal lakes on Isla de Chiloé, south central Chile. Sedimentary geology, 328, 73-86.

Kihara, N., Fujii, N., & Matsuyama, M. (2012) Three-dimensional sediment transport processes on tsunami-induced topography changes in a harbor. Earth, planets and space, 64(10), 787-797.

Kremer, K., Anselmetti, F. S., Evers, F. M., Goff, J., & Nigg, V. (2020) Freshwater (paleo) tsunamis–a review. Earth-science reviews, 103447.

Kremer, K., Hilbe, M., Simpson, G., Decrouy, L., Wildi, W., & Girardclos, S. (2015) Reconstructing 4000 years of mass movement and tsunami history in a deep peri-Alpine lake (Lake Geneva, France-Switzerland). Sedimentology, 62(5), 1305-1327.

Kremer, K., Marillier, F., Hilbe, M., Simpson, G., Dupuy, D., Yrro, B. J., Rachoud-Schneider, A. M., Corboud, P., Bellwald, B., Wildi, W., & Girardclos, S. (2014) Lake dwellers occupation gap in Lake Geneva (France–Switzerland) possibly explained by an earthquake–mass movement–tsunami event during Early Bronze Age. Earth and Planetary Science Letters, 385, 28-39.

Kremer, K., Simpson, G., & Girardclos, S. (2012) Giant Lake Geneva tsunami in ad 563. Nature Geoscience, 5(11), 756-757.

Klyuchevskii, A. V., Demyanovich, V. M., & Klyuchevskaya, A. A. (2012) The possibility of a tsunami on Lake Baikal. In Doklady Earth Sciences (Vol. 442, No. 1, pp. 130-134). SP MAIK Nauka/Interperiodica.

Kuenen, P. H., & Menard, H. W. (1952) Turbidity currents, graded and non-graded deposits. Journal of Sedimentary Research, 22(2), 83-96.

Kuriyama, Y., Chida, Y., Uno, Y., & Honda, K. (2020) Numerical simulation of sedimentation and erosion caused by the 2011 Tohoku Tsunami in Oarai Port, Japan. Marine Geology, 427, 106225.

Lampela, K.M. (2019). Tsunami shoaling theory. Computational Methods and Experimental Measurements XIX & Earthquake Resistant Engineering Structures XII.

Lee, H., & Balachandar, S. (2012) Critical shear stress for incipient motion of a particle on a rough bed. Journal of Geophysical Research: Earth Surface, 117(F1).

Mantz, P. A. (1977) Incipient transport of fine grains and flakes by fluids-extended shield diagram. Journal of the Hydraulics division, 103.

Michel, C., Bleicher, N., Brombacher, C., Hüster Plogmann, H., Ismail-Meyer, K., & Rehazek, A. (2012) Pfahlbauten am Vierwaldstättersee-der steinzeitliche Siedlungsplatz in Kehrsiten. Archäologie der Schweiz, 35(2), 56-71.

Middleton, G. V. (1967) Experiments on density and turbidity currents: III. Deposition of sediment. Canadian Journal of Earth Sciences, 4(3), 475-505.

Montandon, F. (1925) Les Eboulements de la Dent du Midi et du Grammont (Examen critique de la Question du Tauredunum). Le Globe. Revue genevoise de géographie, 46(1), 35-91.

Moore, J. G., Schweickert, R. A., Robinson, J. E., Lahren, M. M., & Kitts, C. A. (2006) Tsunami-generated boulder ridges in Lake Tahoe, California-Nevada. Geology, 34(11), 965-968.

Mountjoy, J. J., Wang, X., Woelz, S., Fitzsimons, S., Howarth, J. D., Orpin, A. R., & Power, W. (2019) Tsunami hazard from lacustrine mass wasting in Lake Tekapo, New Zealand. Geological Society, London, Special Publications, 477(1), 413-426.

Noda, A., Katayama, H., Sagayama, T., Suga, K., Uchida, Y., Satake, K., ... & Okamura, Y. (2007) Evaluation of tsunami impacts on shallow marine sediments: An example from the tsunami caused by the 2003 Tokachi-oki earthquake, northern Japan. Sedimentary Geology, 200(3-4), 314-327.

Nigg, V., Kremer, K., Gierardclos, S., & Anselmettie F. S. (in prep.) Sedimentologic signatures of historic tsunamis in Swiss lakes.

Nigg, V., Wohlwend, S., Hilbe, M., Bellwald, B., Fabbri, S. C., de Souza, G. F., ... & Anselmetti, F. S. (2021) A tsunamigenic delta collapse and its associated tsunami deposits in and around Lake Sils, Switzerland. Natural Hazards, 1-35.

Ontowirjo, B., Paris, R., & Mano, A. (2013) Modeling of coastal erosion and sediment deposition during the 2004 Indian Ocean tsunami in Lhok Nga, Sumatra, Indonesia. Natural hazards, 65(3), 1967-1979.

Paris, R., Fournier, J., Poizot, E., Etienne, S., Morin, J., Lavigne, F., & Wassmer, P. (2010) Boulder and fine sediment transport and deposition by the 2004 tsunami in Lhok Nga (western Banda Aceh, Sumatra, Indonesia): a coupled offshore–onshore model. Marine Geology, 268(1-4), 43-54.

Pritchard, D., & Dickinson, L. (2008) Modelling the sedimentary signature of long waves on coasts: implications for tsunami reconstruction. Sedimentary Geology, 206(1-4), 42-57.

Ramsey, C. B. (2009) Bayesian analysis of radiocarbon dates. Radiocarbon, 51(1), 337-360.

Reimer, P. J., Austin, W. E., Bard, E., Bayliss, A., Blackwell, P. G., Ramsey, C. B., ... & Grootes, P. M. (2020) The IntCal20 northern hemisphere radiocarbon age calibration curve (0–55 cal kBP). Radiocarbon, 62(4), 725-757.

Riou, B., Chaumillon, E., Schneider, J. L., Corrège, T., & Chagué, C. (2020) The sediment-fill of Pago Pago Bay (Tutuila Island, American Samoa): New insights on the sediment record of past tsunamis. Sedimentology, 67(3), 1577-1600.

Roberts, N. J., McKillop, R. J., Lawrence, M. S., Psutka, J. F., Clague, J. J., Brideau, M. A., & Ward, B. C. (2013) Impacts of the 2007 landslide-generated tsunami in Chehalis Lake, Canada. In Landslide science and practice (pp. 133-140). Springer, Berlin, Heidelberg.

Sakuna, D., Szczuciński, W., Feldens, P., Schwarzer, K., & Khokiattiwong, S. (2012) Sedimentary deposits left by the 2004 Indian Ocean tsunami on the inner continental shelf offshore of Khao Lak, Andaman Sea (Thailand). Earth, planets and space, 64(10), 11.

Schlunegger, F., Matter, A., Burbank, D. W., & Klaper, E. M. (1997) Magnetostratigraphic constraints on relationships between evolution of the central Swiss Molasse basin and Alpine orogenic events. Geological Society of America Bulletin, 109(2), 225-241.

Schnellmann, M., Anselmetti, F. S., Giardini, D., & McKenzie, J. A. (2005) Mass movement-induced fold-and-thrust belt structures in unconsolidated sediments in Lake Lucerne (Switzerland). Sedimentology, 52(2), 271-289.

Schnellmann, M., Anselmetti, F.S., Giardini, D., & McKenzie, J. A. (2006) 15,000 Years of mass-movement history in Lake Lucerne: implications for seismic and tsunami hazards. Eclogae Geologicae Helvetiae, 99(3), 409-428.

Schnellmann, M., Anselmetti, F. S., Giardini, D., McKenzie, J. A., & Ward, S. (2002) Prehistoric earthquake history revealed by lacustrine slump deposits: Geology, 30(12), 1131-1134.

Schwarz-Zanetti, G., Deichmann, N., Fäh, D., Giardini, D., Jimenez, M.-J., Masciadri, V., Schibler, R. & Schnellmann, M. (2003) The earthquake in Unterwalden on September 18, 1601: a historico-critical macroseismic evaluation. Eclogae Geologicae Helvetiae, 96(3), 441-450.

Shields, A. (1936) Anwendung der Aehnlichkeitsmechanik und der Turbulenzforschung auf die Geschiebebewegung. PhD Thesis Technical University Berlin.

Siegenthaler, C., Finger, W., Kelts, K. &Wang, S. (1987) Earthquake and seiche deposits in Lake Lucerne, Switzerland. Eclogae Geologicae Helvetiae, 80(1), 241-260.

Smedile, A., De Martini, P. M., Pantosti, D., Bellucci, L., Del Carlo, P., Gasperini, L., ... & Boschi, E. (2011) Possible tsunami signatures from an integrated study in the Augusta Bay offshore (Eastern Sicily—Italy). Marine Geology, 281(1-4), 1-13.

Smedile, A., Molisso, F., Chagué, C., Iorio, M., De Martini, P. M., Pinzi, S., ... & Pantosti, D. (2020) New coring study in Augusta Bay expands understanding of offshore tsunami deposits (Eastern Sicily, Italy). Sedimentology, 67(3), 1553-1576.

Spiske, M., Piepenbreier, J., Benavente, C., & Bahlburg, H. (2013) Preservation potential of tsunami deposits on arid siliciclastic coasts. Earth-Science Reviews, 126, 58-73.

Spiske, M., Weiss, R., Bahlburg, H., Roskosch, J., & Amijaya, H. (2010) The TsuSedMod inversion model applied to the deposits of the 2004 Sumatra and 2006 Java tsunami and implications for estimating flow parameters of palaeo-tsunami. Sedimentary Geology, 224(1-4), 29-37.

Strupler, M., Bacigaluppi, P., Kremer, K., Vetsch, D., Anselmetti, F., Boes, R., & Wiemer, S. (2020) Abschätzung der Gefährdung durch Tsunamis in perialpinen Seen infolge Unterwasserhangrutschungen. Wasser Energie Luft, 112(1), 11-16.

Strupler, M., Danciu, L., Hilbe, M., Kremer, K., Anselmetti, F. S., Strasser, M., & Wiemer, S. (2018a) A subaqueous hazard map for earthquake-triggered landslides in Lake Zurich, Switzerland: Natural Hazards 90(1), 51-78.

Strupler, M., Hilbe, M., Kremer, K., Danciu, L., Anselmetti, F.S., Strasser, M. & Wiemer, S. (2018b) Subaqueous landslide-triggered tsunami hazard for Lake Zurich, Switzerland; Swiss Journal of Geosciences 111(1), 353-371.

Stuiver, M., & Polach, H. A. (1977) Discussion reporting of 14 C data. Radiocarbon, 19(3), 355-363.

Sugawara, D., Minoura, K., Nemoto, N., Tsukawaki, S., Goto, K., & Imamura, F. (2009) Foraminiferal evidence of submarine sediment transport and deposition by backwash during the 2004 Indian Ocean tsunami. Island Arc, 18(3), 513-525.

Suzuki, W., Aoi, S., Sekiguchi, H., & Kunugi, T. (2011) Rupture process of the 2011 Tohoku-Oki mega-thrust earthquake (M9. 0) inverted from strong-motion data. Geophysical Research Letters, 38(7).

Tamura, T., Sawai, Y., Ikehara, K., Nakashima, R., Hara, J., & Kanai, Y. (2015) Shallow-marine deposits associated with the 2011 Tohoku-oki tsunami in Sendai Bay, Japan. Journal of Quaternary Science, 30(4), 293-297.

Tang, H., & Weiss, R. (2015) A model for tsunami flow inversion from deposits (TSUFLIND). Marine geology, 370, 55-62.

Thevenon, F., Adatte, T., Poté, J., & Spangenberg, J. E. (2012) Recent human-induced trophic change in the large and deep perialpine Lake Lucerne (Switzerland) compared to historical geochemical variations. Palaeogeography, Palaeoclimatology, Palaeoecology, 363, 37-47.

Vanzo, D., Peter, S., Vonwiller, L., Buergler, M., Weberndorfer, M., Siviglia, A., et al. (subm.). BASEMENT v3: a modular freeware fro river process modelling over multiple computational backends. Environmental Modelling & Software. https://arxiv.org/abs/2102.12862

Van den Bergh, G. D., Boer, W., De Haas, H., Van Weering, T. C., & Van Wijhe, R. (2003) Shallow marine tsunami deposits in Teluk Banten (NW Java, Indonesia), generated by the 1883 Krakatau eruption. Marine Geology, 197(1-4), 13-34.

Van Rijn, L. C. (2007) Unified view of sediment transport by currents and waves. I: Initiation of motion, bed roughness, and bed-load transport. Journal of Hydraulic engineering, 133(6), 649-667.

Vetsch, D.F., Siviglia, A., Bacigaluppi, P., Bürgler, M., Caponi, F., Conde, D., Gerke, E., Kammerer, S., Koch, A., Peter, S., Vanzo, D., Vonwiller, L. & Weberndorfer, M. (2020) System Manuals of BASEMENT, Version 3.1. Laboratory of Hydraulics, Glaciology and Hydrology (VAW). ETH Zurich. Available from https://www.basement.ethz.ch.

Weiss, R., & Bahlburg, H. (2006) A note on the preservation of offshore tsunami deposits. Journal of Sedimentary Research, 76(12), 1267-1273.

Wentworth, C. K. (1922) A scale of grade and class terms for clastic sediments. The journal of geology, 30(5), 377-392.

Woodruff, J. D., Donnelly, J. P., Mohrig, D., & Geyer, W. R. (2008) Reconstructing relative flooding intensities responsible for hurricane-induced deposits from Laguna Playa Grande, Vieques, Puerto Rico. Geology, 36(5), 391-394.

Yoshikawa, S., Kanamatsu, T., Goto, K., Sakamoto, I., Yagi, M., Fujimaki, M., ... & Sakaguchi, H. (2015) Evidence for erosion and deposition by the 2011 Tohoku-oki tsunami on the nearshore shelf of Sendai Bay, Japan. Geo-Marine Letters, 35(4), 315-328.

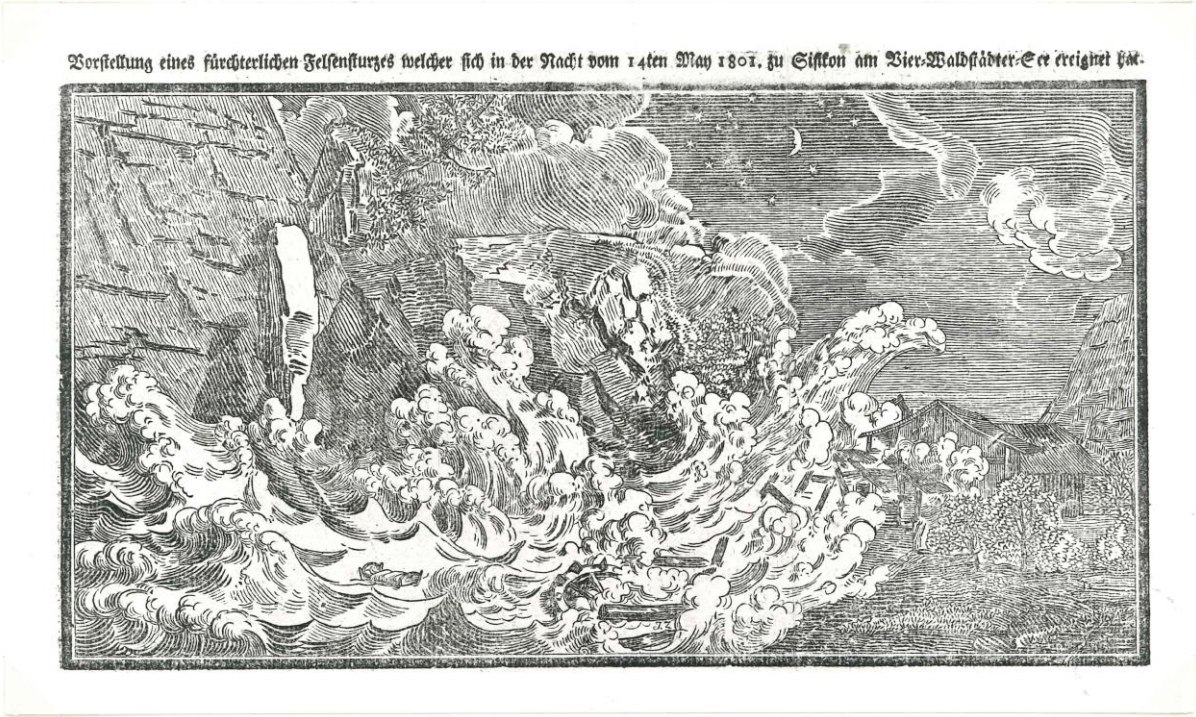

Historical drawing of the 1801 CE Sisikon rockfall-generated impulse wave, which claimed 14 lives (unknown local artist; photograph of the pencil drawing is provided by the Zentralbibliothek Zürich).

6 Freshwater (paleo)tsunamis – a review

Katrina Kremer [1, 2 *], Flavio S. Anselmetti [2], Frederic M. Evers [3], James Goff [4], Valentin Nigg [2]

[1] Swiss Seismological Service, ETH Zurich, Sonneggstrasse 5, 8092 Zürich, Switzerland
[2] Institute of Geological Sciences & Oeschger Centre for Climate Change Research, University of Bern, Baltzerstrasse 1+3, 3012 Bern, Switzerland
[3] Laboratory of Hydraulics, Hydrology and Glaciology (VAW), ETH Zurich, Hönggerbergring 26, 8093 Zürich, Switzerland
[4] Pangea Research Centre, School of Biological, Earth and Environmental Sciences, University of New South Wales, Sydney 2052, Australia

Manuscript published in Earth-Science Reviews (2021)

https://doi.org/10.1016/j.earscirev.2020.103447

Abstract

In freshwater systems (rivers and lakes), historical and recent tsunamis have been documented and their traces have been found in the geological record, but studies of paleotsunamis (prehistorical tsunamis) in such environments are still underrepresented. This contribution reviews paleotsunami studies with a focus on the post-2011 Common Era period and uses historical events to highlight some areas of research that have received little attention. In the past decade, the number of paleotsunami studies has increased and this includes those carried out over freshwater settings. However, studies of lacustrine paleotsunamis compared to studies on marine paleotsunamis are still rare and those for rivers are to our knowledge non-existent. Similarly, studies of historical tsunamis generated by meteorological disturbances have been carried out but there have been none for their paleotsunami counterpart. Thus, within this review, to cover all different aspects of tsunami generation processes in freshwater systems, we have used several historical examples, although there is a notable focus on lacustrine

paleotsunamis. This review shows that future studies of freshwater paleotsunamis are necessary in order to better understand their causes, frequencies and hazard potential.

6.1 Introduction

Tsunami is a Japanese term for "harbor wave" (Darbyshire and Ishiguro, 1957; Goff et al., 2016). The current definition of the term 'tsunami' describes a series of propagating waves of extremely long wavelength and period, usually generated by sudden disturbances of the water column associated with earthquakes occurring below or near the ocean floor. Additional generating mechanisms include volcanic eruptions, subaerial and submarine mass-movements, and bolide or other impacts upon the ocean surface (Tsunami Glossary, 2019). Tsunamis are invariably considered to be associated with marine settings and the earthquakes that cause them, a perception that has been reinforced by recent events such as the 2004 Common Era Indian Ocean and the 2011 CE Tohoku-oki events. While most marine tsunamis are most likely generated by plate displacements along sea-floor ruptures during megathrust earthquakes, recent events such as the 2018 CE Anak Krakatau tsunami (lateral collapse of Anak Krakatau volcano, Grilli et al., 2019; Takagi et al., 2019) indicate that this is by no means always the case.

Rapid displacement of large water masses can occur in any aqueous system. Worldwide historical documents and eyewitness reports have shown that tsunamis do not only occur in open oceans but also in confined fjords (e.g., 1958 CE Lituya Bay impulse wave in Alaska, US: Miller, 1960; Fritz et al., 2009) and in freshwater systems such as rivers and lakes (e.g., Schnellmann et al., 2002; Fritsche et al., 2012; Kremer et al., 2012; Clark et al., 2015; Donaldson et al., 2019; Hu et al., 2020). These historical events allow us to document the existence, causes and consequences of such tsunamis. Unlike historical tsunamis, we only know about the occurrence of paleotsunamis (prehistorical tsunamis) through the traces that they have left behind in the geological record. We distinguish between direct traces that are the deposits of the tsunami itself on lake shores or backwash deposits on the lake floor (Dirksen et al., 2011; Freundt et al., 2006; Moore et al., 2006; Moore et al., 2014) and indirect traces of paleotsunamis that are reflected in the geological record of the causal mechanism (e.g., Schnellmann et al., 2002; Kremer et al., 2012; Bozzano et al., 2009). In the latter case, numerical modelling is used to support the hypothesis that a freshwater paleotsunami occurred and to assess the magnitude of the inferred event (e.g., modelling the tsunamigenic effects of

large mass-movements in lakes; Kremer et al., 2014). In the former case, research on the geological traces of freshwater paleotsunamis is rare.

When searching for "paleotsunamis in lakes" (and its synonyms), around 13 to 1000 results are found on the "web of knowledge" and on "google scholar", respectively. However, the majority of these results refer to marine tsunamis that are recorded in coastal lakes (e.g., Kempf et al., 2017). A review of the literature indicates that there are few publications with a specific focus on paleotsunamis generated in lakes (De Lange and Moon, 2016; Dirksen et al., 2011; Freundt et al., 2006; Kremer et al., 2014; Kremer et al., 2015; Leithold et al., 2019; Moore et al., 2006; Mountjoy et al., 2019; Nigg et al., 2021; Schnellmann et al., 2002; Strupler et al., 2018). There appear to be no publications referring specifically to river paleotsunamis or to paleo-meteotsunamis.

In this study, we use the following definition of a tsunami: "A series of waves that are formed by a sudden displacement of the water, caused in or adjacent to a freshwater system (lake and river) by subaerial and subaqueous mass-movements, volcanic activity, co-seismic fault displacement and meteorological effects" (Fig. 6-1). The preposition "paleo" refers to the prehistoric period where historical (written) documentation is absent. As the historical period varies between countries and cultures, we consider the definition used in the original publications (e.g., In Switzerland, historical documents describe natural hazards already in the 6th century (Gisler et al., 2007) while in New Zealand the first written records are dated around 1840 CE (Clark et al., 2015)). Historical events related to human activity, e.g., mass-movements triggered by construction and quarry works close to the shore, were not considered. In addition, historical wave events generated by e.g., ice avalanches in moraine-dammed proglacial lakes (e.g., Clague and Evans, 2000) were also not included. Many of these lakes have formed due to glacier retreat after the Little Ice Age and are therefore considered only short-term structures in geological terms.

The main objective of this study is to review the literature on paleotsunamis in freshwater systems (rivers, lakes). We focus mainly on the period since the devastating 2011 CE Tohoku-oki tsunami. In particular, we emphasize how increased tsunami awareness has led to a series of follow-up studies that also investigated the lacustrine realm. However, since the number of studies of freshwater paleotsunamis is limited, we also use historical case studies and pre-2011 CE literature to complete a review of the full range of processes that can generate these

events. In the following, we briefly review the historical and prehistorical freshwater tsunami dataset with a focus on the paleotsunamis. We, then, discuss the advances made in paleotsunami research since 2011 CE, the state of current research and propose future research ideas.

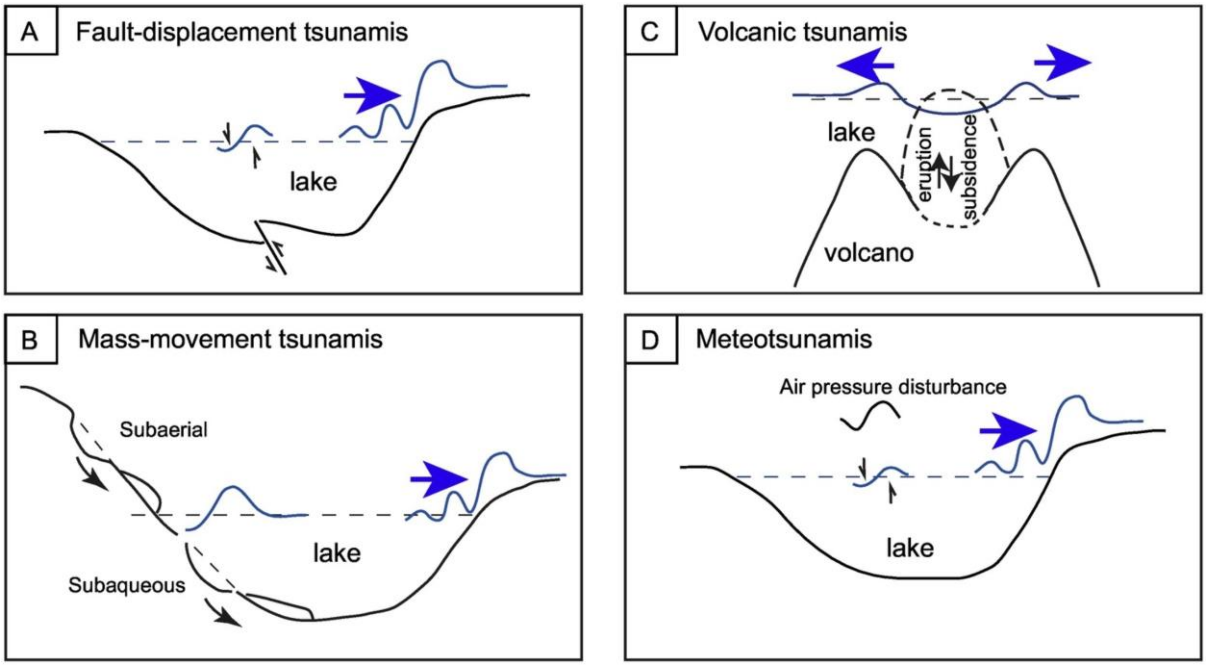

Fig. 6-1: Causes of freshwater tsunamis as mentioned in the definition used for this review.

6.2 Historical studies

As noted, the number of paleotsunami studies is limited and not all processes are covered in the literature. We therefore use historical freshwater tsunamis to fill this gap. The historical case studies covered in this literature review are compiled within Fig. 6-2 and Table 6-1. From this dataset, the main processes causing freshwater tsunamis can be identified. These include fault displacement during earthquakes, mass-movements (subaquatic and subaerial) and volcanic processes, as well as meteorological effects.

The main traces of these historical case studies are the written records. In some cases, the cause of the tsunami has been found in the geological record (e.g., mass-movement deposits in Lake Lucerne in 1601 CE; Schnellmann et al., 2002). In some cases, the deposits laid down by the tsunamis themselves (e.g., Lake Owens in 1872; Smoot et al., 2000) is described (Table 6-1).

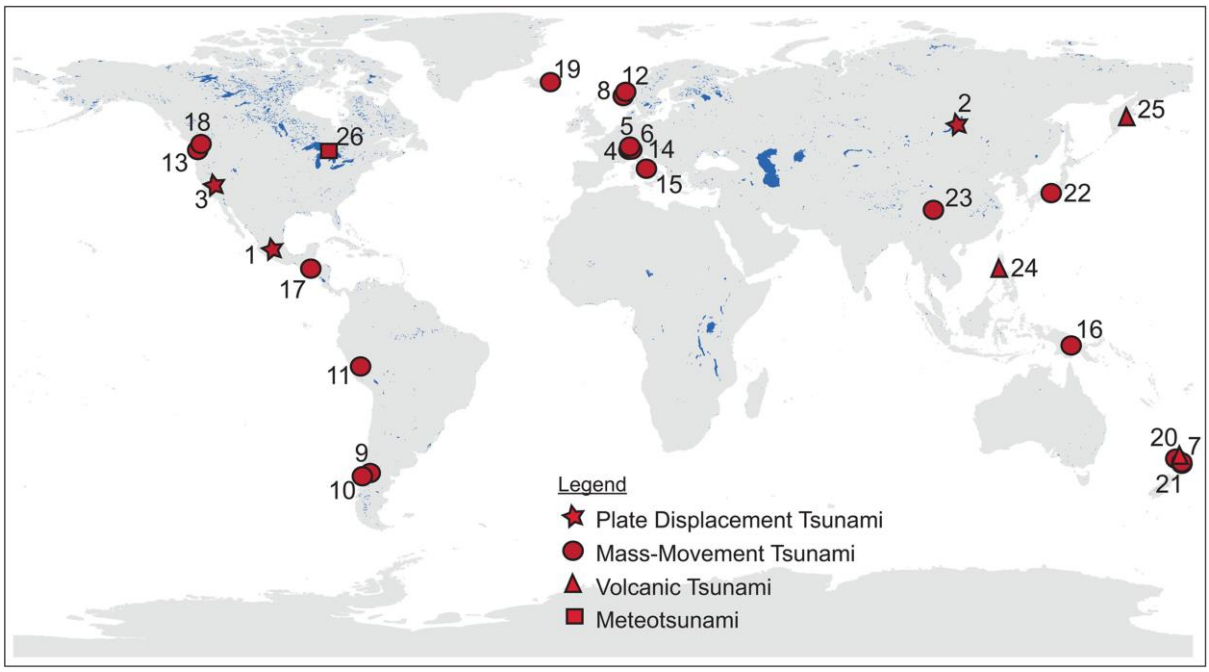

Fig. 6-2: Map showing locations with reported/studied historical freshwater tsunamis. The numbers refer to the case studies listed in Table 6-1.

6.2.1 Fault-displacement tsunamis

Co-seismic tectonic movements along a fault that crosses a lake can generate a tsunami. An historical example may have well occurred in Lake Owens in 1872 CE (Smoot et al., 2000). The reported wave height has been estimated at 37 cm and a graded sand layer has been found in the lake deposits as the evidence of this earthquake triggered tsunami. Another example happened in Lake Baikal during the 1861/1862 CE Tsagan earthquake (Didenkulova and Pelinovsky, 2006; Klyuchevskii et al., 2012; Lunina et al., 2012) that is thought to have caused a tsunami that led to several casualties (Klyuchevskii et al., 2012). However, other studies suggest that this tsunami might have been generated by an earthquake-generated mass-movement (Didenkulova and Pelinovsky, 2006). In Lake Patzcuaro (Mexico), a sedimentary unit identified in a trench is attributed to a resedimentation of lake deposits and is interpreted as being related to a tsunami generated in 1858 CE. However, as with the study in Lake Baikal, the tsunami-generating mechanism is not straightforward and could be related to either fault movement on one of the E-W faults that cross the lake or by the failure of the southwestern flank of the island of Janitzio (Garduno-Monroy et al., 2011; Fig. 6-4; Table 6-2). If Lake Baikal's and Lake Patzcuaro's tsunamis were generated by earthquake-triggered mass movements, then these events fall under Section 6.2.2.

Table 6-1: Historical freshwater tsunamis studied/reported in literature. The numbers refer to their location on the map in Fig. 6-2.

Type of tsunami	Lake	Date (CE)	Evidence of tsunami			Cause	References
			Historical and recent reports	Sedimentological	Modelled		
Fault- displacement tsunamis							
	Lake Patzcuaro (Mexico) (1)	1858	120 adobe houses destroyed by the wave: rising lake level by several meters	Reworked volcanic sands with lithoclasts and remains of ostracods	—	Fault displacement or island flank collapse	Garduno-Monroy et al., 2011
	Lake Baikal (Russia) (2)	1861 / 1862	Several fatalities	—	—		Klyuchevskii et al., 2012; Didenkulova and Pelinovsky, 2006
	Owens Lake (southern California, US) (3)	1872	Wave height of 37 cm	Graded sands	55 cm	Earthquake	Smoot et al., 2000
Mass-movement tsunamis							
Subaqueous	Lake Geneva (Switzerland) (4)	563	Destruction on the lake shore	—	3–12 m (modelled first wave arrival)	Rockfall	Kremer et al., 2012; Schoeneich et al., 2015
Subaqueous	Lake Geneva (Switzerland) (4)	1584	"Stormy" waves; more than five feet water level change; damage and flooding of watersides	—	—	Earthquake - triggered subaqueous mass movement	Fritsche et al., 2012
Subaqueous, subaerial	Lake Lucerne (Switzerland) (5)	1601	Up to 5 m wave height; outflowing river changed periodically flow direction; widespread damage; 9 fatalities	—	6 to >10 m wave height	Earthquake - triggered subaqueous mass movement	Hilbe and Anselmetti, 2015; Schnellmann et al., 2002; Cysat, 1969; Siegenthaler et al., 1987
Subaqueous	Lake Lucerne (Switzerland) (5)	1687	Up to 5 m wave height; two pulses with damaging backflow; inundation; damage mentioned	—	6 to >10 m wave height	Spontaneous delta collapse	Hilbe and Anselmetti, 2015; Bünti, 1973

Type of tsunami	Lake	Date (CE)	Evidence of tsunami			Cause	References
			Historical and recent reports	Sedimentological	Modelled		
Mass-movement tsunamis							
Subaerial	Lake Lauerz (Switzerland) (6)	1806	15 m wave height, around 10 fatalities	—	—	Rockfall	Bussmann and Anselmetti, 2010; Zay, 1807
Subaerial	Lake Taupo (New Zealand) (7)	1846	A tsunami is mentioned in Māori oral accounts	—	—	Mass movement	Clark et al., 2015
Subaerial	Lake Loen (Norway) (8)	1905 & 1936	For both events, tens of meter wave height, many causalities and heavy destruction of houses and farms	—	—	Mass movement	Grimstad and Nesdal, 1991
Subaerial	Lake Taupo (New Zealand) (7)	1910	3 m surge that reached the opposite shore; people swept off their feet and canoes washed away	—	—	Mass movement	Clark et al., 2015
Subaqueous	Lake Nahuel Huapi (Argentina) (9)	1960	2.5 m wave height; wave hit city of Bariloche; 2 fatalities	—	—	Earthquake-triggered mass movement	Barros, 1961; Parsons, 2002; Chapron et al., 2006; Beigt et al., 2016
Subaerial	Lago Cabrera (Yate Volcano, Chile) (10)	1965	25 m wave height and 60 m run-up, three farmer houses destroyed, 27 fatalities	30–40 cm mud	—	15 days of unusual heavy rainfall before the mass movement	Watt et al., 2009
Subaerial	Yanahuin Lake (Peru) (11)	1971	Several tens of meter wave height	—	—	Mass movement	Plafker and Eyzaguirre, 1979
Subaerial	Lake Botnen (Norway) (12)	1978	5–6 m wave height; 15–25 m inland, damage in village	—	—	Mass movement	L'Heureux et al., 2012; Towson and Kaya, 1988
Subaerial	Lake Spirit (USA) (13)	1980	Run-up of 260 m	—	—	Debris avalanches due to volcanic eruption of Mount St Helens volcano	Voight et al., 1983
Subaqueous	Lake Brienz (Switzerland) (14)	1996	50 cm wave noticed by workers	—	—	Spontaneous delta collapse	Girardclos et al., 2007

Type of tsunami	Lake	Date (CE)	Evidence of tsunami		Cause		References
			Historical and recent reports	Sedimentological	Modelled		
Mass-movement tsunamis							
Subaerial	Lake Albano (Italy) (15)	1997	Less than 1 m wave height	—	—	Mass movement	Bozzano et al., 2009; Mazzanti and Bozzano, 2009
Subaerial	Crater lake of Kasu Tephra Cone (Papua New Guinea) (16)	1999	15 m wave height, destruction of 2 houses, flattened vegetation; 11 injuries, 1 fatality	—	—	Mass movement	Wagner et al., 2003
Subaerial	Lake Coatepeque (El Salvador) (17)	2001	2 m wave; 5 fatalities	—	—	Earthquake-triggered mass movement	Bernard, 2009
Subaerial	Chehalis Lake (Canada) (18)	2007	Extensive damage on the shoreline, camping grounds destroyed, 38 m run-up on the opposite shore	—	Max. wave amplitude 37 m	Mass movement	Roberts et al., 2013; Evers, 2017
Subaerial	Oeskjuvaten (Lake Askja, Iceland) (19)	2014	Several tens of meter wave height	—	—	Mass movement	Gylfadóttir et al., 2017
Subaerial	Waikari River (New Zealand) (20)	1863		Thin gravel layer	—	Earthquake-triggered slope failure	Donaldson et al., 2019
Subaerial	Waikairi River (New Zealand) (20)	1931	15 m wave height on a small area	River gravel fining inland, mixed with anthropogenic material (roof nails and crockery)	—	Earthquake-triggered slope failure	Donaldson et al., 2019
Subaerial, subaqueous	Tongario River (New Zealand) (21)	1956	0.9 m tsunami wave observed at the Tongariro River	—	—	Earthquake-triggered most probable delta collapse	Clark et al., 2015
Subaerial	Totsukawa/Kumano River (Japan) (22)	2011	50 m run-up and destruction of Nagatono power plant	—	—	Rainfall-triggered mass movement (Typhoon Talas)	Chigira et al., 2013; Nagata et al., 2014; Fuchs et al., 2016
Subaerial	Jinsha River (China) (23)	2018	Run-up traces, temporary landslide dam	—	50 m run-up on the opposite shore	Mass movement	Hu et al., 2020

Type of tsunami	Lake	Date (CE)	Evidence of tsunami			Cause	References
			Historical and recent reports	Sedimentological	Modelled		
Volcanic tsunamis							
	Taal Lake, Luzon Island (Philippines) (24)	1716	Wave inundated southwestern shore up to 17 m inland	—	—	Sublacustrine eruption	Saderra Maso, 1904, Saderra Maso, 1911; Paris et al., 2014
	Taal Lake, Luzon Island (Philippines) (24)	1749		—	—	Phreatomagmatic eruption	Saderra Maso, 1904, Saderra Maso, 1911; Paris et al., 2014
	Taal Lake, Luzon Island (Philippines) (24)	1754	Waves on the western shore	—	—	Pyroclastic flow	Saderra Maso, 1904, Saderra Maso, 1911; Paris et al., 2014
	Taal Lake, Luzon Island (Philippines) (24)	1911	Western shore hit by 3 m high waves and 20–50 people were drowned	—	—	Pyroclastic flow or atmospheric shock waves due to strong explosions	Saderra Maso, 1904; Paris et al., 2014
	Taal Lake, Luzon Island (Philippines) (24)	1965	190–355 fatalities as wave capsized boats of fleeing residents - waves inundated areas up 4.7 above lake level	—	—	Phreatomagmatic eruption	Moore et al., 1966; Paris et al., 2014
	Lake Karymskoye (Russia) (25)	1996	2 to 30 m wave height	Finely laminated layers of up to 35 cm thickness composed of sand and gravel mixed with pebbles, plant and soil fragments	—	Phreatomagmatic eruption	Belousov and Belousova, 2001; Belousov et al., 2000; Falvard et al., 2018; Torsvik et al., 2010
Meteotsunamis							
Data of historic and recent meteotsunamis are compiled in Bechle et al., 2016	Great lakes (Lake Michigan, Lake Superior, Lake Huron, Lake Erie, Lake Ontario) (26)	1822–2015	m-scale (data are available for most events), damages have been noted in most cases; fatalities in some cases	—	—	Air pressure disturbance	Bechle et al., 2016 and references therein

6.2.2 Mass movement-induced tsunamis

The term “mass movement” is used here for any type of natural gravity-driven mass-movements mobilizing soil, rock, lava, pyroclastic material, ice, and snow (Hungr et al., 2001). Historical reports and recent observations indicate that subaerial and subaqueous mass movements have generated tsunamis in several lakes around the world (Fig. 6-2, Table 6-1). These mass-movements have been generated by a suite of mechanisms such as earthquakes, heavy rainfall, “spontaneous causes” such as over steepening or overloading, and volcanic processes such as avalanches or flank collapses. The majority of the reported historical tsunamis have been caused by subaerial as opposed to subaqueous mass movements (Fig. 6-2).

Mass movements can also generate tsunami-like waves in rivers. Their occurrence is demonstrated in some historical examples (Table 6-1). The largest historical tsunami wave height in New Zealand was the result of a tsunamigenic slope failure into Waikari River in Hawke's Bay, New Zealand in 1931 CE. The reported wave height in 1931 CE was 15 m although its areal extent was small, extending only 150 m length along the river bank and 66 m inland (Donaldson et al., 2019; Tait, 1977).

The 1931 CE slope failure occurred in unconsolidated uplifted loess and marine Plio-Pleistocene sediments that form a 120 m high hill on the western bank of the Waikari River. It was generated by severe ground shaking associated with the 1931 CE Hawke's Bay earthquake (Mw 7.8) that, amongst other things, caused widespread landsliding in the region's river catchments that most probably produced numerous local tsunamis (Davison, 1934; Smith, 1978). Rare historical documents give only general details about the resultant tsunami in the Waikari valley, although it is noted that buildings on the eastern side of the river (Waikari Station) were destroyed by the event (Auckland Star, 1931; Tait, 1977). The ~1.7 10^6 m^3 landslide fell into the river, displacing the water and causing a large impulse wave that inundated Waikari Station. According to the landowner “it also lifted the waters of the river onto the top terrace, surrounding the homestead and washing some of the outbuildings a chain [22 yards/~20 m] or so away” (Tait, 1977, p. 78). The deposit consists primarily of river gravels that fine inland and become mixed with anthropogenic material such as roof nails and crockery (Donaldson et al., 2019). A thinner gravel layer beneath the 1931 CE deposit indicates repeated events have occurred in the area (Fig. 6-3).

This earlier, possibly smaller event, was most likely related to a slope failure generated by the M_w 7.4 1863 CE Hawke's Bay earthquake centered about 100 km south of the Waikari River (Stirling et al., 1998). This evidence for repeated tsunamis suggests that these events occur relatively frequently in the region. Therefore, there is a high probability that numerous past events have occurred not only in this catchment but in regional catchments with similar geology. Adams (1981) reported a similar 1931 CE earthquake-generated slope failure scenario in the larger Mohaka catchment some seven km NE of the Waikari River. It occurred in an unpopulated area and while there were no eyewitnesses to any possible tsunami, the slope failure was noted soon after the earthquake because it dammed the river and continued to do so for the next seven years.

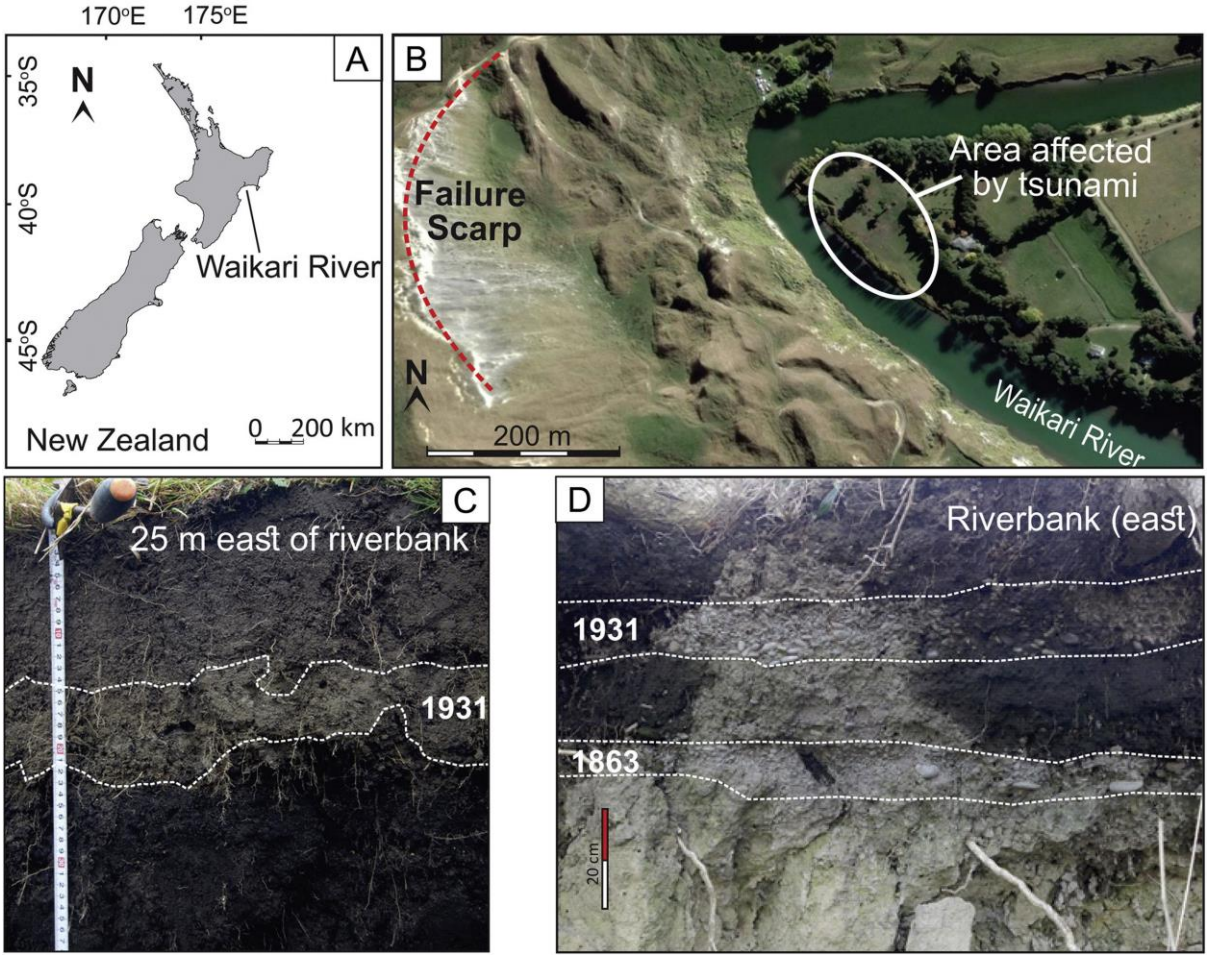

Fig. 6-3: Waikari River: a) Location on east coast, North Island, New Zealand; b) Tsunami site showing failure scarp on the western bank and Waikari Station on the eastern side; c) Gravel and coarse sand layer of 1931 CE tsunami; d) Coarse gravel layers related to the 1931 CE and 1863 CE tsunamis (photos: J. Goff).

6.2.3 Volcanic tsunamis

Volcanic tsunamis are also termed “volcanogenic” (e.g., Freundt et al., 2007) or “volcanism-induced” tsunami. Nishimura (2008) and Paris et al. (2014) discuss several definitions. One of these definitions states “a high wave or surge of water produced by a variety of eruptive and non-eruptive processes at volcanoes” (Begét, 2000). In this review, we use a modified version of this definition: “A high wave or surge of water produced by eruptive processes, mainly underwater explosions and pyroclastic flows”. Other eruption-related processes, such as flank failure entering the water (Paris et al., 2014) are considered to behave similar to subaerial and subaqueous mass-movements and are thus considered in the concept of mass-movement tsunamis. Historical examples of volcanic tsunamis due to phreatomagmatic eruptions have been noted in Taal Lake (Luzon Island, Philippines) and Lake Karymskoye (Belousov and Belousova, 2001; Belousov et al., 2000; Falvard et al., 2018; Saderra Maso, 1904; Moore et al., 1966; Torsvik et al., 2010).

6.2.4 Meteotsunamis

Meteorological tsunamis (or meteotsunamis) are meteorologically generated water waves that have similar characteristics and behavior to classic tsunamis. They are induced by atmospheric perturbations of air pressure and wind (Nomitsu, 1935; Linares et al., 2016). On historical timescales, meteotsunamis have been increasingly recognized in the literature. As one example, Bechle et al. (2016) quantify meteotsunamis based upon seasonality, causes and consequences using the historical record available for the Great Lakes (Canada and USA) from 1822 to 2015 CE. This dataset of Bechle et al. (2016), published in their supplementary material, shows that most of these meteotsunamis have been m-scale waves. The most severe event occurred in Lake Michigan in 1929 CE, where a 6 m high wave caused 10 fatalities. The historical dataset of Bechle et al. (2016) demonstrates that most of the events in the Great Lakes occur from late-spring to mid-summer and are associated with convective storms. As Bechle et al. (2016) summarizes the historical meteotsunami dataset in lakes, these historical events are not listed in detail in Table 6-1. We rather refer to this publication for the individual case studies.

6.3 Paleotsunami studies

As noted, there are only a few studies that have been carried out on paleotsunamis that occurred either in or adjacent to lakes. These studies are summarized in Table 6-2 and Fig. 6-4 (De Lange and Moon, 2016; Dirksen et al., 2011; Freundt et al., 2006; Kremer et al., 2014; Kremer et al., 2015; Leithold et al., 2019; Moore et al., 2006; Schnellmann et al., 2002; Mountjoy et al., 2019; Nigg et al., 2021; Strupler et al., 2018). The interpretation of the occurrence of a paleotsunami is based on either direct observation of their onshore and offshore deposits (Two-Yurts Lake, Lake Managua, Lake Tahoe, Owens Lake; Lake Tarawera; Lake Sils) and/or by modelling the effects of large subaqueous and subaerial mass-movements (Lake Geneva, Lake Lucerne, Lake Tahoe, Lake Tekapo, Lake Crescent, Lake Sils).

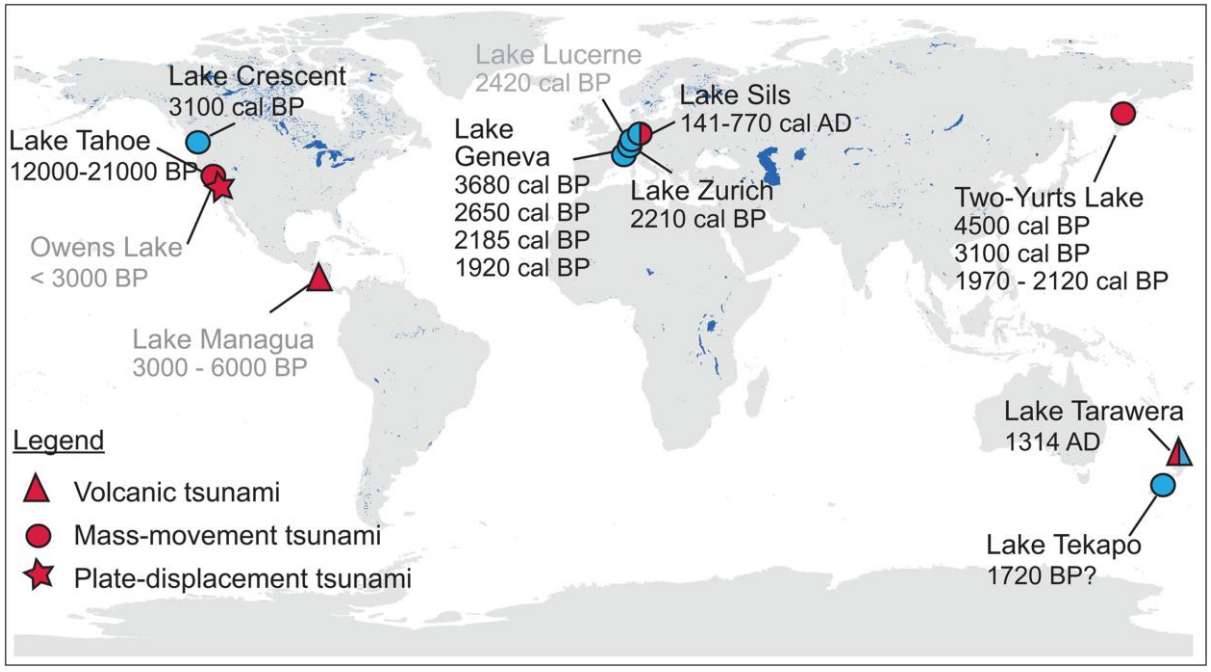

Fig. 6-4: World map showing location of lacustrine paleotsunami studies presented in this review (Table 6-2). Symbols in red represent studies where paleotsunamis have been found based on geological evidence, while blue symbols represent studies where potential paleotsunamis have been modelled based upon a probable generating mechanism. Studies published before 2011 CE are in gray, while post-2011 CE publication are in black font.

6.3.1 Fault-displacement paleotsunamis

In Owens Lake (Southern California, USA), two deposits described as poorly sorted, graded pebbly sand layers were found in sediment cores from the lake floor and are dated to around 300 and 1500 Before Present (BP), respectively (Smoot et al., 2000). The authors proposed that these deposits were caused by the erosion and redeposition of lake sediments because of a

tsunami. As these deposits are associated with liquefaction structures and deformed bedding, the tsunamis may well have been caused by a fault displacement similar to an historical example in 1872 CE (with an earthquake of Mw 7.5–7.7 and a tsunami wave of about 55 cm). This hypothesis is supported by the identification of Holocene fault offsets along the Owens Valley Fault.

6.3.2 Mass-movement paleotsunamis

Lake Lucerne (Switzerland)

In Lake Lucerne, several coeval subaqueous mass movements were identified in reflection seismic data and interpreted as the effects of a paleo-earthquake dated to around 2420 calibrated (cal) BP (Schnellmann et al., 2002). These large coeval mass movements are interpreted as tsunamigenic. The consequences of a sudden water displacement due to one of the largest subaqueous mass-movement (total volume of 11×10^6 m^3, a run-out distance of 1.5 km and a 9 m high failure scar) of this event were modelled by Ward (2001) using the linear water-wave theory. This modelling resulted in waves >3 m high after 1 min after landslide initiation (velocity of 0.15 ms^{-1}) at the shore directly across from the subaquatic mass-movement (Schnellmann et al., 2002). Wave heights of 1–1.5 m reach the city of Lucerne (northwest of the subaqueous landslide location) ~4 mins after subaqueous landslide initiation. So far, no onshore and/or shallow-water deposits have been found for this modelled paleotsunami scenario. Therefore, the consequences are solely based on the interpretation of reflection seismic data and results of the numerical modelling.

Table 6-2: Examples of lacustrine paleotsunamis found in literature and mentioned within this review. Locations are shown in Fig. 6-4.

Lake	Date	Evidence	Wave height	Cause	References
Owens Lake (USA)	Two events younger than 3000 cal BP	Poorly sorted, graded pebbly sand deposits	—	Fault displacement	Smoot et al., 2000
Lake Lucerne (Switzerland)	2420 cal BP	Consequences of large mass movements	Up to 3 m (modelled)	Earthquake-triggered mass movements	Schnellmann et al., 2002
Lake Geneva (Switzerland)	3683 cal BP	Consequences of large mass-movements (failure scar & deposit)	Up to 12 m (modelled)	Earthquake-triggered mass movement	Kremer et al., 2014
Lake Geneva (Switzerland	1920 cal BP; 2185 cal BP; 2650 cal BP	Consequences of large mass-movement deposits originating from the Rhône delta	1–2 m (modelled)	Subaqueous mass movements (delta failures	Kremer et al., 2015
Lake Zurich (Switzerland)	2210 cal BP	Consequences of large mass movement deposits	1–2 m (modelled)	Subaqueous mass movements	Strupler et al., 2018
Lake Tahoe (USA)	12’000–21’000 BP	Sandy, pebble sized gravels, erosion features due to strong current	Up to 50 m (modelled)	Subaqueous mass movement	Moore et al., 2006; Moore et al., 2014

Two-Yurts Lake (Russia)	2100–2000 BP; 2900 BP; 4000 BP	Discontinuous layer of structure-less poorly sorted sands with rounded pebbles and organic material	Up to 10 m (field observation)	Subaerial mass movement	Dirksen et al., 2011
Lake	**Date**	**Evidence**	**Wave height**	**Cause**	**References**
Lake Sils (Switzerland)	141–770 cal CE	Fining-upward coarse sand overlying an organic-rich peat deposit in the off- and onshore realm	2–5 m (modelled)	Subaqueous mass movement (delta failure)	Nigg et al., 2021
Lake Tekapo (New Zealand)	~1720 BP? (~1700 cal BP)	Consequences of subaerial/sublacustrine mass movements	Several meters (modelled)	Mass movements	Mountjoy et al., 2019; Upton and Osterberg, 2007
Lake Crescent (USA)	3100 cal BP	Consequences of a large subaerial mass movement	90–104 m (modelled) following relationship of Clark et al. (2015)	Subaerial mass movement	Leithold et al., 2019
Lake Managua (Nicaragua)	3000–6000 BP	Massive, well sorted sand layer	—	Volcanic eruption	Freundt et al., 2006
Lake Tarawera (New Zealand)	1314 CE	Sharp erosional contact on lacustrine silts and two fining upwards units	6–7 m (modelled with multiple closely spaced pyroclastic flows)	Pyroclastic flows	Magill, 2001; De Lange and Moon, 2016

Lake Geneva (Switzerland)

In Lake Geneva, traces of a large subaqueous failure scar have been identified on the bathymetric map at a water depth greater than 80 m over a horizontal distance of ~5 km (Kremer et al., 2014). The failure escarpment reaches a height of up to 20 m (Fig. 6-5a). The mass-movement deposit has been imaged on reflection seismic profiles as a semi-transparent and chaotic seismic facies that is interpreted as a slide-evolved mass-flow deposit (Fig. 6-5b). The affected surface of this deposit is ~25 km^2 with a volume estimated at 130 10^6 m^3. In recovered sediment cores, the mass-movement deposit consists of deformed and folded sediments with mud clasts (Fig. 6-5c). The event is dated to 3683 ± 128 cal BP. As simultaneous mass-movements occurred along the same seismostratigraphic horizon throughout the lake, the most likely trigger for the mass-movements appears to be an earthquake. The consequences of such a large mass-movement on the water column have been simulated by numerically solving the shallow-water equation in two dimensions following the technique of Simpson and Castelltort (2006). The deposited volume of 130 10^6 m^3, the position of the failure scar, and the extent of the deposit constrained from the reflection seismic data were used as input parameter for the model. The velocity of the mass movement was calculated using the equation from Ward and Day (2002) with a slope gradient of 4° and a runout distance of 2.5 km (Kremer et al., 2014). The resulting first tsunami wave has been estimated to be between 4 and 6 m at Evian (southern slope) and Lausanne (northern slope) after 3 and 6 min, respectively (Fig. 6-5d). In Geneva (at the western end of the lake), wave heights of 1 to 2 m arrive 30 min after the initiation of the mass-movement. At two archeological sites (Preverenges and Morges/Les Roseaux, west of Lausanne), the first wave of 0.75 m is followed by several further waves of 1.7–1.8 m within 15 mins. These sites are characterized by pile dweller settlements that both show an occupation gap coinciding with the timing of the subaqueous mass-movement during the Early Bronze Age (Kremer et al., 2014). Thus, an earthquake-triggered mass-movement tsunami may well explain this time-gap in the pile-dweller occupation (Corboud, 2012; Kremer et al., 2014).

Furthermore, four additional prehistorical mass-movement deposits have been recorded in the reflection seismic data of Lake Geneva. These deposits are dated to around 2650, 2185 and 1920 cal BP (Kremer et al., 2015). The geographical distribution of these deposits suggest that they originated from slope failures of the Rhone Delta at the eastern tip of the lake. Simple modelling approaches have shown that the movement of these sediment volumes might have generated paleotsunamis with minimum wave heights >1 m (Kremer et al., 2015). Two

historically-documented delta failures, one in 1584 CE triggered by an earthquake (Fritsche et al., 2012) and the other in 563 CE triggered by rockfall and laterally consecutive delta failure (Kremer et al., 2012) have also generated tsunamis of different wave heights (Table 6-1). Thus, partial Rhone Delta collapses have produced at least six times tsunamigenic mass-movements over the past ~4000 years. The interpretation of the occurrence of paleotsunami events is based on the modelling of the effects of large mass-movement deposits recorded in the sedimentary archive.

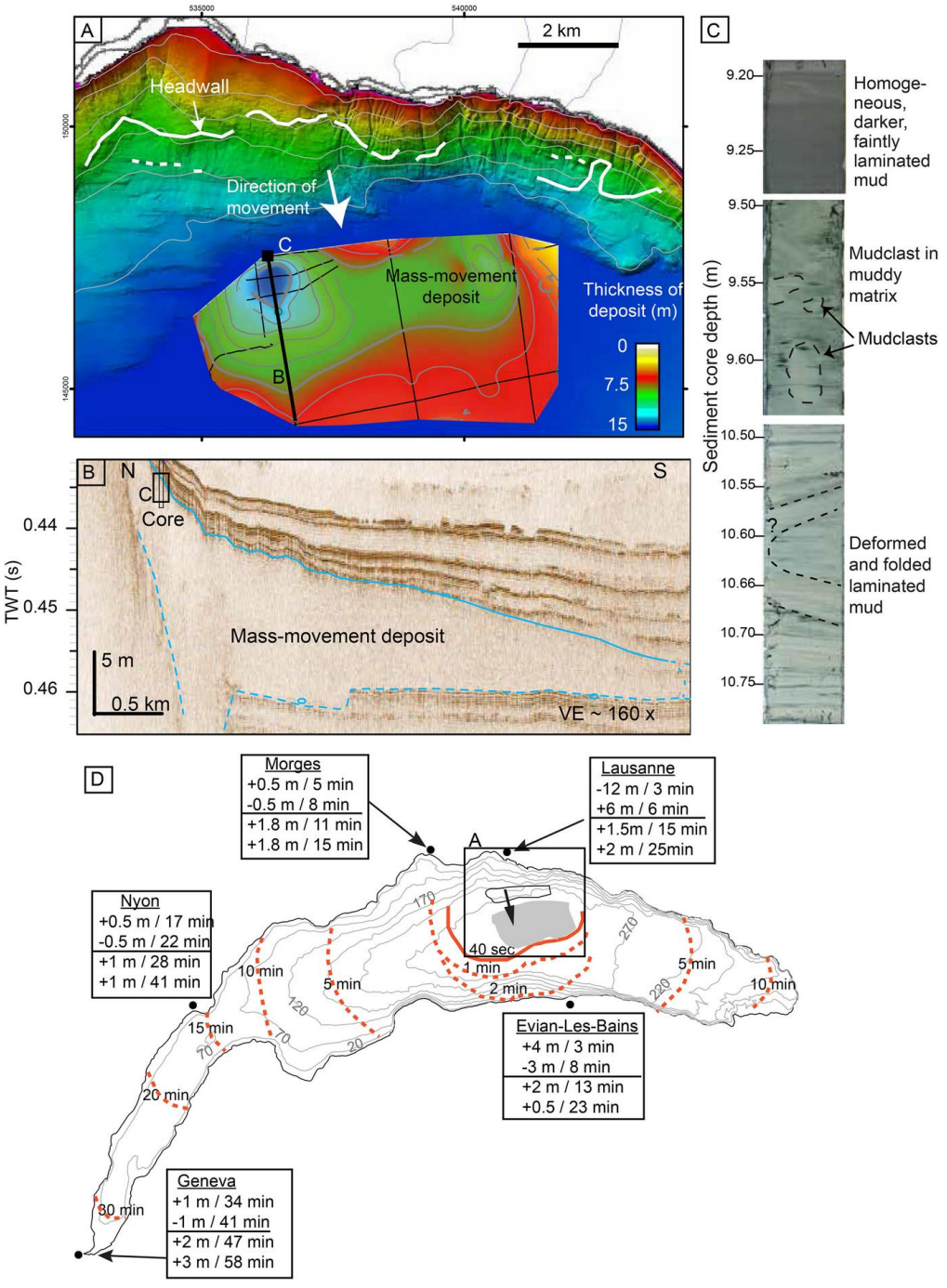

◄ Fig. 6-5: 3683 ± 128 cal BP paleotsunami in Lake Geneva. (A) A former mass movement is recognized in the bathymetric map with traces of the associated headwall (white line). The thickness map is based on reflection seismic data (black lines) and indicates that the up to 15 m thick mass-movement deposit consists of deformed sediment packages. The bold black line marks the location of reflection seismic profiles shown in (B). (B) N-S oriented reflection seismic profile imaging a chaotic to transparent seismic facies that represents the mass-movement deposit. The rectangle shows the position of the sediment core shown in (C). (C) The sediment core shows deformed, mixed and homogeneous sediments interpreted as a slide-evolved mass flow topped by a homogeneous white layer (Kremer et al., 2014). (D) Simulated tsunami propagation assuming a 130×10^6 km^3 slide. Wave height and corresponding arrival times are indicated for selected cities around Lake Geneva. Source of maps is Federal Office of Topography. Parts of the figure have been modified from Kremer et al., 2014.

Lake Zurich (Switzerland)

Traces of basin-wide subaqueous mass movements have been detected in reflection seismic data of Lake Zurich. These are interpreted as earthquake-triggered events and have been dated to ~2210; ~11,600 and ~ 13,670 cal BP (Strasser et al., 2013). Strupler et al. (2018) modelled a tsunami scenario for all documented slides (cumulative volume of around 4 km^3) of the ~2210 cal BP event using GeoClaw (Berger et al., 2011). The strongest effects (run-up and inundation) were noted along the central basin of Lake Zurich with the largest wave heights of around 1.5 m generated 1 min after slide initiation (Strupler et al., 2018). Afterwards, the wave oscillated for the following 10 mins with peak amplitudes of around 0.5 m.

Lake Tahoe (USA)

Evidence of a paleotsunami has been found as a consequence of a large subaqueous mass-movement in Lake Tahoe (Nevada & California, USA; Moore et al., 2014). Moore et al. (2006) describes glacial boulders transported and sorted by strong currents to form a series of underwater ridges. Moreover, high-resolution bathymetry indicates underwater channels, which probably formed through lake-floor scouring at the same time (Moore et al., 2014). Furthermore, erosional surfaces that extend 1 km inland and 30 m above the lake level are overlain by sandy-pebble-sized gravels. It is suggested that the boulders, wave channels and erosional surface overlain by detrital sediment were caused by currents induced by a large tsunami triggered by the giant McKinney Bay landslide (12 km^3). The subaqueous landslide detached from the western wall into the deep Lake Tahoe basin during the late Quaternary, between 12,000 to 21,000 BP (Moore et al., 2014; Moore et al., 2006). The landslide debris is still visible as angular shaped blocks on the bathymetric map. Modelling suggests that rapid movement of the landslide may well have generated a giant tsunami with >50 m wave height

(Ward, 2013). Furthermore, the overtopping of the lake shore by this tsunami may have lowered the lake level by around 10 m (Moore et al., 2014).

Dvuh-yurtochnoe (Two-Yurts) Lake (Russia)

The Two-Yurts lake, formed by a landslide in the Late Pleistocene, was studied by Dirksen et al. (2011) with a focus on the tephrachronology of several Holocene landslide events. Along the eastern shore of the lake, Dirksen et al. (2011) observed a discontinuous layer of structure-less, poorly sorted sands with dispersed rounded pebbles (up to 1 cm in diameter) and reworked organic materials directly overlying landslide deposits, which has been dated to around 2900 ^{14}C BP (3100 cal BP). At another site, 2 km downstream from the lake, a depositional succession occurs that comprises a 10 cm thick structure less, poorly sorted sand layer with dispersed pebbles (up to 5 mm in diameter). This is overlain by a 20 cm thick layer of poorly stratified, moderately sorted sand that is capped by a 5–10 cm thick layer of poorly sorted sand and pebbles mixed with sand and charcoal. The authors concluded that this succession originated from a tsunami caused by a subaerial landslide. Moreover, the authors observed in another nearby smaller lake, a 3 cm-thick layer containing a diatom assemblage similar to that found in Two-Yurts Lake. The diatom assemblage is markedly different from those in the sediments directly below and above, indicating that this layer most likely consists of tsunami-reworked lacustrine sediments from Two-Yurts Lake. Two younger event layers of fine to coarse grained, poorly sorted sand with rounded pebbles are identified and also interpreted as tsunami deposits. These date to between 2000 and 2100 ^{14}C BP (1970–2120 cal BP). A further probable landslide-generated tsunami deposit is dated to ca. 4000 ^{14}C BP (4500 cal BP) indicating that at least four events have occurred between 4500 and 1970 cal BP (Dirksen et al., 2011).

Lake Sils (Switzerland)

A partial collapse of the Isola Delta with a total estimated depositional volume of 6.5 10^6 m^3 has been dated to around 474–770 cal CE (Blass et al., 2005). This is considered to have generated a significant tsunami in Lake Sils. Based on sedimentological core analysis, reflection seismic data and numerical modelling using MassMov2D (version 0.91; Beguería et al., 2009) and GeoClaw (version 4.6.3; Berger et al., 2011), Nigg et al. (2021) proposed a basin-wide tsunami with run-up heights of 3–4 m and an inundation distance of 200 m on the lake shore. The modelled maximum tsunami height at the shoreline generally reached around 2.5–

3.5 m, although they notably exceeded 5 m along the steep shoreline directly opposite the mass movement and in the source area around the shore of the collapsed delta.

Sediment cores taken along an onshore-offshore transect provide evidence for this proposed scenario. An unusual coarse, fining-upward, sand was identified in the shallow-water setting of two apparently separated sub-basins and along the lake shore. The up to 20 cm thick sandy deposit overlies an organic-rich peat with a sharp erosional contact. Towards deeper water, the deposit transforms into a thicker sediment package with multiple fining-upward sequences as well as massive gravel deposits that are considered to have been laid down by pulse-like backwash currents (Nigg et al., 2021). This deposit is topped by a clay capping deposited out of suspension in both the shallow and deeper water settings. This event deposit is in turn overlain by organic-rich deposits that have been radiocarbon dated to 225–419 cal CE (Nigg et al., 2021) which immediately postdates the delta collapse (Blass et al., 2005).

Lake Tekapo (New Zealand)

Several stratigraphic units with coeval mass-movement deposits have been reported from reflection seismic data (Upton and Osterberg, 2007). Mountjoy et al. (2019) modelled the consequences of different mass-movement scenarios and showed that even relative small events with estimated volumes <0.05 10^6 m^3 can generate m-scale tsunamis (Mountjoy et al., 2019). Based on sedimentation rates, an approximate age for one of these horizons has been estimated to around 1720 BP. This suggests that several paleotsunamis may well have occurred at Lake Tekapo, although further dating is needed to better constrain the ages of these events (Mountjoy et al., 2019).

Lake Crescent (USA)

At least four large megaturbidites are recorded in the sedimentary record of Lake Crescent (Leithold et al., 2019). The youngest is dated to around 3100 cal BP and has been linked to the large Sledgehammer Point rockslide which has an estimated volume of 12 10^6 m^3. The proposed tsunami generated by this rockslide had an estimated wave height of between 82 and 104 m (Leithold et al., 2019). This estimation is based on the relationship between subaqueous and maximum observed vertical shoreline run-up height using data from historical landslide tsunamis in lakes and fjords proposed by Clark et al. (2015). It was suggested that this rockslide had been triggered by an earthquake. The older turbidites may well indicate that further earthquake triggered rockslide-tsunamis have occurred (Leithold et al., 2019).

6.3.3 Volcanic paleotsunamis

Lake Managua (Nicaragua)

A sub-plinian to plinian eruption from a vent on the northwestern shore of Chiltepe Peninsula in Lake Managua, 3000–6000 BP, is recorded by a dacite to andesitic tephra ("Mateare Tephra"). A massive dark gray, well-sorted sand layer, the "Mateare sand", has been found at elevations well above beach levels. The geographically widespread distribution of this layer excludes a fluviatile origin and, thus, has been interpreted as a tsunami deposit (Freundt et al., 2006). This tsunami layer has been explained as being generated by pulses of eruption during the initial phase of volcanic activity (Freundt et al., 2006). This pre-2011 study provides a context for the paleotsunami studies carried out since 2011 (Fig. 6-3; Table 6-2).

Lake Tarawera (New Zealand)

New Zealand has a short written-history (since ~1840 CE; Clark et al., 2015), thus in this context an event in 1314 CE is a paleo event. In 1314 CE, multiple pyroclastic flows emitted from Mt. Tarawera during the Kaharoa eruption entered Lake Tarawera. This eruption coincides with the earliest evidence for human settlement in New Zealand (Hogg et al., 2003) and thus, represents a key dating event (De Lange and Moon, 2016). A paleotsunami deposit is described composed of two fining upward sequences overlying with a sharp, erosional basal contact with lacustrine silts. These fining upward units consist of cobbles and gravels originating from beach deposit. Based on the threshold velocities for the entrainment of the different clasts in these units, these layers were interpreted as being the result of two waves of 7 and 1 m high, respectively (Magill, 2001; De Lange and Moon, 2016). De Lange and Moon (2016) showed that multiple, but closely-timed, flows entering the lake were needed to generate the 6–7 m wave height.

6.4 Discussion

6.4.1 Cause of freshwater tsunamis

The above-mentioned examples of paleotsunamis in lakes show that different causal mechanisms can be distinguished: fault displacements, mass movements and volcanic processes (Figs. 6-1A to C). However, these studies do not cover meteotsunamis (Fig. 6-1D) as a further possible mechanism capable of triggering freshwater tsunamis. Indeed, prehistoric examples of meteotsunamis are yet to be reported. Similarly, mass movement-induced tsunami-

like waves in rivers have only been reported in the historical record (Table 6-1). River tsunamis appear to only affect a small geographical area and are deposited in highly dynamic riverine systems. If these historical examples are indicative of the nature and extent of such events, then it is highly likely that evidence for their prehistoric counterparts may well have been eroded. However, evidence for the large slides that caused them may well be preserved in the landscape since they can block entire valleys and create landslide dams. The preservation of these landslides in the environment may well provide a way forward for numerical modelling assessment.

6.4.2 Advances in freshwater paleotsunami research since 2011

This literature review of paleotsunamis in freshwater systems shows that the number of studies has increased since 2011 CE. Pre-2011 CE studies notably described single events (e.g., Schnellmann et al., 2002), while post-2011 CE work contains at least two examples that have shown repeated tsunamis in freshwater systems. Although the recurrence rate is low with around one event per 1000 years (Dirksen et al., 2011; Kremer et al., 2015), these studies show that the hazard related to tsunamis should not be underestimated. Over the past decade, paleotsunami studies modelling the effects of large mass-movements have increased, most probably related to computational advances. Additionally, since 2011 CE the first tsunami-hazard assessment studies have also now been carried out based on the knowledge of freshwater paleotsunamis (e.g., Lake Zurich, Strupler et al., 2018; Lake Tekapo, Mountjoy et al., 2019).

6.4.3 State of current research on freshwater paleotsunamis

There are still only a few lake paleotsunami studies in the literature and none for rivers. The paleotsunami studies found in the literature are from Lakes Owen, Crescent, Managua, Lucerne, Geneva, Zurich, Sils, Two Yurts, Tekapo, Tarawera and Tahoe (Fig. 3 and Table 2) (Smoot et al., 2000; Schnellmann et al., 2002; Freundt et al., 2006; Moore et al., 2006; Dirksen et al., 2011; Kremer et al., 2014; Kremer et al., 2015; Leithold et al., 2019; De Lange and Moon, 2016; Strupler et al., 2018; Mountjoy et al., 2019; Nigg et al., 2021). Six studies report tsunami deposits in the sediments on lake shores (Lakes Managua, Tarawera and Sils) or within the basin (Lakes Owens, Two-Yurts and Tahoe) with the sedimentary evidence differing between study sites. Poorly sorted sands containing pebbles were identified in the Owens Lake

and Two Yurts Lake studies while in Lake Managua a well sorted sand layer was observed. In the investigations at Two-Yurts Lake, organic remains and charcoal were also found in the deposit layers.

In Swiss lakes, besides the documentary evidence for historical tsunamis, paleotsunamis are inferred based on the modelling of the consequences of large prehistoric subaqueous mass-movements on the water column. Deposits corresponding to these inferred paleotsunamis have only been proposed at Lake Sils (Nigg et al., 2021), whereas layers around the other lake shores or in the lake basins are so far missing. It seems reasonable to suggest that the best way forward here is to use modelled inundation data to identify the most likely lake-shore sites for preferential preservation of such deposits. For potential backwash deposits, a study of historically-documented events may serve as a useful guide for the identification of discrete units in sediment cores. Equally, reference to submarine data from equivalent historically-documented marine events such as the 2011 CE Tohoku-oki tsunami may provide guidance on the characteristics of backwash deposits (e.g., Goto et al., 2014).

The fact, that tsunami deposits in freshwater settings are rarely described may be explained by two major differences when compared to their marine counterparts. The first difference arises from geomorphological disparities. In the marine setting, coastal plains are generally much more extensive compared to lacustrine or riverine environments. Deep lakes often have a higher slope gradient along their shores and therefore, the tsunami deposition potential is reduced as no accommodation area is available. Furthermore, sandy beaches around lakes are often restricted in size and associated with fluvial embayments. Thus, the identification of lacustrine tsunami deposits is challenging. The toolkit for the identification of tsunami deposits has mainly been developed on marine tsunamis (Chagué-Goff et al., 2011). There marine microfossil species and saltwater chemistry are often used in the identification of tsunami deposits, all criteria that are absent in the freshwater environment.

Some advances are being made, and like the archive of marine tsunamis in coastal lakes (Bondevik et al., 1997; Hutchinson et al., 1997; Kempf et al., 2017), freshwater tsunamis (e.g., lake tsunamis) have been recorded in bays or smaller nearby lakes or wetlands, as shown in the case of Two-Yurts Lake. As there is a need in fostering the research on freshwater tsunami deposits, we have adapted a conceptual model from Einsele et al. (1996) to indicate the

potential areas where tsunami deposits might be trapped and recorded in and adjacent to lacustrine environments (Fig. 6-6).

Preliminary estimates of the frequency of lacustrine paleotsunamis have also been proposed for both Lake Geneva and Two Yurts Lake (Dirksen et al., 2011; Kremer et al., 2015). For Lake Geneva, six tsunamis (historical and prehistorical) have been identified within the past ~4000 years indicating that the tsunami hazard should not be ignored (Kremer et al., 2015). Although all of the tsunamis in Lake Geneva are related to subaqueous mass-movements, their causes are diverse. The initial triggers of the mass movements are earthquakes, rockfalls, and aseismic delta failures (Kremer et al., 2012; Kremer et al., 2014; Kremer et al., 2015). In Two-Yurts Lake, four tsunami deposits have been recorded within 2000 years, with wave heights between 5 and 10 m (Table 6-2; Dirksen et al., 2011). All were caused by subaerial mass-movements (Dirksen et al., 2011).

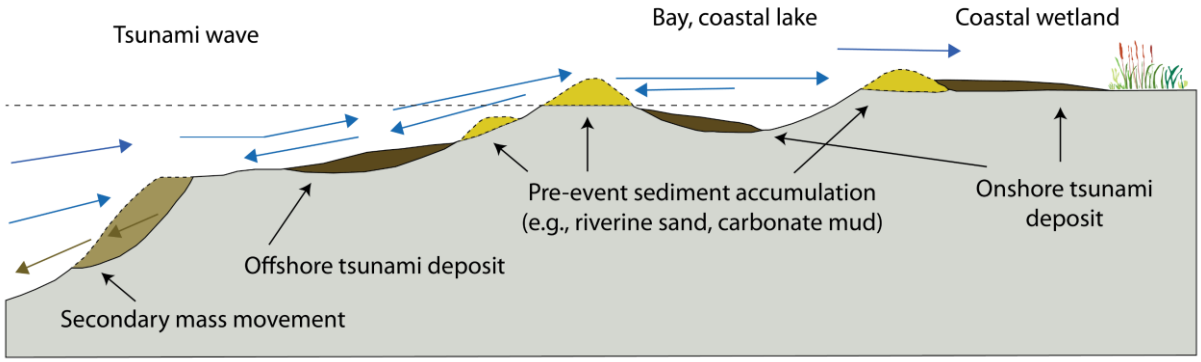

Fig. 6-6: Settings for potential tsunami deposits in lacustrine environments (modified from Einsele et al., 1996).

6.4.4 Future research strategies

Overall, studies of freshwater paleotsunamis are rare, although it is known through historical examples that tsunamis represent a recognized natural hazard that should not be underestimated. For tsunami hazard assessment, it is necessary to know the causes, frequencies, sizes, magnitude, and impacts of tsunamis (Clague et al., 2003 and references therein) and therefore, there is a growing need to carry out further paleotsunami studies. Such studies are of particular importance because some paleotsunamis have been reported from lakes with no historically-documented occurrences (e.g., Lake Managua; Two-Yurts Lake; Lake Tahoe).

Our review indicates that the study on freshwater paleotsunamis is challenging and that more sedimentological studies are needed. Current limitations stem from the fact that at least one of the following conditions need to be fulfilled: (1) tsunami deposits need to be preserved in the sedimentary record and to be distinguished from other type of deposits (such as storms, floods etc.) and/or (2) the traces of the paleotsunami cause needs to be preserved in the geological record so that it can be used for tsunami modelling. Unfortunately, palaeotsunami deposits and even evidence for their generating mechanisms are becoming harder to find on increasingly populated lake shores making it difficult to reconstruct the nature of past events.

To date, hazard assessments around lakes and rivers have only been conducted for the earthquake mass movement-generated tsunami hazard around Lake Zurich, Switzerland (Strupler et al., 2018) and mass movement-triggered tsunami hazard in Lake Tekopa (Mountjoy et al., 2019). Since there are many other lake and river shorelines where residential populations continue to grow, there is an urgent need for tsunami hazard assessements in order to foster awareness and understand the potential risks. In the case of the Lake Zurich study, the subaqueous landslide progression, wave propagation and inundation were calculated with a combination of open source codes including a probabilistic approach. This type of study allows first-order estimations of wave heights to be calculated and tsunami-prone areas to be identified (Strupler et al., 2018). Current work includes a workflow for a rapid screening for tsunami hazard potential on the basis of previous case studies that will be extrapolated using key characteristics (Strupler et al., 2020). These codes and concepts can be readily applied towards other exposed coasts and should be included in future state-of-the-art tsunami hazard assessments.

6.5 Conclusions

Paleotsunamis have been recorded in several lakes around the world. These paleotsunamis have been generated by fault displacements, mass movements (subaerial and subaqueous) and volcanic eruptions. Data from historical tsunamis in freshwater systems have shown that events caused by meteorological disturbances are missing from paleotsunami research. However, most freshwater paleotsunamis appear to be related to subaerial and subaqueous mass-movements, an observation that is supported by historical data.

This review provides first compiled datasets of historical and prehistorical freshwater tsunamis and that, although freshwater tsunamis are rare, they represent a natural hazard that should not be underestimated and that needs to be assessed. Data on the causes, frequencies and extent of freshwater tsunamis are needed in order to assess the tsunami hazard. Given the relative rarity of such events it is therefore crucial that further research is carried out on paleotsunamis in freshwater systems in order to provide a reasonable temporal coverage.

Acknowledgments

This work was supported by the Swiss National Science Foundation (grant numbers: 171017). We thank Elena Tolkova for her help during an earlier version of this manuscript. Reviewer David Tappin, an anonymous reviewer and the guest editor, Kazuhisa Goto, are thanked for their time spent on a previous version of this manuscript and their thoughtful and valuable comments.

References

Adams, J. (1981) Earthquake-dammed lakes in New Zealand. Geology 9 (5):215-219.

Barros, G. (1961) El maremoto del 22 de Mayo de 1960 en las costas de Chile. Publicacion 3012, Departamento de Navegacion e hidrografia de la Armada, Republica de Chile, Santiago, 129 pp.

Bechle, A. J., Wu, C. H., Kristovich, D. A. R, Anderson, E. J., Schwab, D. J. & Rabinovich, A. B. (2016) Meteotsunamis in the Laurentian Great Lakes. Scientific Reports 6, 8.

Begét, J. E. (2000) Volcanic Tsunamis. In: Sigurdsson, H., Houghton. B., Mc Nutt, S. R., Ryme, H., Stix, J. (eds) Encyclopedia of volcanoes. Academic Press, New York. pp 1005–1013.

Beguería, S., Van Asch, T. W., Malet, J. & Gröndahl, S. (2009) A GIS-based numerical model for simulating the kinematics of mud and debris flows over complex terrain. Natural Hazards and Earth System Sciences, 9, 1897-1909.

Beigt, D., Villarosa, G., Gómez, E. A. & Manzoni, C. (2016) Subaqueous landslides at the distal basin of Lago Nahuel Huapi (Argentina): Towards a tsunami hazard evaluation in Northern Patagonian lakes. Geomorphology 268:197-206.

Belousov, A. & Belousova, M. (2001) Eruptive Process, Effects and Deposits of the 1996 and the Ancient Basaltic Phreatomagmatic Eruptions in Karymskoye Lake, Kamchatka, Russia. In: Volcaniclastic Sedimentation in Lacustrine Settings. pp 35-60.

Belousov, A., Voight, B., Belousova, M. & Muravyev, Y. (2000) Tsunamis generated by subaquatic volcanic explosions: Unique data from 1996 eruption in Karymskoye Lake, Kamchatka, Russia. Pure and Applied Geophysics 157 (6-8):1135-1143.

Berger, M. J., George, D. L., LeVeque, R. J. & Mandli, K. T. (2011) The GeoClaw software for depth-averaged flows with adaptive refinement. Advances in Water Resources 34:1195-1206.

Bernard, E. N. (2009) Tsunamis. Vol. 15. Cambridge, Mass: Harvard UP, Print. The Sea.

Blass, A., Anselmetti, F. S., Grosjean, M. & Sturm, M. (2005) The last 1300 years of environmental history recorded in the sediments of Lake Sils (Engadine, Switzerland). Eclogae Geologicae Helvetiae 98:319-332.

Bondevik, S., Mangerud, J., Dawson, S., Dawson, A. & Lohne, Ø. (2003) Record-breaking height for 8000-year-old tsunami in the North Atlantic. Eos, Transactions American Geophysical Union 84 (31):289-293.

Bozzano, F., Mazzanti, P., Anzidei, M., Esposito, C., Floris, M., Fasani, G. B. & Esposito, A. (2009) Slope dynamics of Lake Albano (Rome, Italy): insights from high resolution bathymetry. Earth Surface Processes and Landforms, 34(11), 1469-1486.

Bünti, J. L. (1973) Chronik des Johann Laurentz Bünti, Landammann, 1661–1736. Beiträge zur Geschichte Nidwaldens, 34, 26–27.

Bussmann, F. & Anselmetti, F. S. (2010) Rossberg landslide history and flood chronology as recorded in Lake Lauerz sediments (Central Switzerland). Swiss J Geosci 103:43-59

Chagué-Goff, C., Schneider, J. L., Goff, J. R., Dominey-Howes, D. & Strotz L. (2011) Expanding the proxy toolkit to help identify past events — Lessons from the 2004 Indian Ocean Tsunami and the 2009 South Pacific Tsunami. Earth-Science Reviews 107, 107-122.

Chapron, E., Ariztegui, D., Mulsow, S., Villarosa, G., Pino, M., Outes, V., Juvignié, E. & Crivelli, E. (2006) Impact of the 1960 major subduction earthquake in Northern Patagonia (Chile, Argentina). Quaternary International 158, 58-71.

Chigira, M., Tsou, C. Y., Matsushi, Y., Hiraishi, N. & Matsuzawa, M. (2013) Topographic precursors and geological structures of deep-seated catastrophic landslides caused by Typhoon Talas. Geomorphology, 201, 479-493.

Clague, J. J. & Evans, S. G. (2000) A review of catastrophic drainage of moraine-dammed lakes in British Columbia. Quaternary Science Reviews 19, 1763-1783.

Clague, J. J., Munro, A. & Murty, T. (2003) Tsunami hazard and risk in Canada. Natural Hazards 28 (2-3):433-461.

Clark, K. J., Upton, P., Carey, J., Rosser, B. & Strong, D. (2015) Tsunami and Seiche Hazard Scoping Study for Lakes Tekapo, Pukaki, Ohau, Alexandrina and Ruataniwha, GNS Science Consultancy Report 2014/227. 82 pp.

Corboud, P. (2012) L'archéologie lémanique un siècle après F.A. FOREL, quelques questions encore à résoudre... Archive des Sciences 65:237-248.

Cysat, R. (1969) Collectanea Chronica und denkwürdige Sachen pro Chronica Lucernensi et Helvetiae. Erster Band, zweiter Teil (Eds J. Schmid and D. Schilling), pp. 879–888. Diebold Schilling Verlag, Luzern.

Davison, C. (1934) The Hawke's Bay earthquake of February 3, 1931. Nature 133: 841–842.

Darbyshire, J. & Ishiguro, S. (1957) Tsunamis. Nature 180, 150–151.

De Lange, W. & Moon, V. (2016) Volcanic generation of tsunamis: two New Zealand palaeo-events. In: Submarine Mass Movements and their Consequences. Springer, Cham, S. 559-56.

Didenkulova, I.I. & Pelinovsky, E. N. (2006) Phenomena similar to tsunami in Russian internal basins. Russian Journal of Earth Sciences 8 (6).

Dirksen, O., van den Bogaard, C., Danhara, T. & Diekmann, B. (2011) Tephrochronological investigation at Dvuh-yurtochnoe lake area, Kamchatka: Numerous landslides and lake tsunami, and their environmental impacts. Quaternary International 246 (1):298-311.

Donaldson, G., Goff, J., Chagué, C., Gadd, P. & Fierro, D. (2019) The Waikari River tsunami: New Zealand's largest historical tsunami event. Sedimentary Geology 383:148-158.

Einsele, G., Chough, S. K. & Shiki, T. (1996) Depositional events and their records—an introduction. Sedimentary Geology 104 (1):1-9.

Evers, F. (2017) Spatial propagation of landslide generated impulse waves. Doctoral dissertation No. 24650 and VAW-Mitteilung 244, edited by R. Boes. Zürich, Switzerland: ETH Zurich.

Falvard, S., Paris, R., Belousova, M., Belousov, A., Giachetti, T. & Cuven, S. (2018) Scenario of the 1996 volcanic tsunamis in Karymskoye Lake, Kamchatka, inferred from X-ray tomography of heavy minerals in tsunami deposits. Marine Geology 396:160-170.

Freundt, A., Kutterolf, S., Wehrmann, H., Schmincke, H. U. & Strauch, W. (2006) Eruption of the dacite to andesite zoned Mateare Tephra, and associated tsunamis in Lake Managua, Nicaragua. J Volcanol Geotherm Res 149 (1-2):103-123.

Freundt, A., Strauch, W., Kutterolf, S. & Schmincke, H. U. (2007) Volcanogenic tsunamis in lakes: Examples from Nicaragua and general implications. Pure and Applied Geophysics 164 (2-3):527-545.

Fritsche, S., Fäh D. & Schwarz-Zanetti, G. (2012) Historical intensity VIII earthquakes along the Rhone valley (Valais, Switzerland): primary and secondary effects. Swiss J Geosci 105 (1):1-18.

Fritz, H. M., Mohammed, F. & Yoo, J. (2009) Lituya Bay Landslide Impact Generated Mega-Tsunami 50(th) Anniversary. Pure and Applied Geophysics 166 (1-2):153-175.

Fuchs, H., Evers, F. M. & Boes, R. (2016) Impulse waves in reservoirs: recent research at VAW. Proc. HYDRO 2016, Int. Conf. Hydropower & Dams, Montreux, Switzerland.

Garduno-Monroy, V. H., Soria-Caballero, D. C., Israde-Alcantara, I., Hernandez Madrigal, V. M., Rodriguez-Ramirez, A., Ostroumov, M., Rodriguez-Pascua, M. A., Chacon-Torres, A. & Mora-Chaparro, J. C. (2011) Evidence of tsunami events in the Paleolimnological record of Lake Patzcuaro, Michoacan, Mexico. Geofisica Internacional 50 (2):147-161.

Girardclos, S., Schmidt, O. T., Sturm, M., Ariztegui, D., Pugin, A. & Anselmetti, F. S. (2007) The 1996 AD delta collapse and large turbidite in Lake Brienz. Marine Geology 241 (1-4):137-154.

Gisler, M., Fäh, D. & Masciardri, V. (2007) "Terrae motous factus Est": earthquakes in Switzerland before A.D. 1000. A critical approach. Natural Hazards 43:63–79.
Goff, J., Ebina, Y., Goto, K. & Terry, J. (2016) Defining tsunamis: Yoda strikes back?. Earth-Science Reviews, 159: 271-274.
Goto, K., Ikehara, K., Goff, J., Chagué-Goff, C. & Jaffe, B. (2014) The 2011 Tohoku-oki tsunami — Three years on. Marine Geology 358: 2-11.
Grilli, S. T., Tappin, D. R., Carey, S., Watt, S. F. L., Ward, S. N., Grilli, A. R., Engwell, S. L., Zhang, C., Kirby, J. T., Schmbach, L. & Muin, M. (2019) Modelling of the tsunami from the December 22, 2018 lateral collapse of Anak Krakatau volcano in the Sunda Straits, Indonesia. Scientific Report 9, 11946.
Grimstad, E. & Nesdal, S. (1991) Publikasjon-Norges Geotekniske Institutt. Publikasjon-Norges Geotekniske Institutt 183:1-6.
Gylfadóttir, S. S., Kim, J., Helgason, J. K., Brynjólfsson, S., Höskuldsson, Á., Jóhannesson, T., Harbitz, C. B. & Løvholt, F. (2017) The 2014 Lake Askja rockslide-induced tsunami: Optimization of numerical tsunami model using observed data. Journal of Geophysical Research: Oceans 122 (5):4110-4122.
Heim, A. (1919) Geologie der Schweiz. Tauchnitz, Leipzig.
Hilbe, M. & Anselmetti, F. S. (2015) Mass Movement-Induced Tsunami Hazard on Perialpine Lake Lucerne (Switzerland): Scenarios and Numerical Experiments. Pure and Applied Geophysics 172 (2):545-568.
Hogg, A. G., Higham, T. F. G., Lowe, D. J., Palmer, J. G., Reimer, P. J. & Newnham, R. M. (2003) Wiggle-match date for Polynesian settlement of New Zealand. Antiquity, 77: 116-125.
Hu, Y. X., Yu, Z. Y. & Zhou, J. W. (2020) Numerical simulation of landslide-generated waves during the 11 October 2018 Baige landslide at the Jinsha River. Landslides.
Huber, A. (1982) Felsbewegungen und Uferabbrüche an Schweizer Seen, ihre Ursachen und Auswirkungen, Eclogae geologicae Helvetiae, 75, 563–578.
Hungr, O., Evans, S. G., Bovis, M. J. & Hutchinson, J. N. (2001) A review of the classification of landslides of the flow type. Environmental and Engineering Geoscience 7 (3):221-238.
Hutchinson, I., Clague, J. J. & Mathewes, R. W. (1997) Reconstructing the Tsunami Record on an Emerging Coast: A Case Study of Kanim Lake, Vancouver Island, British Columbia, Canada. Journal of Coastal Research 13: 545-553.
Kempf, P., Moernaut, J., Van Daele, M., Vandoorne, W., Pino, M., Urrutia, R. & De Batist, M. (2017) Coastal lake sediments reveal 5500 years of tsunami history in south central Chile. Quaternary Science Reviews 161:99-116.
Klyuchevskii, A. V., Demyanovich, V. M. & Klyuchevskaya, A. A. (2012) The possibility of a tsunami on Lake Baikal. Doklady Earth Sciences 442 (1):130-134.
Kremer, K., Hilbe, M., Simpson, G., Decrouy, L., Wildi, W. & Girardclos, S. (2015) Reconstructing 4000 years of mass movement and tsunami history in a deep peri-Alpine lake (Lake Geneva, France-Switzerland). Sedimentology 62 (5):1305-1327.
Kremer, K., Marillier, F., Hilbe, M., Simpson, G., Dupuy, D., Yrro, B. J. F., Rachoud-Schneider, A.-M., Corboud, P., Bellwald, B., Wildi, W. & Girardclos, S. (2014) Lake dwellers occupation gap in Lake Geneva (France–Switzerland) possibly explained by an earthquake–mass movement–tsunami event during Early Bronze Age. Earth and Planetary Science Letters 385:28-39.
Kremer, K., Simpson, G. & Girardclos, S. (2012) Giant Lake Geneva tsunami in AD 563. Nature Geoscience 5 (11):756-757.
Leithold EL, Wegmann KW, Bohnenstiehl DR, Joyner CN, Pollen AF (2019) Repeated megaturbidite deposition in Lake Crescent, Washington, USA, triggered by Holocene ruptures of the Lake Creek-Boundary Creek fault system. GSA Bulletin 131, 2039-2055.
L'Heureux, J.-S., Eilertsen, R. S., Glimsdal, S., Issler, D., Solberg, I.-L. & Harbitz, C. B. (2012) The 1978 Quick Clay Landslide at Rissa, Mid Norway: Subaqueous Morphology and Tsunami Simulations. In: Submarine Mass Movements and Their Consequences. Springer Netherlands, pp. 507-516.
Linares, Á., Bechle, A. J. & Wu, C. H. (2016) Characterization and assessment of the meteotsunami hazard in northern Lake Michigan. Journal of Geophysical Research Oceans 121, 7141– 7158.
Lunina, O. V., Andreev, A. V. & Gladkov, A. S. (2012) The Tsagan earthquake of 1862 on Lake Baikal revisited: a study of secondary coseismic soft-sediment deformation. Russian Geology and Geophysics 53 (6):594-610.
Magill, C. R. (2001) Numerical modelling of tsunami generated by mass movement. MSc thesis, University of Waikato. 198 pp.
Maso, S. J. & Saderra, M. (1904) Volcanoes and seismic centers of the Philippines Archipelago. Department of Commerce and Labor, Bureau of the Census of the Philippine Islands, 80 pp.
Maso, S. J. & Saderra, M. (1911) The eruption of Taal volcano, January 30, 1911, Philippines Islands. Department of the Interior, Weather Bureau, Manila.

Mazzanti, P. & Bozzano, F. (2009) An equivalent fluid/equivalent medium approach for the numerical simulation of coastal landslides propagation: theory and case studies. Natural Hazards and Earth System Sciences, 9(6), 1941.

Miller, D. J. (1960) Giant waves in Lituya Bay, Alaska. Geological Survey Professional Paper 354-C. U.S.Government Printing Office, Washington D.C.

Moore, J. G., Nakamura, K. & Alcaraz, A. (1966) The 1965 eruption of Taal volcano. Science 151:955–960.

Moore, J. G., Schweickert, R. A., Robinson, J. E., Lahren, M. M. & Kitts, C. A. (2006) Tsunami-generated boulder ridges in Lake Tahoe, California-Nevada. Geology 34 (11):965-968.

Moore, J. G., Schweickert, R. A. & Kitts, C. A. (2014) Tsunami-generated sediment wave channels at Lake Tahoe, California-Nevada, USA. Geosphere 10 (4):757-768.

Mountjoy, J. J., Wang, X., Woelz, S., Fitzsimons, S., Howarth, J. D., Orpin, A. R. & Power, W. (2019) Tsunami hazard from lacustrine mass wasting in Lake Tekapo, New Zealand. Geological Society, London, Special Publications 477, 413.

Nagata, M., Skano, K., Ueda, Y., & Yasu, H. (2014) Applications by Nara prefecture for utilizing lessons learned from the great floods on Kii peninsula. Interpraevent 2014, Nara, Japan, 404-411.

Nigg, V., Wohlwend, S., Hilbe, M., Bellwald, B., Fabbri, S. C., de Souza, G. F., ... & Anselmetti, F. S. (2021). A tsunamigenic delta collapse and its associated tsunami deposits in and around Lake Sils, Switzerland. Natural Hazards, 1-35.

Nishimura, Y. (2008) Volcanism-induced tsunamis and tsunamiites. Tsunamiites: Features and Implications.

Nomitsu, T. (1935) A theory of tsunamis and seiches produced by wind and barometric gradient. Mem Coll Sci Imp Univ Kyoto A 18(4):201–214.

Paris, R., Switzer, A. D., Belousova, M., Belousov, A., Ontowirjo, B., Whelley, P. L. & Ulvrova, M. (2014) Volcanic tsunami: a review of source mechanisms, past events and hazards in Southeast Asia (Indonesia, Philippines, Papua New Guinea). Natural Hazards 70 (1):447-470.

Parsons, T. (2002) Enciclopedia historica centenaria de Bariloche, 3/5/1902–3/5/2002. Tomo 1, 150.

Plafker, G. & Eyzaguirre, V. R. (1979) Chapter 7 - Rock Avalanche and Wave at Chungar, Peru. In: Voight B (ed) Developments in Geotechnical Engineering, vol 14. Elsevier, pp 269-279.

Roberts, N. J., McKillop, R. J., Lawrence, M. S., Psutka, J. F., Clague, J. J., Brideau, M.-A. & Ward, B. C. (2013) Impacts of the 2007 Landslide-Generated Tsunami in Chehalis Lake, Canada. In: Margottini, C., Canuti, P. & Sassa, K. (eds) Landslide Science and Practice: Volume 6: Risk Assessment, Management and Mitigation. Springer Berlin Heidelberg, Berlin, Heidelberg, pp 133-140.

Saderra Maso, M. (1904) Report on the volcanoes and seismic centers of the Philippines Archipelago. Department of Commerce and Labor, Bureau of the Census of the Philippine Islands, 80 pp.

Schnellmann, M., Anselmetti, F. S., Giardini, D., McKenzie, J. A. & Ward, S. N. (2002) Prehistoric earthquake history revealed by lacustrine slump deposits. Geology 30 (12):1131-1134.

Schoeneich, P., Weidmann, M. & Blomjous, C. (2015) L'énigme du Tauredunum enfin résolue? In: Archives de l'Etat du Valais S (ed) Le Rhône, entre nature et société, vol 29. Cahiers de Vallesia, p 344.

Siegenthaler, C., Finger, W., Kelts, K. & Wang, S. (1987) Earthquake and seiche deposits in Lake Lucerne, Switzerland. Eclogae Geologicae Helvetiae 80:241-260.

Simpson, G. & Castelltort, S (2006) Coupled model of surface water flow, sediment transport and morphological evolution. Computer Geoscience 32, 1600–1614.

Smith, W. D. (1978) Spatial distribution of felt intensities for New Zealand earthquakes. New Zealand Journal. NZ J Geol Geophys 21: 293–311.

Smoot, J. P., Litwin, R. J., Bischoff, J. L. & Lund, S. J. (2000) Sedimentary record of the 1872 earthquake and "Tsunami" at Owens Lake, southeast California, vol 135. vol 135.

Stirling, M., Wesnousky, S. & Berryman, K. (1998) Probabilistic seismic hazard analysis of New Zealand. New Zealand Journal of Geology and Geophysics - N Z J GEOL GEOPHYS 41:355-375.

Strasser, M., Monecke, K., Schnellmann, M. & Anselmetti, F. S. (2013) Lake sediments as natural seismographs: A compiled record of Late Quaternary earthquakes in Central Switzerland and its implication for Alpine deformation. Sedimentology 60, 319-341.

Strupler, M., Danciu, L., Hilbe, M., Kremer, K., Anselmetti, F. S., Strasser, M. & Wiemer, S. (2018) A subaqueous hazard map for earthquake-triggered landslides in Lake Zurich, Switzerland. Natural Hazards: Journal of the International Society for the Prevention and Mitigation of Natural Hazards 90 (1):51-78.

Strupler, M., Anselmetti, F. S., Hilbe, M., Kremer, K. & Wiemer, S. (2019) A workflow for the rapid assessment of the landslide-tsunami hazard in perialpine lakes. International Symposium on Submarine Mass Movements and Their Consequences.

Tait, S. U. (1977) Waikari Station 1840 to 1940. Hawke's Bay Regional Council (HBRC) Report No. AM15-16, HBRC plan No. 4751

Takagi. H., Pratama, M. B., Kurobe, S., Esteban, M., Aranguiz, R. & Ke, B. W. (2019) Analysis of generation and arrival time of landslide tsunami to Palu City due to the 2018 Sulawesi earthquake. Landslides 16 (5):983-991.

Torsvik, T., Paris, R., Didenkulova, I., Pelinovsky, E., Belousov, A. & Belousova, M. (2010) Numerical simulation of a tsunami event during the 1996 volcanic eruption in Karymskoye lake, Kamchatka, Russia. Natural Hazards and Earth System Sciences 10 (11):2359-2369.

Towson, J. M. & Kaya, Y. (1988) Simulations of the waves in Lake Botnen created by the Rissa Landslide. Proceedings of the Institution of Civil Engineers 85 (1):145-160.

Tsunami Glossary (2019) Intergovernmental Oceanographic Commission. Fourth Edition. Paris, UNESCO. IOC Technical Series, 85. (English, French, Spanish, Arabic, Chinese) (IOC/2008/TS/85 rev.4).

Upton, P. & Osterberg, E. C. (2007) Paleoseismicity and mass movements interpreted from seismic-reflection data, Lake Tekapo, South Canterbury, New Zealand. New Zealand Journal of Geology and Geophysics, 50(4), 343-356.

Voight, B., Janda, R., Glicken, H. X. & Douglass, P. M. (1983) Nature And Mechanics Of The Mount St. Helens Rockslide-Avalanche Of 18 May 1980. Geotechnique 33.

Wagner, T. P., McKee, C. O., Kuduon, J. & Kombua, R. (2003). Landslide-induced wave in a small volcanic lake: Kasu Tephra Cone, Papua New Guinea. International Journal of Earth Sciences (Geologische Rundschau) 92, 405-406.

Ward, S. N. (2001) Landslide tsunami: Journal of Geophysical Research, v. 106, p. 11, 201–11, 216.

Ward, S. N. & Day, S. (2002) Suboceanic Landslides. in 2002 Yearbook of Science and Technology, edited by McGraw-Hill (New-York),349-352.

Ward, S. N. (2013) Mega-tsunami: Lake Tahoe: Movie available at http:// www .youtube .com /watch ?v=bxbVEnnmRGQ.

Watt, S. F. L., Pyle, D. M., Naranjo, J.A. & Mather, T. A. (2009) Landslide and tsunami hazard at Yate volcano, Chile as an example of edifice destruction on strike-slip fault zones. Bulletin of Volcanology 71 (5):559.

Zay, K. (1807) Goldau und seine Gegend: wie sie war und was sie geworden. Orell, Füssli und Compagnie, Zürich, 390 pp.

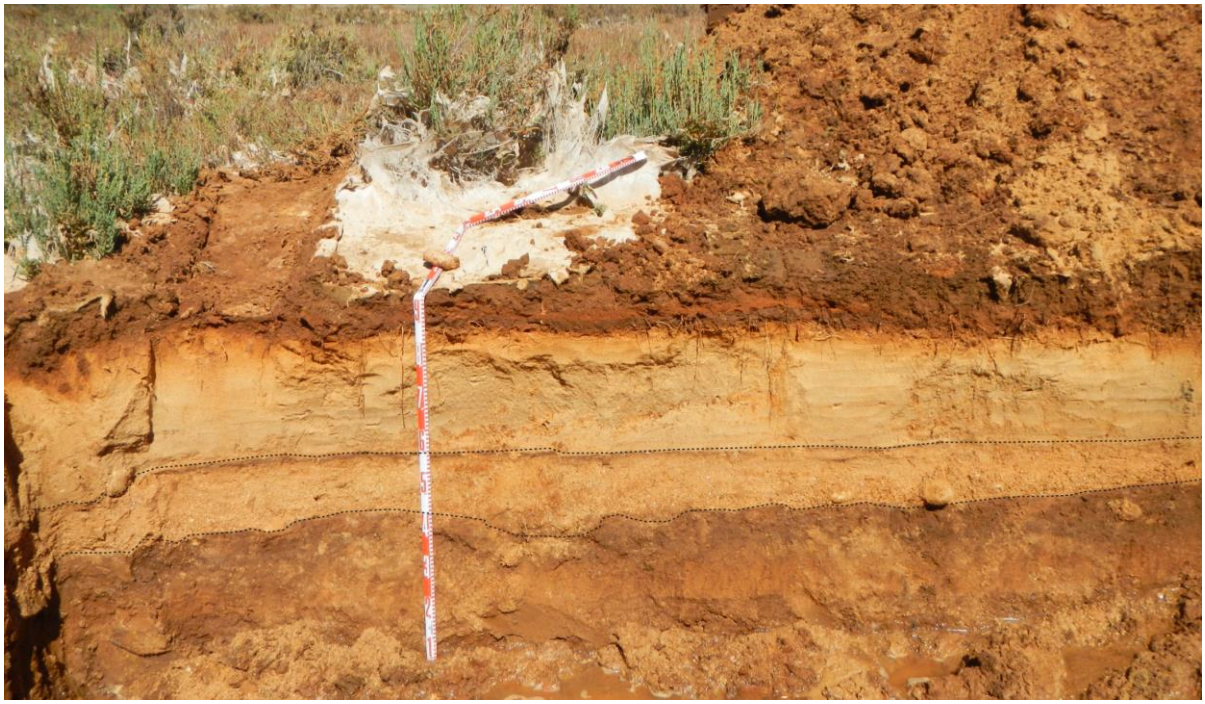

1755 CE Lisbon tsunami deposit investigated in a trench at Rossa Do Veiga (Sagres, Portugal) during the 5th International Tsunami Field Symposium 2017.

7 Conclusions and outlook

7.1 Conclusions

Lake tsunamis have been historically reported as the result of strong regional earthquake-triggered subaqueous mass movements (e.g., 1601 CE Lake Lucerne tsunami), impulse waves generated by subaerial rockfalls and landslides (e.g., 1964 CE Obermatt impulse wave), and apparently spontaneous (e.g., 1687 CE Muota collapse-generated tsunami) as well as externally triggered delta collapses (e.g., 563 CE Lake Geneva tsunami) in Switzerland. The described effects of coastal inundation are severe and would cause injuries, casualties, considerable shoreline damage as well as financial and reputational losses.

Historical documents that describe the coastal effects of these events provide a unique opportunity to characterize the associated hazard of lacustrine tsunamis. Though, the record is limited to the last ~1000 to 1500 years and probably lacks coverage of the entirety of events that took place, especially in remote areas. Moreover, from a geological perspective the historical record is limited to a very short period. However, the natural archive of extreme events preserved within the sedimentary record provides further information on the spatial and temporal occurrence of lake tsunamis.

Previous studies have provided insights into the cascading effects of subaqueous mass movement-generated tsunamis in the lacustrine environment, particularly from the sediment record of deep lake basins and modelling. However, little attention has been paid to the coastal on- and offshore archive of lakes in characterizing the lake-tsunami phenomenon although onshore deposits could potentially confirm the modelling results of past tsunamis and giving hints to their extent and dynamics. The objective of this dissertation is to find and characterize sedimentologically the deposits of the historically mentioned tsunamis. In this thesis, we propose a workflow to study lacustrine tsunami deposits, and we highlight two case studies where this approach has been successfully applied.

The localization of a suitable geological archive is a crucial but enormously challenging task. This is especially true for heavily populated lakeshore areas with developed infrastructure, representative man-made lake promenades, and steep shorelines common to Swiss lakes. Pristine shallow coastal plains and beaches have become rare due to industrialization and the associated growth of civilization. Therefore, the locations where field surveys can be conducted are limited. Moreover, coastal records have become even more fragmentary than they naturally are due to transient depositional conditions. Therefore, the observed limitations and challenges were summarized in Chapter 3 to provide methodological guidelines and considerations for future studies. In a nutshell, historical documents were used to characterize the coastal effects of lake tsunamis generated from subaqueous and subaerial mass movements. Information on the coastal geomorphology (high-resolution topography and bathymetry maps, geological maps and geomorphological field mapping), its temporal evolution (historical maps and borehole logging data), and numerical tsunami propagation and inundation simulations were used to identify locations with a high probability of tsunami inundation, deposition, and preservation for field research. Positive and negative evidence for tsunami depositional signatures observed from multiple field studies were finally presented briefly.

Chapter 4 focuses on the hypothesis of a tsunamigenic prehistoric delta collapse in Lake Sils around 700 CE. Detailed sedimentological analysis on sediment cores recovered from an transect spanning the coastal on- and offshore environment were combined with mineralogical characterization of the lake tributaries and numerical mass-movement and tsunami simulations to reconstruct the lacustrine tsunami event. The results obtained support that the Isola Delta collapse generated a basin-wide tsunami with a numerically simulated inundation distance of 200 m on the adjacent coastal plains, which is supported by a clastic event deposit observed in sediment cores. The up to 20 cm thick deposit observed in sediment cores from the shallow water consists of a fining upward sequence with a sharp basal contact and thins landward. Toward the deeper water (in 20 to 40 m water depth) the well-traceable sedimentary unit transforms into a heterogeneous sediment package that consists of massive gravel as well as single and multiple normal graded sand with mud clasts of laminated pre-event lake deposits that likely originated from pulse-like tsunami backwash currents transporting large amounts of sediment from the on- to the offshore environment. The top of the event deposit is characterized by a ~2 cm thick clay cap that was deposited at the final stage from suspension, indicating large amounts of sediment that were brought into suspension during the event. Radiocarbon dating of an organic-rich unit underlying the event deposit to 225-419 cal CE supports the hypothesis

that the Isola Delta collapse with a minimum estimated depositional volume of 6.5 x 10^6 m^3 (Blass et al., 2005) was tsunamigenic.

Another tsunami-related event deposit was observed in sediment cores recovered along a transect from an offshore depression in the Lucerne Bay, Lake Lucerne, and is discussed in detail in Chapter 5. The up to 60 cm thick, predominantly siliciclastic, normal graded event deposit has a characteristic sharp lower basal contact with coarse carbonate shell fragments at the base, fines upwards from sand to silt and contains terrestrial-derived horizontally bedded wooden particles that become more abundant in the upper part of the deposit. Based on radiocarbon dating of four terrestrial organic macro-remains (leave fragments and conifer needles) from the deposit that yield ages of 1306–1442 cal CE and the sedimentological signatures, the normal graded event deposit was related to the historically reported basin-wide 1601 CE Lake Lucerne tsunami ultimately caused by several subaqueous and a subaerial mass movement (Hilbe and Anselmetti, 2015; Schnellmann et al., 2002; Siegenthaler et a., 1987) triggered by a regional Mw 5.9 earthquake (Fäh et al., 2011). The observed radiocarbon ages provide evidence for sediment remobilization from the on- and offshore Lucerne Bay area, which was further tested using the hydrodynamic simulation software BASEMENT. The Lake Lucerne tsunami was numerically simulated by an instantaneous collapse of 5 m along the area of the second largest mass movement triggered by the 1601 CE earthquake (Hilbe and Anselmetti, 2015). However, the simplification of the numerically simulated tsunami was considered to be a realistic representation the 1601 CE Lake Lucerne tsunami because the simulated wave parameters (e.g., free surface elevation) are comparable to the historically documented values by the Lucerne city clerk Renward Cysat (Cysat, 1969), and with the numerical simulations previously performed by Hilbe and Anselmetti (2015). Based on the wave inundation and bed shear-stresses observed within the Lucerne Bay it was possible to demonstrate that large areas exceed critical values to initiate particle movement and that flow direction and velocity provides evidence that effective sediment transport in the Bay of Lucerne likely was possible during the 1601 CE Lake Lucerne tsunami event.

The literature review on freshwater tsunami discussed in Chapter 6 focuses on case studies of prehistoric events published after the devastating 2011 CE Tohoku-oki tsunami. Briefly, the triggering mechanism of tsunamis in freshwater environments are summarized as those by fault-displacement, subaerial and subaqueous mass movements, volcanic eruptions, and air-pressure disturbances. Because the number of tsunami studies reporting prehistoric events in

the freshwater setting is small, historical events are also presented in this review. This emphasizes the importance of further research to achieve adequate temporal and spatial coverage of freshwater tsunamis in general and to better assess the natural hazards caused by tsunamis, to develop resilient and mitigating solutions.

Returning to the research questions formulated at the beginning of this dissertation, we were able to address some, discard others, and generate new questions for future studies. In particular, the sedimentological signatures of lacustrine deposits were discussed in detail in Chapter 4 and 5, and the observed similarities and differences were mentioned therein. However, it was not possible to establish a tsunami deposit-based event chronology over the past 15'000 years in the on- and offshore. It was also not possible to reconstruct field-derived run-up and inundation estimates. More research is needed to resolve these tasks.

7.2 Outlook

The reconnaissance of lake tsunami deposits is found to be challenging for several reason, including more technical or administrative aspects (e.g., core recovery, highly modified shorelines, and private shore properties), but also because of the geomorphological conditions that must be satisfied for sedimentation and preservation of tsunami deposits over time.

For future studies, I propose to further intensify research on tsunami waves generated from subaerial mass movements in Swiss lakes, as these events are likely to occur more frequently and can be mitigated if their sources can be identified and monitored. On the other hand, the generation mechanisms of tsunami waves from subaqueous mass movements needs to be further investigated through the spatial analysis of mass-movement deposits (using seismic-reflection data and high-resolution bathymetry) to better characterize their failure kinematics. A good opportunity to achieve this is provided by a large dataset of high -resolution bathymetry, and seismic data obtained after the 2018 CE Palu earthquake and tsunami in Indonesia. Incorporation of more adequate subaqueous mass-movements into the numerical simulation will then increase the robustness of the associated numerical solutions.

For the reconnaissance of lakeshore tsunami deposits, it is strongly recommended to collaborate with archeological surveys. In particular, the excavation of pile dwelling with trenches on the lakeshore could provide essential information about past events. In addition,

the 3D view of trenches allows investigation of the lateral continuity of the associated deposits, which may also be discontinuous and patchy, which is difficult to assess with sediment coring. Further, the shallow-water environment could be studied more comprehensively with a bunch of gravity cores to study erosional signatures from past tsunami events via high-resolution dating.

Finally, including sediment transport in numerical simulations will further increase knowledge of lake tsunami-induced sediment remobilization. This may help for the identification of suitable depositional environments for future sedimentological studies. The hydro- and morphodynamical freeware BASEMENT, will include this capability in its next versions (BASEMNET v3.2 onwards).

References

Blass, A., Anselmetti, F. S., Grosjean, M., & Sturm, M. (2005) The last 1300 years of environmental history recorded in the sediments of Lake Sils (Engadine, Switzerland). Eclogae Geologicae Helvetiae, 98(3), 319-332.

Cysat, R. (1969) Collectanea Chronica und denkwürdige Sachen pro Chronica Lucernensi et Helvetiae. Erster Band, zweiter Teil (Eds J. Schmid and D. Schilling), pp. 879– 888. Diebold Schilling Verlag, Luzern.

Fäh, D., Giardini, D., Kästli, P., Deichmann, N., Gisler, M., Schwarz-Zanetti, G., ... & Eberhard, D. (2011) ECOS-09 earthquake catalogue of Switzerland release 2011 report and database. Public catalogue, 17. 4. 2011. Swiss Seismological Service ETH Zurich. *RISK*.

Hilbe, M., & Anselmetti, F. S. (2015) Mass movement-induced tsunami hazard on perialpine Lake Lucerne (Switzerland): scenarios and numerical experiments. Pure and Applied Geophysics, 172(2), 545-568.

Schnellmann, M., Anselmetti, F. S., Giardini, D., McKenzie, J. A., & Ward, S. N. (2002) Prehistoric earthquake history revealed by lacustrine slump deposits. Geology, 30(12), 1131-1134.

Siegenthaler, C., Finger, W., Kelts, K., & Wang, S. (1987) Earthquake and seiche deposits in Lake Lucerne, Switzerland. Eclogae Geologicae Helvetiae, 80(1), 241-260.

Appendix A

Supplementary material to Chapter 3

Sedimentological signatures of historic tsunamis in Swiss lakes

Valentin Nigg[1], Katrina Kremer[1, 2], Stéphanie Girardclos[3], Flavio S. Anselmetti[1]

[1] Institute of Geological Sciences and Oeschger Centre for Climate Change Research, University of Bern, Baltzerstrasse 1+3, 3012 Bern, Switzerland

[2] Swiss Seismological Service, ETH Zurich, Sonneggstrasse 5, 8092 Zürich, Switzerland

[3] Department of Earth Sciences and Institute of Environmental Science, University of Geneva, Rue des Maraîchers 13, 1205 Geneva, Switzerland [4]

Table A1: Sediment core ID, applied coring system, and locations given in the Swiss coordinate system LV95

Lake	Location	Core ID	Coring system	Total depth (m)	Swiss Coordinates (LV95) East (m)	North (m)
Lucerne	Ennetbürgen	EB17-1	Pürckhauer	2.00	2674351	1204230
		EB17-2	Pürckhauer	2.00	2674333	1204229
		EB17-3	Pürckhauer	2.00	2674310	1204221
		EB17-3	Pürckhauer	2.00	2674355	1204272
	Chappelmatt	CP18-1A	Geoprobe 6620DT	7.20	2673831	1213105
		CP18-1B	Geoprobe 6620DT	7.80	2673832	1213110
		CP18-2A	Geoprobe 6620DT	6.00	2673837	1213125
		CP18-2B	Geoprobe 6620DT	7.20	2673838	1213130
		CP18-3A	Geoprobe 6620DT	4.80	2673848	1213149
		CP18-3B	Geoprobe 6620DT	5.40	2673849	1213155
		CP18-4A	Geoprobe 6620DT	3.60	2673892	1213173
		CP18-4B	Geoprobe 6620DT	4.20	2673889	1213174
	Tanzenberg	HT18-1A	Geoprobe 6620DT	8.40	2673184	1209044
		HT18-1B	Geoprobe 6620DT	1.20	2673186	1209042
		HT18-1C	Geoprobe 6620DT	6.60	2673187	1209042
		HT18-2A	Geoprobe 6620DT	7.20	2673209	1209055

Lake	Location	Core ID	Coring system	Total depth (m)	Swiss Coordinates (LV95) East (m)	North (m)
Lake		HT18-3A	Geoprobe 6620DT	8.40	2673258	1209114
Lucerne		HT18-4A	Geoprobe 6620DT	3.60	2673266	1209129
	Tribschen	STO18_1A	Geoprobe 6620DT	4.80	2667610	1210282
		STO18_1B	Geoprobe 6620DT	5.60	2667610	1210285
		STO18_2A	Geoprobe 6620DT	4.80	2667628	1210283
		STO18_2B	Geoprobe 6620DT	4.20	2667629	1210279
		STO18_3A	Geoprobe 6620DT	4.80	2667674	1210296
		STO18_3B	Geoprobe 6620DT	5.40	2667677	1210297
		STO18_4A	Geoprobe 6620DT	4.80	2667704	1210293
		STO18_4B	Geoprobe 6620DT	4.20	2667705	1210291
	Lucerne Bay	LU18-1	UWITECT piston	3.40	2666807	1211720
		LU18-2	UWITECT piston	3.20	2666662	1211710
		LU18-3	UWITECT piston	3.20	2666482	1211708
		LU18-4	UWITECT piston	7.20	2667619	1210858
Lake	Lausanne	LS18-1	Pürckhauer	2.00	2535107	1152582
Geneva	St. Sulpice	STS18-1	Pürckhauer	2.00	2532268	1151122
		STS18-2	Pürckhauer	2.00	2532272	1151105
		STS18-3	Pürckhauer	2.00	2532300	1151114
		STS18-8	Pürckhauer	2.00	2533217	1151847
		STS18-9	Pürckhauer	2.00	2533218	1151873
	Collonges-Bellerive	TCS18-1	Pürckhauer	2.00	2503854	1122263
		TCS18-2	Pürckhauer	2.00	2503861	1122256
		TCS18-3	Pürckhauer	2.00	2503864	1122258
		TCS18-4	Pürckhauer	2.00	2503867	1122247
		TCS18-5	Pürckhauer	2.00	2503874	1122246
		TCS18-6	Pürckhauer	2.00	2503884	1122257
		TCS18-7	Pürckhauer	2.00	2503886	1122396
	Sciez	SC18-1	Pürckhauer	2.00	2517798	1132569
		SC18-2	Pürckhauer	2.00	2517800	1132614
		SC18-3	Pürckhauer	2.00	2517803	1132647
		SC18-4	Pürckhauer	2.00	2517788	1132682
	Nernier	NE18-1	Pürckhauer	2.00	2513243	1135700
Lake Sils	Sils Baselgia	SIL06-8	Pürckhauer	0.85	2’777’946	1’145’042
		SIL09-1	Geoprobe 6620DT	5.15	2’777’997	1’145’056
		SIL09-2	Geoprobe 6620DT	3.40	2’777’979	1’145’050
		SIL09-3	Geoprobe 6620DT	3.62	2’777’960	1’145’045
		SIL09-4	Geoprobe 6620DT	3.94	2’777’944	1’145’035
		SIL09-5	Geoprobe 6620DT	3.70	2’777’926	1’145’026
		SIL09-6	Geoprobe 6620DT	4.30	2’777’943	1’145’076
		SIL09-7	Geoprobe 6620DT	2.27	2’777’929	1’145’069
		SIL09-8	Geoprobe 6620DT	4.22	2’777’920	1’145’064

Lake	Location	Core ID	Coring system	Total depth (m)	Swiss Coordinates (LV95) East (m)	Swiss Coordinates (LV95) North (m)
Lake Sils		SIL09-9	Geoprobe 6620DT	3.71	2’777’903	1’145’057
		SIL09-10	Geoprobe 6620DT	4.55	2’777’940	1’145’062
		SIL09-11	Geoprobe 6620DT	2.54	2’778’025	1’145’179
		SIL09-12	Geoprobe 6620DT	1.93	2’778’065	1’145’204
	Lagrev Basin	SIL10-1	Percussion core	0.90	2’777’820	1’144’985
		SIL10-2	Percussion core	1.82	2’777’768	1’144’941
		SIL10-3	Percussion core	1.56	2’777’717	1’144’902
		SIL10-4	Percussion core	1.93	2’777’656	1’144’860
		SIL10-5	Percussion core	1.81	2’777’599	1’144’837
		SIL10-6	Percussion core	1.71	2’777’505	1’144’790
		SIL10-7	Percussion core	0.56	2’777’739	1’144’918
		SIL18-1	Percussion core	0.50	2’777’819	1’144’993
		SIL18-2	Percussion core	0.88	2’777’808	1’145’006
		SIL18-3	Percussion core	0.80	2’777’784	1’145’021
		SIL18-4	Percussion core	1.05	2’777’821	1’144’908
		SIL18-5	Percussion core	1.00	2’777’840	1’144’908
	Sils Baselgia	SIL18-6	Percussion core	0.82	2’777’772	1’145’067
		SIL18-7	Percussion core	0.67	2’777’735	1’144’273
		SIL18-8	Percussion core	0.59	2’777’878	1’144’126
		SIL18-9	Percussion core	0.62	2’777’819	1’144’135
		SIL18-10	Percussion core	0.51	2’777’793	1’144’168

Appendix B

Supplementary material to Chapter 4

A tsunamigenic delta collapse and its associated deposits in and around Lake Sils, Switzerland

Valentin Nigg[1], Stephan Wohlwend[2], Michael Hilbe[1], Benjamin Bellwald[3], Stefano C. Fabbri[1], Gregory F. de Souza[4], Florian Donau[2], Reto Grischott[2], Michael Strasser[5], Flavio S. Anselmetti[1]

[1] Institute of Geological Sciences and Oeschger Centre for Climate Change Research, University of Bern, Baltzerstrasse 1+3, 3012 Bern, Switzerland

[2] Geological Institute, ETH Zurich, Sonneggstrasse 5, 8092 Zürich, Switzerland

[3] Volcanic Basin Petroleum Research (VBPR), Høienhald, Blindernveien 5, 0361 Oslo, Norway

[4] Institute of Geochemistry and Petrology, ETH Zurich, Clausiusstrasse 25, 8092 Zürich, Switzerland

[5] Department of Geology, University of Innsbruck, Innrain 52, 6020 Innsbruck, Austria

Onshore sediment cores

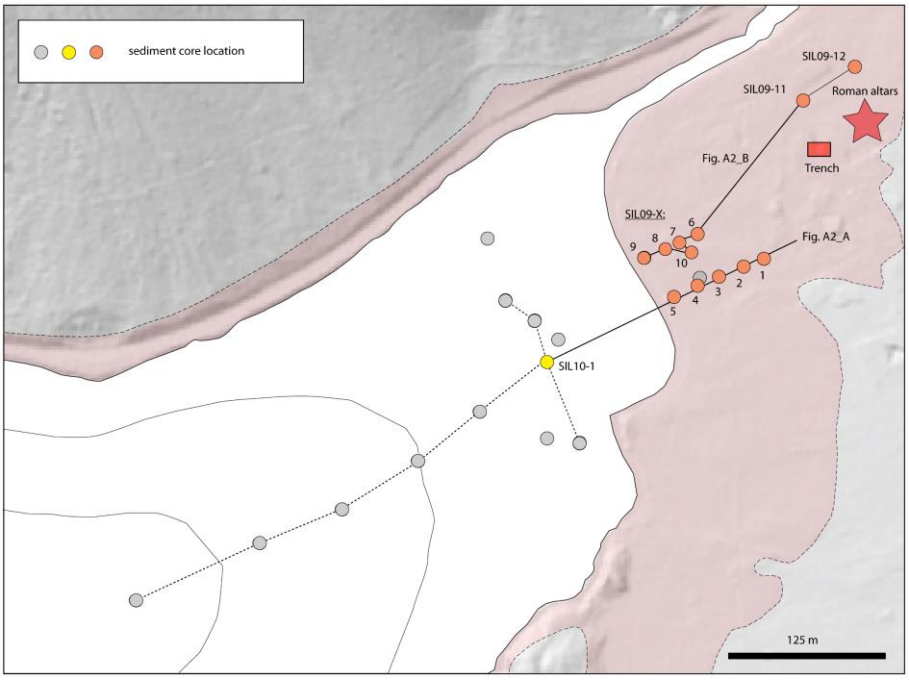

Fig. B1: Detail map of the coastal plain at show onshore sediment core location and core label.

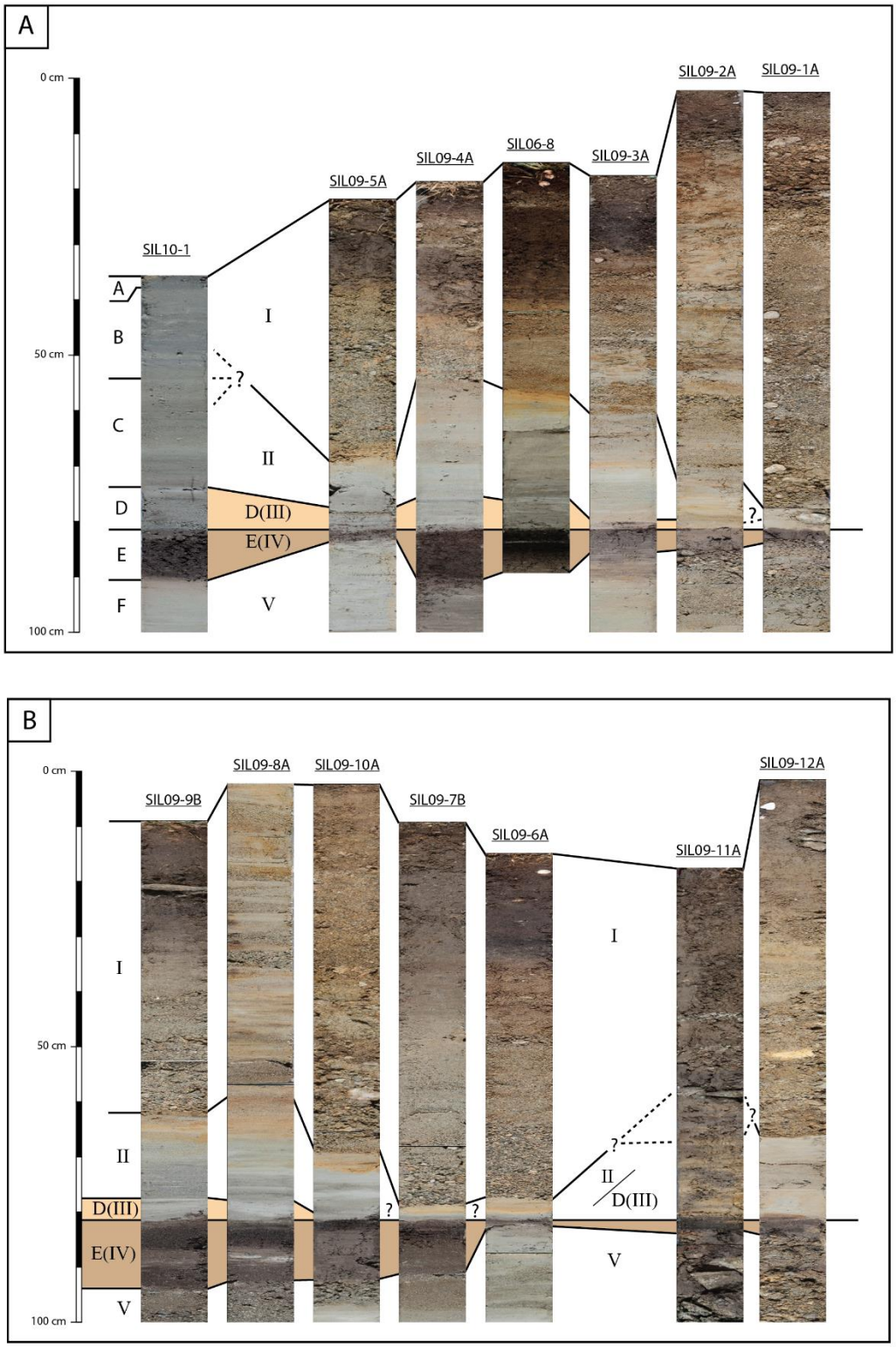

Fig. B2: Core line scan images and lithological interpretation of onshore sediments (see Fig. A1 for core location). Lithological units are labelled according to the descriptions in the manuscript.

Numerical tsunami modeling – total failed volume estimation

For the volume estimation of the Isola Delta collapse two different scenarios were calculated (Fig. A1). The total failed volume is 1.33 10^6 m^3 (scenario S01r) and 1.71 10^6 m^3 (scenario S01a), respectively. The total volume consists of three individual packages with different initial heights above todays lake floor.

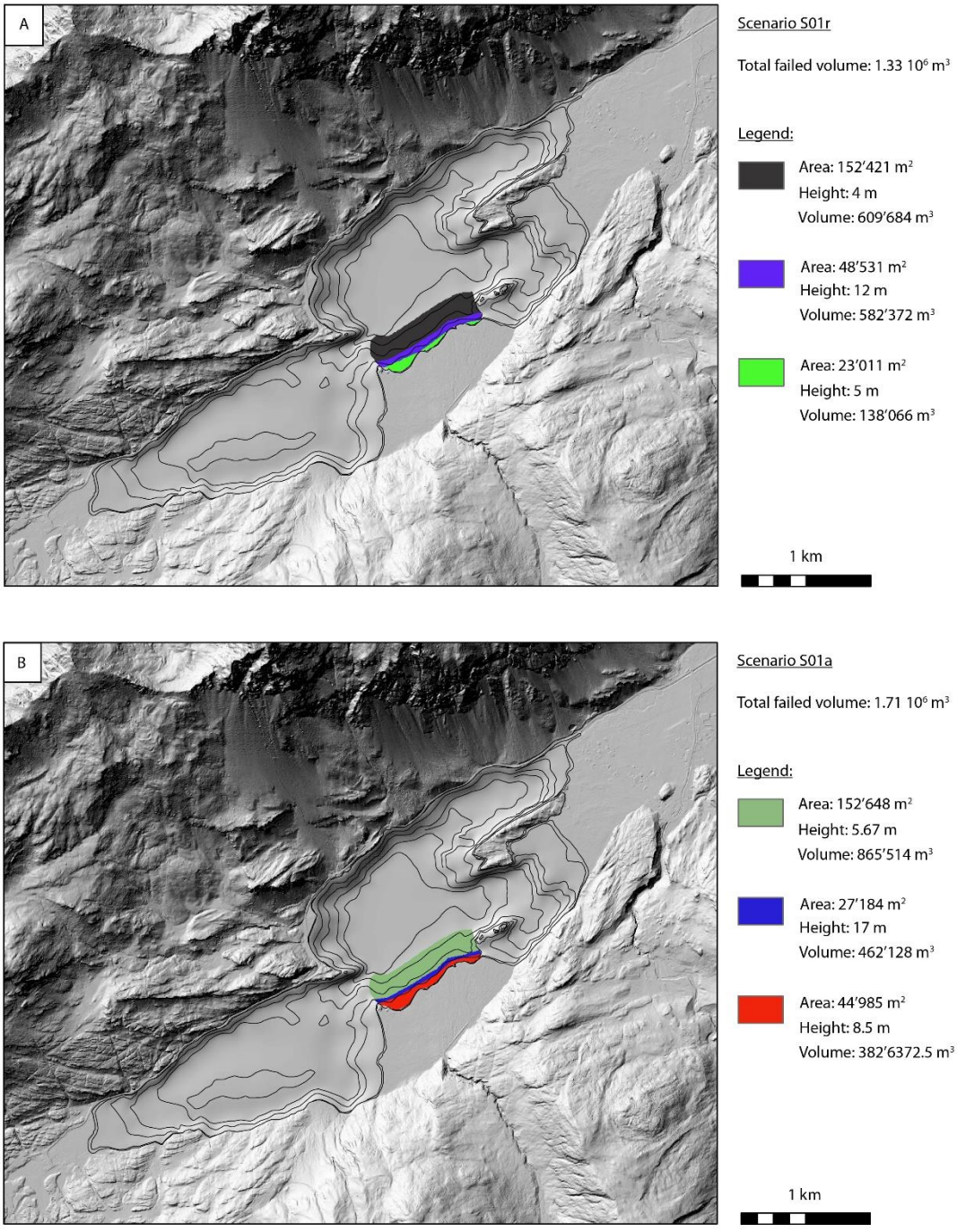

Fig. B3: Total failed delta volume of the two different numerical modelled scenario S01r (A) and S01a (B).

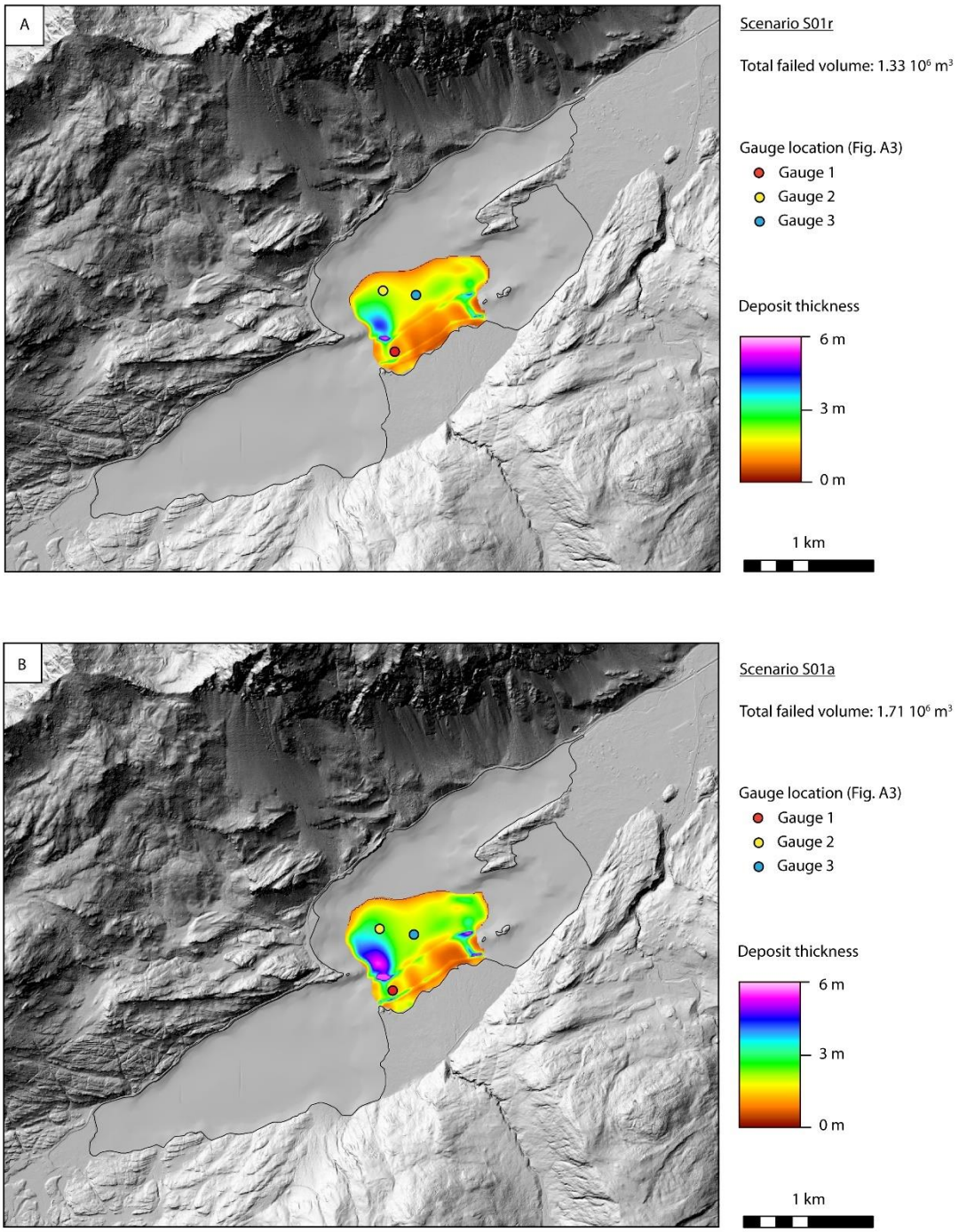

Fig. B4: Simulated mass-movement deposit of the two different numerical simulations S01r and S01a, with the initial volumes shown in Fig. B1.

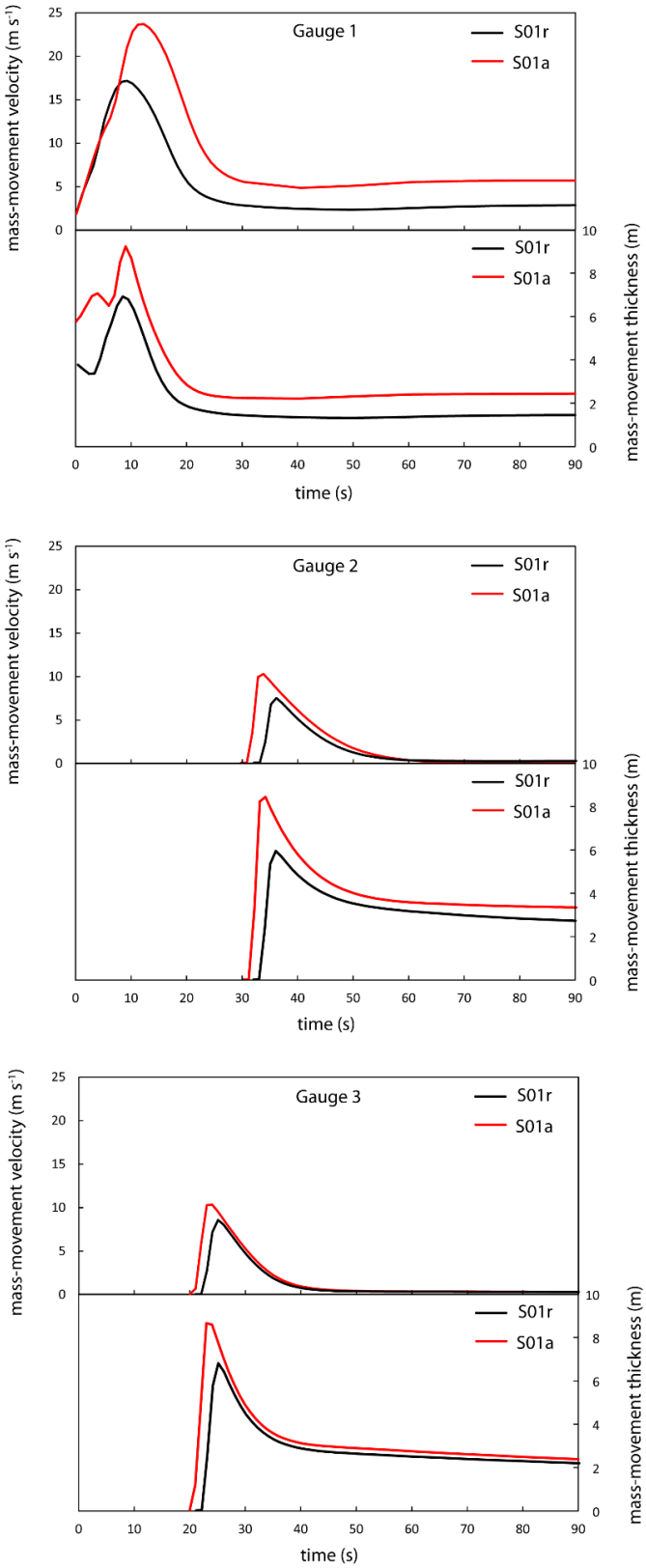

Fig. B5: Time series of simulated mass-movement velocity and thickness at the gauge location (see Fig. B2 for exact position) of the two different numerical simulations S01r and S01a.

Table B1: Sediment core locations in Swiss coordinate system LV95

Core ID	East (m)	North (m)	Water depth (m) or m a.s.l	Length (cm)	Study
SIL06-8	2'777'946	1'145'042	na	85	this study
SIL09-1	2'777'997	1'145'056	1798.54	515	this study
SIL09-2	2'777'979	1'145'050	1798.25	340	this study
SIL09-3	2'777'960	1'145'045	1797.88	362	this study
SIL09-4	2'777'944	1'145'035	1797.67	394	this study
SIL09-5	2'777'926	1'145'026	1797.52	370	this study
SIL09-6	2'777'943	1'145'076	1797.67	430	this study
SIL09-7	2'777'929	1'145'069	1797.49	227	this study
SIL09-8	2'777'920	1'145'064	1797.96	422	this study
SIL09-9	2'777'903	1'145'057	1797.37	371	this study
SIL09-10	2'777'940	1'145'062	1797.13	455	this study
SIL09-11	2'778'025	1'145'179	1798.15	254	this study
SIL09-12	2'778'065	1'145'204	1798.12	193	this study
SIL10-1	2'777'820	1'144'985	1.7	90	this study
SIL10-2	2'777'768	1'144'941	4.3	182	this study
SIL10-3	2'777'717	1'144'902	20.0	156	this study
SIL10-4	2'777'656	1'144'860	28.4	193	this study
SIL10-5	2'777'599	1'144'837	35.0	181	this study
SIL10-6	2'777'505	1'144'790	39.4	171	this study
SIL10-7	2'777'739	1'144'918	12.0	56	this study
SIL18-1	2'777'819	1'144'993	<3	50	this study
SIL18-2	2'777'808	1'145'006	<3	88	this study
SIL18-3	2'777'784	1'145'021	<3	80	this study
SIL18-4	2'777'821	1'144'908	<3	105	this study
SIL18-5	2'777'840	1'144'908	<3	100	this study
SIL18-6	2'777'772	1'145'067	<3	82	this study
SIL18-7	2'777'735	1'144'273	<3	67	this study
SIL18-8	2'777'878	1'144'126	<3	59	this study
SIL18-9	2'777'819	1'144'135	<3	62	this study
SIL18-10	2'777'793	1'144'168	<3	51	this study
Sis03-2	2'774'670	1'142'384	27	97.5	Blass et al. (2005)
Sis03-22	2'777'252	1'144'698	46	84	Blass et al. (2005)
Sis03-23	2'777'593	1'144'855	34	78	Blass et al. (2005)
Sis03-28	2'777'045	1'144'572	48	92	Blass et al. (2005)
PSS94-2	2'777'452	1'144'701	~70	811	Ohlendorf (1998)
PSS94-5	2'777'452	1'144'702	~42	283	Ohlendorf (1998)

Table B2: Mineralogical composition of sediment samples from core SIL10-1, SIL10-5, and SIL09 in volume percentage.

Core subsample	Composite depth (cm)	Lithological unit	Qtz (vol%)	Pl (vol%)	Kfs (vol%)	CPx (vol%)	Mca (vol%)	Chl (vol%)	Dol (vol%)	Cc (vol%)	Srp (vol%)	Am (vol%)	Tlc (vol%)
SIL10-1-46	40	D (clay cap)	15	9	2	1	38	28	1	1	2	4	0
SIL10-1-51	45	D	30	12	3	1	24	22	1	1	1	3	1
SIL10-1-54	48	E	12	5	1	1	39	34	3	0	2	4	0
SIL10-1-76	70	F	17	5	2	2	33	33	1	0	3	3	0
SIL10-5A-78	67	C	11	5	6	2	26	34	1	2	5	9	0
SIL10-5A-87	76	D (clay cap)	13	7	2	3	29	33	0	1	6	5	0
SIL10-5A-91	80	D	28	17	2	1	27	18	2	1	2	4	0
SIL10-5-98	87	D	17	6	1	1	36	36	1	0	0	4	0
SIL10-5B-20	116	D	31	8	0	1	31	22	3	1	1	2	0
SIL10-5B-70	166	D	23	6	1	1	36	27	2	1	2	2	0
SIL09-4A-44	44	II	13	27	4	0	36	15	0	0	1	4	0
SIL09-4A-49	49	II	15	16	2	1	41	20	0	0	1	5	0
SIL09-4A-52	52	II	23	18	1	1	37	14	1	0	1	4	0
SIL09-4A-60	60	II	21	19	1	1	41	13	0	0	1	3	0
SIL09-4A-85	85	V	23	19	1	1	28	22	1	1	1	3	0

Notes: Mineral abbreviations are Qtz = quartz; Pl = plagioclase; Kfs = K-feldspar; CPx = clinopyroxene; Mca = white mica; Chl = chlorite; Dol = dolomite; Cc = calcite; Srp = serpentine; Am = amphibole; and Tlc = talc.

Table B3: Mineralogical composition of the sand-sized riverine bedload samples collected at Lake Sils major tributaries in volume percentage.

Riverine bedload sample	Qtz (vol%)	Pl (vol%)	Kfs (vol%)	CPx (vol%)	Mca (vol%)	Chl (vol%)	Dol (vol%)	Cc (vol%)	Srp (vol%)	Am (vol%)	Tlc (vol%)
1: Aua da Fedoz	61.02	19.46	2.52	2.61	5.06	2.06	2.78	0.00	0.00	3.66	0.83
2: Lavatera	84.02	5.36	1.18	1.25	1.48	2.81	0.73	0.43	1.94	0.79	0.00
3: Lavatera + Ova dal Mulin	87.51	5.5	0.87	1.17	1.02	1.76	0.00	0.00	1.76	0.42	0.00
4: Ova de la Roda	73.62	13.38	6.85	2.82	0.42	0.73	0.00	0.98	0.00	0.75	0.00
5: Ova dal Crot	71.63	16.1	7.99	2.22	0.65	1.07	0.00	0.00	0.00	0.34	0.00
6: Fadacla	74.22	11.30	4.56	1.38	2.68	1.00	4.28	0.00	0.00	0.58	0.00

Notes: Mineral abbreviations are Qtz = quartz; Pl = plagioclase; Kfs = K-feldspar; CPx = clinopyroxene; Mca = white mica; Chl = chlorite; Dol = dolomite; Cc = calcite; Srp = serpentine; Am = amphibole; and Tlc = talc.

Table B4: Elemental concentrations of inorganic and total carbon, total nitrogen, and total sulfur in C sediment samples from core SIL10-1.

Core subsample	Composite depth (cm)	Lithological units	IC (wt%)	$CaCO_3$ (wt%)	TC (wt%)	TOC (wt%)	TN (wt%)	TS (wt%)	C/N (mol mol^{-1})
SIL10-1-34	28	C	0	0	4.08	4.08	0.347	1.449	13.7
SIL10-1-39	33	C	0	0	3.35	3.35	0.300	1.178	13.0
SIL10-1-42	36	C	0	0	4.56	4.56	0.411	1.509	12.9
SIL10-1-46	40	D (clay cap)	0	0	1.58	1.58	0.091	0.194	20.2
SIL10-1-48	42	D	0	0	0.20	0.20	0.014	0.016	16.8
SIL10-1-52	46	D	0.19	1.62	1.67	1.48	0.109	0.020	15.8
SIL10-1-53	47	E	0	0	8.74	8.74	0.492	0.282	20.7
SIL10-1-55	49	E	0	0	38.75	38.75	2.221	0.894	20.4
SIL10-1-59	53	E	0	0	23.52	23.52	1.546	0.295	17.7
SIL10-1-62	56	F	0	0	2.08	2.08	0.141	0.016	17.2
SIL10-1-67	61	F	0	0	1.11	1.11	0.076	0.007	17.0
SIL10-1-72	66	F	0	0	1.40	1.40	0.103	0.011	15.9
SIL10-1-77	71	F	0	0	0.02	0.02	0.007	0	3.8
SIL10-1-84	78	F	0	0	1.78	1.78	0.113	0	18.4
SIL10-1-89	83	F	0	0	0.41	0.41	0.045	0.048	10.7

Notes: IC = inorganic carbon; $CaCO_3$ = calcium carbonate; TC = total carbon; TOC = total organic carbon; TN = total nitrogen; TS = total sulfur; and C/N = carbon/nitrogen ratio. TOC concentrations a calculated from the difference between IC and TC concentrations. C/N ratios are calculated from TOC and TN concentrations and are given as weight/weight ratios.

Table B5: Elemental concentrations of inorganic and total carbon, total nitrogen, and total sulfur in C sediment samples from core SIL10-5.

Core subsample	Composite depth (cm)	Lithological units	IC (wt%)	$CaCO_3$ (wt%)	TC (wt%)	TOC (wt%)	TN (wt%)	TS (wt%)	C/N (mol mol^{-1})
SIL10-5A-82	71	C	0	0	1.03	1.03	0.121	0.068	9.9
SIL10-5A-84	73	C	0	0	0.86	0.86	0.074	0.084	13.6
SIL10-5A-86	75	C	0	0	0.87	0.87	0.095	0.034	10.6
SIL10-5A-88	77	D (clay cap)	0	0	7.18	7.18	0.509	0.116	16.5
SIL10-5A-90	79	D	0.11	0.92	0.62	0.51	0.015	0.029	39.7
SIL10-5A-98	87	D	0.03	0.28	0.73	0.70	0.067	0.019	12.2
SIL10-5A-103	92	D	0.26	2.22	1.11	0.85	0.059	0.017	16.7
SIL10-5B-10	106	D	0.29	2.42	0.76	0.47	0.016	0.041	34.3
SIL10-5B-20	116	D	0.35	2.94	0.78	0.43	0.018	0.016	27.8
SIL10-5B-30	126	D	0.28	2.38	0.74	0.46	0.017	0.019	31.4
SIL10-5B-60	156	D	0.19	1.60	0.67	0.48	0.018	0.030	31.0
SIL10-5B-70	166	D	0.26	2.21	0.78	0.52	0.015	0.020	40.2
SIL10-5B-80	176	D	0.26	2.22	0.63	0.37	0.012	0.019	36.4

Notes: IC = inorganic carbon; $CaCO_3$ = calcium carbonate; TC = total carbon; TOC = total organic carbon; TN = total nitrogen; TS = total sulfur; and C/N = carbon/nitrogen ratio. TOC concentrations a calculated from the difference between IC and TC concentrations. C/N ratios are calculated from TOC and TN concentrations and are given as weight/weight ratios.

Table B6: Elemental concentrations of inorganic and total carbon, total nitrogen, and total sulfur in C sediment samples from core SIL09-4.

Core subsample	Composite depth (cm)	Lithological units	IC (wt%)	$CaCO_3$ (wt%)	TC (wt%)	TOC (wt%)	TN (wt%)	TS (wt%)	C/N (mol mol^{-1})
SIL09-4A-0-12-44	40	II	0	0	0.30	0.30	0.036	0	9.8
SIL09-4A-0-12-49	45	II	0	0	0.68	0.68	0.144	0	5.5
SIL09-4A-0-12-53	49	II	0	0	0.37	0.37	0.038	0	11.4
SIL09-4A-0-12-57	53	II	0	0	0.46	0.46	0.033	0	16.4
SIL09-4A-0-12-61	57	II	0	0	0.58	0.58	0.038	0	17.7
SIL09-4A-0-12-65	61	D(III)	0	0	1.23	1.23	0.110	0.019	13.1
SIL09-4A-0-12-68	64	E(IV)	0	0	38.63	38.63	1.707	0.972	26.4
SIL09-4A-0-12-73	69	E(IV)	0	0	42.94	42.94	1.968	1.613	25.5
SIL09-4A-0-12-78	74	V	0	0	4.34	4.34	0.275	0.276	18.4
SIL09-4B-6-18-33	79	V	0	0	1.46	1.46	0.102	0.047	16.7
SIL09-4B-6-18-38	84	V	0	0	1.42	1.42	0.296	0.025	5.6
SIL09-4B-6-18-43	89	VI	0	0	0.61	0.61	0.048	0.022	14.9
SIL09-4A-12-24-12	94	VI	0	0	0.38	0.38	0.028	0.023	15.7
SIL09-4A-12-24-17	99	VI	0	0	0.21	0.21	0.019	0.012	13.0

Notes: IC = inorganic carbon; $CaCO_3$ = calcium carbonate; TC = total carbon; TOC = total organic carbon; TN = total nitrogen; TS = total sulfur; and C/N = carbon/nitrogen ratio. TOC concentrations a calculated from the difference between IC and TC concentrations. C/N ratios are calculated from TOC and TN concentrations and are given as weight/weight ratios.

Appendix C

Supplementary material to Chapter 5

Offshore tsunami deposits: evidence from sediment cores and numerical simulations of wave propagation of the 1601 CE Lake Lucerne Event

Valentin Nigg[1], Paola Bacigaluppi[2], David F. Vetsch[2], Hendrik Vogel[1], Katrina Kremer[3] and Flavio S. Anselmetti[1]

[1] Institute of Geological Sciences and Oeschger Centre for Climate Change Research, University of Bern, Baltzerstrasse 1+3, CH-3012 Bern (valentin.nigg@geo.unibe.ch)

[2] Institute of Hydraulics, Hydrology and Glaciology, ETH Zurich, Hönggerbergring 26, CH-8093 Zürich

[3] Swiss Seismological Service, ETH Zurich, Sonneggstrasse 5, CH-8093 Zürich, Switzerland

Table C1: Lake surface sediment samples: sample ID, macroscopic description of the sedimentological composition, D_{50} of the grain-size distribution measured with laser diffraction analysis, and CH1903+ LV95 coordinates of sample location.

Sample ID	Macroscopic description	D_{50} (µm)	Coordinates (CH1903+ / LV95)
S_1	Carbonate mud with coarse organic	45	2'667'325/1'211'284
S_2	Carbonate mud with coarse organic	58	2'667'282/1'211'571
S_3	Poorly sorted siliciclastic sand with gravel	340	2'667'957/1'211'689
S_4	Carbonate mud with coarse organic	45	2'668'777/1'210'976

Table C2: Lake surface sediment samples: TC, TOC, TIC, $CaCO_3$, TN, and TS concentrations as well as the molar C/N ratio.

Sample ID	TC (wt.%)	TOC (wt.%)	TIC (wt.%)	$CaCO_3$ (wt.%)	TN (wt.%)	C/N ratio (mol mol^{-1})	TS (wt.%)
LS-1	11.91	2.21	9.70	80.78	0.28	6.7	0.00
LS-2	11.84	2.42	9.41	78.42	0.30	6.8	0.00
LS-3	1.04	0.43	0.61	5.12	0.05	7.5	0.00
LS-4	5.71	2.48	3.23	26.93	0.24	9.0	0.00

Table C3: Sediment core total composite length and CH1903+ LV95 coordinates of sediment core location.

Core ID	Total composite depth (cm)	Coordinates (CH1903+ / LV95)
LU18-1	283.5	2'666'807/1'211'720
LU18-2	287.5	2'666'662/1'211'710
LU18-3	217.5	2'666'482/1'211'707

Table C4: Volume estimation of Unit 2 based on thickness of Unit 2 observed in sediment cores LU18-1, -2, and -3 and estimated depositional area (see Fig. 5-2B).

Area	Area (m^3)	Thickness of Unit 2 (m)	Volume (m^3)
A1	10'395	0.40	4'158
A2	14'507	0.64	9'285
A3	8'148	0.67	5'469
Total estimated Volume			18'902

Table C5: Lake surface sediment samples: Core ID, total composite depth, sedimentary unit, and TC, TOC, TIC, $CaCO_3$, TN, TS concentrations, as well as the molar C/N ratio.

Core ID	Total composite depth (cm)	Sedimentary unit	TC (wt.%)	TOC (wt.%)	TIC (wt.%)	$CaCO_3$ (wt.%)	TN (wt.%)	C/N ratio (mol mol^{-1})	TS (wt.%)
LU18-2	0.5	Unit 1	12.36	3.37	8.99	74.90	0.43	6.79	0.00
	10.5	Unit 1	11.03	2.19	8.85	73.69	0.27	6.90	0.06
	20.5	Unit 1	11.42	1.54	9.88	82.32	0.15	8.53	0.08
	30.5	Unit 1	10.26	1.73	8.52	71.00	0.11	13.10	0.00
	40.5	Unit 2	4.95	2.97	1.98	16.49	0.13	20.13	0.03
	50.5	Unit 2	3.88	2.16	1.72	14.30	0.11	16.44	0.00
	60.5	Unit 2	2.70	0.94	1.77	14.72	0.06	14.29	0.00
	70.5	Unit 2	2.08	0.34	1.74	14.53	0.00	-	0.00
	80.5	Unit 2	2.14	0.52	1.62	13.47	0.00	-	0.00
	90.5	Unit 2	1.94	0.31	1.63	13.62	0.00	-	0.00
	100.5	Unit 2	1.81	0.17	1.64	13.66	0.00	-	0.00
LU18-1	84.0	Unit 3	6.29	1.94	4.35	36.21	0.17	9.82	0.03
	84.5	Unit 3	3.54	1.93	1.62	13.46	0.13	12.77	0.00
	85.5	Unit 3	7.84	1.39	6.45	53.74	0.13	9.41	0.04
	86.5	Unit 3	5.86	1.56	4.30	35.82	0.11	11.91	0.06
	87.5	Unit 3	6.06	1.99	4.07	33.93	0.13	13.12	0.06
	88.5	Unit 3	6.01	1.93	4.07	33.93	0.13	12.66	0.08
	89.5	Unit 3	5.08	1.82	3.26	27.11	0.12	13.09	0.10
	90.5	Unit 3	5.21	1.34	3.87	32.24	0.11	10.60	0.06
	91.5	Unit 3	5.59	1.33	4.26	35.49	0.12	9.80	0.23
	92.0	Unit 3	3.88	0.89	2.98	24.85	0.07	11.64	0.11
	93.0	Unit 3	2.55	0.45	2.10	17.50	0.00	-	0.04
	94.0	Unit 3	2.44	0.43	2.01	16.73	0.03	12.63	0.04
	95.0	Unit 4	3.38	0.52	2.85	23.76	0.04	11.39	0.03
	96.0	Unit 4	4.71	0.22	4.48	37.34	0.00	-	0.00

Gauge data

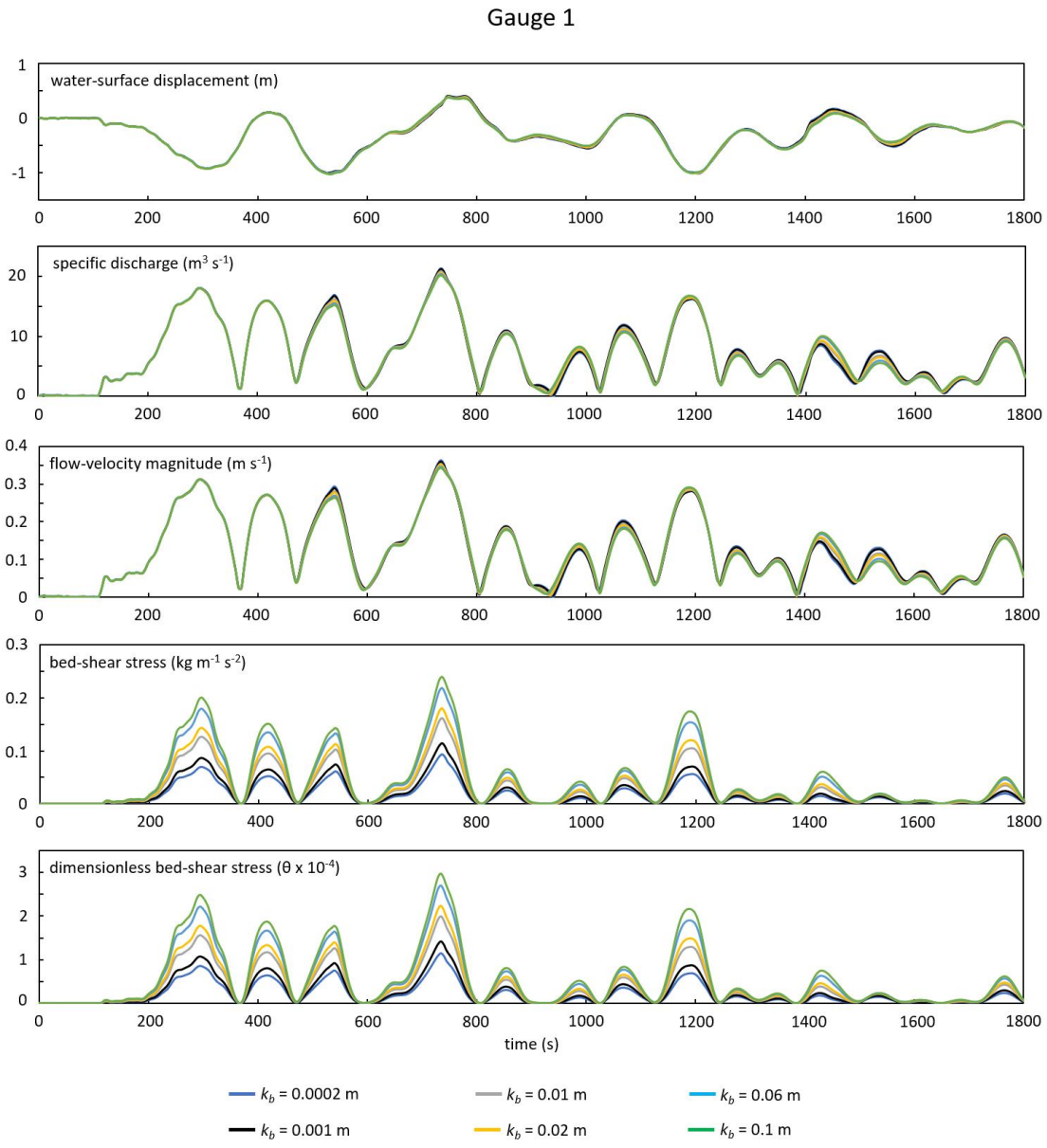

Fig. C1: Main parameters obtained from Gauge 1 for the sensitivity analysis of the bed roughness (k_b): water-surface displacement, specific discharge, flow-velocity magnitude, bed shear-stress, and dimensionless bed shear-stress. See Fig. 5-2 for the detailed gauge location.

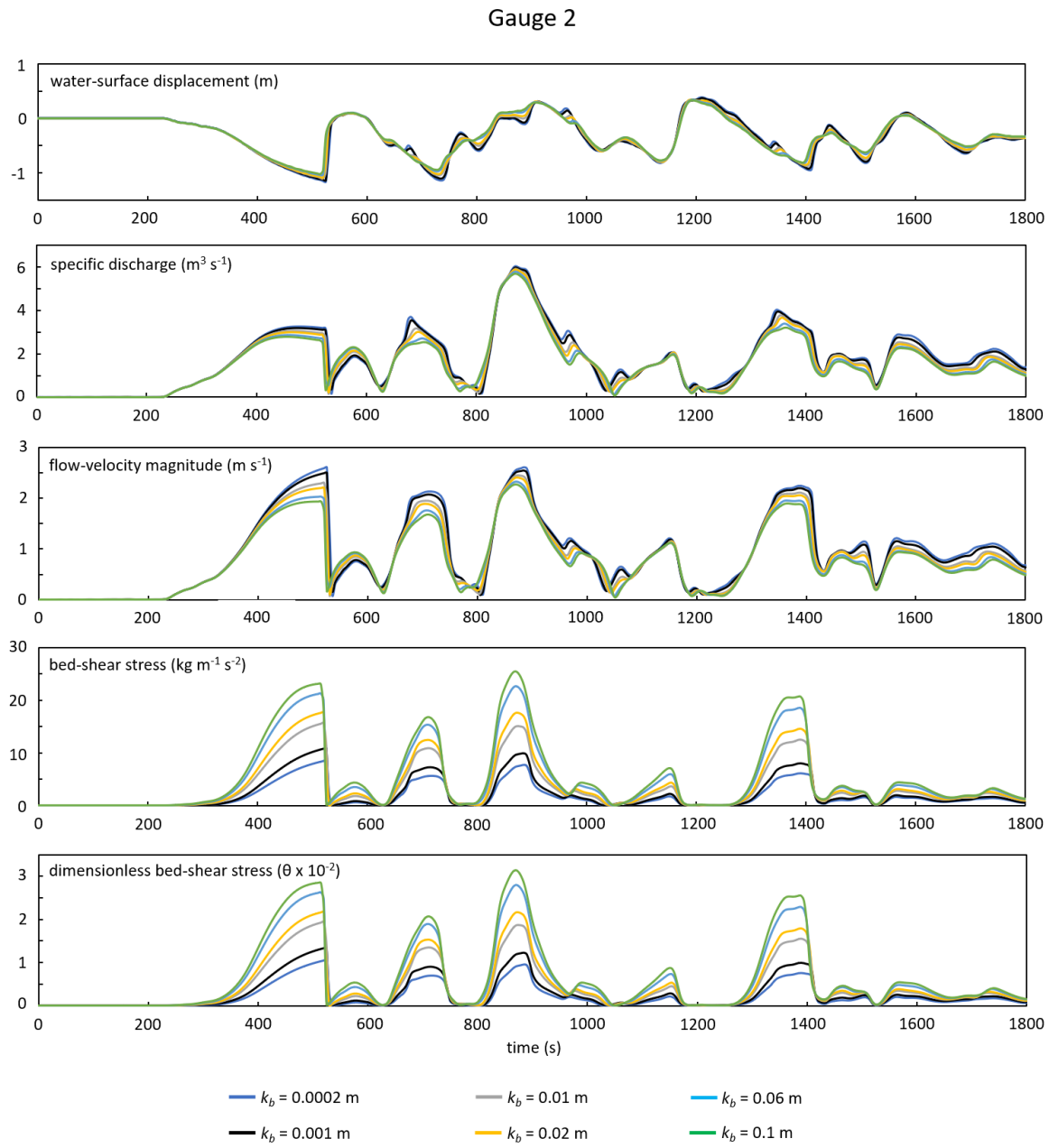

Fig. C2: Main parameters obtained from Gauge 2 for the sensitivity analysis of the bed roughness(k_b): water-surface displacement, specific discharge, flow-velocity magnitude, bed shear-stress, and dimensionless bed shear-stress. See Fig. 5-2 for the detailed gauge location.

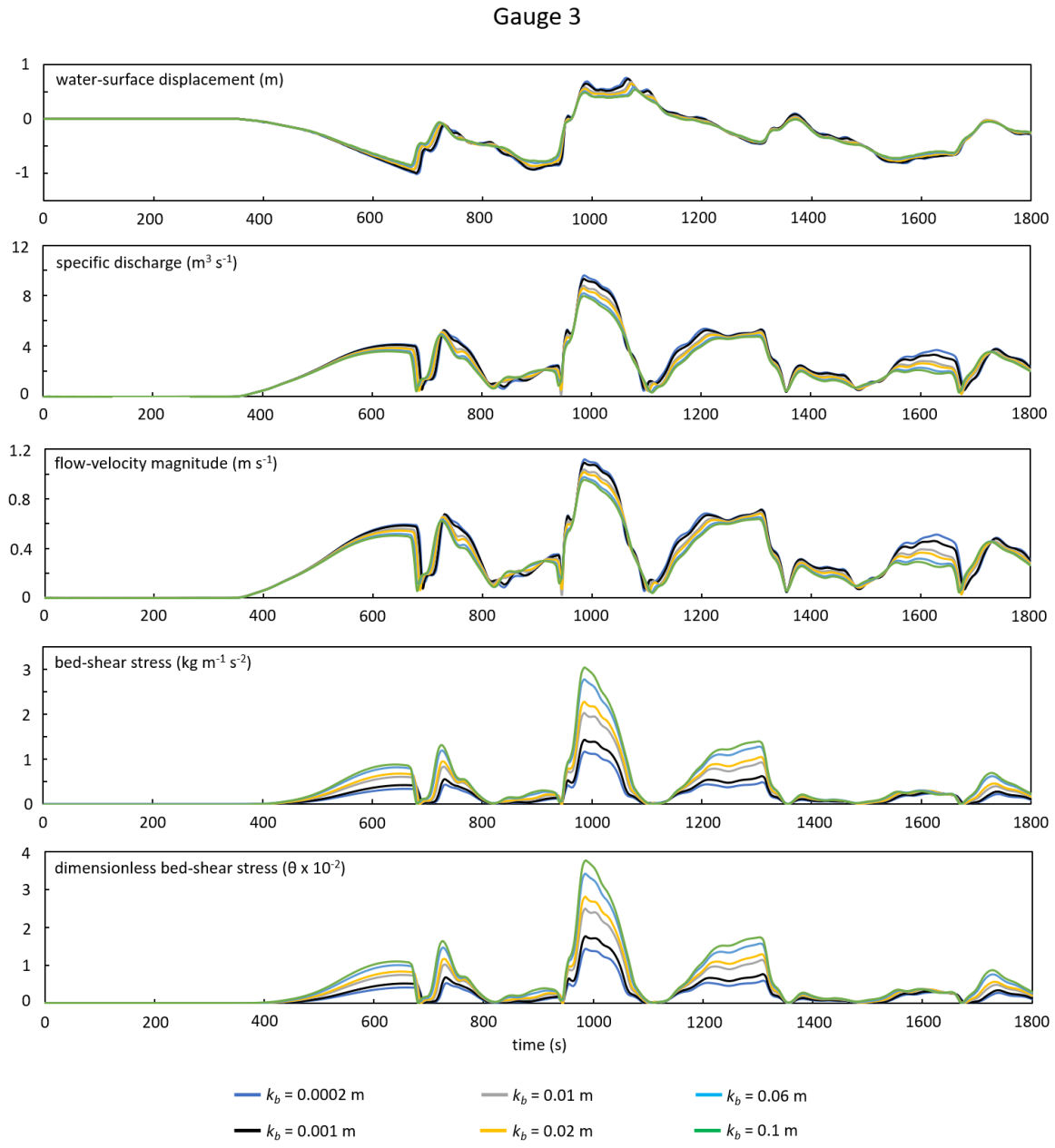

Fig. C3: Main parameters obtained from Gauge 3 for the sensitivity analysis of the bed roughness (k_b): water-surface displacement, specific discharge, flow-velocity magnitude, bed shear-stress, and dimensionless bed shear-stress. See Fig. 5-2 for the detailed gauge location.

Table C6: Area exceeding the dimensionless bed shear-stress (θ) of 0.03 and calculated volumes of eroded sediment with different homogeneous erosion thicknesses.

Simulation	Area (m^2)	Volume of eroded sediment (m^3) calculated with different homogeneous thicknesses of erosion on the area				
	$\theta \geq 0.03$	0.02 m	0.05 m	0.1 m	0.15 m	0.2 m
LU-S1	195503.2	3910.1	9775.2	19550.3	29325.5	39100.6
LU-S2	275519.4	5510.4	13776.0	27551.9	41327.9	55103.9
LU-S3	378890	7517.8	18794.5	37589.0	56383.5	75178.0
LU-S4	434414.2	8688.3	21720.7	43441.4	65162.1	86882.8
LU-S5	525417.2	10508.3	26270.9	52541.7	78812.6	105083.4
LU-S6	566827.3	11336.5	28341.4	56682.7	85024.1	113365.4

Bibliography of Chapter covers

Chapter 3

Triner, F. J. (1806) Vue d'une partie du Lac de Lovertz et de l'ile de Schwanau. Swiss National Library. https://www.helveticarchives.ch/detail.aspx?ID=480881

Chapter 4

Scheuchzer, J. J. (1723) Ouresiphoites Helveticus, sive, itinera per Helvetiae alpinas regiones facta annis MDCCII, MDCIII, MDCCIV, MDCCV, MDCCVI, MDCCVII, MDCCIX, MDCCX, MDCCXI (...). Lugduni Batavorum [Leiden]: typis ac sumptibus Petri van der Aa, MDCCXXIII. http://dx.doi.org/10.3931/e-rara-22519

Chapter 5

Martini, M. (1597) Luzern, Ansicht der Stadt, Martiniplan. Staatsarchiv Luzern, StALU PL 5255. https://query-staatsarchiv.lu.ch/detail.aspx?ID=119483

Chapter 6

Unknown Artist (1801) Felssturz in Sisikon 1801. 108.03-BI-6229. Zentralbibliothek Zürich, Graphische Sammlaung und Fotoarchiv.

Declaration of Consent

on the basis of Article 18 of the PromR Phil.-nat. 19

Name, First name: *Nigg, Valentin*

Matriculation number: *10-119-865*

Study program: *Doctoral studies in Earth Sciences (Geology)*

Bachelor ☐ Master ☐ Dissertation ☑

Title of the thesis: Sedimentological signatures of lacustrine tsunamis

Supervisors: Prof. Dr. F.S. Anselmetti
PD Dr. Hendrik Vogel

I declare herewith that this thesis is my own work and that I have not used any sources other than those stated. I have indicated the adoption of quotations as well as thoughts taken from other authors as such in the thesis. I am aware that the Senate pursuant to Article 36 paragraph1 litera r of the University Act of September 5th, 1996 and Article 69 of the University Statute of June 7th, 2011is authorized to revoke the title awarded on the basis of this thesis.

For the purposes of evaluation and verification of compliance with the declaration of originality and the regulations governing plagiarism, I hereby grant the University of Bern the right to process my personal data and to perform the acts of use this requires, in particular, to reproduce the written thesis and to store it permanently in a database, and to use said database, or to make said database available, to enable comparison with future theses submitted by others.

_____

Place/Date

_____

Signature